

1. REPORT NUMBER CA15-2582	2. GOVERNMENT ASSOCIATION NUMBER	3. RECIPIENT'S CATALOG NUMBER
4. TITLE AND SUBTITLE Analysis of Multi-span Bridges Using OpenSees		5. REPORT DATE October 2016
		6. PERFORMING ORGANIZATION CODE
7. AUTHOR Abdullah Almutairi, Jinchi Lu, Ning Wang, and Ahmed Elgamal		8. PERFORMING ORGANIZATION REPORT NO. UCSD
		9. PERFORMING ORGANIZATION NAME AND ADDRESS Department of Structural Engineering School of Engineering University of California, San Diego La Jolla, California 92093-0
12. SPONSORING AGENCY AND ADDRESS California Department of Transportation Division of Engineering Services 1801 30th St., MS-9-2/5i Sacramento, California 95816		10. WORK UNIT NUMBER
		11. CONTRACT OR GRANT NUMBER 65A0530
		13. TYPE OF REPORT AND PERIOD COVERED Final Report
		14. SPONSORING AGENCY CODE

15. SUPPLEMENTARY NOTES
 Prepared in cooperation with the State of California Department of Transportation.

16. ABSTRACT
 Seismic response parametric studies of multi-span bridges were performed using OpenSees. The models investigated were derived from three bridge configurations (the Salinas River Bridge, the Samoa Channel Bridge, and the Eureka Channel Bridge). Nonlinear Time History Analysis (THA) was conducted for 14 input motions provided by Caltrans. The THA procedures and results are presented in this report. Results of the Equivalent Static Analysis (ESA) procedure are presented as well. To facilitate the conducted analyses, the user interface MSBridge, in which FE computations are performed using OpenSees, was further developed and employed.

In the Salinas River Bridge model, the columns were modeled using the force-based beam-column element (based on the plastic hinge integration method BeamWithHinges) with an idealized bi-linear moment-curvature relationship. The column foundation response was represented by p-y and t-z springs. For the Samoa Channel Bridge and the Eureka Channel Bridge models, the pier columns were modeled using the nonlinear fiber section and the force-based beam-column element with the distributed plasticity integration method (forceBeamColumn). The pier foundation response was modeled by Foundation Matrix. In all cases, an elastic abutment model was employed for simplicity.

Comparison of the ESA and THA average results shows that the difference in displacement demand is about 12% for the Salinas River Bridge (for both longitudinal and transverse directions). For the Samoa Channel Bridge and the Eureka Channel Bridge models, the differences are 5.8% and 27.5%, respectively, in the longitudinal direction. The differences between the ESA and THA results in the transverse direction are 1

17. KEY WORDS Finite Element, Time History Analysis, Equivalent Static Analysis, Seismic Response, Highway Bridge	18. DISTRIBUTION STATEMENT Unlimited	
19. SECURITY CLASSIFICATION (of this report) Unclassified	20. NUMBER OF PAGES 217	21. COST OF REPORT CHARGED



**STRUCTURAL SYSTEMS
RESEARCH PROJECT**

Report No.
SSRP-16/01

**ANALYSIS OF MULTI-SPAN
BRIDGES USING OPENSEES**

by

ABDULLAH ALMUTAIRI

JINCHI LU

NING WANG

AHMED ELGAMAL

Final Report Submitted to the California Department of
Transportation (Caltrans) under Contract No. 65A0530.

October 2016

Department of Structural Engineering
University of California, San Diego
La Jolla, California 92093-0085

University of California, San Diego
Department of Structural Engineering
Structural Systems Research Project

Report No. SSRP-16/01

Analysis of Multi-span Bridges Using OpenSees

by

Abdullah Almutairi

Graduate Student Researcher, UC San Diego

Jinchi Lu

Associate Project Scientist, UC San Diego

Ning Wang

UC San Diego

and

Ahmed Elgamal

Professor, UC San Diego

Final Report Submitted to the California Department of
Transportation under Contract No. 65A0530

Department of Structural Engineering
University of California, San Diego
La Jolla, California 92093-0085

October 2016

DISCLAIMER

This document is disseminated in the interest of information exchange. The contents of this report reflect the views of the authors who are responsible for the facts and accuracy of the data presented herein. The contents do not necessarily reflect the official views or policies of the State of California or the Federal Highway Administration. This publication does not constitute a standard, specification or regulation. This report does not constitute an endorsement by the California Department of Transportation of any product described herein.

For individuals with sensory disabilities, this document is available in Braille, large print, audiocassette, or compact disk. To obtain a copy of this document in one of these alternate formats, please contact: the Division of Research and Innovation, MS-83, California Department of Transportation, P.O. Box 942873, Sacramento, CA 94273-0001.

ACKNOWLEDGMENTS

The research described in this report was supported by the California Department of Transportation (Caltrans) with Dr. Charles Sikorsky as the project manager. This support is most appreciated. In addition, we are grateful for the valuable technical suggestions, comments and contributions provided by Caltrans engineers, particularly Dr. Toorak Zokaie, Mr. Yeo (Tony) Yoon, Dr. Mark Mahan, Dr. Anoosh Shamsabadi, and Mr. Steve Mitchell.

EXECUTIVE SUMMARY

Seismic response parametric studies of multi-span bridges were performed using OpenSees. The models investigated were derived from three bridge configurations (the Salinas River Bridge, the Samoa Channel Bridge, and the Eureka Channel Bridge). Nonlinear Time History Analysis (THA) was conducted for 14 input motions provided by Caltrans. The THA procedures and results are presented in this report. Results of the Equivalent Static Analysis (ESA) procedure are presented as well. To facilitate the conducted analyses, the user interface MSBridge, in which FE computations are performed using OpenSees, was further developed and employed.

Comparison of the ESA and THA average results shows that the difference in displacement demand is about 12% for the Salinas River Bridge (for both longitudinal and transverse directions). For the Samoa Channel Bridge and the Eureka Channel Bridge models, the differences are 5.8% and 27.5%, respectively, in the longitudinal direction. The differences between the ESA and THA results in the transverse direction are 15.8% and 4.5%, respectively, for the above 2 bridges.

To further identify the main causes of difference between ESA and THA results, a parametric study was performed for a OSB (Ordinary Standard Bridge) model, in which focus was placed on the transverse direction response only. A series of models of increasing complexity were studied in an attempt to separate influence of column nonlinear response, foundation p-y springs, and the added resistance provided at the bridge end-bents and abutments. With all nonlinear mechanisms engaged, the difference was in the neighborhood of 10%.

ABSTRACT

Seismic response parametric studies of multi-span bridges were performed using OpenSees. The models investigated were derived from three bridge configurations (the Salinas River Bridge, the Samoa Channel Bridge, and the Eureka Channel Bridge). Nonlinear Time History Analysis (THA) was conducted for 14 input motions provided by Caltrans. The THA procedures and results are presented in this report. Results of the Equivalent Static Analysis (ESA) procedure are presented as well. To facilitate the conducted analyses, the user interface MSBridge, in which FE computations are performed using OpenSees, was further developed and employed.

In the Salinas River Bridge model, the columns were modeled using the force-based beam-column element (based on the plastic hinge integration method `BeamWithHinges`) with an idealized bi-linear moment-curvature relationship. The column foundation response was represented by p-y and t-z springs. For the Samoa Channel Bridge and the Eureka Channel Bridge models, the pier columns were modeled using the nonlinear fiber section and the force-based beam-column element with the distributed plasticity integration method (`forceBeamColumn`). The pier foundation response was modeled by Foundation Matrix. In all cases, an elastic abutment model was employed for simplicity.

Comparison of the ESA and THA average results shows that the difference in displacement demand is about 12% for the Salinas River Bridge (for both longitudinal and transverse directions). For the Samoa Channel Bridge and the Eureka Channel Bridge models, the differences are 5.8% and 27.5%, respectively, in the longitudinal direction. The differences between the ESA and THA results in the transverse direction are 15.8% and 4.5%, respectively, for the above 2 bridges.

To further identify the main causes of difference between ESA and THA results, a parametric study was performed for a OSB (Ordinary Standard Bridge) model, in which focus was placed on the transverse direction response only. A series of models of increasing complexity were studied in an attempt to separate influence of column nonlinear response, foundation p-y springs, and the added resistance provided at the bridge end-bents and abutments. With all nonlinear mechanisms engaged, the difference was in the neighborhood of 10%.

TABLE OF CONTENTS

DISCLAIMER.....	IV
ACKNOWLEDGMENTS	V
EXECUTIVE SUMMARY	VI
ABSTRACT.....	VII
TABLE OF CONTENTS	VIII
LIST OF TABLES	XIII
LIST OF FIGURES	XVI
1 INTRODUCTION.....	1
1.1 Background.....	1
1.2 Report Scope and Layout.....	1
2 THE SALINAS RIVER BRIDGE	3
2.1 Bridge Description and Geometric Configuration.....	3
2.2 OpenSees Bridge FE Model and Mode Shapes	3
2.3 Equivalent Static Analysis (ESA).....	4
2.3.1 ESA in the Longitudinal Direction	5
2.3.2 ESA in the Transverse Direction	5
2.4 Nonlinear Time History Analysis	6
2.4.1 Maximum Displacement and Acceleration.....	7
2.4.2 Response Time Histories	12
2.5 Summary	17
2.6 Conclusions.....	17
3 THE SAMOA CHANNEL BRIDGE	18
3.1 Bridge Description	18
3.2 Geometric Configuration	19
3.3 OpenSees FE Modeling	22
3.4 Mode Shape Analysis	23
3.5 Equivalent Static Analysis (ESA).....	25
3.5.1 ESA in the Longitudinal Direction	25
3.5.2 ESA in the Transverse Direction	25
3.6 Nonlinear Time History Analysis	27

3.6.1	Maximum Displacement and Acceleration.....	27
3.6.2	Response Time History.....	32
3.7	Summary.....	39
3.8	Conclusions.....	39
3.9	Analysis of Samoa Bridge with Stiff Foundation Matrix.....	40
3.9.1	Mode Shape Analysis.....	40
3.9.2	Equivalent Static Analysis (ESA).....	42
3.9.2.1	ESA in the Longitudinal Direction.....	42
3.9.2.2	ESA in the Transverse Direction.....	42
3.9.3	Nonlinear Time History Analysis.....	43
3.9.3.1	Maximum Displacement and Acceleration.....	43
3.9.3.2	Response Time History.....	49
3.9.4	Summary.....	54
3.9.5	Conclusions.....	54
4	THE EUREKA CHANNEL BRIDGE.....	55
4.1	Bridge Description.....	55
4.2	Geometric Configuration.....	56
4.3	OpenSees Finite Element Modeling.....	58
4.4	Mode Shape Analysis.....	58
4.5	Equivalent Static Analysis (ESA).....	60
4.5.1	ESA in the Longitudinal Direction.....	60
4.5.2	ESA in the Transverse Direction.....	60
4.6	Nonlinear Time History Analysis.....	62
4.6.1	Maximum Displacement and Acceleration.....	62
4.6.2	Response Time History.....	67
4.7	Summary.....	74
4.8	Conclusions.....	74
5	SUMMARY AND CONCLUSIONS.....	75
5.1	Summary.....	75
5.2	Conclusions.....	75
APPENDIX A	MSBRIDGE: MULTI-SPAN BRIDGE ANALYSIS.....	77

A.1	General Overview	77
A.2	Capabilities Added in the Current Updated Version of MSBridge	78
APPENDIX B	BASE INPUT MOTIONS	82
APPENDIX C	BRIDGE TRANSVERSE DIRECTION STUDY (COMPARISON OF ESA AND THA RESULTS).....	89
C.1	Introduction.....	89
C.1.1	Purpose of Study.....	89
C.1.2	Salient Modeling Considerations.....	90
C.1.3	Report Layout	90
C.2	Typical Bent.....	91
C.2.1	ESA Comparison for MSBridge and wFrame	91
C.3	Case 1: Single Bent Model with Rigid Base and Linear Columns.....	95
C.3.1	Comparison of ESA and THA Results	95
C.4	Case 2: Single Bent Model with Linear Soil Springs and Linear Columns.....	97
C.4.1	Comparison of ESA and THA Results	97
C.5	Case 3: Single Bent Model with Rigid Base and Nonlinear Columns	99
C.5.1	Comparison of ESA and THA Results	99
C.6	Case 4: Single Bent Model with Linear Soil Springs and Nonlinear Columns	102
C.6.1	Comparison of ESA and THA Results	102
C.7	Case 5: Single Bent Model with Nonlinear Soil Springs and Nonlinear Columns	105
C.7.1	Transverse Pushover Loading.....	105
C.7.2	Comparison of ESA and THA Results	107
C.8	Case 6: Multi-bent Model with Nonlinear Soil Springs and Nonlinear Columns	110
C.9	Case 7: Multi-bent Model with End-bents.....	111
C.9.1	Comparison of ESA and THA Results	112
C.10	Case 8: Salinas River Bridge Model.....	116
C.10.1	Comparison of ESA and THA Results	118
C.11	Summary and Conclusions	123
C.11.1	Summary.....	123
C.11.2	Conclusions.....	123
APPENDIX D	SALINAS BRIDGE MODELING DETAILS	125

D.1	Column.....	125
D.2	Soil Springs.....	126
D.3	Deck and Bentcap	128
D.4	Abutment.....	128
APPENDIX E THE SAMOA CHANNEL BRIDGE MODELING DETAILS		129
E.1	Column.....	129
E.2	Foundation Matrix	129
E.3	Deck.....	133
E.4	Abutment.....	133
E.5	ESA	133
APPENDIX F THE EUREKA CHANNEL BRIDGE MODELING DETAILS		135
F.1	Column.....	135
F.2	Foundation Matrix	135
F.3	Deck.....	136
F.4	Abutment.....	136
APPENDIX G COLUMN NONLINEAR FIBER SECTIONS FOR THE SAMOA CHANNEL BRIDGE AND THE EUREKA CHANNEL BRIDGE.....		137
APPENDIX H VERIFICATIONS OF MSBRIDGE RESPONSE MECHANISMS.....		144
G.1	Bridge Model	145
G.1.1	Longitudinal Column Response Profile.....	145
G.1.2	Transverse Column Response Profile.....	147
G.2	Pushover Analysis.....	148
G.2.1	Forced-based Pushover Analysis	149
G.2.2	Displacement-based Pushover Analysis	150
G.2.3	Nonlinear Fiber Section	151
G.3	Mode Shapes Analysis.....	153
G.4	Abutment Model	156
G.4.1	Elastic Abutment Model	156
G.4.2	Roller Abutment Model	157
G.4.3	SDC Abutment Model	158
G.5	Foundation Model.....	160

G.5.1	Rigid Base.....	160
G.5.2	Soil Springs.....	161
G.5.3	Foundation Matrix	164
G.6	Advanced Options.....	175
REFERENCES.....		188

LIST OF TABLES

Table 2.1. Natural Periods and Frequencies for Salinas Bridge	2
Table 2.2. Comparison of MSBridge and wFrame Results for ESA of Salinas Bridge	5
Table 2.3. Longitudinal ESA Parameters for Salinas Bridge	6
Table 2.4. Longitudinal ESA Result for Salinas Bridge	6
Table 2.5. Transverse ESA Parameters for Bent 4	6
Table 2.6. Transverse ESA Result for Salinas Bridge	6
Table 2.7. Salinas Bridge Deck Maximum Displacement	8
Table 2.8. Salinas Bridge Deck Maximum Acceleration	9
Table 3.1. Column Heights for Samoa Bridge.....	22
Table 3.2. Natural Periods and Frequencies for Samoa Bridge	23
Table 3.3. Longitudinal ESA Parameters for Samoa Bridge	26
Table 3.4. Longitudinal ESA Result for Samoa Bridge.....	26
Table 3.5. Transverse ESA Parameters for Pier S-8.....	26
Table 3.6. Transverse ESA Result for Pier S-8	26
Table 3.7. Samoa Bridge Deck Maximum Displacement.....	28
Table 3.8. Samoa Bridge Deck Maximum Acceleration	29
Table 3.9. Natural Periods and Frequencies for Samoa Bridge with Stiff Foundation Matrix.....	40
Table 3.10. Natural Periods and Frequencies for Samoa Bridge with Rigid Pier Base.....	40
Table 3.11. Longitudinal ESA Parameters for Samoa Bridge with Stiff Foundation Matrix.....	42
Table 3.12. Longitudinal ESA Result for Samoa Bridge with Stiff Foundation Matrix	42
Table 3.13. Transverse ESA Parameters for Pier S-8.....	43
Table 3.14. Transverse ESA Result for Samoa Bridge with Stiff Foundation Matrix	43
Table 3.15. Deck Maximum Displacement for Samoa Bridge with Stiff Foundation Matrix.....	45
Table 3.16. Deck Maximum Acceleration for Samoa Bridge with Stiff Foundation Matrix	46
Table 4.1. Column Heights for Eureka Bridge	57
Table 4.2. Natural Periods and Frequencies for Eureka Bridge	58
Table 4.3. Longitudinal ESA Parameters for Eureka Bridge.....	61
Table 4.4. Longitudinal ESA Result for Eureka Bridge	61
Table 4.5. Transverse ESA Parameters for Pier E-6.....	61
Table 4.6. Transverse ESA Result for Eureka Bridge	61

Table 4.7. Eureka Bridge Deck Maximum Displacement	63
Table 4.8. Eureka Bridge Deck Maximum Acceleration.....	64
Table B.1. Input Motions Employed in the Nonlinear THA	83
Table B.2. Intensity Measures of the 14 Motions.....	84
Table C.1. Comparison of MSBridge and wFrame Results for the transverse ESA	94
Table C.2 Comparison of transverse ESA displacement demand and THA maximum displacement (ESA displacement demand for an individual motion is based on the response spectrum of that motion)	96
Table C.3 Maximum Column Shear Forces and Bending Moments (Transverse).....	96
Table C.4 Comparison of transverse ESA displacement demand and THA maximum displacement (ESA displacement demand for an individual motion is based on the response spectrum of that motion)	98
Table C.5 Maximum Column Shear Forces and Bending Moments (Transverse).....	98
Table C.6 Comparison of transverse ESA displacement demand and THA maximum displacement (ESA displacement demand for an individual motion is based on the response spectrum of that motion)	100
Table C.7 Maximum Column Shear Forces and Bending Moments (Transverse).....	100
Table C.8 Comparison of transverse ESA displacement demand and THA maximum displacement (ESA displacement demand for an individual motion is based on the response spectrum of that motion)	103
Table C.9 Maximum Column Shear Forces and Bending Moments (Transverse).....	103
Table C.10 Comparison of transverse ESA displacement demand and THA maximum displacement (ESA displacement demand for an individual motion is based on the response spectrum of that motion)	107
Table C.11 Maximum Column Shear Forces and Bending Moments (Transverse).....	108
Table C.12 Comparison of transverse ESA displacement demand and THA maximum displacement (ESA displacement demand for an individual motion is based on the response spectrum of that motion)	113
Table C.13 Comparison of Cases 5 and 7 for THA maximum displacement.....	113
Table C.14 Maximum Column Shear Forces and Bending Moments (Transverse).....	114

Table C.15 Comparison of transverse ESA displacement demand and THA maximum displacement (ESA displacement demand for an individual motion is based on the response spectrum of that motion)	119
Table C.16 Comparison of Cases 5 and 8 for THA maximum displacement.....	119
Table C.17 Maximum Column Shear Forces and Bending Moments (Transverse).....	120
Table C.18 Comparison of the average ESA displacement demand and THA maximum displacement for all the studied models	123
Table D.1. Salinas River Bridge Deck Material and Section Properties	128
Table D.2. Salinas River Bridge Bentcap Properties	128
Table E.1. Samoa Bridge Foundation Matrix Coefficients (Wang 2015)	132
Table E.2. Samoa Bridge Constant Foundation Matrix Coefficients for All Bents (Wang 2015)	133
Table E.3. Bridge Deck Material and Section Properties for Samoa Bridge (Wang 2015)	133
Table F.1. Bent Foundation Matrix Coefficients for Eureka Bridge (Wang 2015).....	135
Table F.2. Material and Section Properties of the Bridge Deck for Eureka Bridge (Wang 2015)	136
Table H.1 MSBridge Feature-Verification Cases.....	146
Table H.2 Special Cases for Rigid Beam on Elastic Foundation (Hetenyi 1946)	161

LIST OF FIGURES

Figure 2.1 General layout of Salinas Bridge (Caltrans 2016).....	1
Figure 2.2 Sectional details of Salinas Bridge: (a) deck; (b) Type I shaft cross section	1
Figure 2.3 Salinas Bridge FE model created in MSBridge (dimensions in ft): (a) plan view; (b) elevation view; (c) close-up of 3D view; (d) side view of a bent (typical).....	2
Figure 2.4 Salinas Bridge mode shapes: (a) first mode; (b) second mode; (c) third mode; (d) fourth mode; and (e) fifth mode	3
Figure 2.5 Acceleration response spectrum (ARS) curve employed in Caltrans (2005).....	4
Figure 2.6 ARS curve employed in the ESA	5
Figure 2.7 Bridge deck maximum longitudinal displacement	10
Figure 2.8 Bridge deck maximum transverse displacement	10
Figure 2.9 Bridge deck maximum longitudinal acceleration.....	11
Figure 2.10 Bridge deck maximum transverse acceleration.....	11
Figure 2.11 Column top longitudinal response time histories of Column 1 of Bent 7 for Simulation 1: a) acceleration; b) displacement; c) bending moment; and (d) base excitation ROCKS1N1.....	13
Figure 2.12 Column top longitudinal moment-curvature response of Column 1 of Bent 7 for Simulation 1	14
Figure 2.13 Deformed mesh (factor of 100) for Simulation 1 at the maximum displacement step (grey lines represent undeformed mesh): (a) entire bridge; (b) close-up of Bents 6, 7, and 8 (from left to right)	14
Figure 2.14 Column top longitudinal response time histories of Column 1 of Bent 7 for Simulation 4: (a) acceleration; (b) displacement; (c) bending moment; (d) base excitation ROCKS1N4.....	15
Figure 2.15 Column top longitudinal moment-curvature response of Column 1 of Bent 7 for Simulation 4	16
Figure 2.16 Deformed mesh (factor of 100) for Simulation 4 at the step of the maximum displacement (14 in @ 19.2 seconds) (grey lines represent undeformed mesh): (a) entire bridge; (b) close-up of Bents 6, 7, and 8 (from left to right).....	16

Figure 3.1 Bridge configuration: (a) Samoa Channel Bridge, Eureka geotechnical array, Middle Channel Bridge and Eureka Channel Bridge (Map Data @ 2015 Google) and (b) photo of the Samoa Channel Bridge (http://www.strongmotioncenter.org)	18
Figure 3.2 Layout of instrumentation at Samoa Bridge (http://www.strongmotioncenter.org): (a) elevation view; (b) plan view	19
Figure 3.3 Samoa Bridge: (a) elevation and bridge deck of Pier S-8; (b) column detail of Piers S-8 and S-9; (c) column detail of other piers except Piers S-8 and S-9	21
Figure 3.4 Samoa Bridge FE mesh created in MSBridge: (a) 3D view; (b) elevation view; (c) plan view	23
Figure 3.5 Mode shapes for Samoa Bridge: (a) first mode; (b) second mode; (c) third mode; (d) fourth mode; and (e) fifth mode	24
Figure 3.6 ARS curve employed in the ESA	25
Figure 3.7 Bridge deck maximum longitudinal displacement	30
Figure 3.8 Bridge deck maximum transverse displacement	30
Figure 3.9 Bridge deck maximum longitudinal acceleration.....	31
Figure 3.10 Bridge deck maximum transverse acceleration.....	31
Figure 3.11 Pier S-8 column top longitudinal response time histories for Simulation 1: (a) acceleration; (b) displacement; (c) bending moment; (d) base excitation ROCKS1N1	33
Figure 3.12 Column top longitudinal moment-curvature response for Simulation 1: (a) Pier S-4; (b) Pier S-8; (c) Pier S-19.....	34
Figure 3.13 Deformed mesh (factor of 100) for Simulation 1 at the maximum displacement step (grey lines represent undeformed mesh): (a) entire bridge; (b) close-up of Bents 6, 7, and 8 (from left to right)	35
Figure 3.14 Pier S-8 column top longitudinal response time histories for Simulation 4: (a) acceleration; (b) displacement; (c) bending moment; (d) base excitation ROCKS1N4	36
Figure 3.15 Column top longitudinal moment-curvature response for Simulation 4: (a) Pier S-4; (b) Pier S-8; (c) Pier S-19.....	37
Figure 3.16 Deformed mesh (factor of 100) for Simulation 4 at the maximum displacement step (grey lines represent undeformed mesh): (a) entire bridge; (b) close-up of Bents 6, 7, and 8 (from left to right)	38
Figure 3.17 Stiff foundation matrix employed	40

Figure 3.18 Mode shapes for Samoa Bridge with stiff foundation matrix: (a) first mode; (b) second mode; (c) third mode; (d) fourth mode; and (e) fifth mode	41
Figure 3.19 Bridge deck maximum longitudinal displacement	47
Figure 3.20 Bridge deck maximum transverse displacement	47
Figure 3.21 Bridge deck maximum longitudinal acceleration.....	48
Figure 3.22 Bridge deck maximum transverse acceleration.....	48
Figure 3.23 Pier S-8 column top longitudinal response time histories for Simulation 1: (a) acceleration; (b) displacement; (c) bending moment; (d) base excitation ROCKS1N1	50
Figure 3.24 Pier S-8 column top longitudinal moment-curvature response for Simulation 1	51
Figure 3.25 Deformed mesh (factor of 200) for Simulation 1 at the maximum displacement step (grey lines represent undeformed mesh): (a) entire bridge; (b) close-up of Bents 6, 7, and 8 (from left to right)	51
Figure 3.26 Pier S-8 column top longitudinal response time histories for Simulation 8: (a) acceleration; (b) displacement; (c) bending moment; (d) base excitation ROCKS1P1	52
Figure 3.27 Pier S-8 column top longitudinal moment-curvature response for Simulation 8	53
Figure 3.28 Deformed mesh (factor of 200) for Simulation 8 at the maximum displacement step (grey lines represent undeformed mesh): (a) entire bridge; (b) close-up of Bents 6, 7, and 8 (from left to right)	53
Figure 4.1 Bridge configuration: (a) Samoa Bridge, Eureka Geotechnical Array, Middle Channel Bridge and Eureka Bridge (Map Data @ 2015 Google) and (b) photo of the Eureka Bridge (http://www.strongmotioncenter.org)	55
Figure 4.2 Layout of instrumentation at Eureka Bridge (http://www.strongmotioncenter.org): (a) elevation view; (b) plan view	56
Figure 4.3 Eureka Bridge: (a) elevation and bridge deck	57
Figure 4.4 Eureka Bridge FE mesh created in MSBridge: (a) 3D view; (b) elevation view; (c) plan view	58
Figure 4.5 Mode shapes for Eureka Bridge: (a) first mode; (b) second mode; (c) third mode; (d) fourth mode; and (e) fifth mode	59
Figure 4.6 ARS curve employed in the ESA	60
Figure 4.7 Bridge deck maximum longitudinal displacement	65
Figure 4.8 Bridge deck maximum transverse displacement	65

Figure 4.9 Bridge deck maximum longitudinal acceleration.....	66
Figure 4.10 Bridge deck maximum transverse acceleration.....	66
Figure 4.11 Pier E-7 Column top longitudinal response time histories for Simulation 2: a) acceleration; b) displacement; c) bending moment; d) base excitation ROCKS1N2	68
Figure 4.12 Column top longitudinal moment-curvature response for Simulation 2 (motion ROCKS1N2): (a) Pier E-6; (b) Pier E-7; (c) Pier E-13	69
Figure 4.13 Deformed mesh (factor of 100) for Simulation 1 (motion ROCKS1P2) at the maximum displacement step (grey lines represent undeformed mesh): (a) entire bridge; (b) close-up of Piers 6, 7, and 8 (from left to right).....	70
Figure 4.14 Pier E-7 column top longitudinal response time histories for Simulation 9: (a) acceleration; (b) displacement; (c) bending moment; (d) base excitation ROCKS1P2	71
Figure 4.15 Column top longitudinal moment-curvature response for Simulation 9 (motion ROCKS1P2): (a) Pier E-6; (b) Pier E-7; (c) Pier E-13	72
Figure 4.16 Deformed mesh (factor of 100) for Simulation 9 (motion ROCKS1P2) at the maximum displacement step (grey lines represent undeformed mesh): (a) entire bridge; (b) close-up of Piers 6, 7, and 8 (from left to right).....	73
Figure A.1 Global coordinate system employed in MSBridge.....	78
Figure B.1 Longitudinal PGA histograms of the first 14 input motions	83
Figure B.2 Acceleration time histories of the input motion components for Rock site (non-pulse- like motions).....	85
Figure B.3 Acceleration time histories of the input motion components for Rock site (pulse-like motions).....	86
Figure B.4 Pseudo-Spectral Acceleration for rock site (non-pulse-like motions).....	87
Figure B.5 Pseudo-Spectral Acceleration for rock site (pulse-like motions)	88
Figure C.1 Typical bent of Salinas Bridge (dimensions in ft)	92
Figure C.2 Idealized bilinear moment-curvature relationship employed for the columns (plastic moment = 6,100 kip-ft; yield curvature = 2.92×10^{-5} rad/in).....	93
Figure C.3 Idealized bilinear moment-curvature relationship employed for the pile shafts (plastic moment = 19,400 kip-ft; yield curvature = 8.23×10^{-5} rad/in).....	93
Figure C.4 Shear force versus transverse displacement for pushover analysis	94
Figure C.5 Single bent model for Case 1 (with rigid base at mudline)	95

Figure C.6 Single bent model for Case 2	97
Figure C.7 Single bent model for Case 3 (with rigid base at mudline)	99
Figure C.8 Moment-curvature response at column top for Motion #1 ROCKS1N1 (Red part shows the end of shaking)	101
Figure C.9 Moment-curvature response at column top for Motion #2 ROCKS1N2 (Red part shows the end of shaking)	101
Figure C.10 Single bent model for Case 4	102
Figure C.11 Moment-curvature response at column top for Motion #1 ROCKS1N1 (Red part shows the end of shaking)	104
Figure C.12 Moment-curvature response at column top for Motion #2 ROCKS1N2 (Red part shows the end of shaking)	104
Figure C.13 Single bent model for Case 5	105
Figure C.14 Pushover load versus transverse displacement for the transverse ESA	106
Figure C.15 Axial force versus transverse displacement for the transverse ESA	106
Figure C.16 Moment-curvature response at column top for Motion #1 ROCKS1N1 (Red part shows the end of shaking)	108
Figure C.17 Moment-curvature response at column top for Motion #2 ROCKS1N2 (Red part shows the end of shaking)	109
Figure C.18 Multi-bent model for Case 6	110
Figure C.19 First transverse mode of the multi-bent model (period = 2.0 seconds): (a) plan view; (b) 3D view	110
Figure C.20 Multi-bent model with end-bents: (a) plan view; (b) 3D view; (c) bent close-up ...	111
Figure C.21 First transverse mode of the multi-bent model (period = 1.94 seconds)	112
Figure C.22 Moment-curvature response at column top for Column 1 of Bent 6 for Motion #1 ROCKS1N1 (Red part shows the end of shaking)	114
Figure C.23 Moment-curvature response at column top for Column 1 of Bent 6 for Motion #2 ROCKS1N2 (Red part shows the end of shaking)	115
Figure C.24 Abutment and column response in pushover analysis	117
Figure C.25 First transverse mode of Salinas River Bridge (period = 1.91 seconds): (a) plan view; (b) 3D view	118

Figure C.26 Moment-curvature response at column top for Column 1 of Bent 6 for Motion #1 ROCKS1N1 (Red part shows the end of shaking).....	120
Figure C.27 Abutment (left or right) transverse resisting force-displacement response for Motion #1 ROCKS1N1 (Red part shows the end of shaking).....	121
Figure C.28 Moment-curvature response at column top for Column 1 of Bent 6 for Motion #2 ROCKS1N2 (Red part shows the end of shaking).....	121
Figure C.29 Abutment (left or right) transverse resisting force-displacement response for Motion #2 ROCKS1N2 (Red part shows the end of shaking).....	122
Figure D.1 Bi-linear moment-curvature relationship: (a) column; (b) pile shaft	125
Figure D.2 Idealized soil P-Y curve at depth of 0.5 ft (Caltrans, 2005).....	126
Figure D.3 Idealized soil P-Y curve at depth of 16.5 ft (Caltrans, 2005).....	126
Figure D.4 Idealized soil P-Y curve at depth of 17.5 ft (Caltrans, 2005).....	126
Figure D.5 Idealized soil P-Y curve at depth of 106.5 ft (Caltrans, 2005).....	127
Figure D.6 Idealized soil T-Z curves (Caltrans, 2005)	127
Figure D.7 Idealized soil Q-Z curves (Caltrans, 2005).....	127
Figure E.1 Column moment-curvature relationship in the longitudinal direction for: (a) Pier S-8 and Pier S-9; (b) other piers	130
Figure E.2 Column moment-curvature relationship in the transverse direction for: (a) Pier S-8 and Pier S-9; (b) other piers	131
Figure E.3 Foundation matrix definition	132
Figure E.4 Acceleration response spectrum employed in the ESA	134
Figure H.1 Bridge deformed shape in the longitudinal direction	145
Figure H.2 Longitudinal displacement response profile for column 1 of bent 6.....	147
Figure H.3 Bridge deformed shape in the transverse direction	148
Figure H.4 Transverse displacement response profile for column 1 of bent 6.....	148
Figure H.5 Longitudinal displacement response time history at elevation of -3 ft for column 1 of bent 6.....	149
Figure H.6 Longitudinal displacement response time history at elevation of -3 ft for column 1 of bent 6.....	150
Figure H.7 Longitudinal displacement response time history at elevation of -3 ft for column 1 of bent 6.....	151

Figure H.8 Longitudinal Displacement Response Time History at Elevation of -3 ft for Column 1 of Bent 6 [Linear Columns]	152
Figure H.9 Longitudinal Displacement Response Time History at Elevation of -3 ft for Column 1 of Bent 6 [Non-linear Columns]	152
Figure H.10 Bridge natural periods and natural frequencies	153
Figure H.11 Mode Shapes for the bridge model: (a) first mode; (b) second mode; (c) third mode; (d) fourth mode; and (e) fifth mode	154
Figure H.12 Longitudinal displacement response time history at elevation of -3 ft for column 2 of bent 6 [Elastic Abutment]	157
Figure H.13 Longitudinal displacement response time history at elevation of -3 ft for column 2 of bent 6 [Roller Abutment]	158
Figure H.14 Longitudinal displacement response time history at elevation of -3 ft for column 2 of bent 6 [SDC 2010 Sand]	159
Figure H.15 Longitudinal displacement response time history at elevation of -3 ft for column 2 of bent 6 [Elastic zero stiffness Abutment]	160
Figure H.16 Foundation types available in MSBridge	161
Figure H.17 Soil springs foundation type	162
Figure H.18 A simplified single pile model.....	162
Figure H.19 Deformed shape with soil springs foundation model	163
Figure H.20 Longitudinal pile response	164
Figure H.21 Foundation matrix for each bent.....	165
Figure H.22 A simplified two-span bridge model	165
Figure H.23 Deformed shape with foundation matrix model	166
Figure H.24 Longitudinal displacement response time history at elevation of -3 ft for column 1 of bent 2 [rigid].....	166
Figure H.25 Longitudinal displacement response time history at elevation of -3 ft for column 1 of bent 2 [infinite foundation stiffnesses]	167
Figure H.26 Local coordination system for the foundation matrix (Elgamal et al. 2014).....	167
Figure H.27 Foundation matrix for each bent.....	168
Figure H.28 Deformed Shape with foundation matrix model [case 2].....	168

Figure H.29 Longitudinal displacement response time history at elevation of -3 ft for column 1 of bent 2 [rigid].....	169
Figure H.30 Longitudinal displacement response time history at elevation of -3 ft for column 1 of bent 2 [horizontal displacement is permitted].....	170
Figure H.31 Foundation matrix for each bent.....	171
Figure H.32 Deformed shape with foundation matrix mode [case 3].....	171
Figure H.33 Longitudinal displacement response time history at elevation of -3 ft for column 1 of bent 2 [rigid].....	172
Figure H.34 Longitudinal displacement response time history at elevation of -3 ft for column 1 of bent 2 [rotation is permitted].....	172
Figure H.35 Foundation matrix for each bent.....	173
Figure H.36 Deformed shape with foundation matrix [case 4]	173
Figure H.37 Longitudinal displacement response time history at elevation of -3 ft for column 1 of bent 2 [rigid].....	174
Figure H.38 Longitudinal displacement response time history at elevation of -3 ft for column 1 of bent 2 [horizontal displacement and rotation are permitted]	175
Figure H.39 Advanced options	176
Figure H.40 the general scheme of a deck hinge, which consists of 2 compression connectors (located at both deck edges) and cables. (Elgamal et al. 2014)	176
Figure H.41 Definition of deck hinges	177
Figure H.42 FE mesh of 11-span model with one deck hinge included.....	178
Figure H.43 Deformed shape with deck hinge	178
Figure H.44 Longitudinal displacement response time history at elevation of -3 ft for column 1 of bent 6 [without deck hinge]	179
Figure H.45 Longitudinal displacement response time history at elevation of -3 ft for column 1 of bent 6 [with high stiffness bearing]	179
Figure H.46 Deck hinge Force-Displacement response	180
Figure H.47 Deformed shape for time step 1.....	181
Figure H.48 Deformed shape for time step 3.....	181
Figure H.49 Deck hinge Force-Displacement response	182
Figure H.50 Deck hinge displacement response time history [1 bearing].....	183

Figure H.51 Deck hinge displacement response time history [3 bearings]	183
Figure H.52 Deck hinge displacement response time history [5 bearings]	184
Figure H.53 Deformed shape for time step 1.....	185
Figure H.54 Deformed shape for time step 200.....	185
Figure H.55 Deck hinge Force-Displacement response [Edge Element 1]	186
Figure H.56 Deck hinge Force-Displacement response [Edge Element 2]	186
Figure H.57 Deck hinge Force-Displacement response [Cable Element 1]	187
Figure H.58 Deck hinge Force-Displacement response [Cable Element 2]	187

1 INTRODUCTION

1.1 Background

In this report, seismic response studies of multi-span bridges were performed using OpenSees. The models investigated were derived from three bridge configurations, namely, the Salinas River Bridge, the Samoa Channel Bridge and the Eureka Channel Bridge. The studies were conducted using the Finite Element (FE) framework OpenSees (ver. 2.5.0), an open source software for simulating the seismic response of structural and geotechnical systems (Mazzoni et al. 2009, McKenna et al. 2010). Since 1998, OpenSees has been under development by the Pacific Earthquake Engineering Research (PEER).

To facilitate the conducted OpenSees analyses, the user interface MSBridge (Elgamal *et al.* 2014; Lu *et al.* 2015) was further developed and employed. MSBridge is a PC-based graphical pre- and post-processor (user-interface) for conducting nonlinear FE studies of multi-span bridge systems. The analysis options available in MSBridge include i) Pushover analysis; ii) Mode shape analysis; iii) Single and multiple three-dimensional (3D) seismic Time History Analyses (THA); iv) Equivalent Static Analysis (ESA) (Caltrans 2013); and v) Pushover analysis of soil movements (imposed displacement profile). For further information about MSBridge, along with the newly added capabilities, please see APPENDIX A.

Nonlinear Time History Analysis (THA) was conducted for 14 input motions (ranging from 0.32g-0.71g for peak acceleration) provided by Caltrans. Further details regarding these motions are provided in APPENDIX B. The THA procedures and results are presented in this report. Results of the corresponding Equivalent Static Analysis (ESA) procedure are presented and compared to the THA average displacement demand outcome.

1.2 Report Scope and Layout

A preliminary study was conducted first to compare ESA and THA results for an OSB (Ordinary Standard Bridge) model. Focus was placed on response in the transverse direction. The THA effort employed a set of 14 input ground motions provided by Caltrans (Further details regarding these motions are provided in APPENDIX B). A series of models of increasing complexity were studied in an attempt to separate influence of column nonlinear response, foundation p-y springs, and the added resistance provided at the bridge-end bents and abutments. A single bent model was studied first, followed by models of the entire bridge (to include the abutment end-effects). On this basis, it was noted that: i) Linear models of the bridge bent resulted in essentially identical response (ESA and THA); ii) Nonlinearity of the columns and base soil springs (p-y and t-z) caused a difference of about 25%; and iii) When the abutment effects were included, the difference actually decreased to somewhere in the neighborhood of 10%. Details of this preliminary study are included in APPENDIX C.

Overall, this report is composed of five chapters. Chapter 2 presents the analysis procedures and results for the Salinas River Bridge idealization (with model properties included in APPENDIX D). The analysis procedures and results for the Samoa Channel Bridge and the Eureka Channel

Bridge idealizations are presented in Chapters 3 and 4, respectively. Finally, a brief assessment of outcomes and conclusions is included in Chapter 5.

In the conducted nonlinear analyses for the Samoa Channel Bridge and the Eureka Channel Bridge, the pier columns were modeled using nonlinear Fiber section and the force-based beam-column element (`forceBeamcolumn`) with the distributed plasticity integration method. Details of the modeling techniques for the Samoa Channel Bridge and the Eureka Channel Bridge are described in APPENDIX E and APPENDIX F, respectively. Furthermore, APPENDIX G lists the OpenSees Tcl code snippets of the column nonlinear Fiber sections for the Samoa Channel Bridge and the Eureka Channel Bridge (as an example for modeling columns of arbitrary cross section and reinforcement steel layout).

In the initial stage of this research, an effort was made to illustrate and verify the MSBridge salient features and capabilities. Details of the MSBridge feature-verification effort are presented and discussed in APPENDIX H. In the conducted verification analyses, a number of idealized bridge configurations were employed. Each of these configurations allowed for simple and systematic assessment of the particular response feature being verified.

2 THE SALINAS RIVER BRIDGE

2.1 Bridge Description and Geometric Configuration

The January 1997 flooding along the Salinas River resulted in major damage to the North Bound Salinas River Bridge which was built in 1938 (Caltrans 2005). A new Salinas River Bridge (hereinafter referred to as “Salinas Bridge”, see Figure 2.1 for the general plan) was designed as the replacement structure (Caltrans 2005).

Salinas Bridge is a reinforced concrete box-girder bridge with 11 spans. According to Caltrans (2005), the following characteristics are provided:

- Each span is 140 ft long, and the substructure consists of multiple two-column bents.
- The soil profile of the riverbed consists of very loose sand for the top 20 ft followed by 30 ft of loose sand and 150 ft of dense sand thereafter.
- Ground water was encountered near the surface of the streambed, and there is a moderate to high potential for liquefaction.
- The site is located approximately 4 miles from the King City-Reliz Fault with a maximum credible earthquake of moment magnitude 7.
- Peak bedrock acceleration is estimated at 0.5g.

Figure 2.2 shows a sectional view of the bridge deck along with the pile shaft reinforcement details. The four-cell box girder is 42.5 ft wide by 5.75 ft deep; and the deck and soffit slabs are 8 in and 6 in thick, respectively.

2.2 OpenSees Bridge FE Model and Mode Shapes

Earlier, Salinas Bridge was studied by Caltrans (2005) using wFrame, a two-dimensional (2D) program for pushover analysis of bridge bents and frames (Mahan 2005). The analysis procedure and results were reported in Caltrans (2005). The FE model employed in this study (Figure 2.3) was created in MSBridge based on the wFrame model described in the above-mentioned Caltrans report (for purposes of comparison). Thus, uniform column height (48 ft) and span length (140 ft) were employed in this 3D model (Figure 2.3). Details of the employed modeling techniques and associated model properties are included in APPENDIX D. Comparison of MSBridge and wFrame pushover analysis for the Salinas Bridge model is presented in Section 2.3.

The force-based beam-column element (`beamWithHinges`) based on the plastic hinge integration method (Scott and Fenves 2006; Scott and Ryan 2013) with an idealized bi-linear moment-curvature relationship was used to model the columns and the pile shafts (Caltrans 2005). The deck and the bentcap were considered to be linear elastic.

An elastic abutment model, where the transverse abutment resistance was taken as a fraction of the longitudinal resistance provided by Caltrans (2005) was assumed for simplicity (Aviram *et al.* 2008a, 2008b). According to the Caltrans (2005) model, a pin connection was implemented at the base of the abutment.

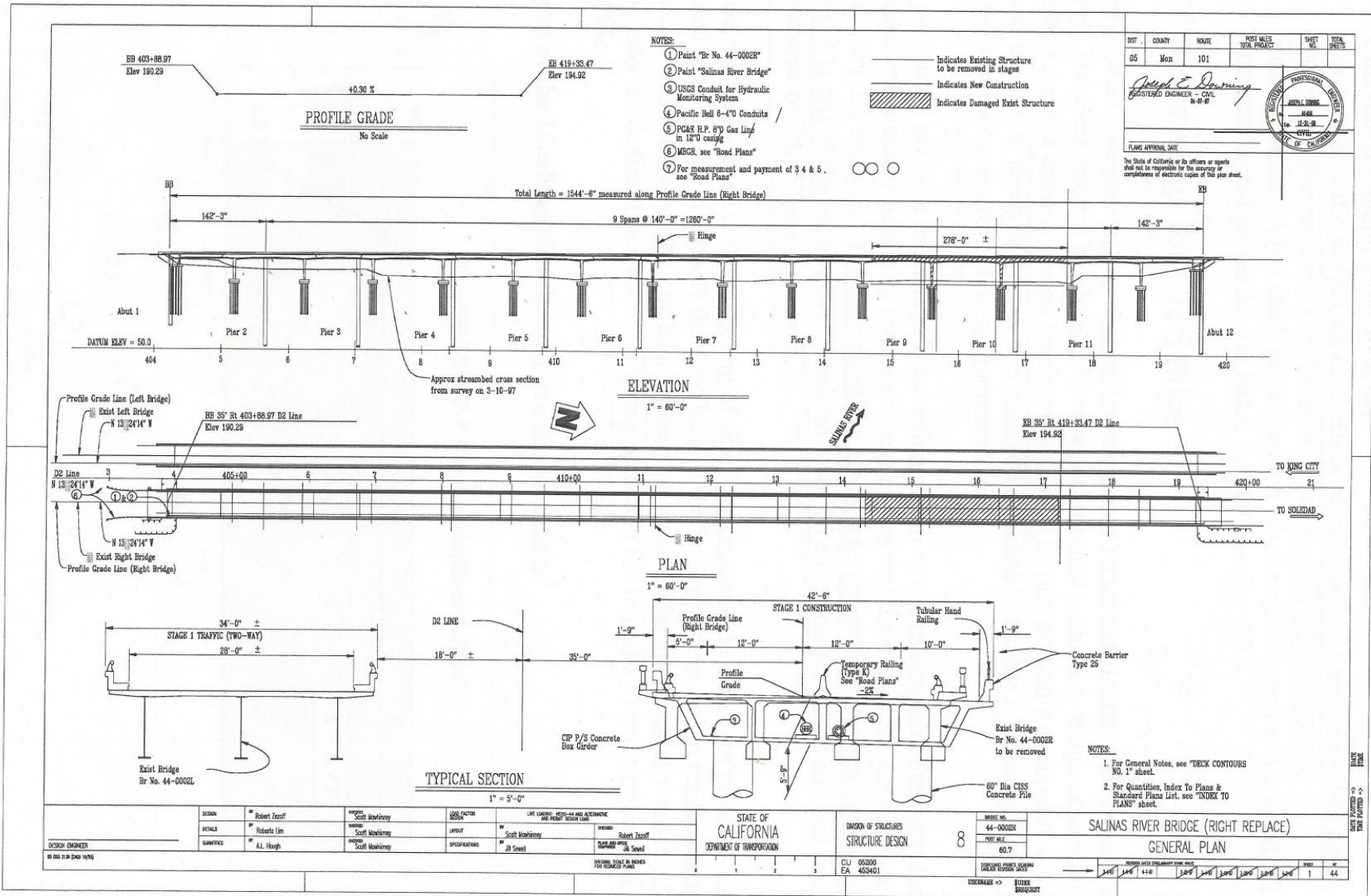
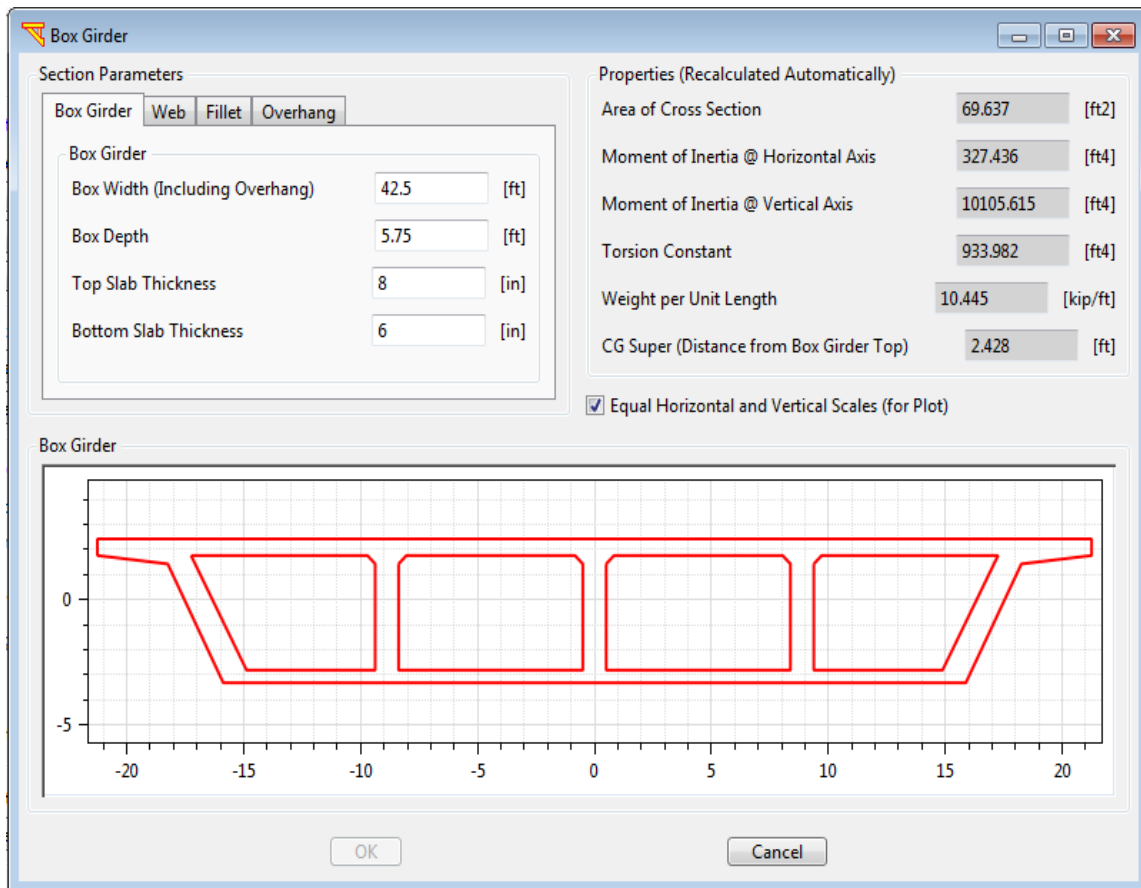
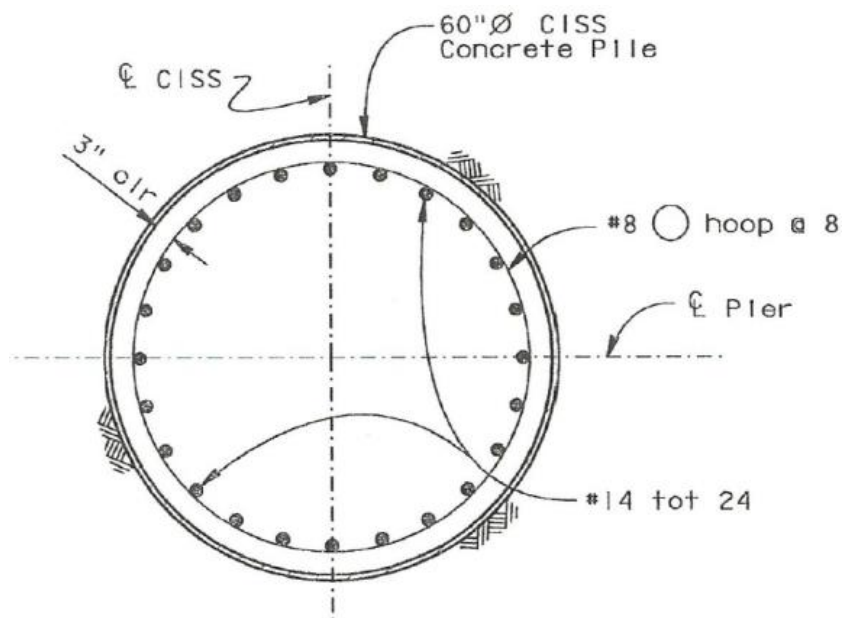


Figure 2.1 General layout of Salinas Bridge (Caltrans 2016)



a)



b)

Figure 2.2 Sectional details of Salinas Bridge: (a) deck; (b) Type I shaft cross section

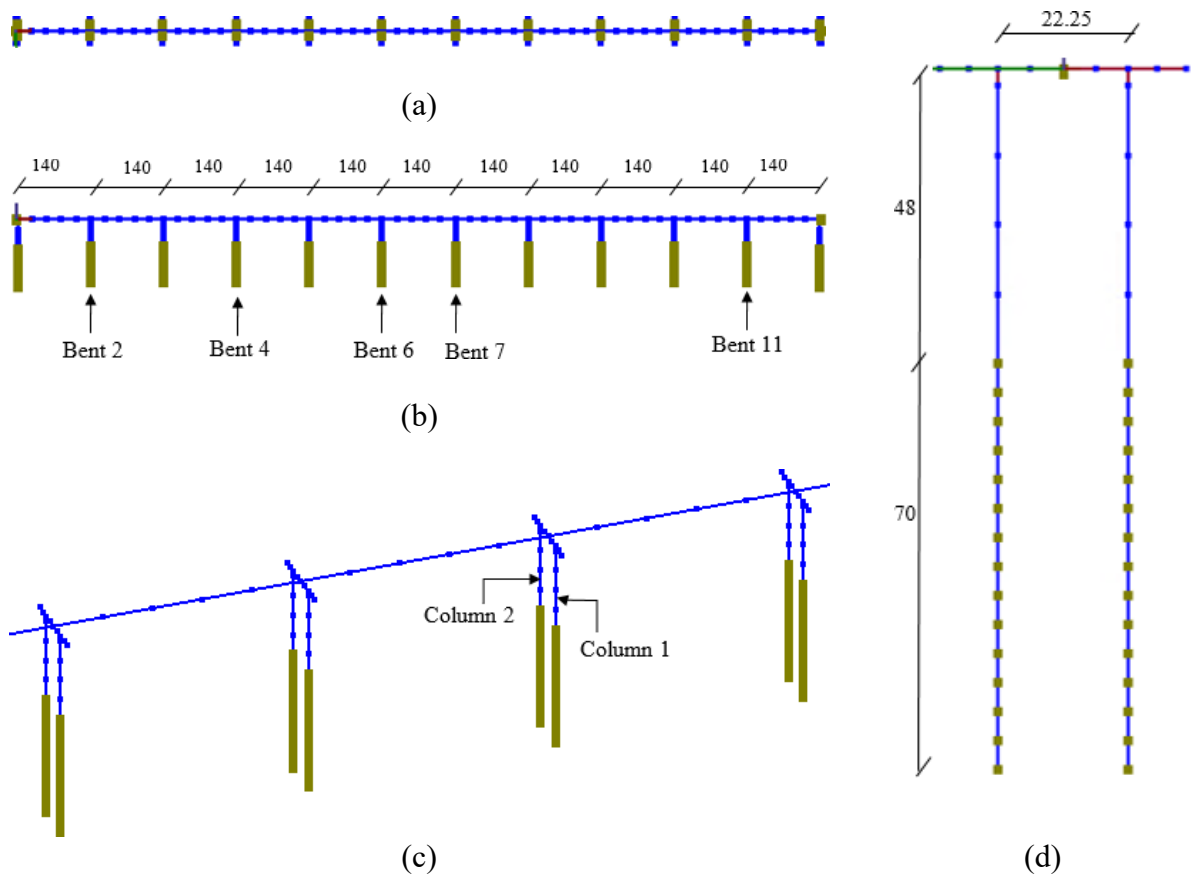


Figure 2.3 Salinas Bridge FE model created in MSBridge (dimensions in ft): (a) plan view; (b) elevation view; (c) close-up of 3D view; (d) side view of a bent (typical)

The foundation response was modeled by the p-y and t-z soil springs defined by Caltrans (2005) as shown in APPENDIX D. In this p-y springs foundation representation, lateral soil resistance is provided as the p-y springs interact with the pile shafts (Caltrans 2005). Similarly, vertical soil resistance is provided by the t-z and Q-z springs.

Using this model (Figure 2.3), mode shape analysis, the first five mode shapes (Table 2.1) are shown in Figure 2.4. ESA, and seismic excitation results are shown in the following sections.

Table 2.1. Natural Periods and Frequencies for Salinas Bridge

Mode	Natural period (sec)	Natural Frequency (Hz)
1*	1.89	0.53
2	1.72	0.58
3**	1.62	0.62
4	1.47	0.68
5	1.08	0.92

* Fundamental mode in the Transverse direction

** Fundamental mode in the Longitudinal direction

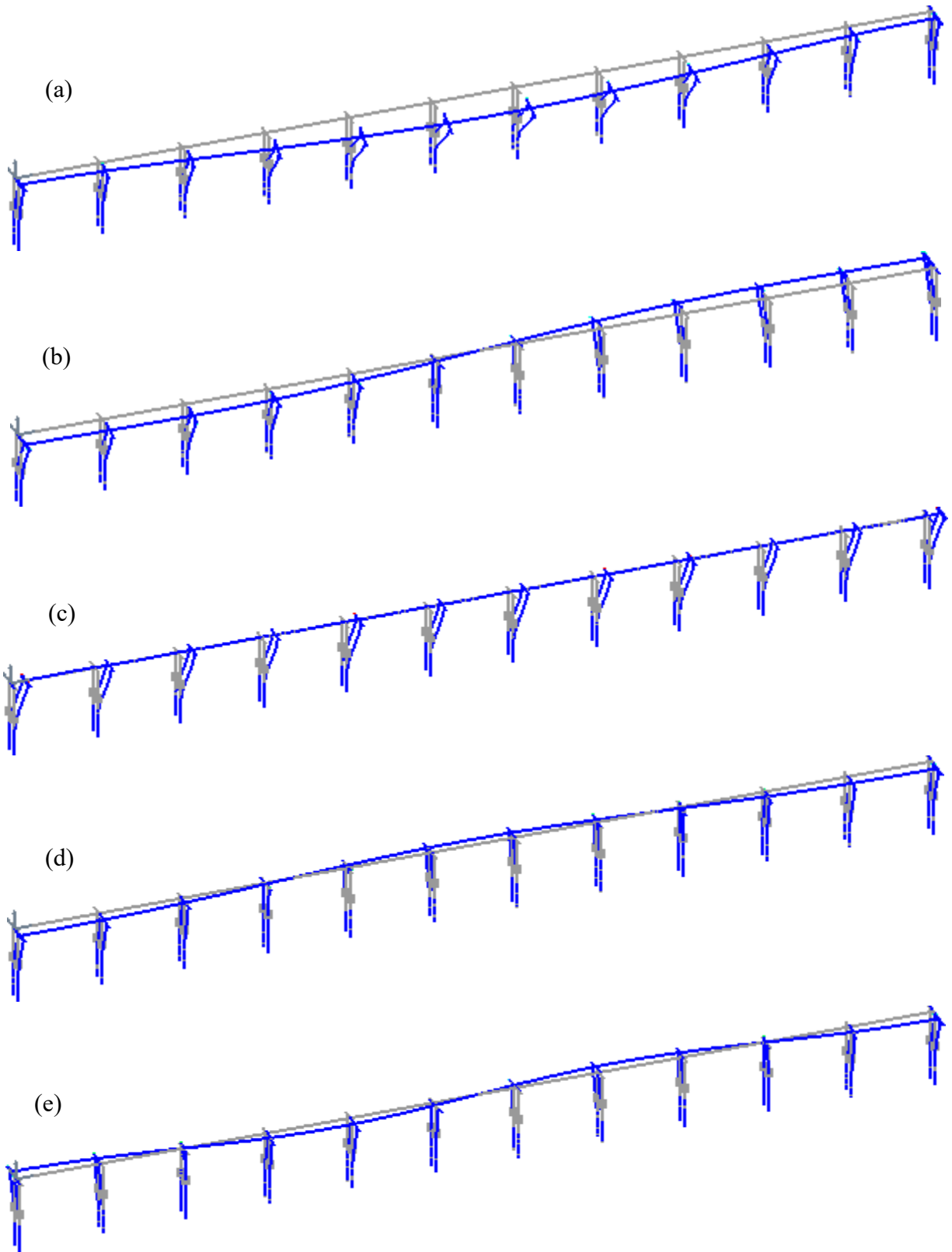


Figure 2.4 Salinas Bridge mode shapes: (a) first mode; (b) second mode; (c) third mode; (d) fourth mode; and (e) fifth mode

2.3 Equivalent Static Analysis (ESA)

Caltrans (2005) presents the results of an ESA of the Salinas Bridge using wFrame (Mahan 2005). A comparison with this study was conducted first using MSBridge with the ARS (Figure 2.5) employed by Caltrans (2005). To conduct ESA in MSBridge, please refer to the MSBridge user manual (Elgamal et al. 2014).

In the longitudinal ESA, the entire bridge system (Figure 2.3) was engaged. The bridge system was pushed in the longitudinal direction until plastic moment was reached (Figure D.1). The pushover load was applied at the bridge center (i.e., the span between Bents 6 and 7 (Figure 2.3)).

In the transverse ESA, an individual bent (Bent 4, as a typical representative) was employed. The bent was pushed along bridge transverse direction (Figure 2.3) until plastic moment was reached (Figure D.1). The pushover load was applied at the bentcap center (i.e., the bentcap center between the 2 columns (Figure 2.3)).

Note that in this comparison study, rigid bentcaps were assumed in MSBridge for longitudinal ESA in order to do comparison with wFrame (since wFrame is a 2D program while a full 3D model was employed in MSBridge). However, the actual bentcap properties (Table D.2) were used in Transverse ESA for both MSBridge and wFrame.

The results are listed in Table 2.2. In general, good agreement (Table 2.2) was noted in the MSBridge and wFrame results in the longitudinal and transverse ESA Salinas Bridge study. The relative differences in initial stiffness between MSBridge and wFrame were 1%, and 2.6% in the longitudinal and transverse directions, respectively.

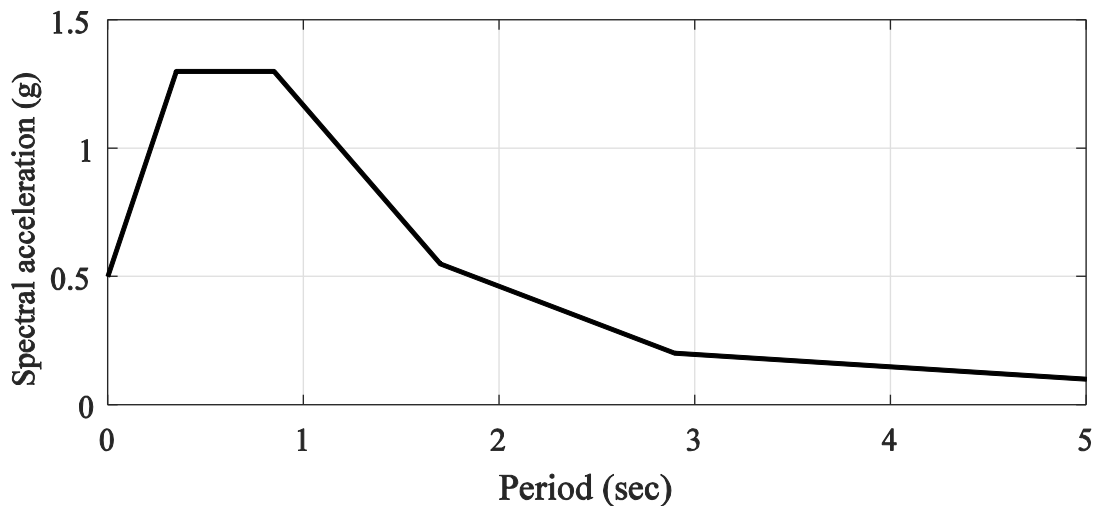


Figure 2.5 Acceleration response spectrum (ARS) curve employed in Caltrans (2005)

Table 2.2. Comparison of MSBridge and wFrame Results for ESA of Salinas Bridge

Program	Longitudinal ESA			Transverse ESA		
	MSBride	wFrame	Difference	MSBridge	wFrame	Difference
Yield Displacement (in)	5.2	4.87	6.8%	9.4	9.76	3.4%
Pushover Load (kip)	4222	3961.5	6.6%	376	382.4	1.7%
Initial Stiffness (kip/in)	805	813.5	1.0%	40	39	2.6%
Period (seconds)	1.63	1.62	0.6%	2.21	2.24	1.3%
Displacement Demand (in)	14.8	15.37	3.7%	18.8	18.6	1.1%

For the purpose of the current study, ESA was conducted in the longitudinal and transverse directions. Figure 2.6 shows the acceleration response spectrum (ARS) employed in the ESA (derived by Caltrans from the provided corresponding set of input seismic motions).

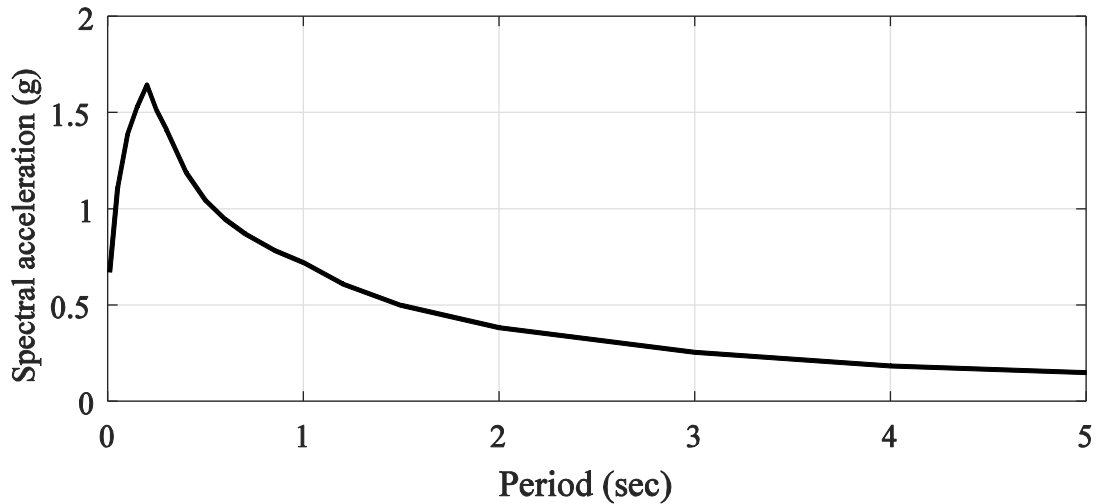


Figure 2.6 ARS curve employed in the ESA

2.3.1 ESA in the Longitudinal Direction

Table 2.3 lists the parameters related to the longitudinal ESA. The pushover load at initial yielding (i.e., plastic moment was reached) was about 24% of the tributary dead load (Table 2.3). Table 2.4 shows the longitudinal ESA result for Salinas Bridge. The displacement demand is 12.5 in for the longitudinal ESA (Table 2.4).

2.3.2 ESA in the Transverse Direction

Table 2.5 (also shown in Table 2.2) lists the parameters related to the transverse ESA (Bent 4, typical). The pushover load at initial yielding (i.e., plastic moment was reached) was about 20% of the tributary dead load (Table 2.5). Table 2.6 shows the transverse ESA result for Salinas Bridge. The displacement demand is 16.8 in for the transverse ESA (Table 2.6).

Table 2.3. Longitudinal ESA Parameters for Salinas Bridge

Parameter	Value
Tributary dead load (kip)	20,850.8
Tributary mass (kip-sec ² /in)	54.0
Pushover load at initial yielding (kip)	5004.19
Yield displacement (in)	6.5
Initial stiffness (kip/in)	768.0
Period (sec)	1.7

Table 2.4. Longitudinal ESA Result for Salinas Bridge

Parameter	Longitudinal Direction
Displacement Demand (in)	12.5

Table 2.5. Transverse ESA Parameters for Bent 4

Parameter	Value
Tributary dead load (kip)	1912.4
Tributary mass (kip-sec ² /in)	4.9
Pushover load at initial yielding (kip)	376
Yield displacement (in)	9.4
Initial stiffness (kip/in)	40
Period (sec)	2.21

Table 2.6. Transverse ESA Result for Salinas Bridge

Pier # (see Figure 2.3a)	Displacement Demand in Transverse Direction (in)
Bent 4 (typical bent)	16.8

2.4 Nonlinear Time History Analysis

Nonlinear THA was conducted for the 14 input motions provided by Caltrans (APPENDIX B). Uniform base excitation was studied using each of these input ground motions. In future studies, a more representative investigation can be conducted with input ground motion varying along the depth of the foundation shafts (and possibly along the lateral extent of the bridge configuration).

Rayleigh damping was used with a 5% damping ratio (defined at the periods of 1.6 and 2.1 seconds) in the nonlinear THA. For the time integration scheme, the Newmark average acceleration method ($\gamma = 0.5$ and $\beta = 0.25$) was employed.

Variable time-stepping scheme (`VariableTransient`) was used in the conducted Nonlinear THA. The starting value for each step was 0.005 second (the time step of the input motions), and the minimum time step was 5×10^{-5} second (upon splitting of time step when needed).

2.4.1 Maximum Displacement and Acceleration

Table 2.7 lists Salinas Bridge deck maximum displacement for 28 simulations from the nonlinear THA (the 14 motions were employed as both bridge longitudinal and transverse input). Among the simulations with longitudinal component only (Simulations 1-14), Simulation 9 (motion ROCKS1P2) gave the least maximum displacement (8.2 in) while Simulation 4 (motion ROCKS1N4) gave the largest maximum displacement (14.0 in). The maximum displacement of Table 2.7 are also presented in graphical format against Peak Ground Acceleration (PGA) in Figure 2.7 and Figure 2.8.

The Salinas Bridge columns generally deformed more in the transverse direction, compared to the longitudinal direction, when subjected to the same input excitation (Table 2.7). This general trend was also noted in the ESA displacement demand results (Table 2.4 and Table 2.6).

Table 2.8 list Salinas Bridge deck maximum acceleration for the 28 simulations. Among the simulations with longitudinal component only (Simulations 1-14), Simulations 2 (motion ROCKS1N2) and 9 (motion ROCKS1P2) gave the least maximum acceleration (0.3g) while Simulations 4 (motion ROCKS1N4) and 11 (motion ROCKS1P4) gave the largest maximum acceleration (0.45g). The maximum acceleration of Table 2.8 are also presented in graphical format against PGA in Figure 2.9 and Figure 2.10.

Table 2.7. Salinas Bridge Deck Maximum Displacement

Simulation	Longitudinal Input	Transverse Input	Longitudinal Displacement (in)	Transverse Displacement (in)
1	ROCKS1N1 (0.7g)	-	12.6	0
2	ROCKS1N2 (0.38g)	-	8.3	0
3	ROCKS1N3 (0.32g)	-	9.4	0
4	ROCKS1N4 (0.34g)	-	14.0	0
5	ROCKS1N5 (0.53g)	-	10.5	0
6	ROCKS1N6 (0.42g)	-	9.8	0
7	ROCKS1N7 (0.36g)	-	11.8	0
8	ROCKS1P1 (0.71g)	-	13.1	0
9	ROCKS1P2 (0.44g)	-	8.2	0
10	ROCKS1P3 (0.48g)	-	11.0	0
11	ROCKS1P4 (0.32g)	-	13.8	0
12	ROCKS1P5 (0.67g)	-	9.4	0
13	ROCKS1P6 (0.41g)	-	9.7	0
14	ROCKS1P7 (0.4g)	-	12.7	0
Average			11.0	
15	-	ROCKS1N1 (0.7g)	0	14.0
16	-	ROCKS1N2 (0.38g)	0	13.8
17	-	ROCKS1N3 (0.32g)	0	10.4
18	-	ROCKS1N4 (0.34g)	0	15.8
19	-	ROCKS1N5 (0.53g)	0	16.8
20	-	ROCKS1N6 (0.42g)	0	14.0
21	-	ROCKS1N7 (0.36g)	0	14.1
22	-	ROCKS1P1 (0.71g)	0	15.4
23	-	ROCKS1P2 (0.44g)	0	14.2
24	-	ROCKS1P3 (0.48g)	0	17.0
25	-	ROCKS1P4 (0.32g)	0	14.6
26	-	ROCKS1P5 (0.67g)	0	21.0
27	-	ROCKS1P6 (0.41g)	0	14.0
28	-	ROCKS1P7 (0.4g)	0	12.7
Average				14.8

Notes:

- ESA longitudinal displacement demand is 12.5 in, corresponding to a difference of 11.8% (compared to the average THA maximum displacement of 11 in)
- ESA transverse displacement demand is 16.8 in, corresponding to a difference of 11.7% (compared to the average THA maximum displacement of 14.8 in)

Table 2.8. Salinas Bridge Deck Maximum Acceleration

Simulation	Longitudinal Input	Transverse Input	Longitudinal Acceleration (g)	Transverse Acceleration (g)
1	ROCKS1N1 (0.7g)	-	0.42	0
2	ROCKS1N2 (0.38g)	-	0.30	0
3	ROCKS1N3 (0.32g)	-	0.33	0
4	ROCKS1N4 (0.34g)	-	0.45	0
5	ROCKS1N5 (0.53g)	-	0.37	0
6	ROCKS1N6 (0.42g)	-	0.34	0
7	ROCKS1N7 (0.36g)	-	0.41	0
8	ROCKS1P1 (0.71g)	-	0.43	0
9	ROCKS1P2 (0.44g)	-	0.30	0
10	ROCKS1P3 (0.48g)	-	0.38	0
11	ROCKS1P4 (0.32g)	-	0.45	0
12	ROCKS1P5 (0.67g)	-	0.34	0
13	ROCKS1P6 (0.41g)	-	0.34	0
14	ROCKS1P7 (0.4g)	-	0.42	0
15	-	ROCKS1N1 (0.7g)	0	0.35
16	-	ROCKS1N2 (0.38g)	0	0.31
17	-	ROCKS1N3 (0.32g)	0	0.34
18	-	ROCKS1N4 (0.34g)	0	0.36
19	-	ROCKS1N5 (0.53g)	0	0.38
20	-	ROCKS1N6 (0.42g)	0	0.36
21	-	ROCKS1N7 (0.36g)	0	0.42
22	-	ROCKS1P1 (0.71g)	0	0.37
23	-	ROCKS1P2 (0.44g)	0	0.31
24	-	ROCKS1P3 (0.48g)	0	0.38
25	-	ROCKS1P4 (0.32g)	0	0.36
26	-	ROCKS1P5 (0.67g)	0	0.41
27	-	ROCKS1P6 (0.41g)	0	0.36
28	-	ROCKS1P7 (0.4g)	0	0.37

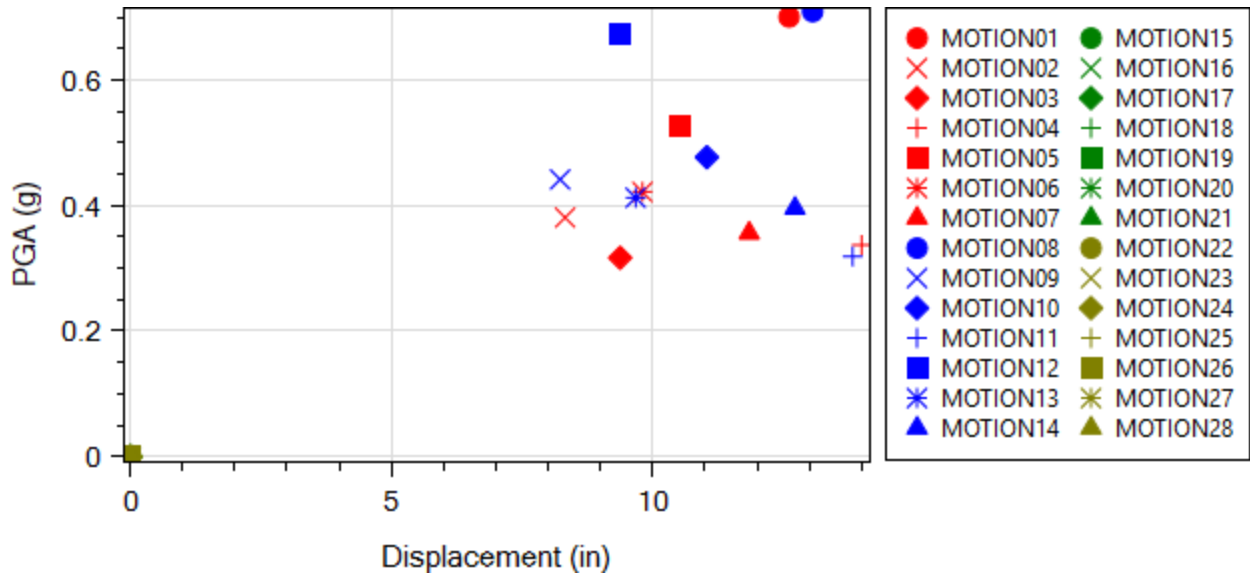


Figure 2.7 Bridge deck maximum longitudinal displacement

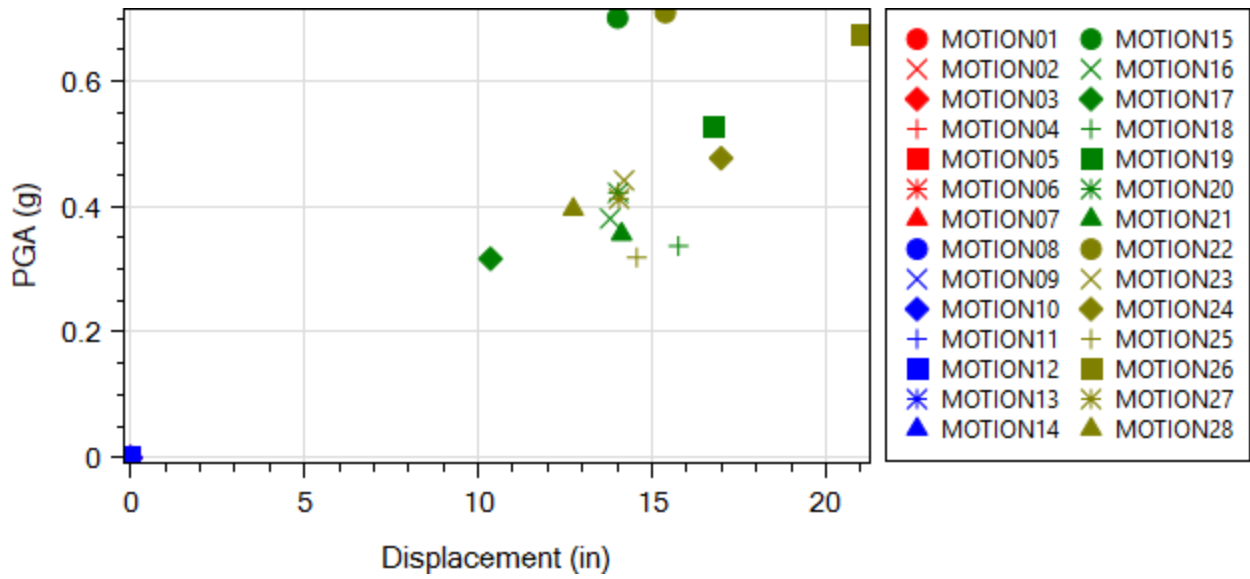


Figure 2.8 Bridge deck maximum transverse displacement

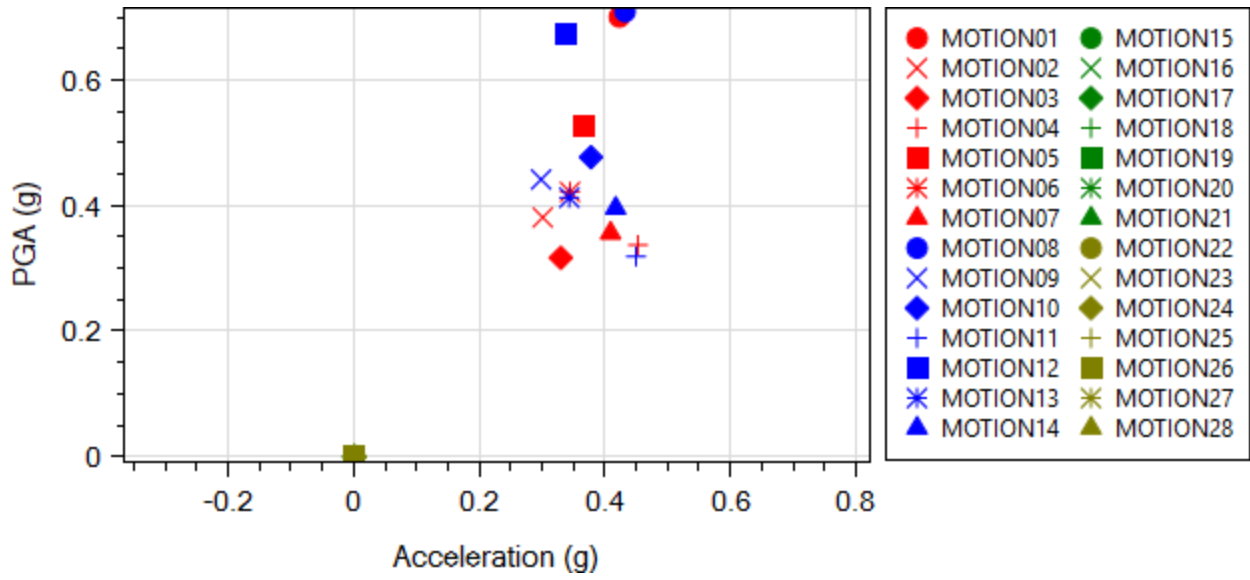


Figure 2.9 Bridge deck maximum longitudinal acceleration

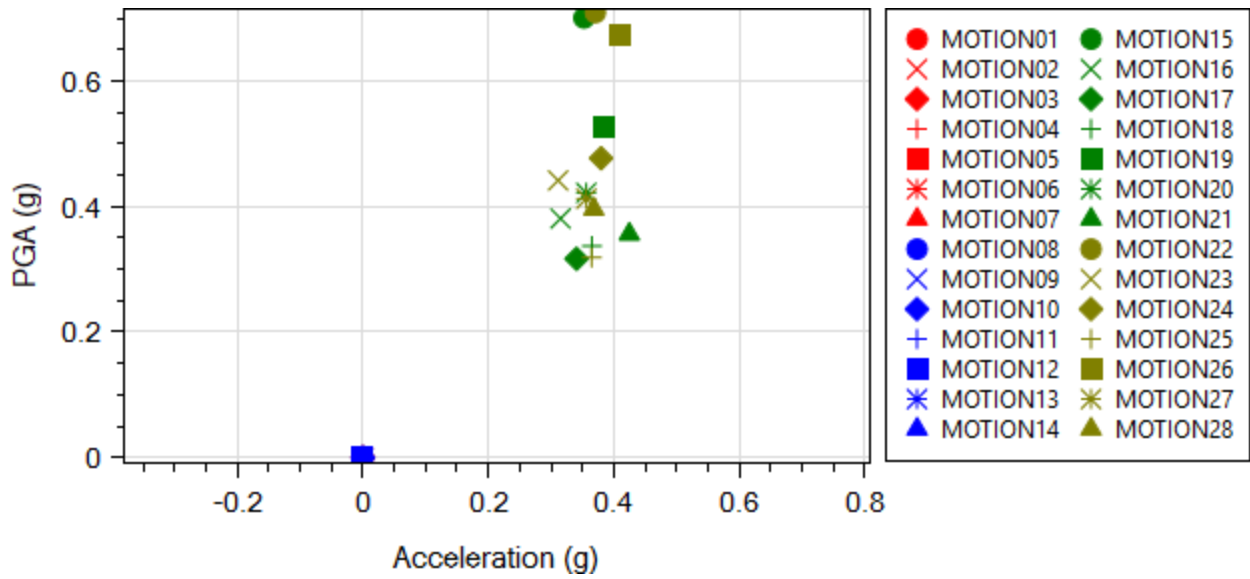


Figure 2.10 Bridge deck maximum transverse acceleration

2.4.2 Response Time Histories

In this section, response time histories for Column 1 of Bent 7 (i.e., the middle bent, see Figure 2.3) for 2 representative simulations (Simulations 1 and 4) are presented (Longitudinal seismic excitation).

1) Simulation 1 (Longitudinal Input ROCKS1N1)

For Simulation 1, the deck maximum displacement is 12.6 in (Table 2.7). Figure 2.11 displays the column longitudinal response time histories. The input motion ROCKS1N1 is shown in Figure 2.11d for reference.

Figure 2.12 displays the moment-curvature response at the column top. A maximum bending moment of 6,100 kip-ft was reached as expected upon yielding (Figure 2.12). A level of yielding may be seen in the column response (Figure 2.11c). The deformed mesh when the deck maximum displacement was reached (i.e., 12.6 in as shown in Table 2.7) is shown in Figure 2.13.

2) Simulation 4 (Longitudinal Input ROCKS1N4)

The deck maximum displacement is 14.0 in for Simulation 4 (Table 2.7). The column longitudinal response time histories are displayed in Figure 2.14. Figure 2.15 shows the moment-curvature response at the column top. A maximum bending moment of 6,100 kip-ft was also reached as expected upon yielding (Figure 2.14). The deformed mesh when the deck maximum displacement was reached (i.e., 14.0 in as shown in Table 2.7) is shown in Figure 2.16.

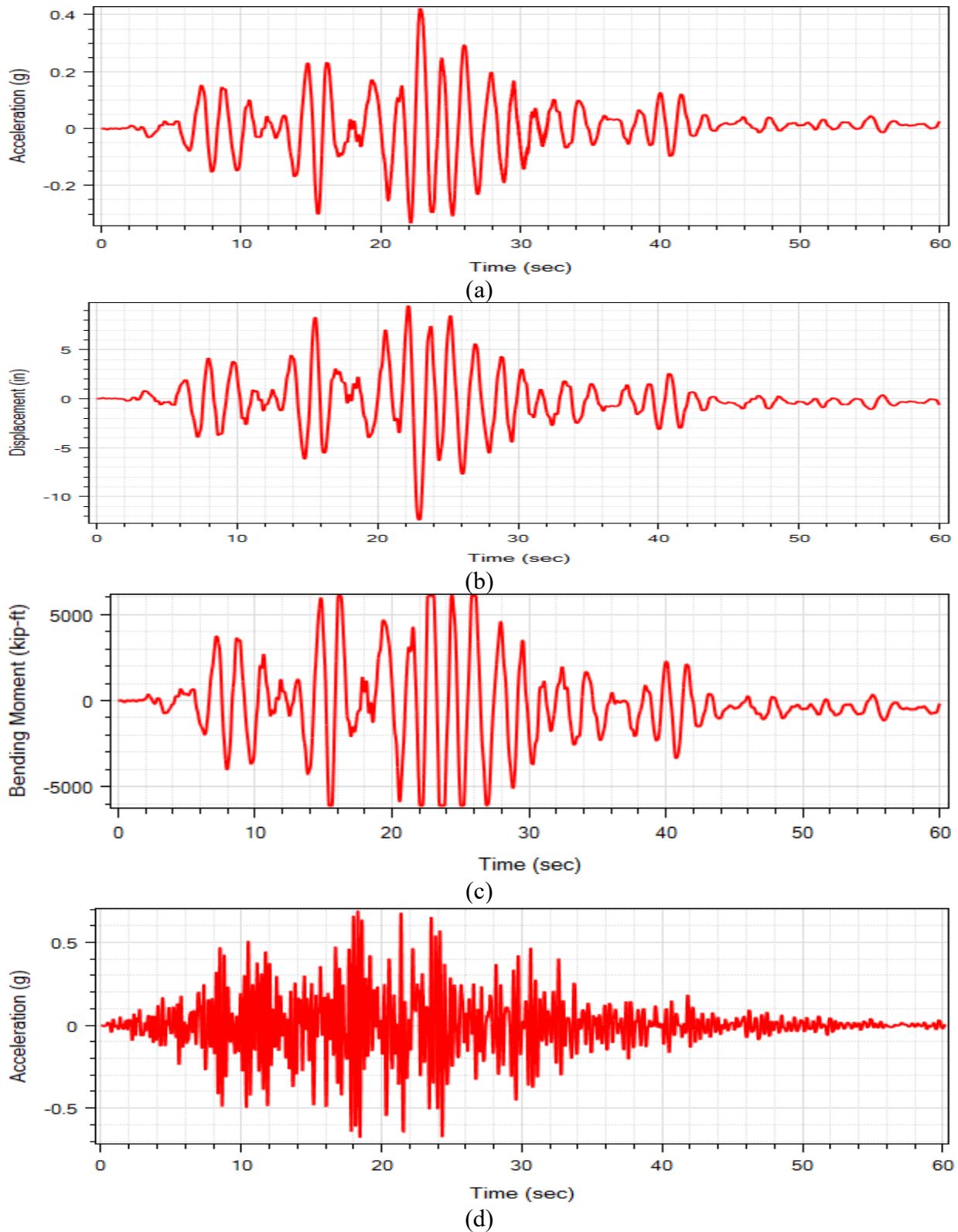


Figure 2.11 Column top longitudinal response time histories of Column 1 of Bent 7 for Simulation 1: a) acceleration; b) displacement; c) bending moment; and (d) base excitation ROCKS1N1

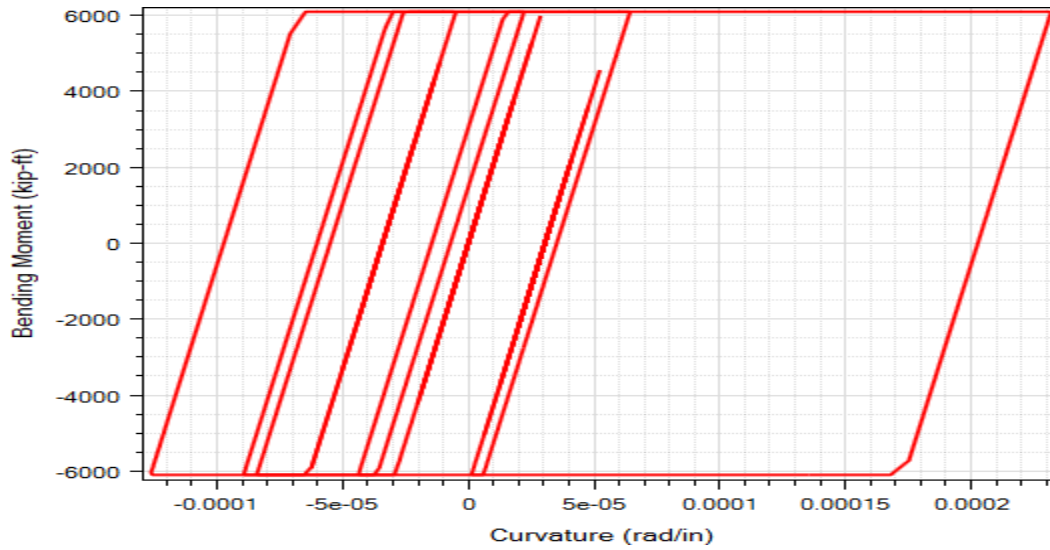


Figure 2.12 Column top longitudinal moment-curvature response of Column 1 of Bent 7 for Simulation 1

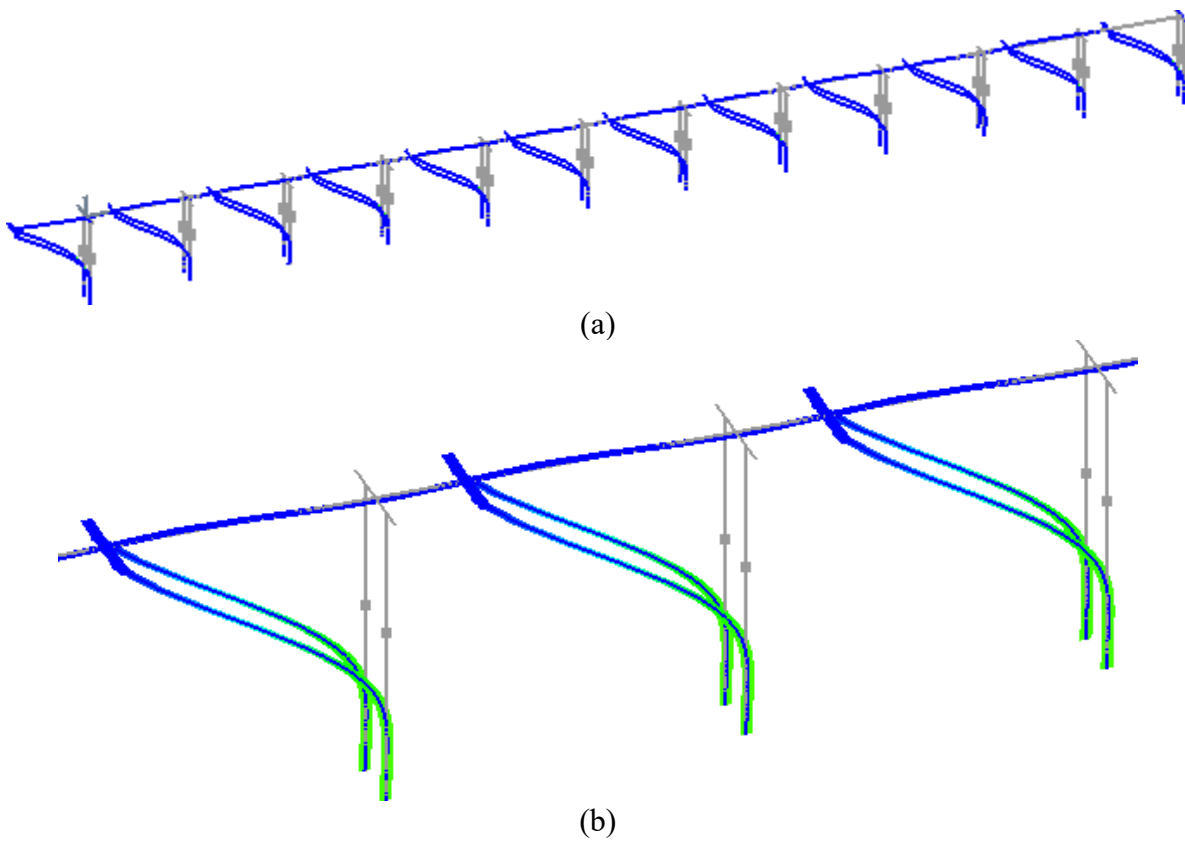
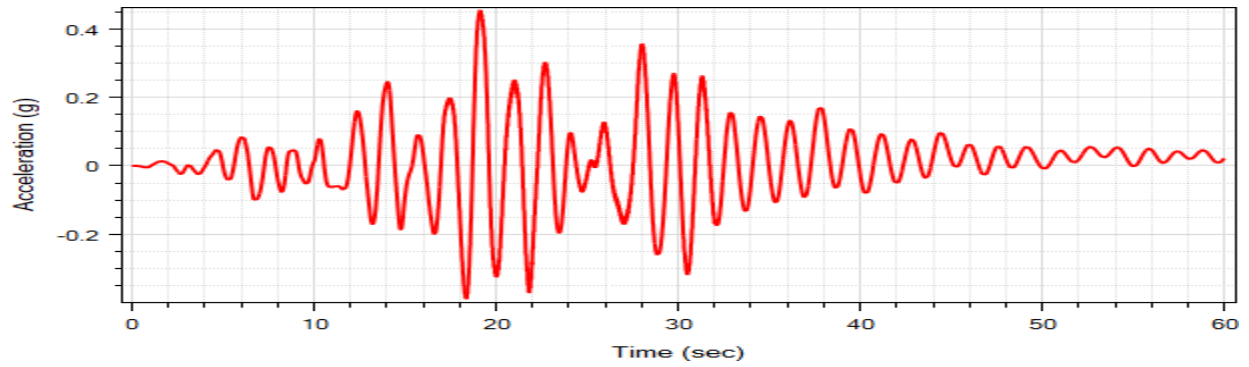
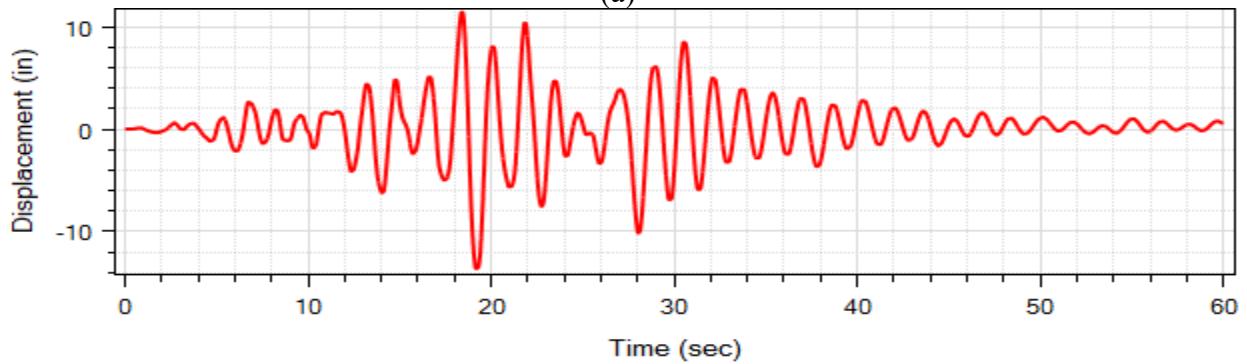


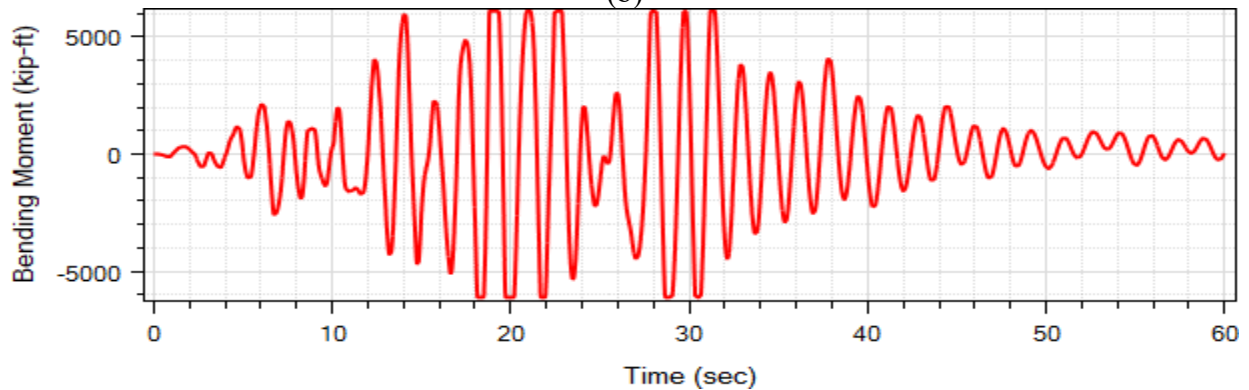
Figure 2.13 Deformed mesh (factor of 100) for Simulation 1 at the maximum displacement step (grey lines represent undeformed mesh): (a) entire bridge; (b) close-up of Bents 6, 7, and 8 (from left to right)



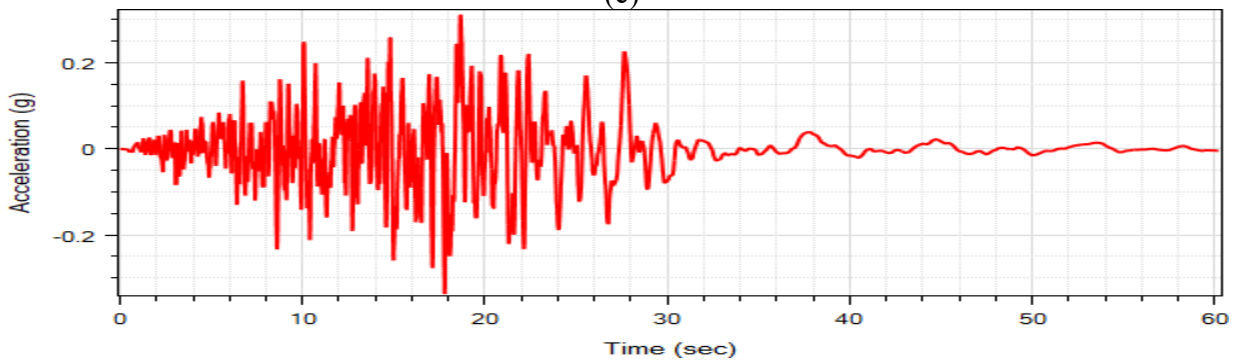
(a)



(b)



(c)



(d)

Figure 2.14 Column top longitudinal response time histories of Column 1 of Bent 7 for Simulation 4: (a) acceleration; (b) displacement; (c) bending moment; (d) base excitation ROCKS1N4

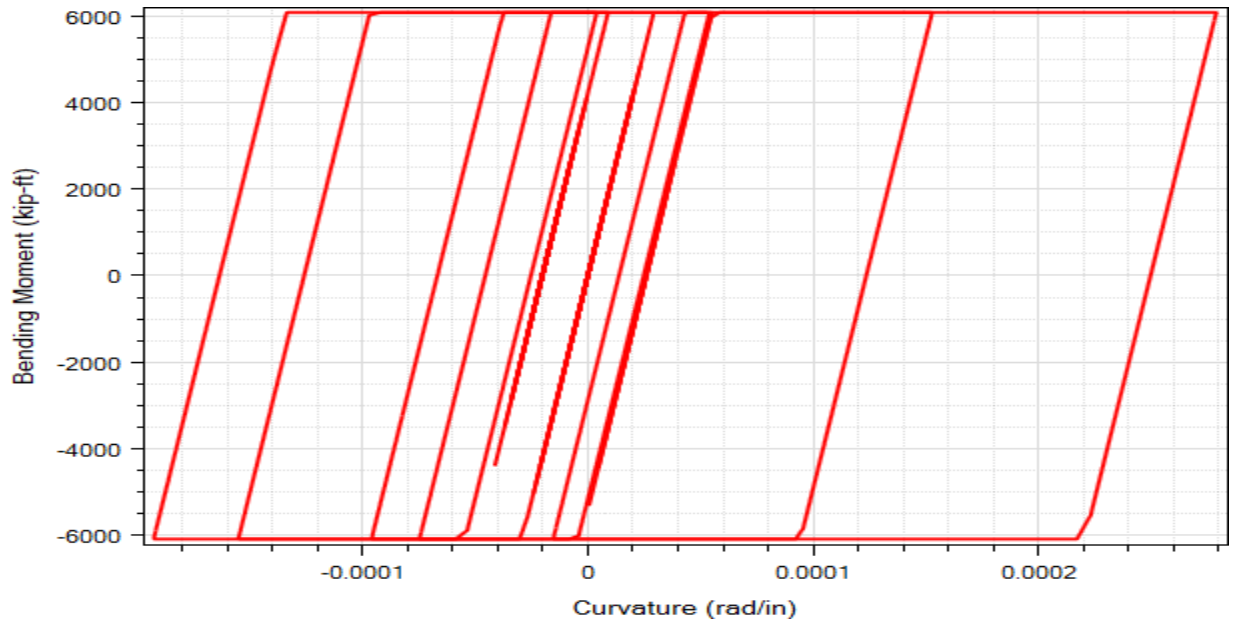


Figure 2.15 Column top longitudinal moment-curvature response of Column 1 of Bent 7 for Simulation 4

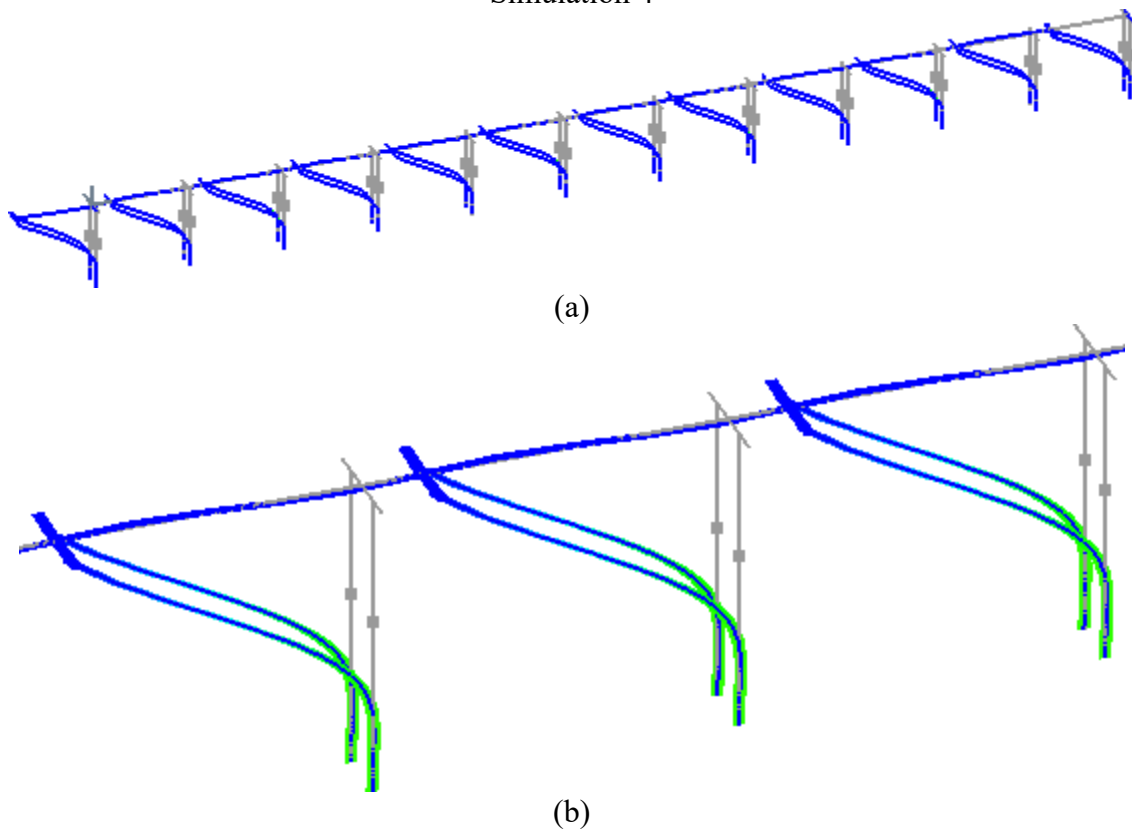


Figure 2.16 Deformed mesh (factor of 100) for Simulation 4 at the step of the maximum displacement (14 in @ 19.2 seconds) (grey lines represent undeformed mesh): (a) entire bridge; (b) close-up of Bents 6, 7, and 8 (from left to right)

2.5 Summary

Salinas Bridge was modeled in OpenSees. A recently developed user interface MSBridge was employed for pre- and post-processing in the conducted OpenSees analysis. Nonlinear THA was conducted for the 14 input motions provided by Caltrans. The average THA maximum displacement is 11 inches in the bridge longitudinal direction and 14.8 inches in the transverse direction. ESA was also conducted for Salinas Bridge using MSBridge.

2.6 Conclusions

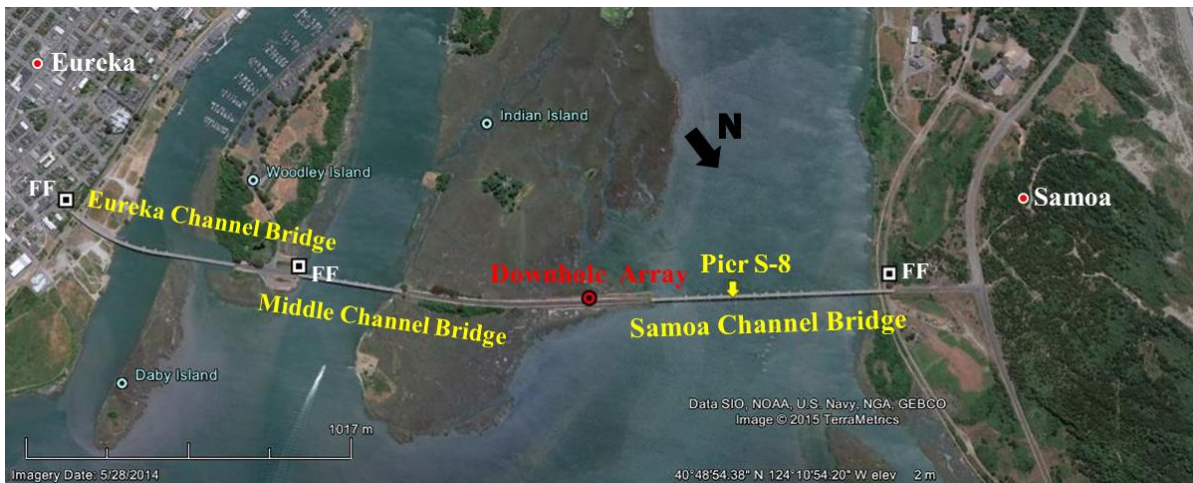
1. For the employed ESA spectrum, column displacement demand was 12.5 inches in the longitudinal direction and 16.8 inches in the transverse direction.
2. For the investigated set of ground motions in the OpenSees analysis:
 - 2.1 In the longitudinal direction, about 36% of the shaking events resulted in column displacement demand that exceeded that of the ESA. This demand reached a maximum of 12% in excess of that from the corresponding ESA.
 - 2.2 In the transverse direction, about 14% of the shaking events resulted in column displacement demand that exceeded that of the ESA. This demand reached a maximum of 25% in excess of that from the corresponding ESA.

3 THE SAMOA CHANNEL BRIDGE

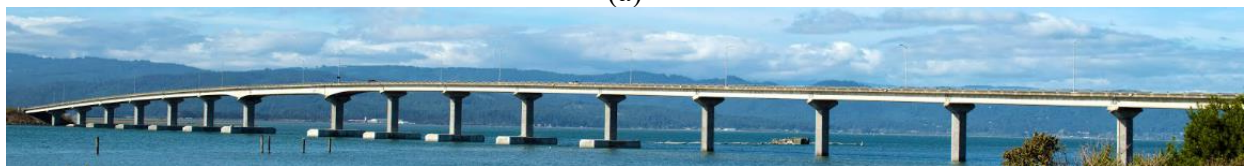
3.1 Bridge Description

The 20-span Samoa Channel Bridge (hereinafter referred to as “Samoa Bridge”, Figure 3.1) near Eureka in northern California is a 2506 ft (764 m) long and 34 ft (10.4 m) wide structure connecting Samoa Peninsula and Indian Island (Figure 3.2). The bridge was designed in 1968, constructed in 1971 and underwent a seismic retrofit in 2002 (Caltrans 1968; Caltrans 2002b) (Shamsabadi and Taciroglu 2013). The bridge superstructure, which consists of cast-in place reinforced concrete deck and four pre-cast pre-stressed concrete I-girders, is supported by 19 single hexagonal concrete pier bents on pile group foundations. For convenience, the piers (including abutments) are numbered #1 through #21 from Indian Island side to Samoa Peninsula side. Typical span length is 120 ft (36.6 m) long except the main channel, which is 225 ft (68.6 m) long extending from centerline of pier 8 to the centerline of pier 9.

Samoa Bridge is heavily instrumented as shown in Figure 3.2 in order to record any significant earthquake excitation. There are 33 accelerometers in total on the Samoa Bridge System, including 24 accelerometers on the bridge structure, 6 accelerometers on the pile foundations, and 3 accelerometers at a nearby free field site. Sensors on the structure are oriented in the longitudinal and transverse direction of the bridge and sensors at the free field are oriented in the north-south, east-west and vertical directions.



(a)



(b)

Figure 3.1 Bridge configuration: (a) Samoa Channel Bridge, Eureka geotechnical array, Middle Channel Bridge and Eureka Channel Bridge (Map Data @ 2015 Google) and (b) photo of the Samoa Channel Bridge (<http://www.strongmotioncenter.org>)

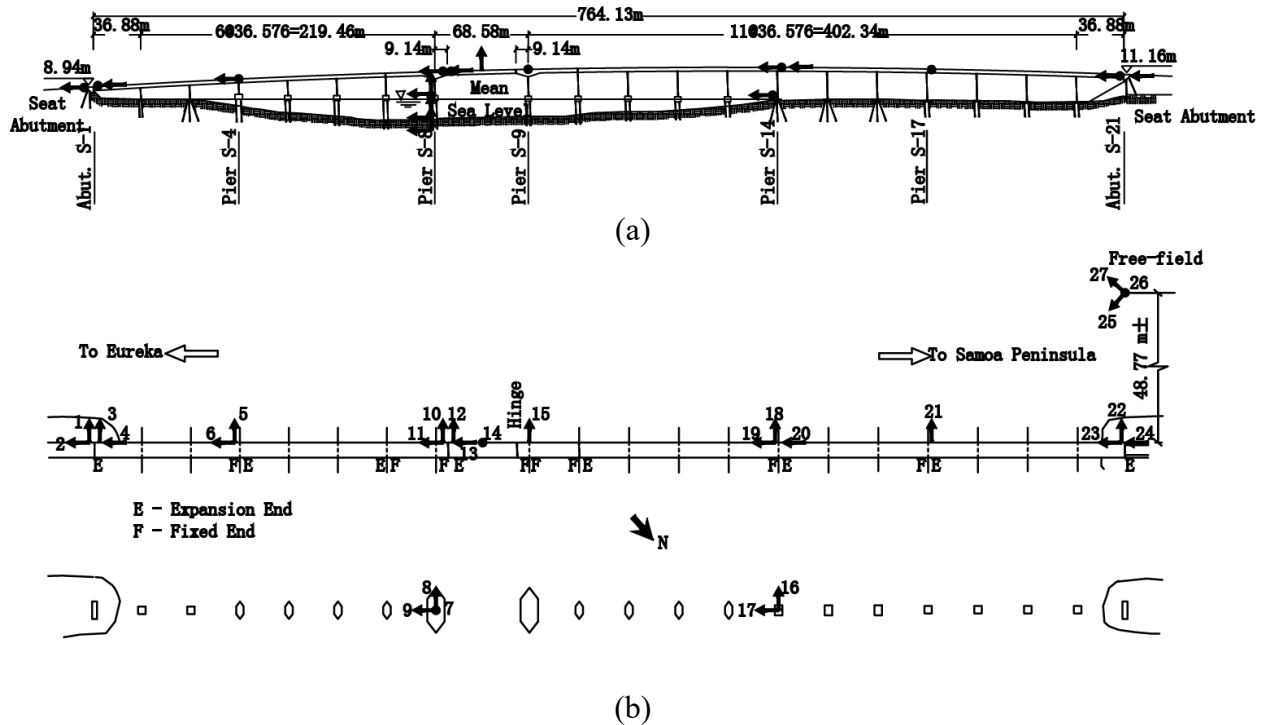
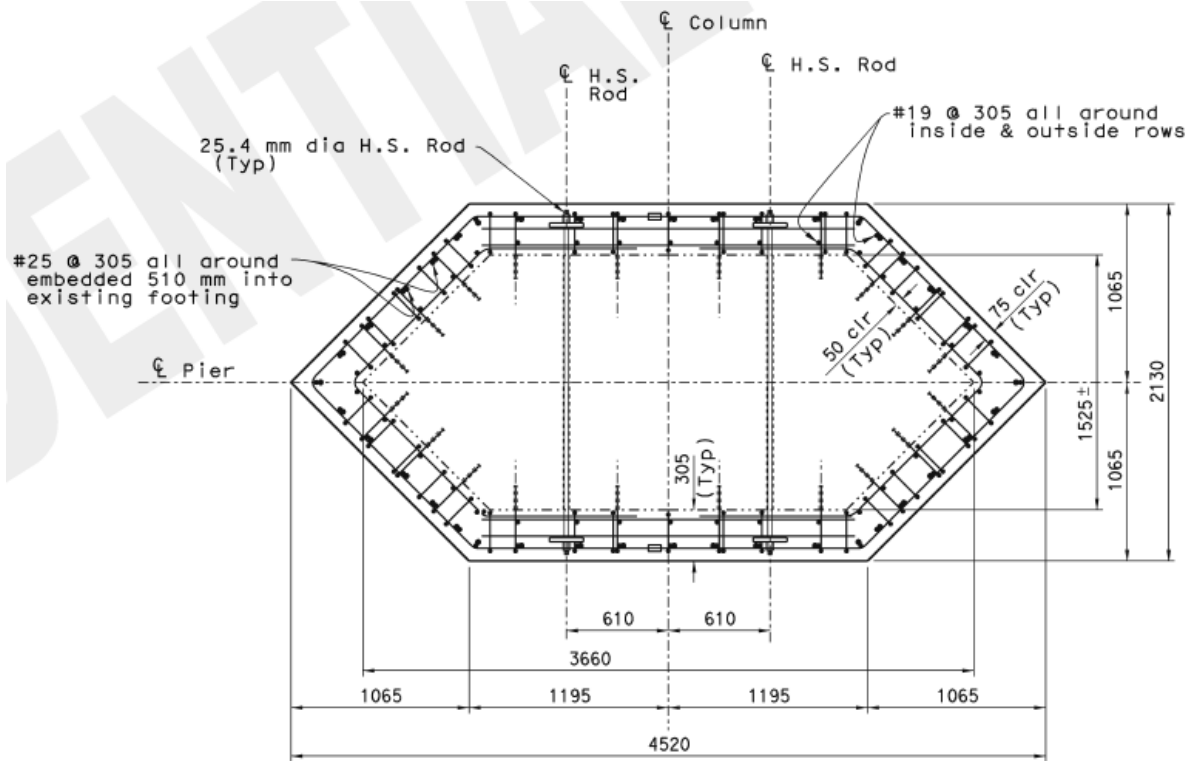


Figure 3.2 Layout of instrumentation at Samoa Bridge (<http://www.strongmotioncenter.org>): (a) elevation view; (b) plan view

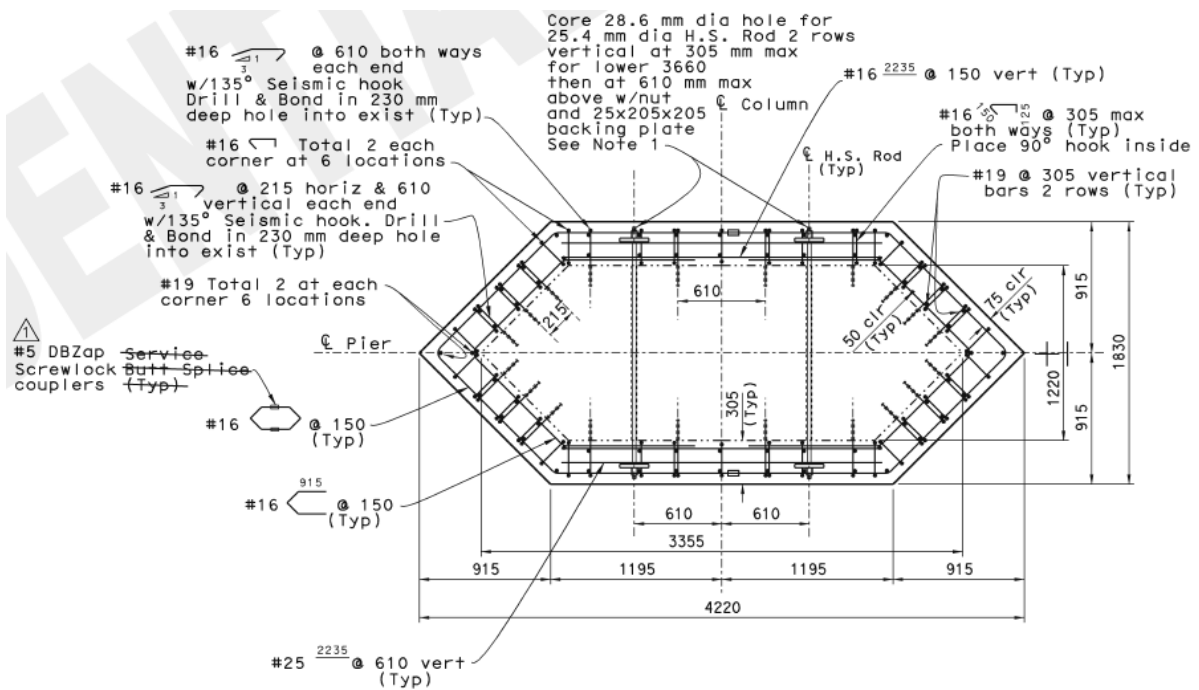
The abutments and piers were founded originally on pile-group foundations consisting of driven pre-cast pre-stressed concrete piles. Referenced to the mean sea level (MSL), elevation of the mud line varies from -51.8 ft (-15.8 m) below Pier S-8 to +3 ft (+0.9 m) at Pier S-20. Eleven pile groups (from S-3 to S-13) have a pile cap located above the mudline with a maximum value of +54.9 ft (+16.72 m) (elevation of cap base) at Pier S-8 (Figure 3.3a)

3.2 Geometric Configuration

Figure 3.3 shows the elevation view of Samoa Bridge, the column reinforcement details at Pier S-8 and S-9, and the column reinforcement details at the piers other than Pier S-8 and S-9. The columns are precast pre-stressed concrete I-girders along with cast-in-place concrete slabs are supported on concrete seat-type abutments and the hammerhead cap beams of column type piers. The column/pier heights of this vertical curved bridge range from 20.3 ft (6.19 m; for Pier S-3) to 42.3 ft (12.9 m; for Pier S-14) as depicted in Figure 3.2 with no deck offset and no column top rigid link. Moreover, Table 3.1 shows the column heights for each pier.



(b)



(c)

Figure 3.3 Samoa Bridge: (a) elevation and bridge deck of Pier S-8; (b) column detail of Piers S-8 and S-9; (c) column detail of other piers except Piers S-8 and S-9

Table 3.1. Column Heights for Samoa Bridge

Pier # (see Figure 3.2a)	Column Heights (ft)
Pier S-2	36.49
Pier S-3	32.04
Pier S-4	34.86
Pier S-5	39.34
Pier S-6	43.03
Pier S-7	45.41
Pier S-8	46.49
Pier S-9	48.23
Pier S-10	49.01
Pier S-11	47.98
Pier S-12	46.15
Pier S-13	44.28
Pier S-14	53.87
Pier S-15	51.47
Pier S-16	49.07
Pier S-17	46.16
Pier S-18	43.76
Pier S-19	38.87
Pier S-20	36.47

3.3 OpenSees FE Modeling

Figure 3.4 shows the FE mesh of the Samoa Bridge model. To facilitate the conducted analyses, a recently developed user interface MSBridge was employed (please see APPENDIX A for more information about MSBridge).

In the conducted OpenSees analyses, the pier columns were modeled using the nonlinear Fiber section as shown in APPENDIX G and the forceBeamColumn (with the distributed plasticity integration method) element was employed. The deck was considered linearly elastic and the bentcap was ignored (the pier column top was considered to extend to the deck CG). Elastic abutment model was employed (for simplicity). The Foundation Matrix technique was employed to model the pier column base. The employed modeling techniques and associated model properties are presented in APPENDIX E.

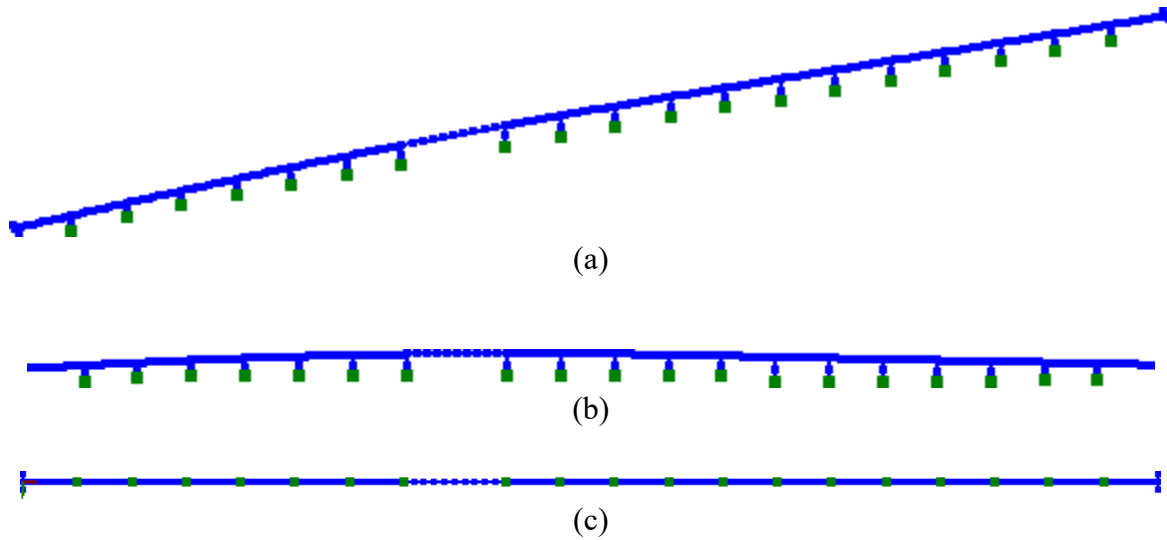


Figure 3.4 Samoa Bridge FE mesh created in MSBridge: (a) 3D view; (b) elevation view; (c) plan view

Foundation Matrix

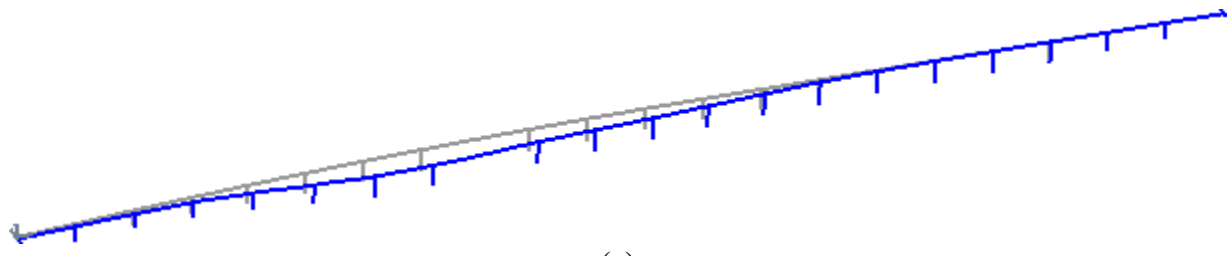
Linear lateral springs were attached to the base of bridge structure (bottom of the pier column) to account for stiffness of the underlying pile foundations and the soil-foundation-structure interaction. Determination of linear foundation stiffness was achieved through the extended OpenSees-SNOPT framework (Gill *et al.* 2002; Wang 2015). Spring values were calibrated by minimizing sum of squared errors by comparing the computed and recorded seismic response at the location of sensors (bridge deck and pile cap response) for the selected observation period. The evaluated base spring values obtained from the optimization problem are defined as the matrix of foundation stiffness coefficients (k_x and k_y see APPENDIX E), which were obtained by conducting pushover analysis on individual bent FE model (Wang 2015).

3.4 Mode Shape Analysis

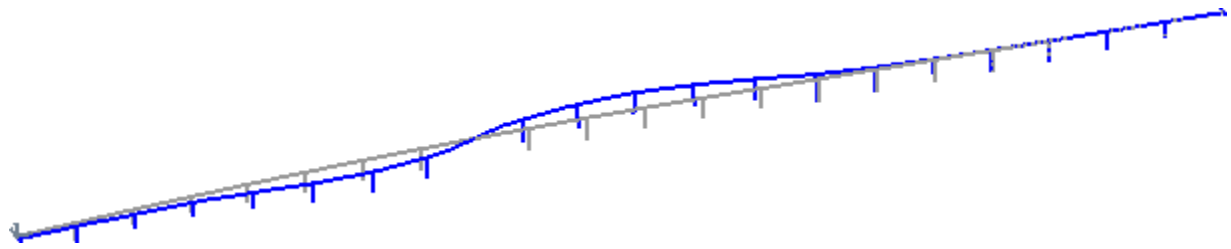
This section shows the response from Mode shape analysis. The natural periods of the first five modes are listed in Table 3.2, and the corresponding mode shapes are shown in Figure 3.5.

Table 3.2. Natural Periods and Frequencies for Samoa Bridge

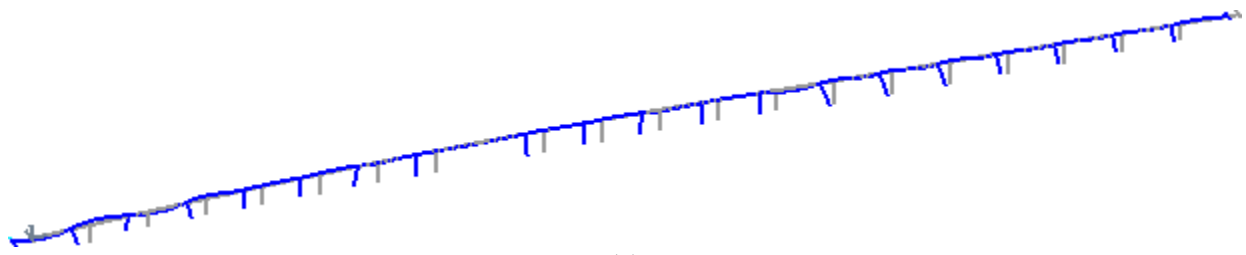
Mode	Natural period (sec)	Natural Frequency (Hz)
1	1.14	0.88
2	0.96	1.04
3	0.91	1.10
4	0.73	1.36
5	0.68	1.48



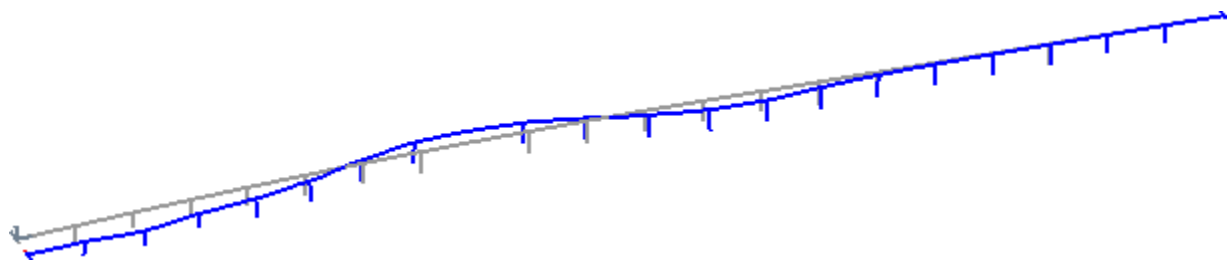
(a)



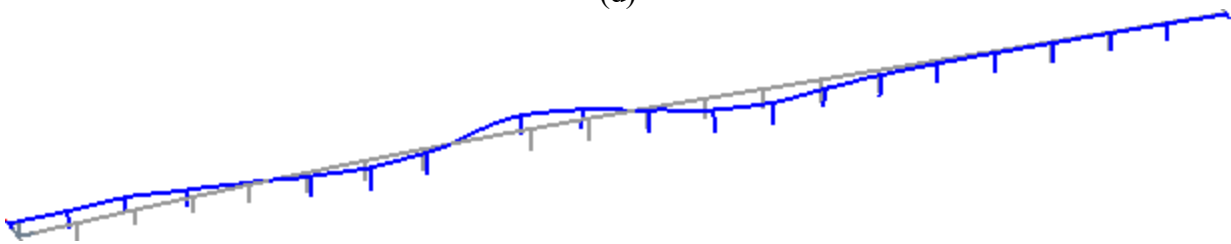
(b)



(c)



(d)



(e)

Figure 3.5 Mode shapes for Samoa Bridge: (a) first mode; (b) second mode; (c) third mode; (d) fourth mode; and (e) fifth mode

3.5 Equivalent Static Analysis (ESA)

ESA was conducted for Samoa Bridge in the longitudinal and transverse directions. For the procedure to conduct ESA in MSBridge, please refer to the MSBridge user manual (Elgamal et al. 2014). Figure 3.6 shows the ARS curve employed in the ESA.

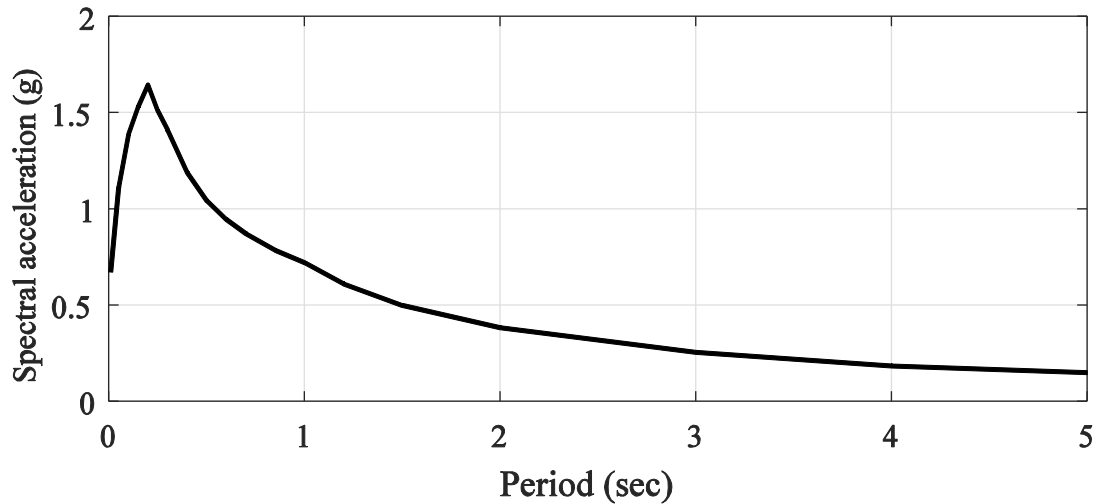


Figure 3.6 ARS curve employed in the ESA

3.5.1 ESA in the Longitudinal Direction

The entire bridge system (Figure 3.4) was employed in the longitudinal ESA. The bridge system was pushed along the bridge deck (longitudinal) direction until initial yielding occurred (when the curvature reached 5×10^{-5} rad/in based on the moment-curvature shown in Figure E.1). The pushover load was applied at the bridge center (i.e., near Bent 11, see Figure 3.4).

Table 3.3 lists the parameters related to the longitudinal ESA. The pushover load at initial yielding was about 40% of the tributary dead load (Table 3.3). Table 3.4 shows the longitudinal ESA result for Samoa Bridge. The displacement demand is 6.9 in for the longitudinal ESA (Table 3.4).

3.5.2 ESA in the Transverse Direction

Transverse ESA was conducted for Pier S-8 (Pier S-8 was chosen in order to compare ESA and THA results later on, since maximum displacement in the THA occurs in Pier S-8). The pier was pushed along the bridge transverse direction (Figure 3.4) until initial yielding occurred (when the curvature reached 3×10^{-5} rad/in based on the moment-curvature shown in Figure E.2). The pushover load was applied at the pier top (Figure 3.4).

Table 3.5 lists the parameters related to the transverse ESA (for Pier S-9). Table 3.6 shows the transverse ESA result for Samoa Bridge (for Pier S-9). The displacement demand for Pier S-9 is 14.4 inches for the transverse ESA (Table 3.6).

Table 3.3. Longitudinal ESA Parameters for Samoa Bridge

Parameter	Value
Tributary dead load (kip)	21,618.6
Tributary mass (kip-sec ² /in)	56.0
Pushover load at initial yielding (kip)	8,561.0
Yield displacement (in)	3.8
Initial stiffness (kip/in)	2,274.15
Period (sec)	1.0

Table 3.4. Longitudinal ESA Result for Samoa Bridge

Parameter	Longitudinal Direction
Displacement Demand (in)	6.9

Table 3.5. Transverse ESA Parameters for Pier S-8

Parameter	Value
Tributary dead load (kip)	1590.8
Tributary mass (kip-sec ² /in)	4.1
Pushover load at initial yielding (kip)	585.4
Yield displacement (in)	12.57
Initial stiffness (kip/in)	46.56
Period (sec)	1.87

Table 3.6. Transverse ESA Result for Pier S-8

Pier # (see Figure 3.2a)	Displacement Demand in Transverse Direction (in)
Pier S-8	14.1

3.6 Nonlinear Time History Analysis

Nonlinear THA was conducted for the 14 input motions provided by Caltrans (see APPENDIX B for the characteristics of the 14 motions). The input motions were applied directly at the pier base and both abutments.

Rayleigh damping was used with a 5% damping ratio (defined at the periods of 0.91 and 1.14 second) in the nonlinear THA. For the time integration scheme, the Newmark average acceleration method ($\gamma = 0.5$ and $\beta = 0.25$) was employed.

Variable time-stepping scheme (`VariableTransient`) was used in the analysis. The starting value for each step was 0.005 second (same as the time step of the input motions) and the minimum time step was 5×10^{-5} second (upon splitting of time step when needed).

3.6.1 Maximum Displacement and Acceleration

Table 3.7 lists Samoa Bridge deck maximum displacement for the 28 simulations from the nonlinear THA. Among the simulations with longitudinal component only (Simulations 1-14), Simulations 6 (motion ROCKS1N6) and 13 (motion ROCKS1P6) gave the least maximum displacement (5.9 in) while Simulations 4 (motion ROCKS1N4) and 11 (motion ROCKS1P4) gave the largest maximum displacement (9.1 in). The maximum displacement of Table 3.7 are also presented in graphical format against PGA in Figure 3.7 and Figure 3.8.

The Samoa Bridge piers also generally deformed more in the transverse direction, compared to the longitudinal direction, when subjected to the same input excitation (Table 3.7). This might be due to the more flexible transverse pier response, compared to that in the longitudinal direction (Table 3.3 and Table 3.5).

Table 3.8 displays Salinas Bridge deck maximum acceleration for the 28 simulations. Among the simulations with longitudinal component only (Simulations 1-14), Simulations 6 (motion ROCKS1N6) and 13 (motion ROCKS1P6) gave the least maximum acceleration (0.56g) while Simulation 1 (ROCKS1N1) gave the largest maximum acceleration (0.82g). The maximum acceleration of Table 3.8 are also presented in graphical format against PGA in Figure 3.9 and Figure 3.10.

Table 3.7. Samoa Bridge Deck Maximum Displacement

Simulation	Longitudinal Input	Transverse Input	Longitudinal Displacement (in)	Transverse Displacement (in)
1	ROCKS1N1 (0.7g)	-	6.6	0
2	ROCKS1N2 (0.38g)	-	6.9	0
3	ROCKS1N3 (0.32g)	-	7.2	0
4	ROCKS1N4 (0.34g)	-	9.1	0
5	ROCKS1N5 (0.53g)	-	7.5	0
6	ROCKS1N6 (0.42g)	-	5.9	0
7	ROCKS1N7 (0.36g)	-	7.1	0
8	ROCKS1P1 (0.71g)	-	7.0	0
9	ROCKS1P2 (0.44g)	-	7.0	0
10	ROCKS1P3 (0.48g)	-	8.1	0
11	ROCKS1P4 (0.32g)	-	9.1	0
12	ROCKS1P5 (0.67g)	-	7.9	0
13	ROCKS1P6 (0.41g)	-	5.9	0
14	ROCKS1P7 (0.4g)	-	6.9	0
Average			7.3	
15	-	ROCKS1N1 (0.7g)	0	12.1
16	-	ROCKS1N2 (0.38g)	0	9.8
17	-	ROCKS1N3 (0.32g)	0	16.9
18	-	ROCKS1N4 (0.34g)	0	13.1
19	-	ROCKS1N5 (0.53g)	0	9.1
20	-	ROCKS1N6 (0.42g)	0	11.1
21	-	ROCKS1N7 (0.36g)	0	13.4
22	-	ROCKS1P1 (0.71g)	0	12.2
23	-	ROCKS1P2 (0.44g)	0	9.7
24	-	ROCKS1P3 (0.48g)	0	9.2
25	-	ROCKS1P4 (0.32g)	0	13.6
26	-	ROCKS1P5 (0.67g)	0	8.5
27	-	ROCKS1P6 (0.41g)	0	11.2
28	-	ROCKS1P7 (0.4g)	0	16.2
Average				11.9

Notes:

- ESA longitudinal displacement demand is 6.9 in, corresponding to a difference of 5.8% (compared to the average THA maximum displacement of 7.3 in)
- ESA transverse displacement demand is 14.1 in, corresponding to a difference of 15.8% (compared to the average THA maximum displacement of 11.9 in)

Table 3.8. Samoa Bridge Deck Maximum Acceleration

Simulation	Longitudinal Input	Transverse Input	Longitudinal Acceleration (g)	Transverse Acceleration (g)
1	ROCKS1N1 (0.7g)	-	0.82	0
2	ROCKS1N2 (0.38g)	-	0.65	0
3	ROCKS1N3 (0.32g)	-	0.65	0
4	ROCKS1N4 (0.34g)	-	0.76	0
5	ROCKS1N5 (0.53g)	-	0.73	0
6	ROCKS1N6 (0.42g)	-	0.56	0
7	ROCKS1N7 (0.36g)	-	0.70	0
8	ROCKS1P1 (0.71g)	-	0.81	0
9	ROCKS1P2 (0.44g)	-	0.65	0
10	ROCKS1P3 (0.48g)	-	0.75	0
11	ROCKS1P4 (0.32g)	-	0.77	0
12	ROCKS1P5 (0.67g)	-	0.76	0
13	ROCKS1P6 (0.41g)	-	0.56	0
14	ROCKS1P7 (0.4g)	-	0.64	0
15	-	ROCKS1N1 (0.7g)	0	1.40
16	-	ROCKS1N2 (0.38g)	0	1.30
17	-	ROCKS1N3 (0.32g)	0	1.20
18	-	ROCKS1N4 (0.34g)	0	1.18
19	-	ROCKS1N5 (0.53g)	0	1.16
20	-	ROCKS1N6 (0.42g)	0	1.25
21	-	ROCKS1N7 (0.36g)	0	1.14
22	-	ROCKS1P1 (0.71g)	0	1.44
23	-	ROCKS1P2 (0.44g)	0	1.30
24	-	ROCKS1P3 (0.48g)	0	1.17
25	-	ROCKS1P4 (0.32g)	0	1.16
26	-	ROCKS1P5 (0.67g)	0	1.17
27	-	ROCKS1P6 (0.41g)	0	1.26
28	-	ROCKS1P7 (0.4g)	0	1.19

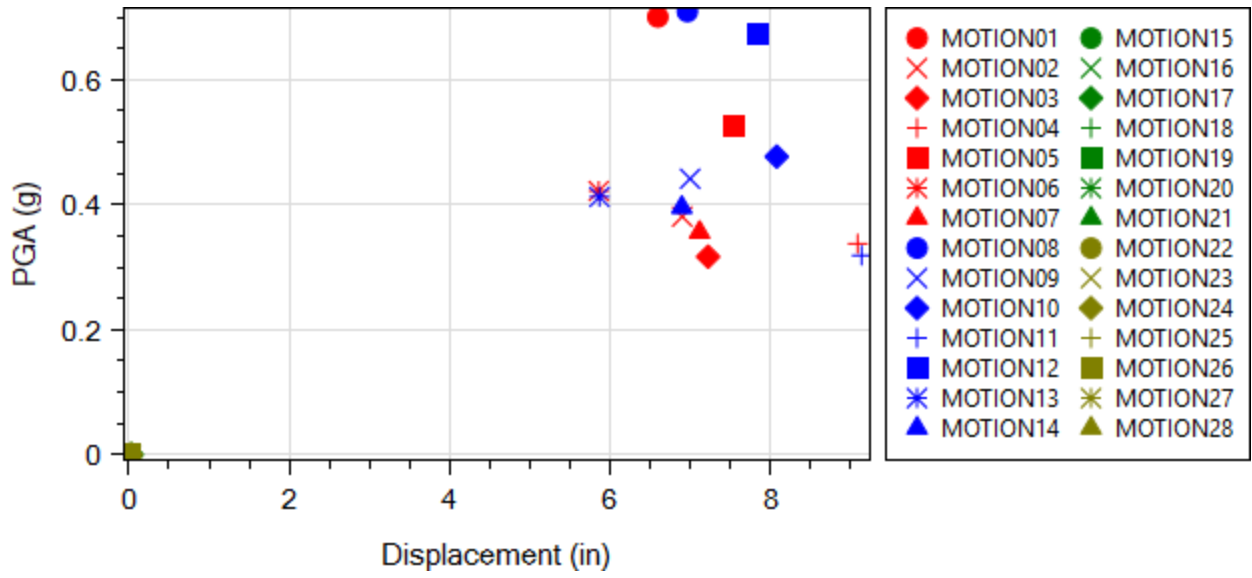


Figure 3.7 Bridge deck maximum longitudinal displacement

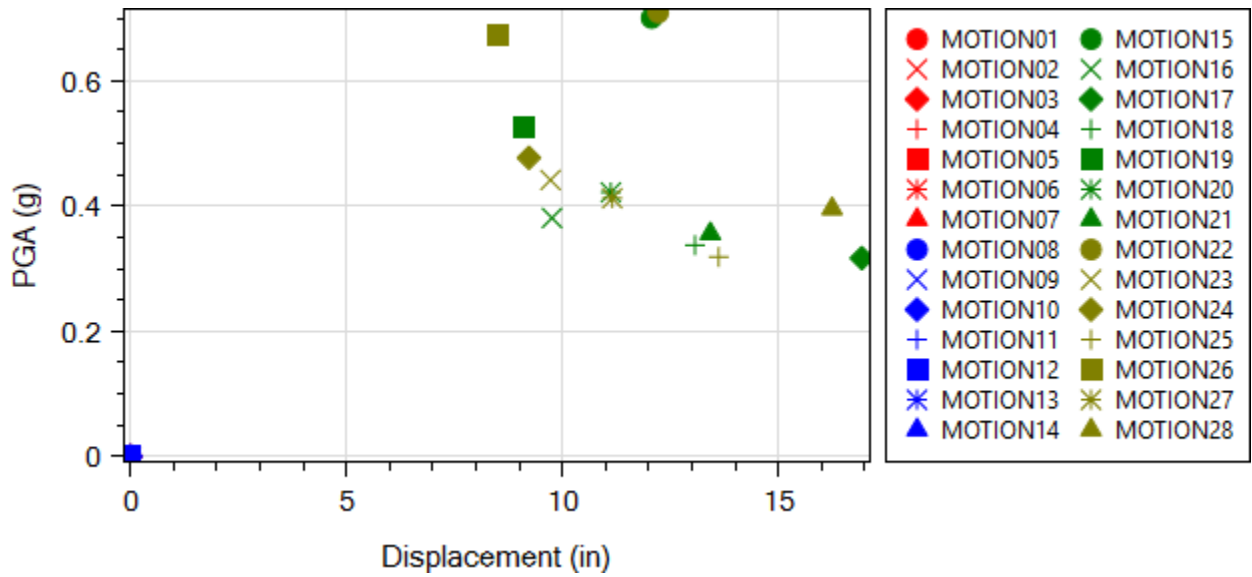


Figure 3.8 Bridge deck maximum transverse displacement

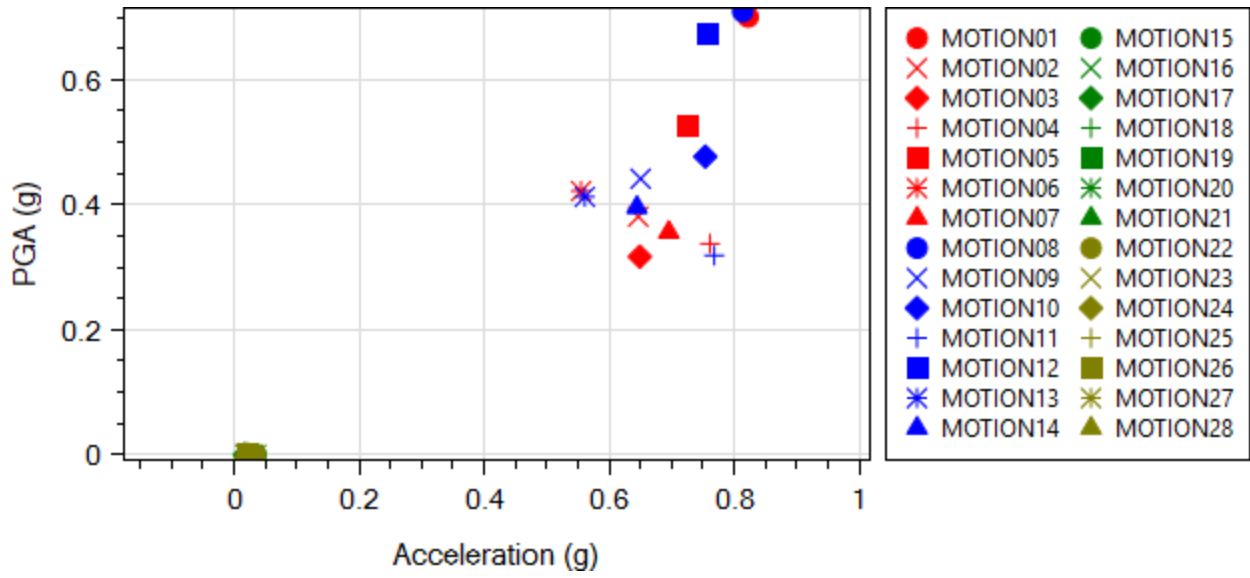


Figure 3.9 Bridge deck maximum longitudinal acceleration

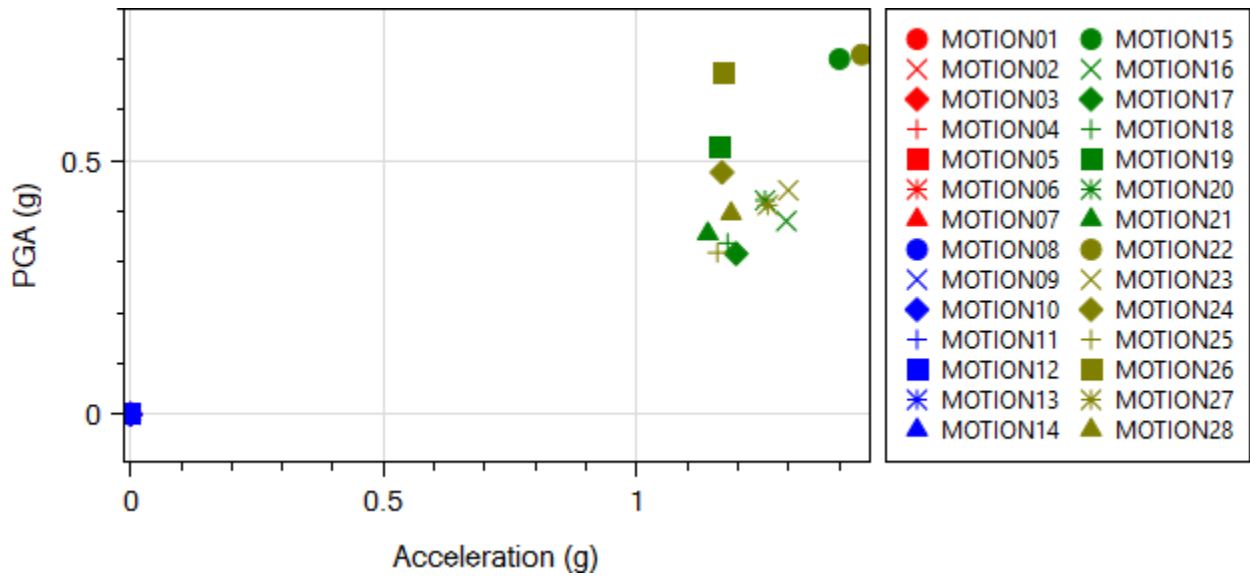


Figure 3.10 Bridge deck maximum transverse acceleration

3.6.2 Response Time History

In this section, response time histories for Pier S-8 (see Figure 3.4) from 2 representative simulations (Simulations 1 and 4) are presented (Longitudinal seismic excitation).

1) Simulation 1 (motion ROCKS1N1)

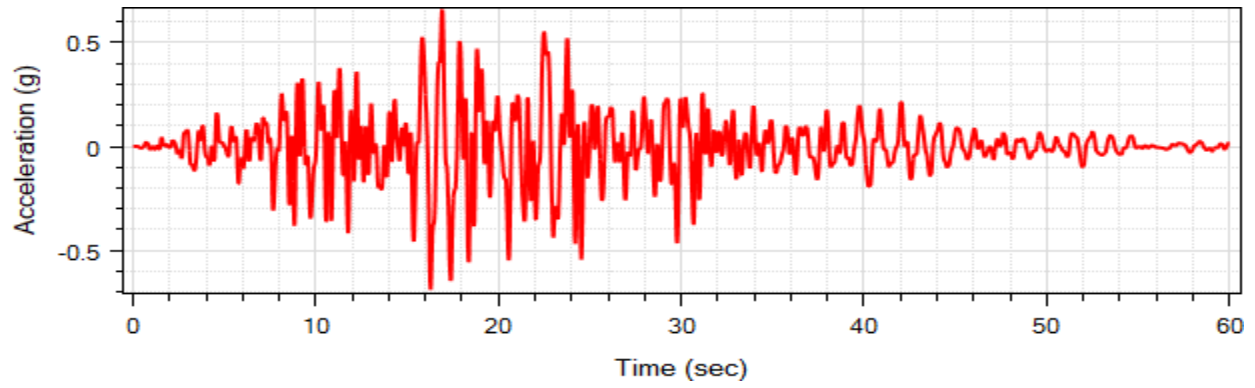
For Simulation 1, the deck maximum displacement is 6.6 in (Table 3.7). The pier top longitudinal response time histories at Pier S-8 are displayed in Figure 3.11 where the displacement time history refers to the displacement at the pier top. The input motion ROCKS1N1 is also shown in Figure 3.11d for reference.

Figure 3.12 displays the moment-curvature response at the pier top for selected piers. A maximum bending moment of 12,000 kip-ft was reached for Pier S-8 (Figure 3.12). The deformed mesh when the deck maximum displacement was reached (i.e., 6.6 in as shown in Table 3.7) is shown in Figure 3.13.

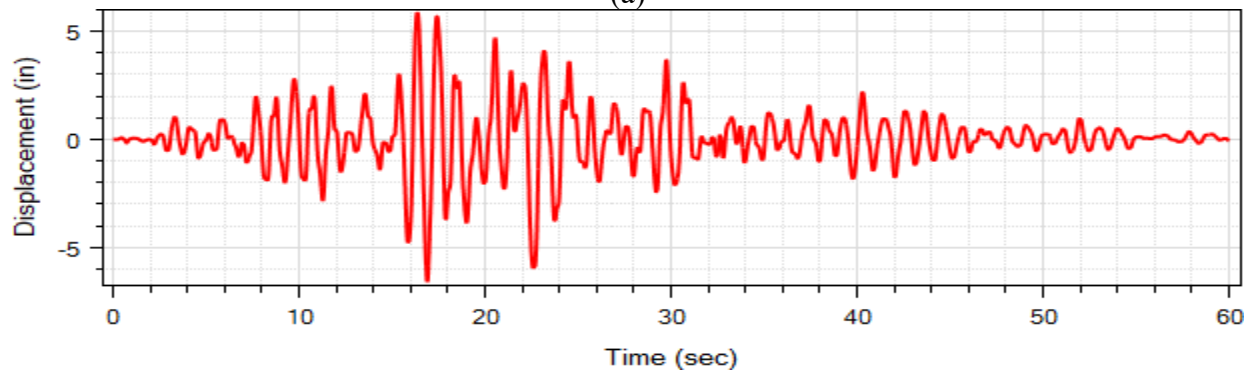
2) Simulation 4 (motion ROCKS1N4)

For Simulation 4, the deck maximum displacement is 9.1 in (Table 3.7). The pier top longitudinal response time histories at Pier S-8 are displayed in Figure 3.14. The input motion ROCKS1N4 is also shown in Figure 3.14d for reference.

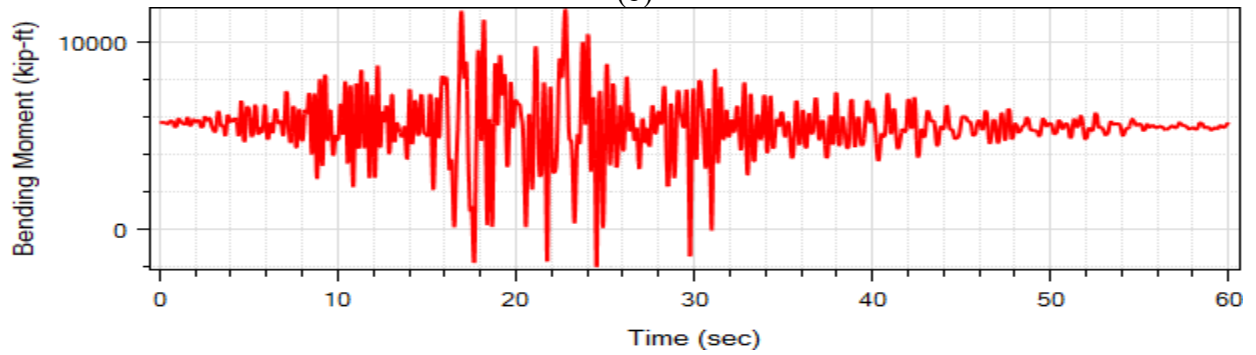
Figure 3.15 displays the moment-curvature response at the pier top for selected piers. A maximum bending moment of 14,500 kip-ft was reached for Pier S-8 (Figure 3.12). (Figure 3.12). The deformed mesh when the deck maximum displacement was reached for Motion 4 ROCKS1N4 (i.e., 9.1 in as shown in Table 3.7) is shown in Figure 3.16.



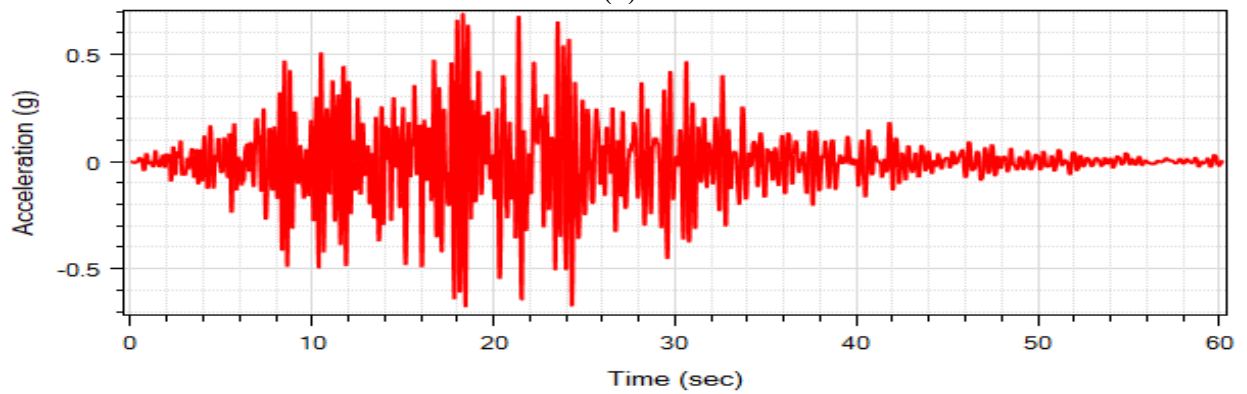
(a)



(b)

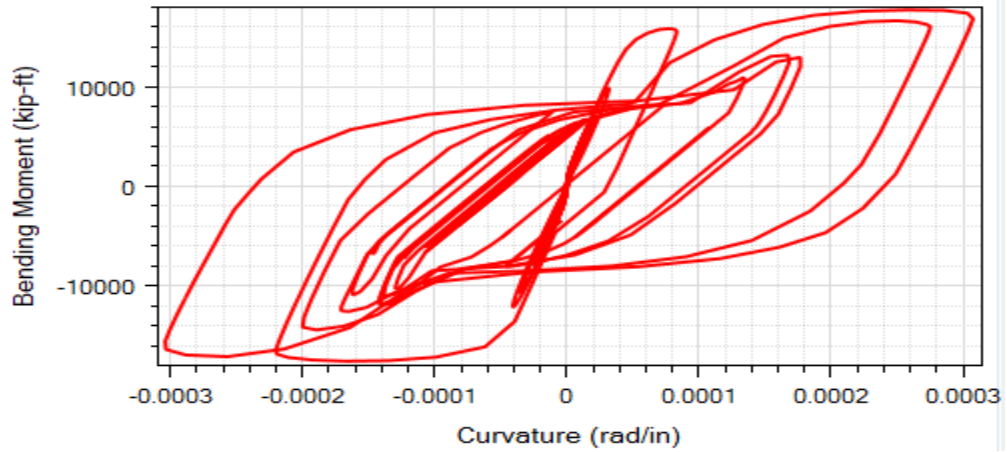


(c)

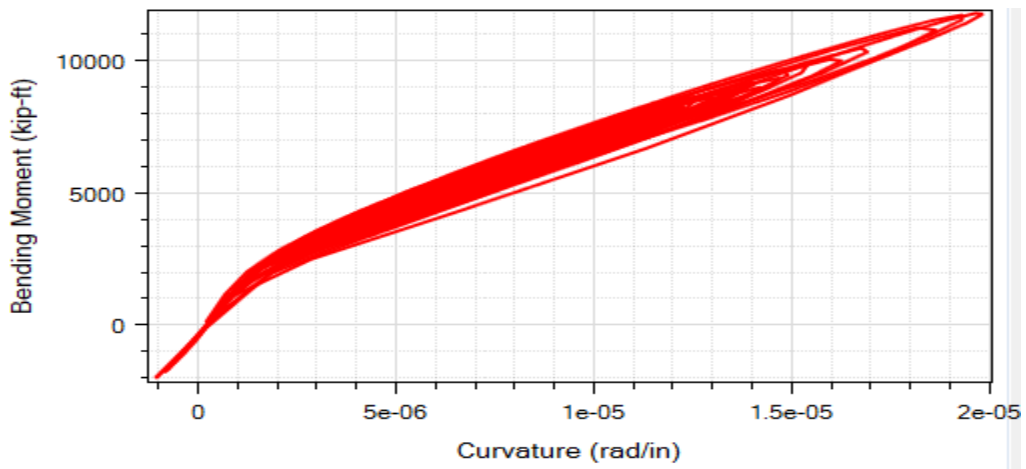


(d)

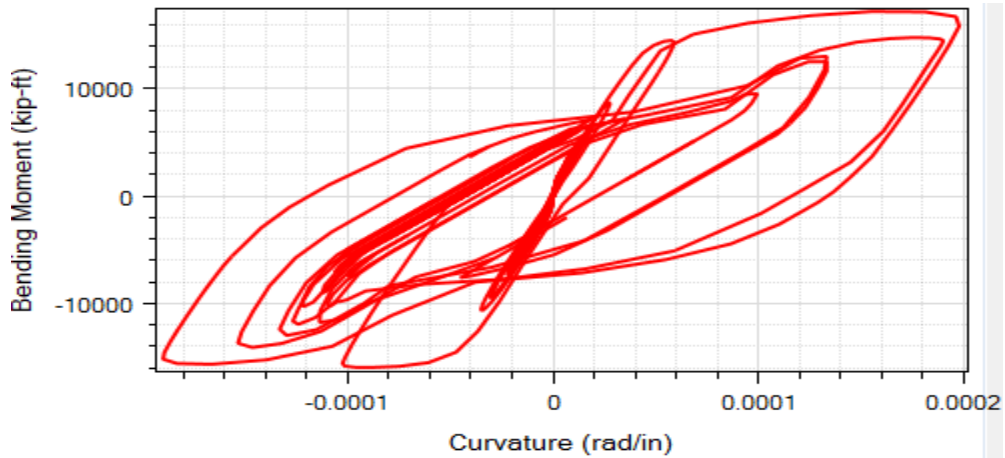
Figure 3.11 Pier S-8 column top longitudinal response time histories for Simulation 1: (a) acceleration; (b) displacement; (c) bending moment; (d) base excitation ROCKS1N1



(a)

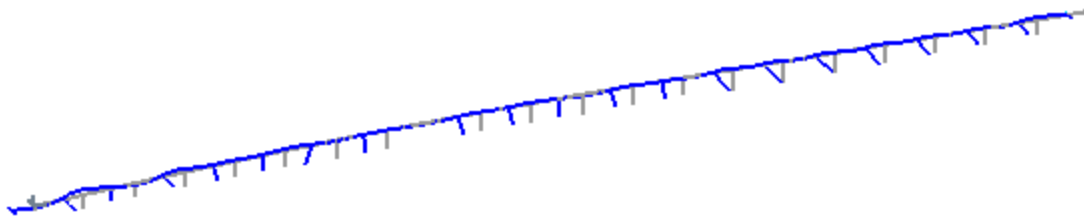


(b)

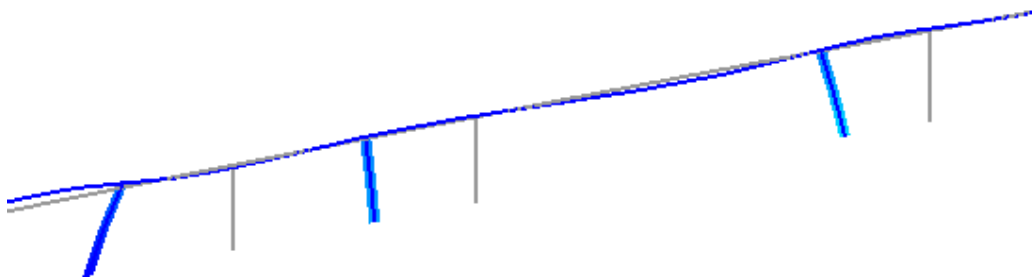


(c)

Figure 3.12 Column top longitudinal moment-curvature response for Simulation 1: (a) Pier S-4; (b) Pier S-8; (c) Pier S-19



(a)



(b)

Figure 3.13 Deformed mesh (factor of 100) for Simulation 1 at the maximum displacement step (grey lines represent undeformed mesh): (a) entire bridge; (b) close-up of Bents 6, 7, and 8 (from left to right)

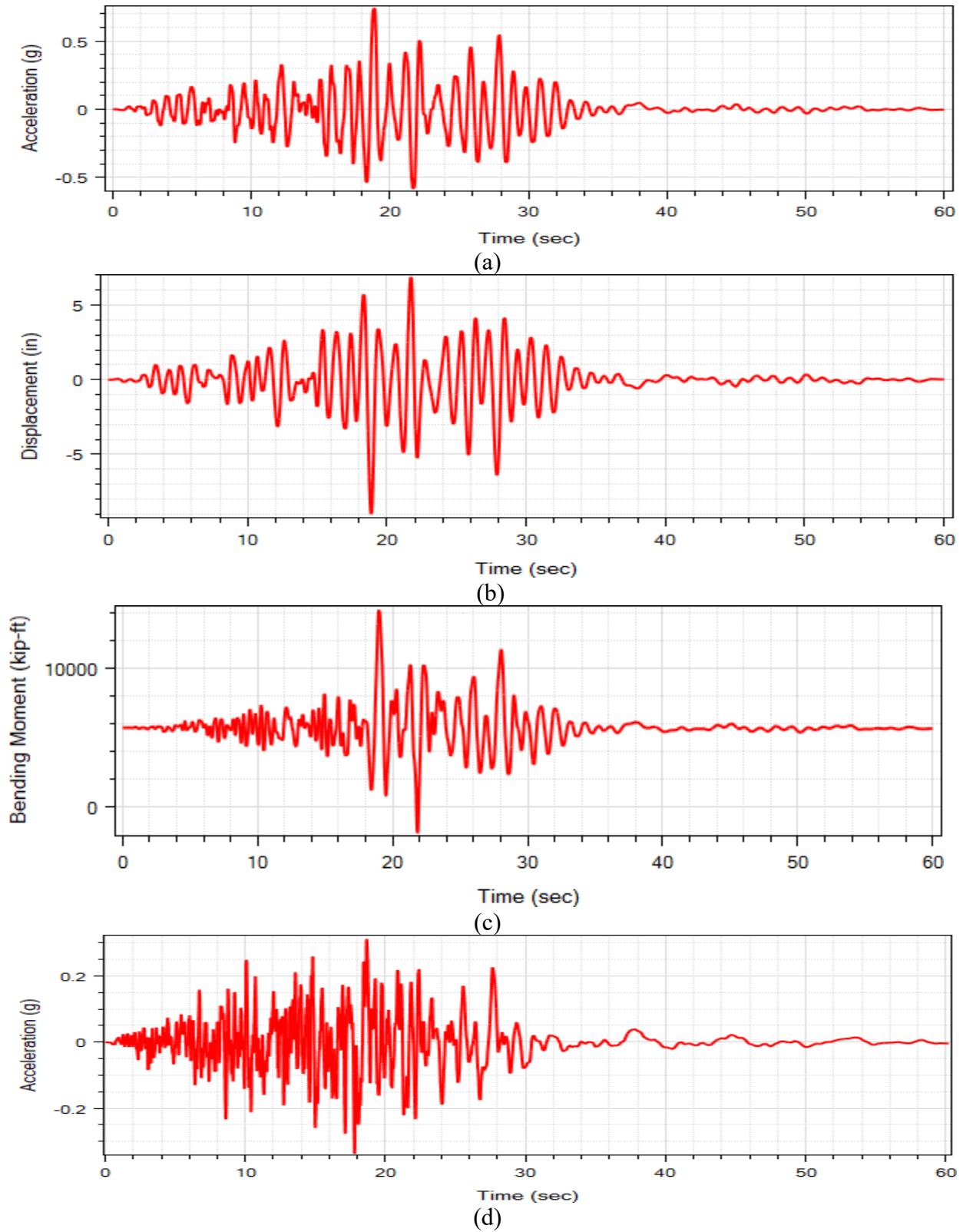


Figure 3.14 Pier S-8 column top longitudinal response time histories for Simulation 4: (a) acceleration; (b) displacement; (c) bending moment; (d) base excitation ROCKS1N4

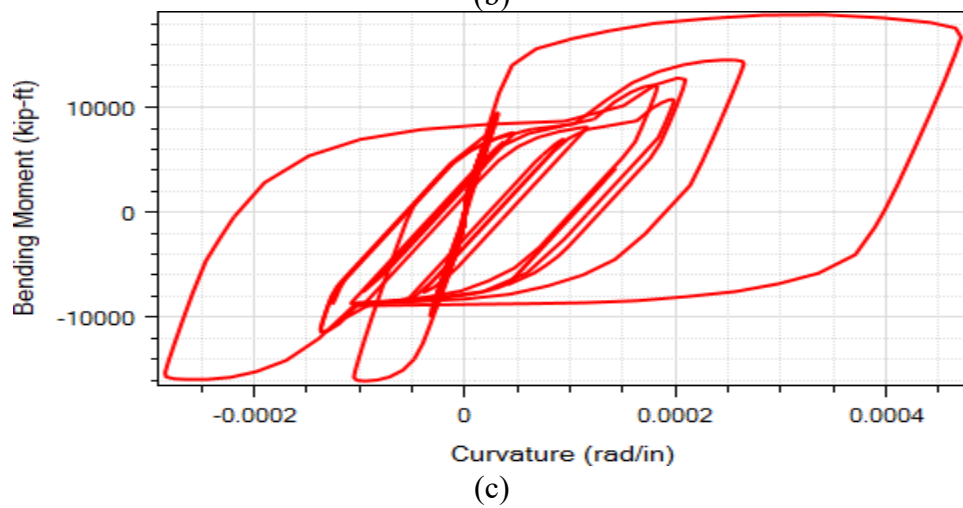
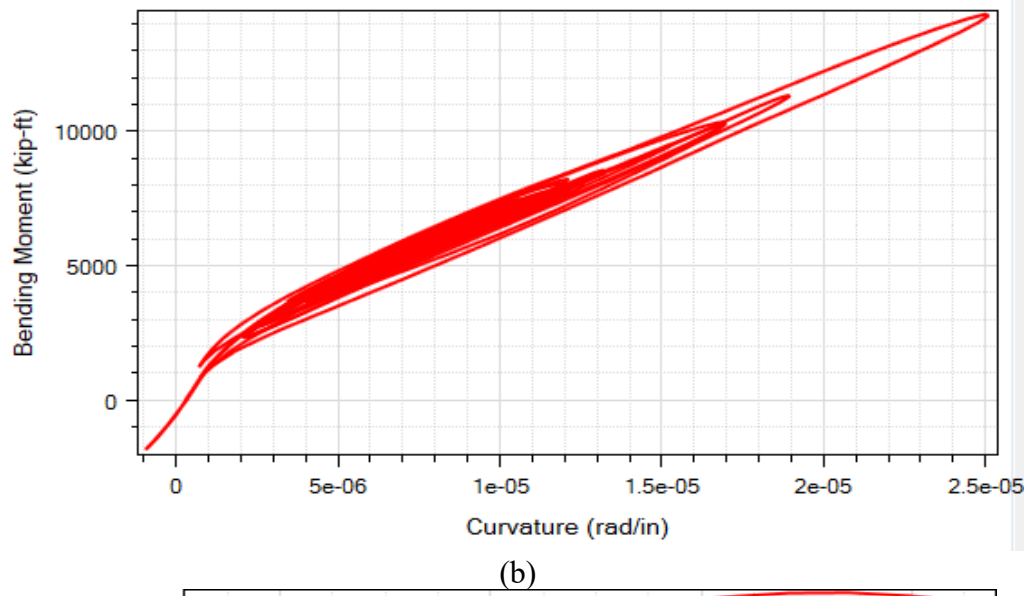
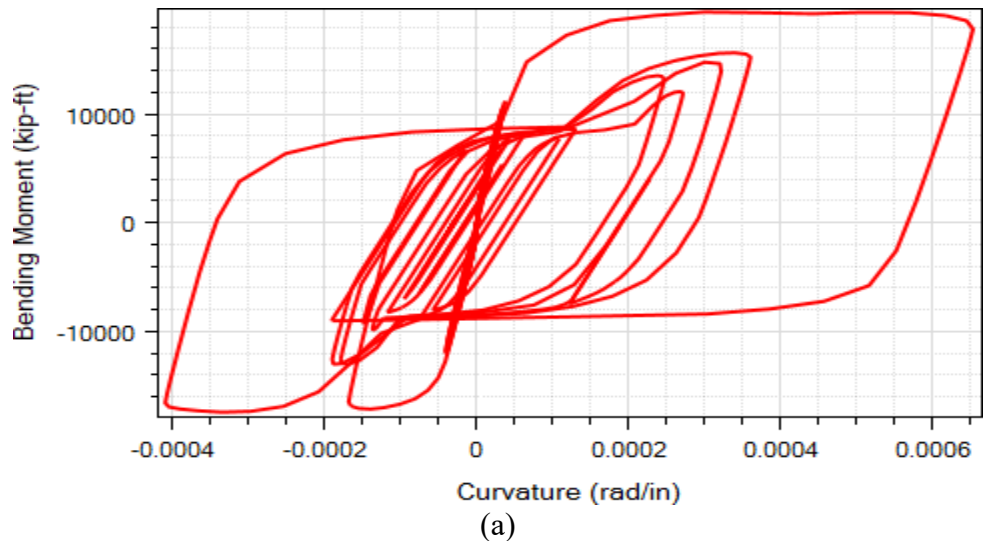


Figure 3.15 Column top longitudinal moment-curvature response for Simulation 4: (a) Pier S-4; (b) Pier S-8; (c) Pier S-19

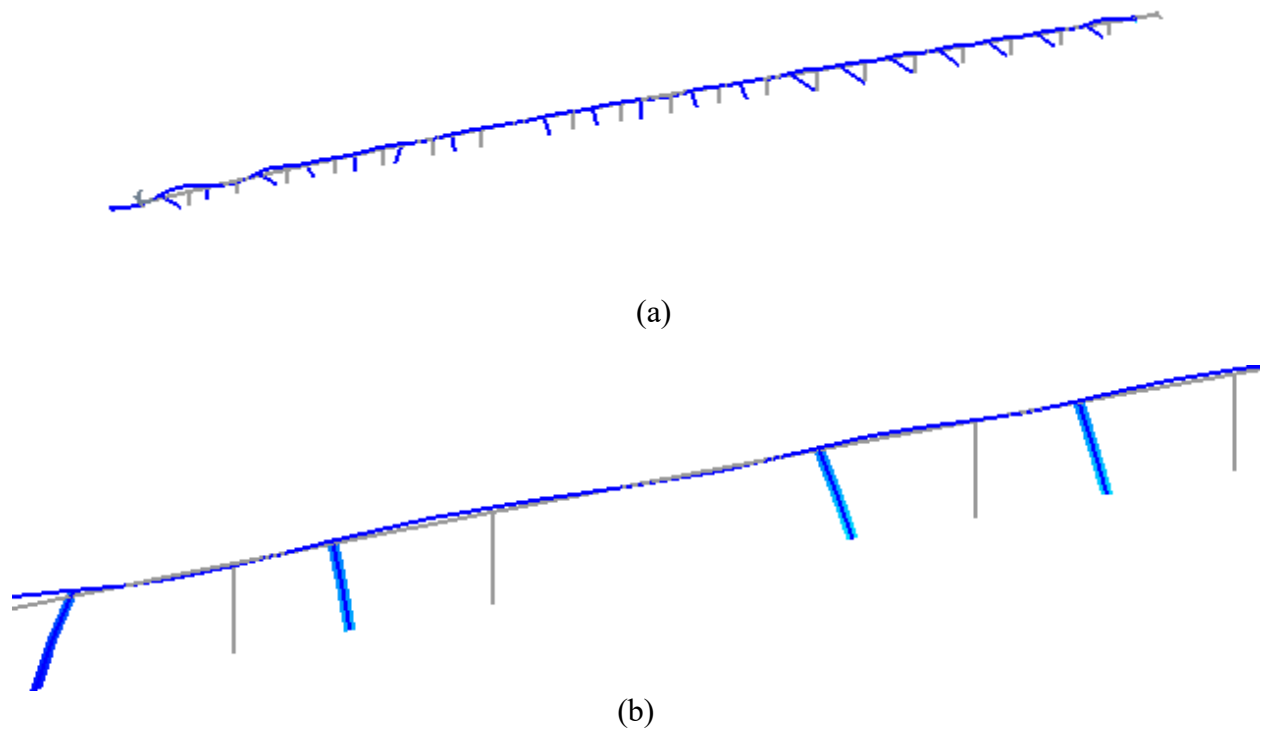


Figure 3.16 Deformed mesh (factor of 100) for Simulation 4 at the maximum displacement step (grey lines represent undeformed mesh): (a) entire bridge; (b) close-up of Bents 6, 7, and 8 (from left to right)

3.7 Summary

Samoa Bridge was modeled in OpenSees. A recently developed user interface MSBridge was employed for pre- and post-processing in the conducted OpenSees analysis. Nonlinear THA was conducted for the 14 input motions provided by Caltrans. The average THA maximum displacement is 7.3 inches in the bridge longitudinal direction and 11.9 inches in the transverse direction. ESA was also conducted for Samoa Bridge using MSBridge.

3.8 Conclusions

1. For the employed ESA spectrum, column displacement demand was 6.9 inches in the longitudinal direction and 14.1 inches in the transverse direction.
2. For the investigated set of ground motions in the OpenSees analysis:
 - 2.1 In the longitudinal direction, about 64% of the shaking events resulted in column displacement demand that exceeded that of the ESA. This demand reached a maximum of 32% in excess of that from the corresponding ESA.
 - 2.2 In the transverse direction, about 14% of the shaking events resulted in column displacement demand that exceeded that of the ESA. This demand reached a maximum of 20% in excess of that from the corresponding ESA.

3.9 Analysis of Samoa Bridge with Stiff Foundation Matrix

There are scenarios where foundations are built on stiff and competent soils. The resulting foundation matrix is typically a stiff one with large coefficients. In this section, analysis of Samoa Bridge was conducted with a much stiffer foundation matrix (Figure 3.17), compared the foundation matrix employed in previous sections (APPENDIX E). The results of Mode shape analysis, ESA, and Nonlinear THA are presented and discussed in this section.

K =	SDx	SDy	SDz	SRx	Sry	SRz	
	150000	0	0	0	0	0	SDx
	0	150000	0	0	0	0	SDy
	0	0	650000	0	0	0	SDz
	0	0	0	3.00E+09	0	0	SRx
	0	0	0	0	3.00E+09	0	Sry
	0	0	0	0	0	7.00E+08	SRz

Figure 3.17 Stiff foundation matrix employed

3.9.1 Mode Shape Analysis

This section shows the response from mode shape analysis. The natural periods of the first five modes are listed in Table 3.9, and the corresponding mode shapes are shown in Figure 3.18.

Comparison of Stiff Foundation Matrix Case with Rigid Base Case

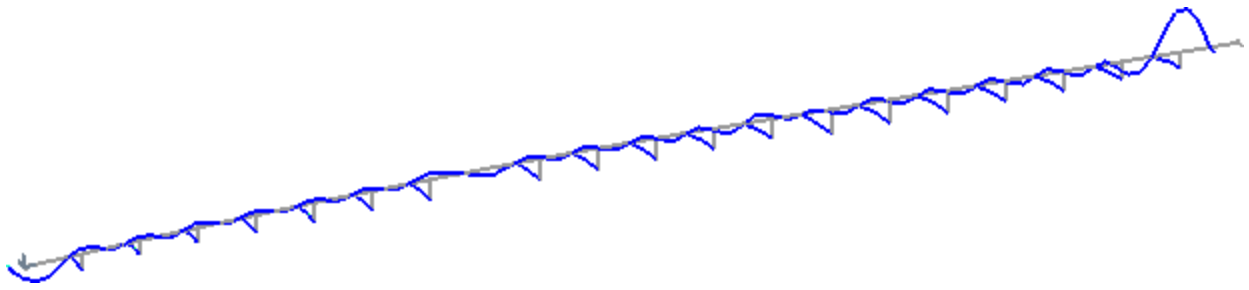
For comparison purposes, Mode shape analysis was also conducted for Samoa Bridge with rigid pier base. The natural periods and frequencies are shown in Table 3.10. It is seen that both Table 3.9 and Table 3.10 are almost identical, which indicates that the stiff foundation matrix employed in this section (Figure 3.17) is essentially equivalent to the rigid base.

Table 3.9. Natural Periods and Frequencies for Samoa Bridge with Stiff Foundation Matrix

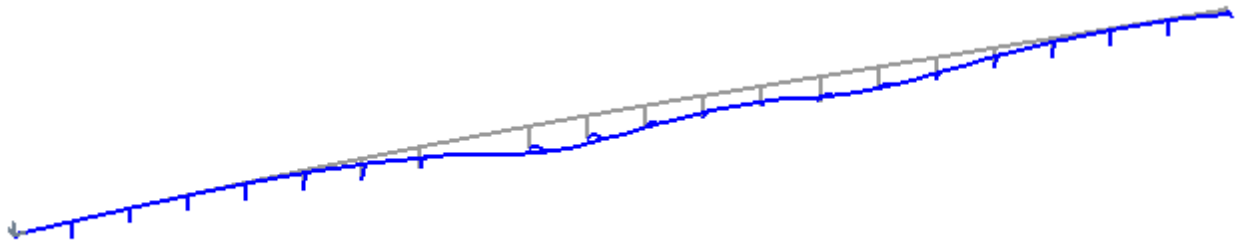
Mode	Natural Period (sec)	Natural Frequency (Hz)
1	0.36	2.77
2	0.32	3.15
3	0.31	3.22
4	0.309	3.24
5	0.308	3.25

Table 3.10. Natural Periods and Frequencies for Samoa Bridge with Rigid Pier Base

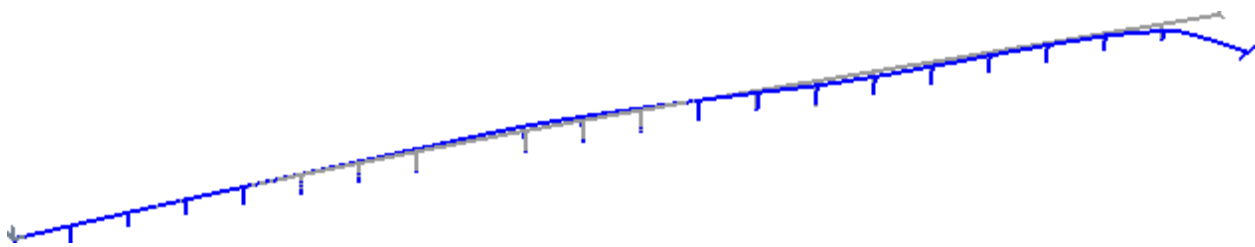
Mode	Natural Period (sec)	Natural Frequency (Hz)
1	0.36	2.78
2	0.32	3.16
3	0.309	3.23
4	0.3073	3.254
5	0.3072	3.255



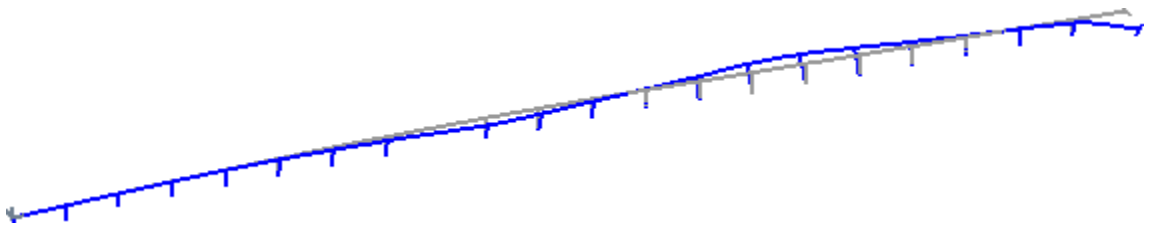
(a)



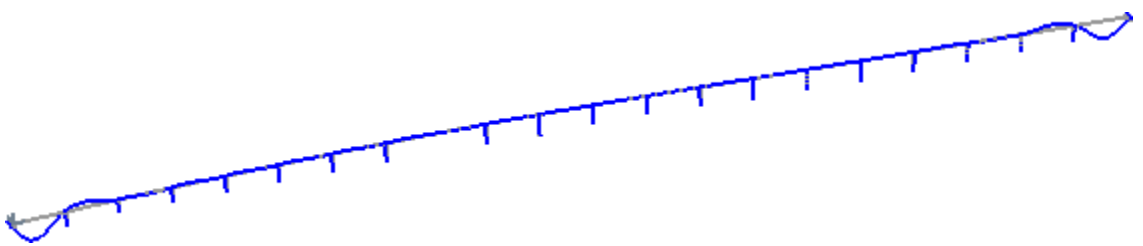
(b)



(c)



(d)



(e)

Figure 3.18 Mode shapes for Samoa Bridge with stiff foundation matrix: (a) first mode; (b) second mode; (c) third mode; (d) fourth mode; and (e) fifth mode

3.9.2 Equivalent Static Analysis (ESA)

ESA was conducted in the bridge longitudinal and transverse directions. For the procedure to conduct ESA in MSBridge, please refer to the MSBridge user manual (Elgamal *et al.* 2014) with Figure 3.6 showing the employed ARS curve.

3.9.2.1 ESA in the Longitudinal Direction

The entire bridge system (Figure 3.4) was employed in the longitudinal ESA. The bridge system was pushed along the bridge deck (longitudinal) direction until initial yielding occurred (when the curvature reached 5×10^{-5} rad/in based on the moment-curvature shown in Figure E.1). The pushover load was applied at the bridge center (i.e., near Bent 11, see Figure 3.4).

Table 3.11 lists the parameters related to the longitudinal ESA. The pushover load at initial yielding was about 48% of the tributary dead load (Table 3.11). Table 3.12 shows the longitudinal ESA result. The displacement demand is 3.0 in for the longitudinal ESA (Table 3.12).

3.9.2.2 ESA in the Transverse Direction

Transverse ESA was conducted for Pier S-8. The pier was pushed along the bridge transverse direction (Figure 3.4) until initial yielding occurred (when the curvature reached 3×10^{-5} rad/in based on the moment-curvature shown in Figure E.2). The pushover load was applied at the pier top (Figure 3.4).

Table 3.13 lists the parameters related to the transverse ESA. Table 3.14 shows the transverse ESA result for Samoa Bridge. The displacement demand for Pier S-8 is 4.0 inches for the transverse ESA (Table 3.14).

Table 3.11. Longitudinal ESA Parameters for Samoa Bridge with Stiff Foundation Matrix

Parameter	Value
Tributary dead load (kip)	21,374.8
Tributary mass (kip-sec ² /in)	55.3
Pushover load at initial yielding (kip)	10,259.9
Yield displacement (in)	1.43
Initial stiffness (kip/in)	7,192.58
Period (sec)	0.55

Table 3.12. Longitudinal ESA Result for Samoa Bridge with Stiff Foundation Matrix

Parameter	Longitudinal Direction
Displacement Demand (in)	3.0

Table 3.13. Transverse ESA Parameters for Pier S-8

Parameter	Value
Tributary dead load (kip)	1579
Tributary mass (kip-sec ² /in)	4.1
Pushover load at initial yielding (kip)	840.8
Yield displacement (in)	2.41
Initial stiffness (kip/in)	349.5
Period (sec)	0.68

Table 3.14. Transverse ESA Result for Samoa Bridge with Stiff Foundation Matrix

Pier # (see Figure 3.2a)	Displacement Demand in Transverse Direction (in)
Pier S-8	4.0

3.9.3 Nonlinear Time History Analysis

Nonlinear THA was conducted for the 14 input motions provided by Caltrans. The input motions were applied directly at the pier base as well as at both abutments.

Rayleigh damping was used with a 5% damping ratio (defined at the periods of 0.36 and 0.32 second) in the nonlinear THA. For the time integration scheme, the Newmark average acceleration method ($\gamma = 0.5$ and $\beta = 0.25$) was employed.

Variable time-stepping scheme (`VariableTransient`) was used in the analysis. The starting value for each step was 0.005 second (same as the time step of the input motions) and the minimum time step was 5×10^{-5} second (upon splitting of time step when needed).

3.9.3.1 Maximum Displacement and Acceleration

Table 3.15 lists the deck maximum displacement for the 28 simulations from the nonlinear THA. Among the simulations with longitudinal component only (Simulations 1-14), Simulations 11 (motion ROCKS1P4) gave the least maximum displacement (2.16 in) while Simulation 7 (motion ROCKS1N7) gave the largest maximum displacement (2.67 in). The maximum displacement of Table 3.15 are also presented in graphical format against PGA in Figure 3.19 and Figure 3.20.

Table 3.16 displays the deck maximum acceleration for the 28 simulations. Among the simulations with longitudinal component only (Simulations 1-14), Simulation 3 (motion ROCKS1N3) gave the least maximum acceleration (0.674g) while Simulation 1 (motion ROCKS1N1) gave the largest maximum acceleration (0.868g). The maximum acceleration of Table 3.16 are also presented in graphical format against PGA in Figure 3.21 and Figure 3.22.

Table 3.15. Deck Maximum Displacement for Samoa Bridge with Stiff Foundation Matrix

Simulation	Longitudinal Input	Transverse Input	Longitudinal Displacement (in)	Transverse Displacement (in)
1	ROCKS1N1 (0.7g)	-	2.60	0
2	ROCKS1N2 (0.38g)	-	2.45	0
3	ROCKS1N3 (0.32g)	-	2.24	0
4	ROCKS1N4 (0.34g)	-	2.18	0
5	ROCKS1N5 (0.53g)	-	2.24	0
6	ROCKS1N6 (0.42g)	-	2.45	0
7	ROCKS1N7 (0.36g)	-	2.67	0
8	ROCKS1P1 (0.71g)	-	2.59	0
9	ROCKS1P2 (0.44g)	-	2.43	0
10	ROCKS1P3 (0.48g)	-	2.44	0
11	ROCKS1P4 (0.32g)	-	2.16	0
12	ROCKS1P5 (0.67g)	-	2.18	0
13	ROCKS1P6 (0.41g)	-	2.42	0
14	ROCKS1P7 (0.4g)	-	2.41	0
Average			2.4	
15	-	ROCKS1N1 (0.7g)	0	4.40
16	-	ROCKS1N2 (0.38g)	0	2.32
17	-	ROCKS1N3 (0.32g)	0	2.49
18	-	ROCKS1N4 (0.34g)	0	2.33
19	-	ROCKS1N5 (0.53g)	0	2.43
20	-	ROCKS1N6 (0.42g)	0	2.77
21	-	ROCKS1N7 (0.36g)	0	2.85
22	-	ROCKS1P1 (0.71g)	0	4.46
23	-	ROCKS1P2 (0.44g)	0	2.39
24	-	ROCKS1P3 (0.48g)	0	2.62
25	-	ROCKS1P4 (0.32g)	0	2.34
26	-	ROCKS1P5 (0.67g)	0	4.38
27	-	ROCKS1P6 (0.41g)	0	2.78
28	-	ROCKS1P7 (0.4g)	0	2.70
Average				2.9

Notes:

- ESA longitudinal displacement demand is 3.0 in, corresponding to a difference of 20.3% (compared to the average THA maximum displacement of 2.4 in)
- ESA transverse displacement demand is 4.0 in, corresponding to a difference of 26.3% (compared to the average THA maximum displacement of 2.9 in)

Table 3.16. Deck Maximum Acceleration for Samoa Bridge with Stiff Foundation Matrix

Simulation	Longitudinal Input	Transverse Input	Longitudinal Acceleration (g)	Transverse Acceleration (g)
1	ROCKS1N1 (0.7g)	-	0.868	0
2	ROCKS1N2 (0.38g)	-	0.751	0
3	ROCKS1N3 (0.32g)	-	0.674	0
4	ROCKS1N4 (0.34g)	-	0.680	0
5	ROCKS1N5 (0.53g)	-	0.685	0
6	ROCKS1N6 (0.42g)	-	0.795	0
7	ROCKS1N7 (0.36g)	-	0.781	0
8	ROCKS1P1 (0.71g)	-	0.865	0
9	ROCKS1P2 (0.44g)	-	0.748	0
10	ROCKS1P3 (0.48g)	-	0.717	0
11	ROCKS1P4 (0.32g)	-	0.677	0
12	ROCKS1P5 (0.67g)	-	0.726	0
13	ROCKS1P6 (0.41g)	-	0.792	0
14	ROCKS1P7 (0.4g)	-	0.717	0
15	-	ROCKS1N1 (0.7g)	0.125	3.59
16	-	ROCKS1N2 (0.38g)	0.042	1.34
17	-	ROCKS1N3 (0.32g)	0.022	1.01
18	-	ROCKS1N4 (0.34g)	0.047	1.57
19	-	ROCKS1N5 (0.53g)	0.052	1.74
20	-	ROCKS1N6 (0.42g)	0.046	2.14
21	-	ROCKS1N7 (0.36g)	0.038	1.58
22	-	ROCKS1P1 (0.71g)	0.125	3.62
23	-	ROCKS1P2 (0.44g)	0.051	1.34
24	-	ROCKS1P3 (0.48g)	0.054	1.74
25	-	ROCKS1P4 (0.32g)	0.048	1.59
26	-	ROCKS1P5 (0.67g)	0.121	3.41
27	-	ROCKS1P6 (0.41g)	0.048	2.16
28	-	ROCKS1P7 (0.4g)	0.028	0.96

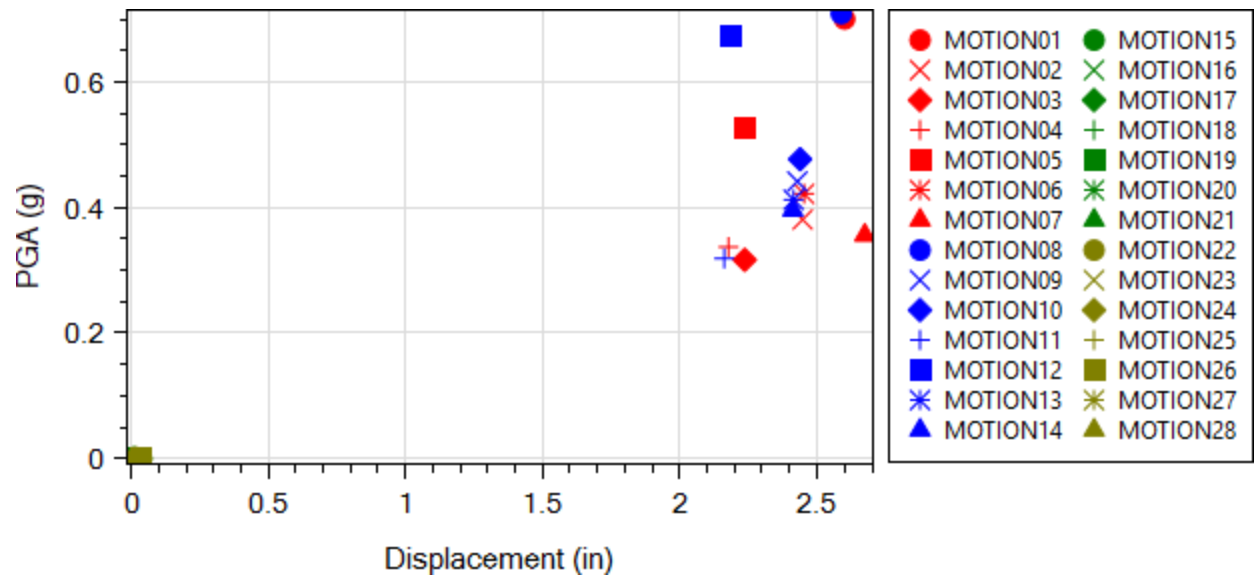


Figure 3.19 Bridge deck maximum longitudinal displacement

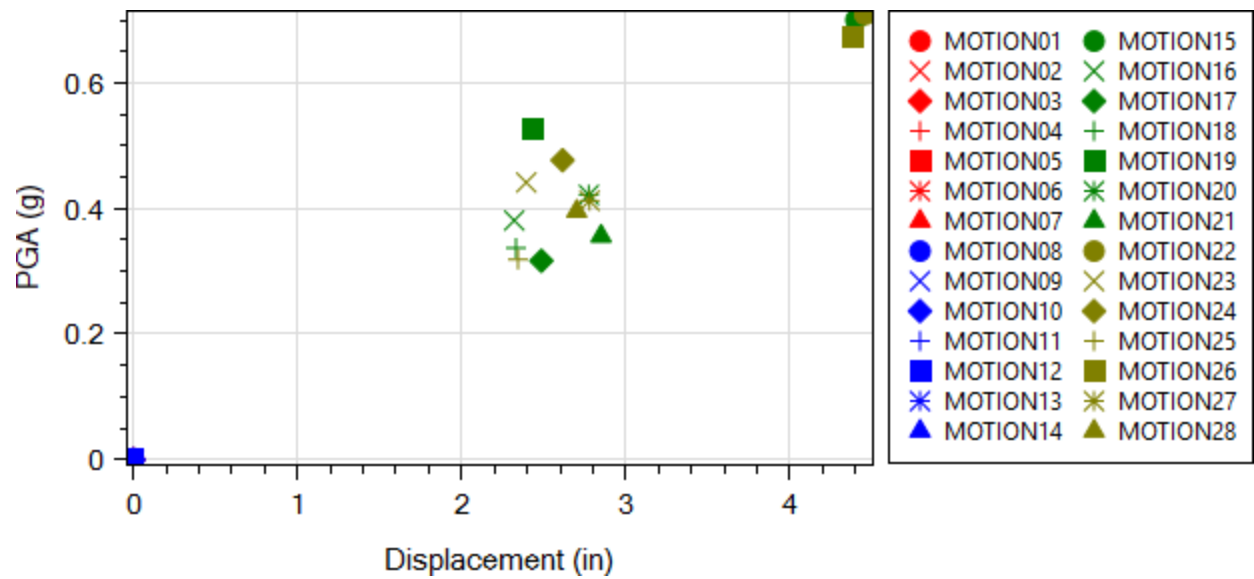


Figure 3.20 Bridge deck maximum transverse displacement

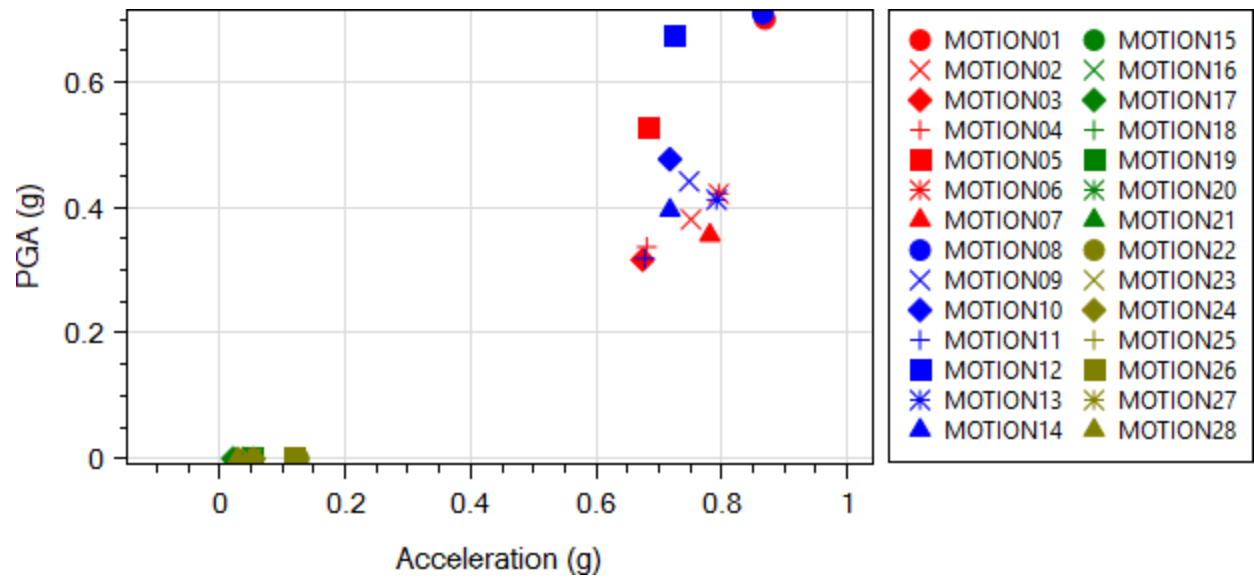


Figure 3.21 Bridge deck maximum longitudinal acceleration

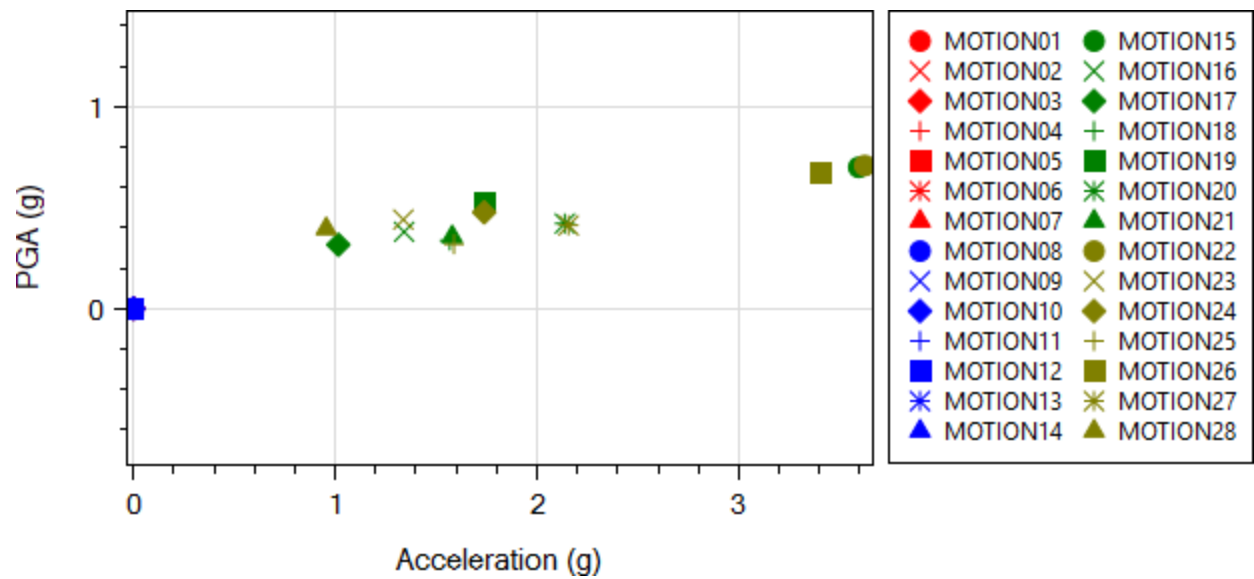


Figure 3.22 Bridge deck maximum transverse acceleration

3.9.3.2 Response Time History

In this section, response time histories for Pier S-8 (see Figure 3.4) from 2 representative simulations (Simulations 1 and 8) are presented (Longitudinal seismic excitation).

1) Simulation 1 (motion ROCKS1N1)

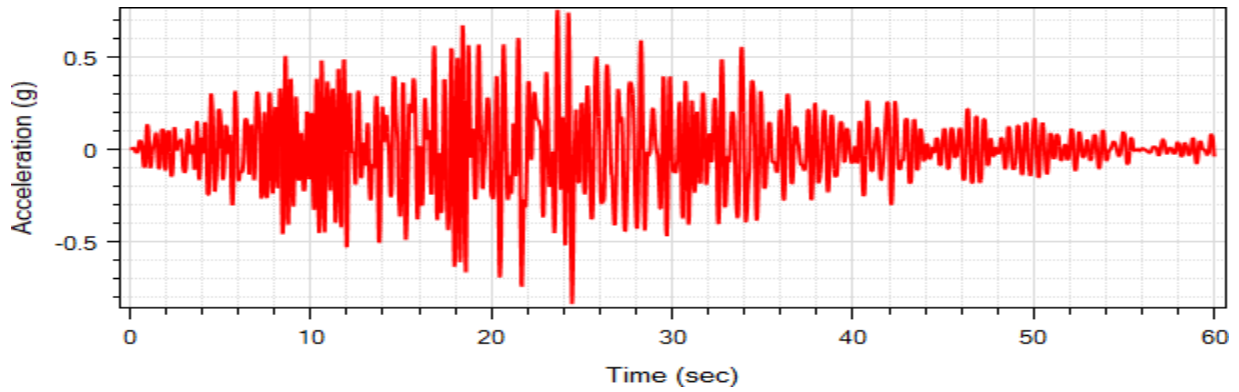
For Simulation 1, the deck maximum displacement is 2.6 in (Table 3.15). The pier top longitudinal response time histories at Pier S-8 are displayed in Figure 3.23 where the displacement time history refers to the displacement at the pier top. The input motion ROCKS1N1 is shown in Figure 3.23d for reference.

Figure 3.24 displays the moment-curvature response at the pier top. A maximum bending moment of 19,500 kip-ft was reached (Figure 3.24). The deformed mesh when the deck maximum displacement was reached (i.e., 2.6 in as shown in Table 3.15) is shown in Figure 3.25.

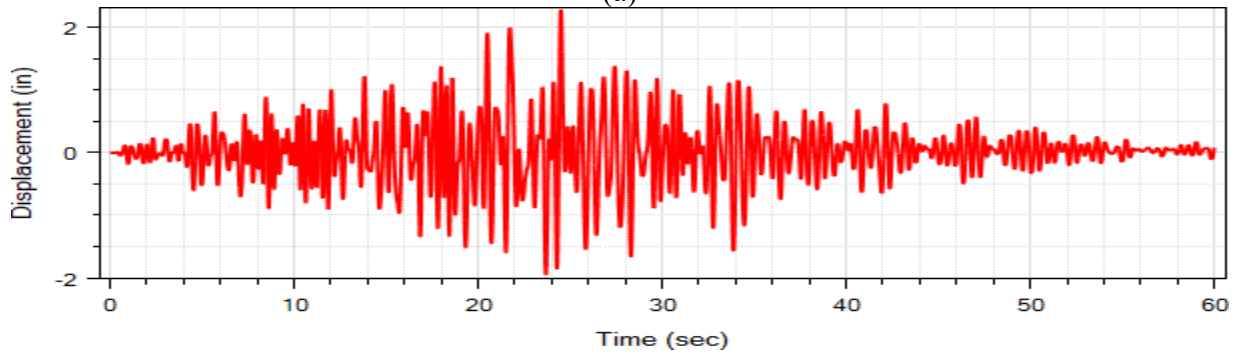
2) Simulation 8 (motion ROCKS1P1)

For Simulation 8, the deck maximum displacement is 2.59 in (Table 3.15). The pier top longitudinal response time histories at Pier S-8 are displayed in Figure 3.26. The input motion ROCKS1P1 is shown in Figure 3.26d for reference.

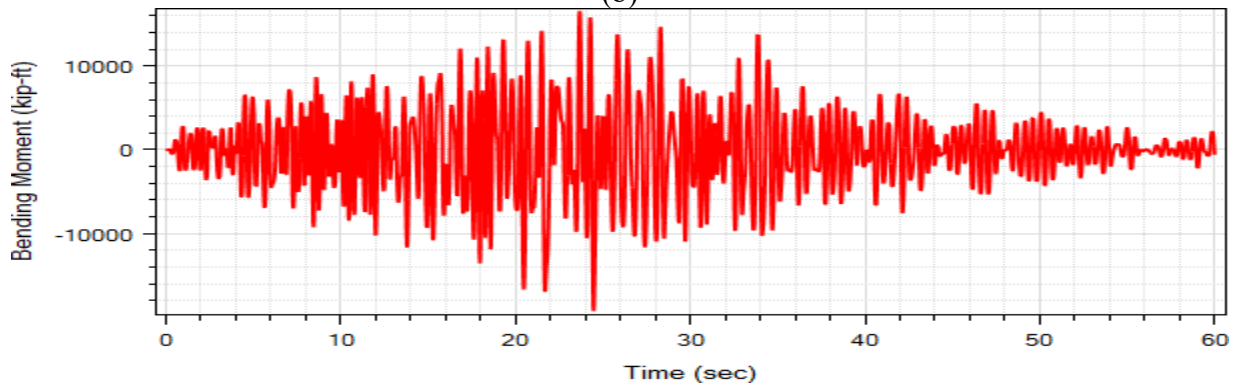
Figure 3.27 displays the moment-curvature response at the pier top. A maximum bending moment of 19,200 kip-ft was reached (Figure 3.27). The deformed mesh when the deck maximum displacement was reached (i.e., 2.59 in as shown in Table 3.15) is shown in Figure 3.28.



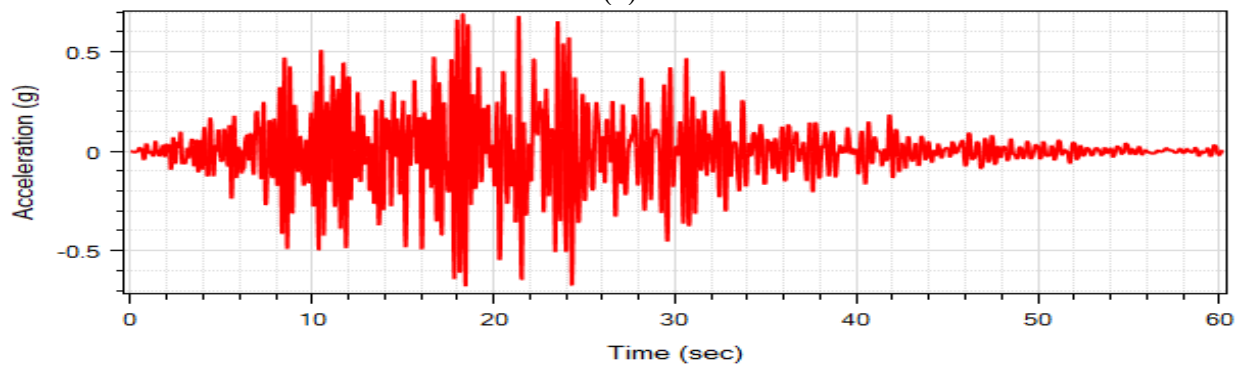
(a)



(b)



(c)



(d)

Figure 3.23 Pier S-8 column top longitudinal response time histories for Simulation 1: (a) acceleration; (b) displacement; (c) bending moment; (d) base excitation ROCKS1N1

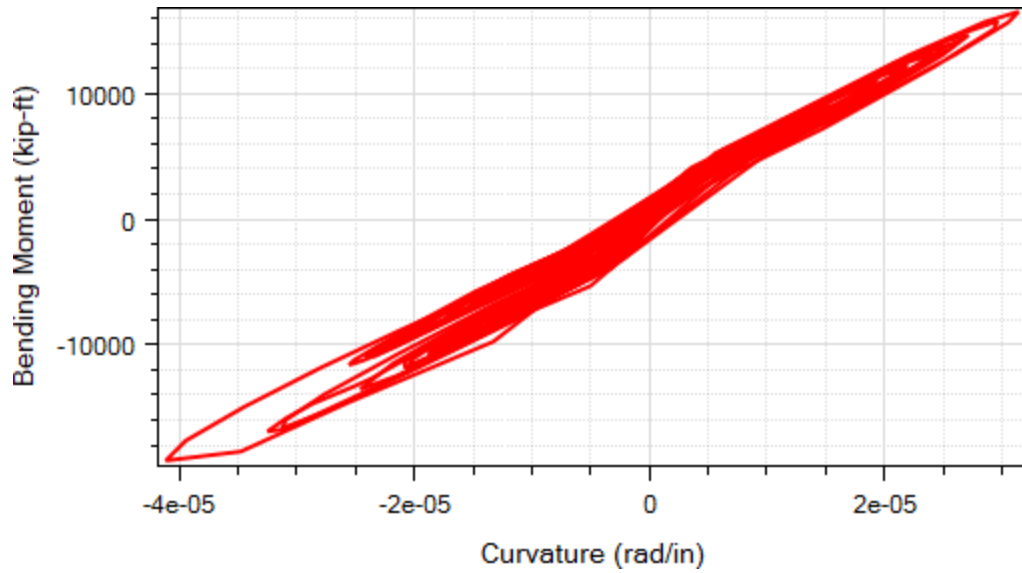


Figure 3.24 Pier S-8 column top longitudinal moment-curvature response for Simulation 1

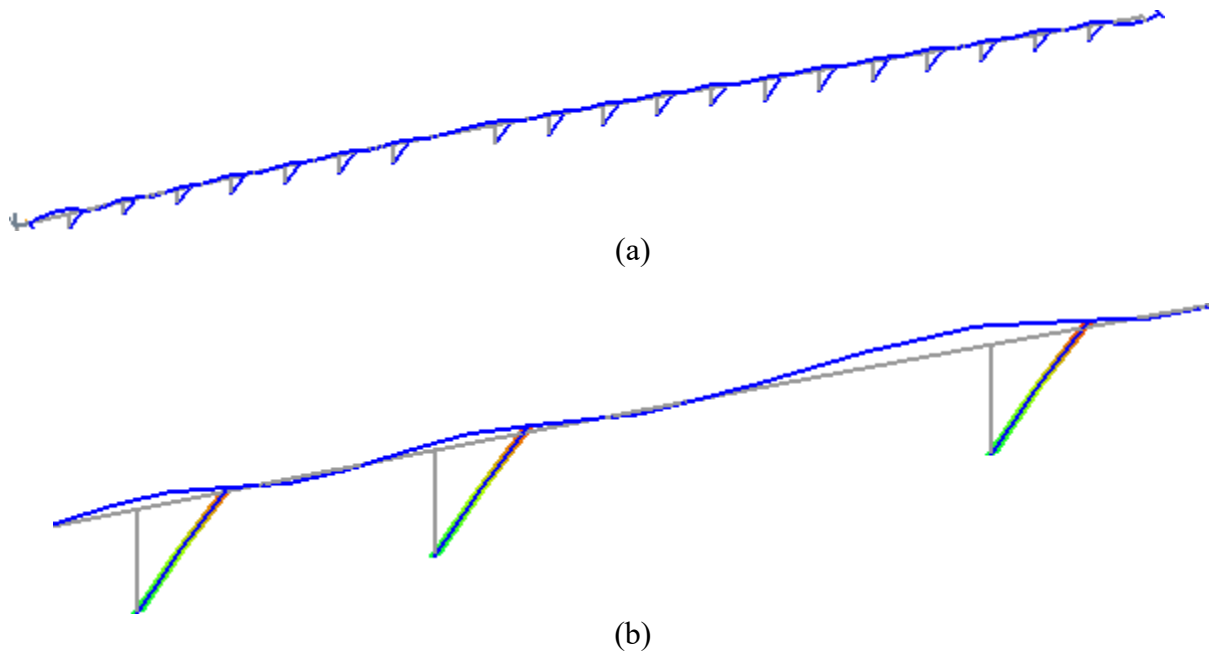
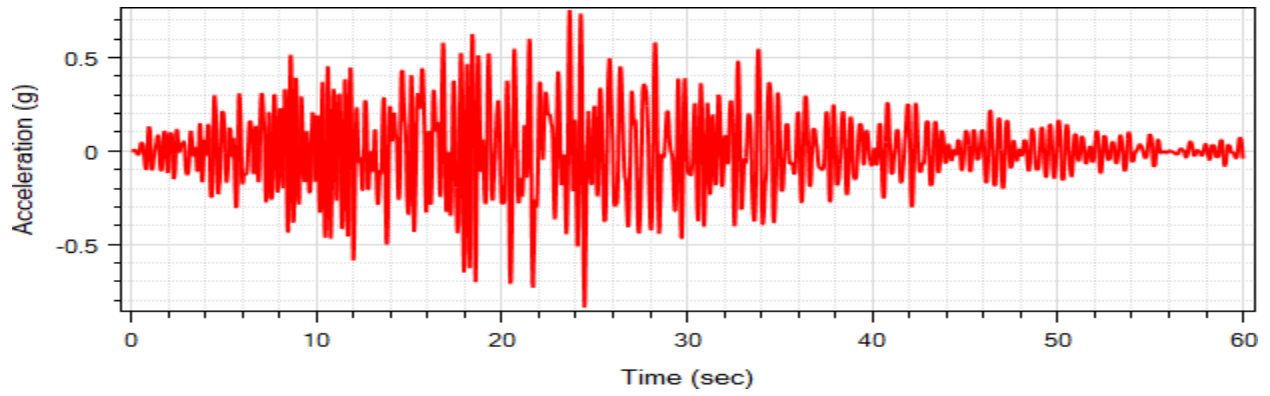
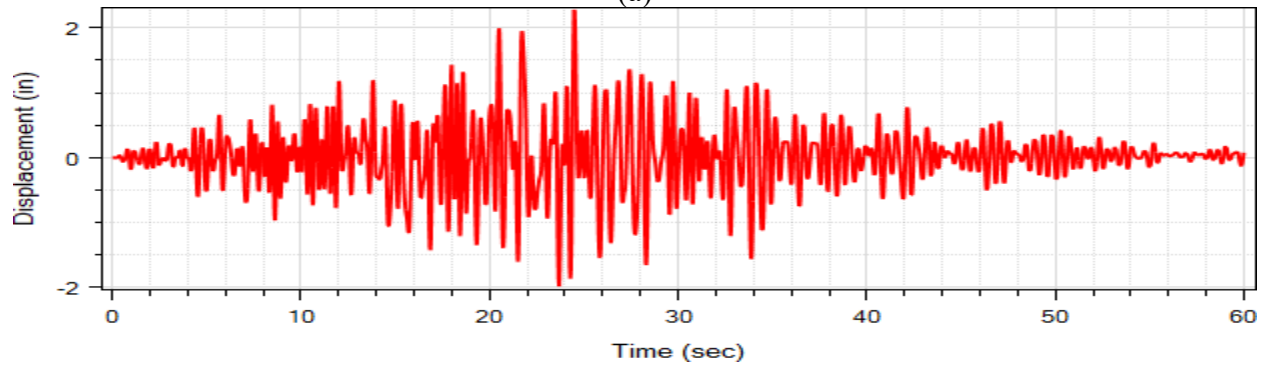


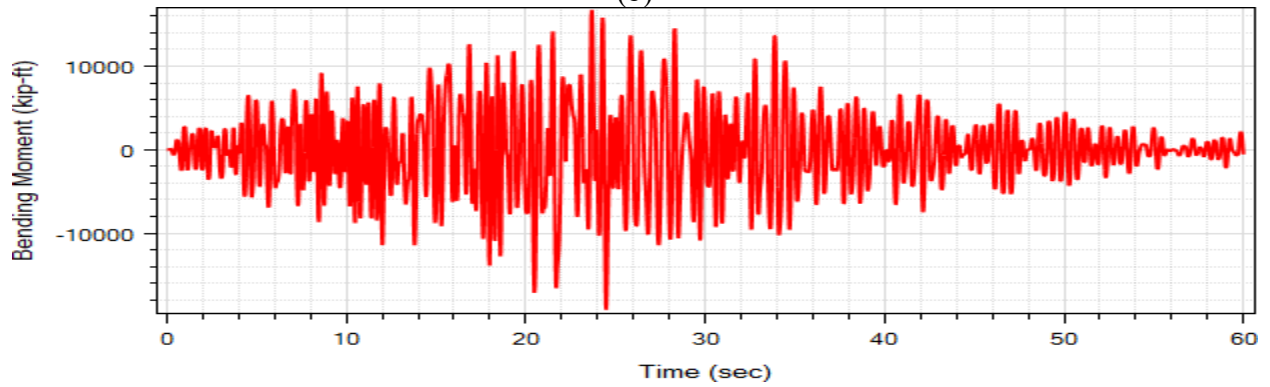
Figure 3.25 Deformed mesh (factor of 200) for Simulation 1 at the maximum displacement step (grey lines represent undeformed mesh): (a) entire bridge; (b) close-up of Bents 6, 7, and 8 (from left to right)



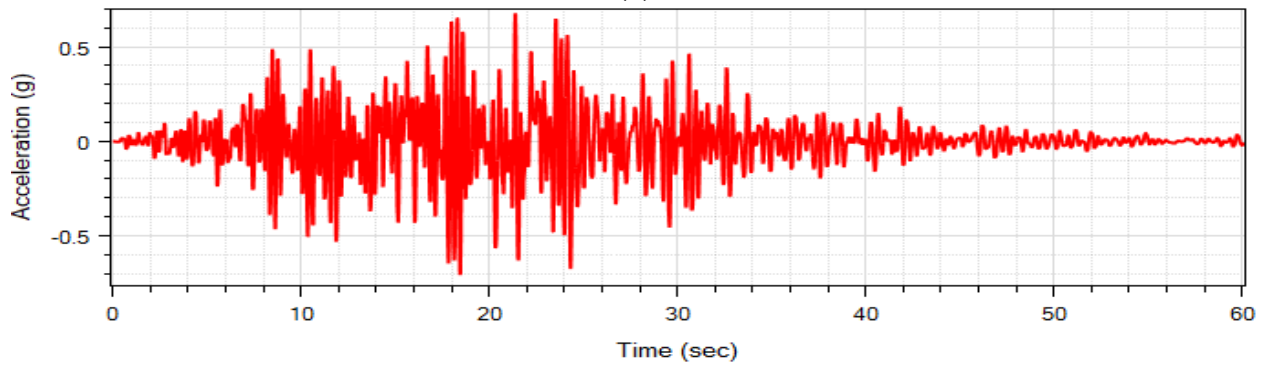
(a)



(b)



(c)



(d)

Figure 3.26 Pier S-8 column top longitudinal response time histories for Simulation 8: (a) acceleration; (b) displacement; (c) bending moment; (d) base excitation ROCKS1P1

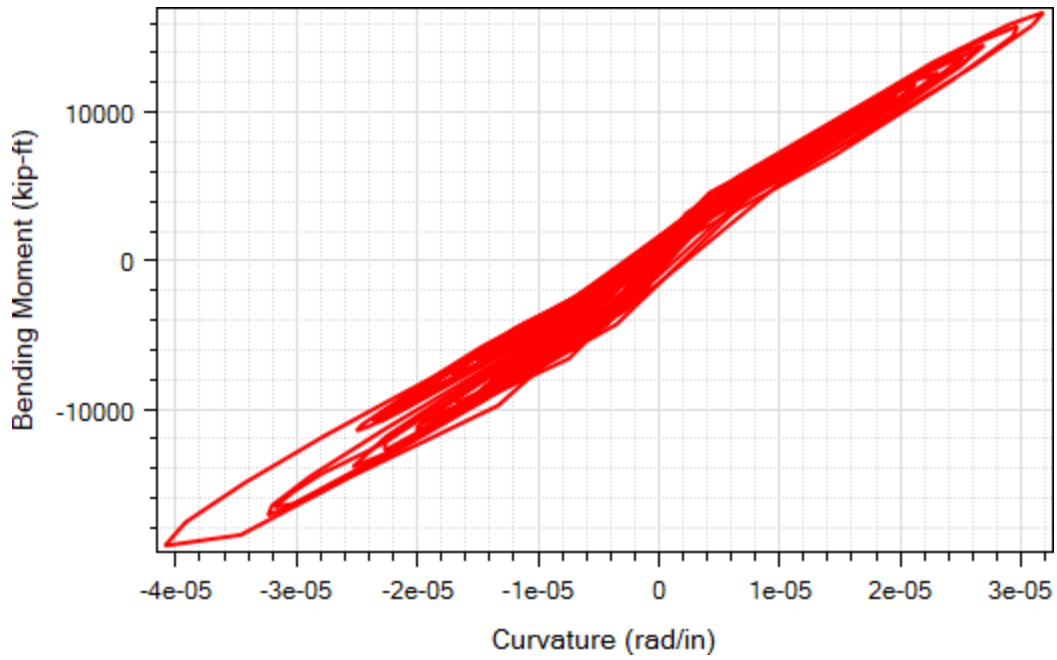


Figure 3.27 Pier S-8 column top longitudinal moment-curvature response for Simulation 8

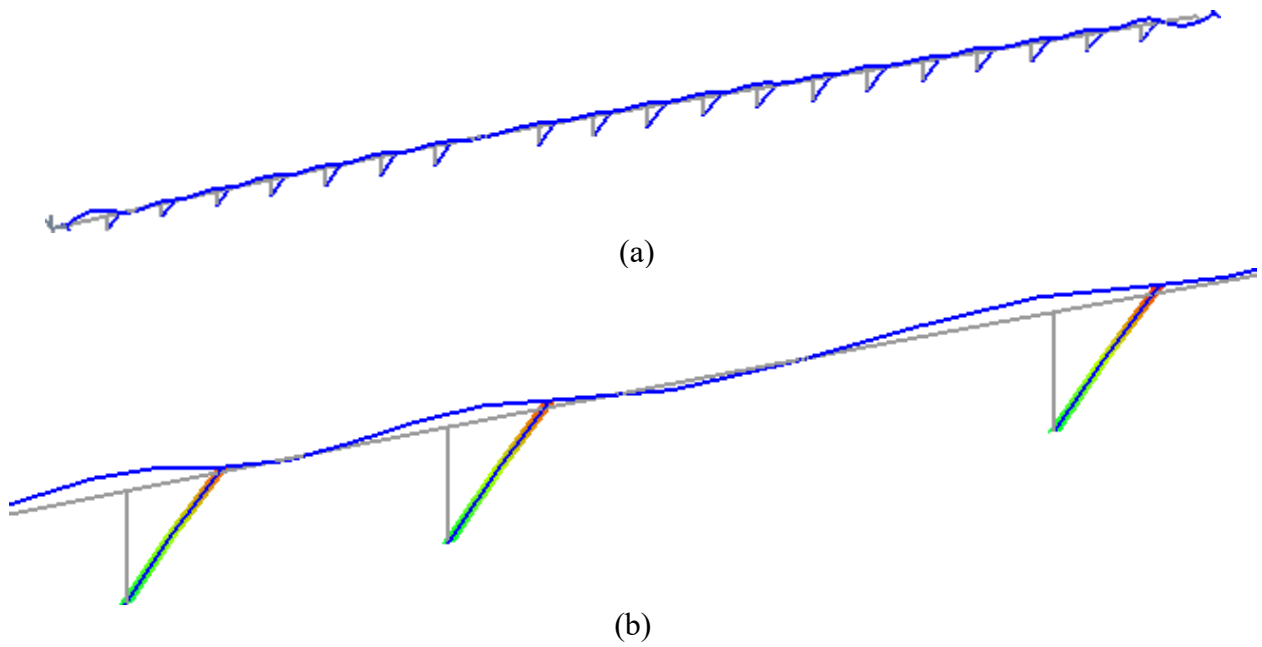


Figure 3.28 Deformed mesh (factor of 200) for Simulation 8 at the maximum displacement step (grey lines represent undeformed mesh): (a) entire bridge; (b) close-up of Bents 6, 7, and 8 (from left to right)

3.9.4 Summary

Samoa Bridge with a stiff foundation matrix was modeled in OpenSees. A recently developed user interface MSBridge was employed for pre- and post-processing in the conducted OpenSees analysis. Nonlinear THA was conducted for the 14 input motions provided by Caltrans. The average THA maximum displacement is 2.4 inches in the bridge longitudinal direction and 2.9 inches in the transverse direction. ESA was also conducted for Samoa Bridge using MSBridge.

3.9.5 Conclusions

1. For the employed ESA spectrum, column displacement demand was 3.0 inches in the longitudinal direction and 4.0 inches in the transverse direction.
2. For the investigated set of ground motions in the OpenSees analysis:
 - 2.1 In the longitudinal direction, none of the shaking events resulted in column displacement demand that exceeded that of the ESA.
 - 2.2 In the transverse direction, about 21% of the shaking events resulted in column displacement demand that exceeded that of the ESA. This demand reached a maximum of 12% in excess of that from the corresponding ESA.

4 THE EUREKA CHANNEL BRIDGE

4.1 Bridge Description

The 15-span Eureka Channel Bridge (hereinafter referred to as “Eureka Bridge”, Figure 4.1) near Eureka in northern California is a 1,815.75 ft (553.44 m) long and 34 ft (10.36 m) wide structure, supported by 14 single hexagonal concrete pier bents on pile group foundations (Figure 4.2). From Abutment 1 at south-bound, the alignment of span has a 1,014.3 ft (309.157 m) length on a 1,800 ft (548.64 m) radius curve and a 802.4 ft (244.573 m) straight segment at Abutment 16 to north-bound. The bridge piers are labeled from the Eureka area to Samoa area as Pier E-1 (abutment), Pier E-2, Pier E-3 and so on. Length of span is in a range of 81 ft (24.69 m) to 190 ft (57.91 m) with main channel between pier 7 and pier 8.



(a)



(b)

Figure 4.1 Bridge configuration: (a) Samoa Bridge, Eureka Geotechnical Array, Middle Channel Bridge and Eureka Bridge (Map Data @ 2015 Google) and (b) photo of the Eureka Bridge (<http://www.strongmotioncenter.org>)

Eureka Bridge is heavily instrumented as shown in Figure 4.2 in order to record any significant earthquake excitation. There are 27 accelerometers in total on the Eureka Bridge System, including 18 accelerometers on the bridge structure, 6 accelerometers on the pile foundations, and 3 accelerometers at a nearby free field site. Sensors on the structure are oriented in the longitudinal and transverse direction of the bridge and sensors at the free field are oriented in the north-south, east-west and vertical directions.

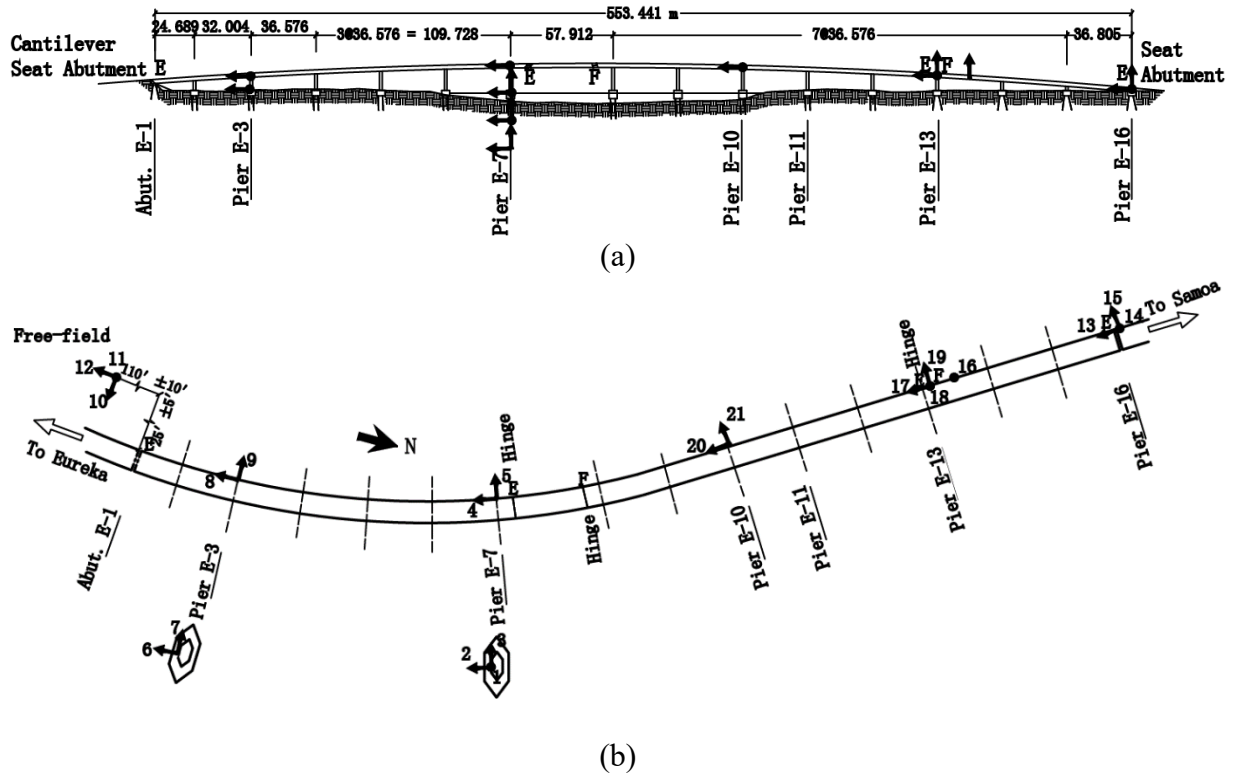


Figure 4.2 Layout of instrumentation at Eureka Bridge (<http://www.strongmotioncenter.org>): (a) elevation view; (b) plan view

4.2 Geometric Configuration

Figure 4.3 shows the elevation view of Eureka Bridge. Moreover, Figure 3.3b shows the column reinforcement details at Pier E-7. Precast pre-stressed concrete I-girders along with cast-in-place concrete slabs (16.5 cm of thickness) are supported on concrete seat-type abutments and the hammerhead cap beams of column type piers. The height of the columns/piers ranges from 7.8 ft (2.39 m; for Pier E-15) to 40.2 ft (12.25 m; for Pier E-6) as depicted in Figure 4.2. The offset between column top and the deck was not represented in this study and no column top rigid link. Moreover, Table 4.1 shows the column heights for each pier.

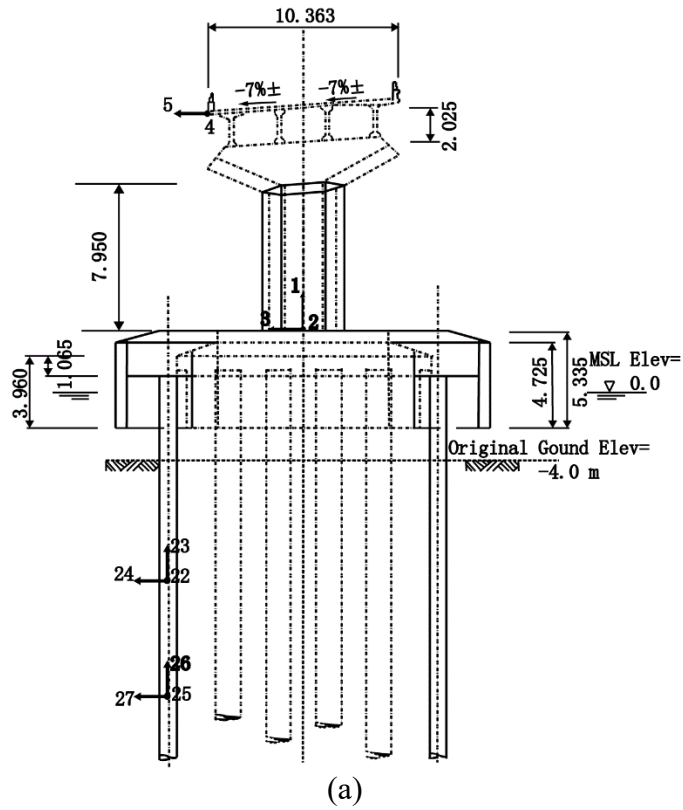


Figure 4.3 Eureka Bridge: (a) elevation and bridge deck

Table 4.1. Column Heights for Eureka Bridge

Pier # (see Figure 4.2a)	Column Height (ft)
Pier E-2	32.40
Pier E-3	37.57
Pier E-4	42.41
Pier E-5	45.89
Pier E-6	53.00
Pier E-7	42.24
Pier E-8	40.59
Pier E-9	39.28
Pier E-10	35.08
Pier E-11	39.50
Pier E-12	32.95
Pier E-13	26.36
Pier E-14	21.81
Pier E-15	19.54

4.3 OpenSees Finite Element Modeling

The employed modeling techniques and associated model properties are presented in APPENDIX F. To facilitate the conducted analyses, a recently developed user interface MSBridge was employed (please see Appendix A for more information about MSBridge). Figure 4.4 shows the Eureka Bridge model created in MSBridge. The pier columns were modeled using the nonlinear Fiber section and the forceBeamColumn (with the distributed plasticity integration method) element was employed as shown in APPENDIX G. The deck was considered linearly elastic and the bentcap was ignored (the pier column top was considered to extend to the deck CG). Elastic abutment model was employed (for simplicity). The pier column base was not fixed. Instead, the Foundation Matrix technique (see Section 3.3 for the further discussion) was employed to model the pier column base.

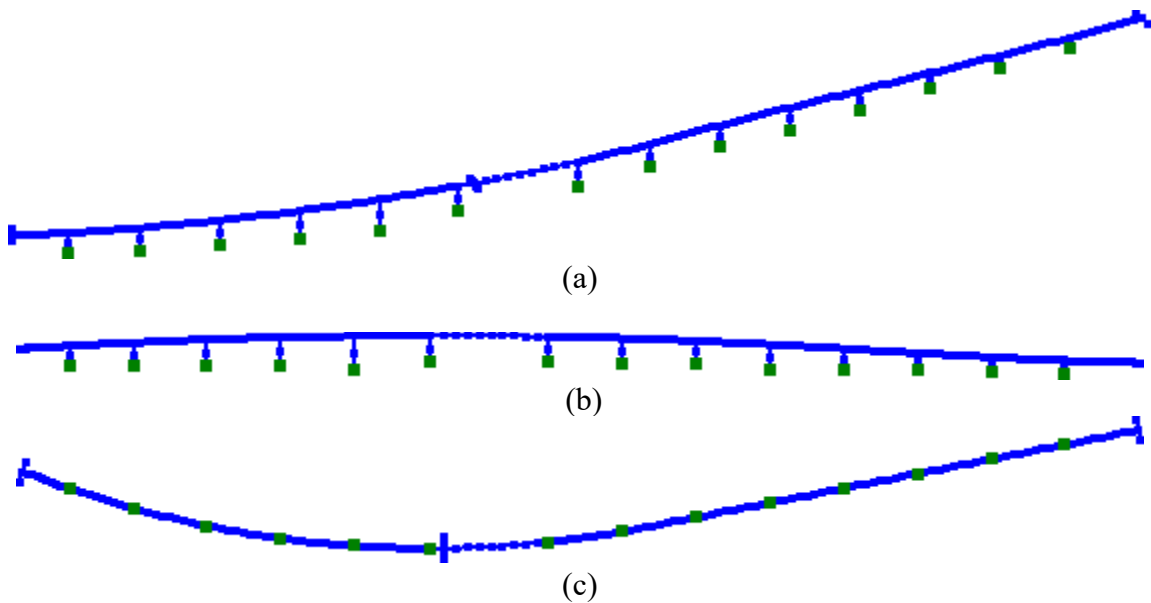


Figure 4.4 Eureka Bridge FE mesh created in MSBridge: (a) 3D view; (b) elevation view; (c) plan view

4.4 Mode Shape Analysis

This section shows the response from Mode shape analysis. The natural periods of the first five modes are listed in Table 4.2, and the corresponding mode shapes are shown in Figure 4.5.

Table 4.2. Natural Periods and Frequencies for Eureka Bridge

Mode	Natural Period (sec)	Natural Frequency (Hz)
1	1.24	0.80
2	1.18	0.85
3	1.02	0.98
4	0.89	1.12
5	0.85	1.18

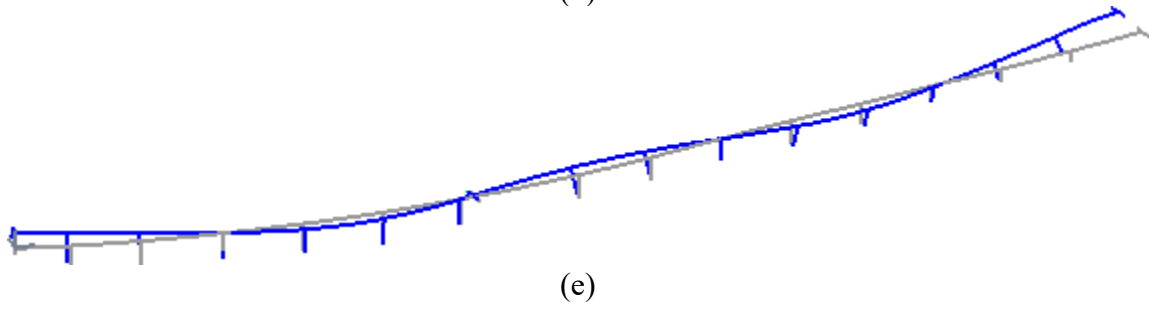
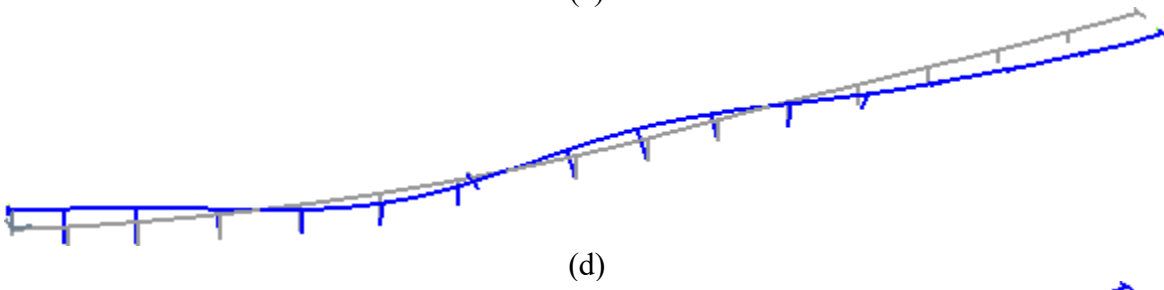
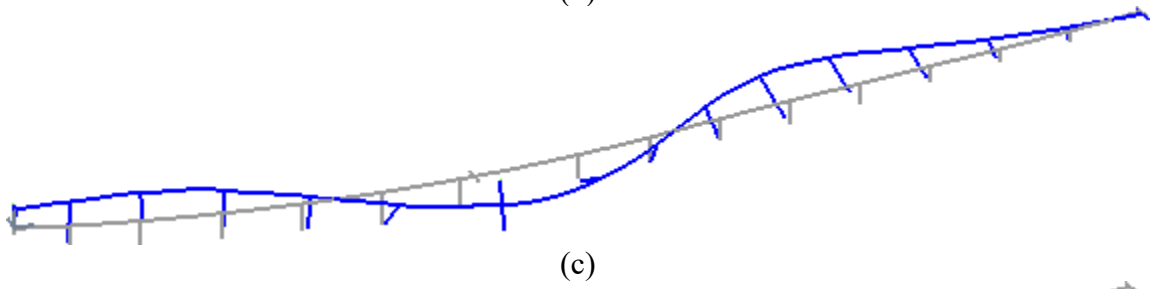
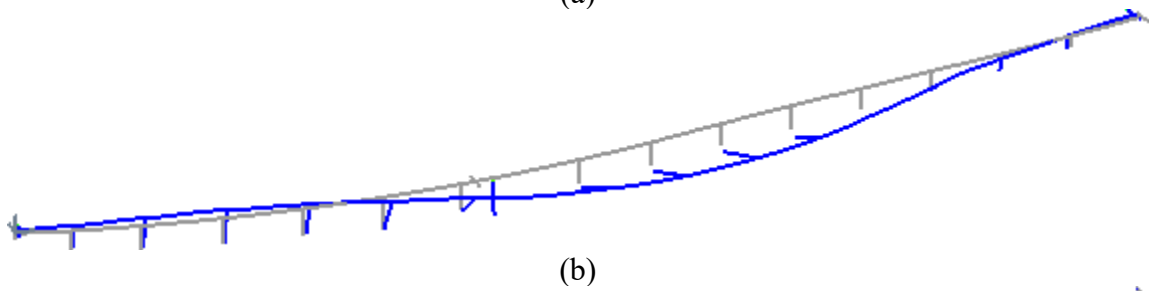
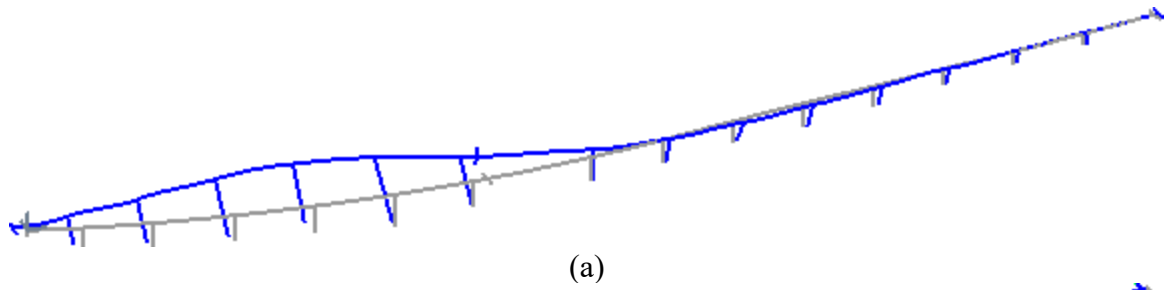


Figure 4.5 Mode shapes for Eureka Bridge: (a) first mode; (b) second mode; (c) third mode; (d) fourth mode; and (e) fifth mode

4.5 Equivalent Static Analysis (ESA)

ESA was conducted for Eureka Bridge in the bridge longitudinal and transverse directions. For the procedure to conduct ESA in MSBridge, please refer to the MSBridge user manual (Elgamal *et al.* 2014). Figure 4.6 shows the ARS curve employed in the ESA.

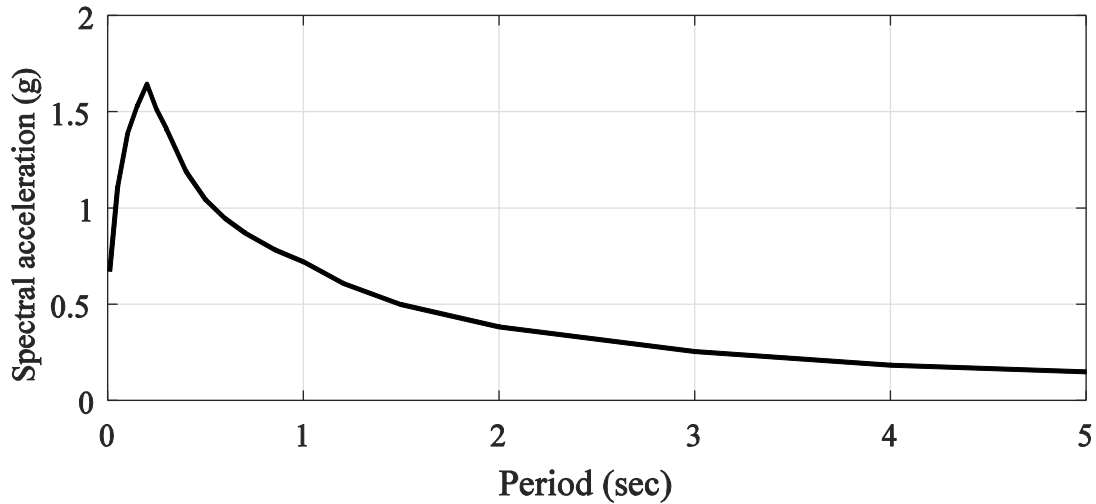


Figure 4.6 ARS curve employed in the ESA

4.5.1 ESA in the Longitudinal Direction

The entire bridge system (Figure 4.4) was employed in the longitudinal ESA. The bridge system was pushed along the bridge deck (longitudinal) direction until initial yielding occurred (when the curvature reached 5×10^{-5} rad/in based on the moment-curvature shown in Figure E.1). The pushover load was applied at the bridge center.

Table 4.3 lists the parameters related to the longitudinal ESA. The pushover load at initial yielding was about 42% of the tributary dead load (Table 4.3). Table 4.4 shows the longitudinal ESA result for Eureka Bridge. The displacement demand is 6.1 in for the longitudinal ESA (Table 4.4).

4.5.2 ESA in the Transverse Direction

Transverse ESA was conducted for Pier E-6 (Pier E-6 was chosen in order to compare ESA and THA results later on, since maximum displacement in the THA occurs in Pier E-6). The pier was pushed along the bridge transverse direction (Figure 4.4) until initial yielding occurred (when the curvature reached 3×10^{-5} rad/in based on the moment-curvature shown in Figure E.2). The pushover load was applied at the pier top (Figure 4.4).

Table 4.5 lists the parameters related to the transverse ESA. Table 4.6 shows the transverse ESA result for Eureka Bridge. The displacement demands for Pier E-6 is 13.1 inches for the transverse ESA (Table 4.6).

Table 4.3. Longitudinal ESA Parameters for Eureka Bridge

Parameter	Value
Tributary dead load (kip)	14,586.9
Tributary mass (kip-sec ² /in)	37.8
Pushover load at initial yielding (kip)	6,126.5
Yield displacement (in)	3.4
Initial stiffness (kip/in)	1807.1
Period (sec)	0.9

Table 4.4. Longitudinal ESA Result for Eureka Bridge

Parameter	Longitudinal Direction
Displacement Demand (in)	6.1

Table 4.5. Transverse ESA Parameters for Pier E-6

Parameter	Value
Tributary dead load (kip)	1,080.64
Tributary mass (kip-sec ² /in)	2.8
Pushover load at initial yielding (kip)	459
Yield displacement (in)	12.5
Initial stiffness (kip/in)	36.7
Period (sec)	1.74

Table 4.6. Transverse ESA Result for Eureka Bridge

Pier # (see Figure 4.2a)	Displacement Demand in Transverse Direction (in)
Pier E-6	13.1

4.6 Nonlinear Time History Analysis

Nonlinear THA was conducted for the 14 input motions provided by Caltrans (see APPENDIX B for the characteristics of the 14 motions). The input motions were applied directly at the column base as well as at both abutments.

Rayleigh damping was used with a 5% damping ratio (defined at the periods of 1.24 and 0.94 second) in the nonlinear THA. For the time integration scheme, the Newmark average acceleration method ($\gamma = 0.5$ and $\beta = 0.25$) was employed.

Variable time-stepping scheme (`VariableTransient`) was used in the analysis. The starting value for each step was 0.005 second (same as the time step of the input motions) and the minimum time step was 5×10^{-5} second (upon splitting of time step when needed).

4.6.1 Maximum Displacement and Acceleration

Table 4.7 lists Eureka Bridge deck maximum displacement for the 28 simulations from the nonlinear THA. Among the simulations with longitudinal component only (Simulations 1-14), Simulation 14 (motion ROCKS1P7) gave the least maximum displacement (4.0 in) while Simulation 9 (motion ROCKS1P2) gave the largest maximum displacement (5.5 in). Note that the deck maximum displacement is recorded in the local coordinate system (APPENDIX A). Thus, the longitudinal maximum displacement refers to the displacement along the tangential direction of the bridge at a given superstructure location. The maximum displacement of Table 4.7 are also presented in graphical format against PGA in Figure 4.7 and Figure 4.8.

Table 4.8 list Eureka Bridge deck maximum acceleration for the 28 simulations. Among the simulations with longitudinal component only (Simulations 1-14), Simulation 4 (motion ROCKS1N4) gave the least maximum acceleration (0.73g) while Simulation 9 (motion ROCKS1P2) gave the largest maximum acceleration (1.05g). Note that the deck maximum acceleration also is recorded in the local coordinate system (APPENDIX A). Thus, the longitudinal maximum acceleration refers to the acceleration along the tangential direction of the bridge at a given superstructure location. The maximum acceleration of Table 4.8 are also presented in graphical format against PGA in Figure 4.9 and Figure 4.10.

Table 4.7. Eureka Bridge Deck Maximum Displacement

Simulation	Longitudinal Input	Transverse Input	Longitudinal Displacement (in)	Transverse Displacement (in)
1	ROCKS1N1 (0.7g)	-	4.4	3.3
2	ROCKS1N2 (0.38g)	-	5.2	3.1
3	ROCKS1N3 (0.32g)	-	4.2	3.7
4	ROCKS1N4 (0.34g)	-	4.1	4.5
5	ROCKS1N5 (0.53g)	-	5.0	3.4
6	ROCKS1N6 (0.42g)	-	4.1	3.9
7	ROCKS1N7 (0.36g)	-	3.5	3.3
8	ROCKS1P1 (0.71g)	-	4.5	3.3
9	ROCKS1P2 (0.44g)	-	5.5	3.1
10	ROCKS1P3 (0.48g)	-	4.6	3.4
11	ROCKS1P4 (0.32g)	-	4.2	4.5
12	ROCKS1P5 (0.67g)	-	4.2	3.3
13	ROCKS1P6 (0.41g)	-	4.1	3.9
14	ROCKS1P7 (0.4g)	-	4.0	3.6
Average			4.4	
15	-	ROCKS1N1 (0.7g)	6.0	15.5
16	-	ROCKS1N2 (0.38g)	4.6	12.6
17	-	ROCKS1N3 (0.32g)	7.1	19.2
18	-	ROCKS1N4 (0.34g)	5.7	16.9
19	-	ROCKS1N5 (0.53g)	3.5	8.7
20	-	ROCKS1N6 (0.42g)	4.5	12.1
21	-	ROCKS1N7 (0.36g)	4.8	12.1
22	-	ROCKS1P1 (0.71g)	6.0	15.4
23	-	ROCKS1P2 (0.44g)	4.6	12.5
24	-	ROCKS1P3 (0.48g)	3.6	9.2
25	-	ROCKS1P4 (0.32g)	5.7	17.0
26	-	ROCKS1P5 (0.67g)	4.1	9.4
27	-	ROCKS1P6 (0.41g)	4.6	12.0
28	-	ROCKS1P7 (0.4g)	7.1	19.0
Average				13.7

Notes:

- ESA longitudinal displacement demand is 6.1 in, corresponding to a difference of 27.5% (compared to the average THA maximum displacement of 4.4 in)
- ESA transverse displacement demand is 13.1 in, corresponding to a difference of 4.5% (compared to the average THA maximum displacement of 13.7 in)

Table 4.8. Eureka Bridge Deck Maximum Acceleration

Simulation	Longitudinal Input	Transverse Input	Longitudinal Acceleration (g)	Transverse Acceleration (g)
1	ROCKS1N1 (0.7g)	-	0.80	0.59
2	ROCKS1N2 (0.38g)	-	1.01	0.47
3	ROCKS1N3 (0.32g)	-	0.76	0.59
4	ROCKS1N4 (0.34g)	-	0.73	0.64
5	ROCKS1N5 (0.53g)	-	0.95	0.62
6	ROCKS1N6 (0.42g)	-	0.78	0.67
7	ROCKS1N7 (0.36g)	-	0.66	0.59
8	ROCKS1P1 (0.71g)	-	0.81	0.59
9	ROCKS1P2 (0.44g)	-	1.05	0.46
10	ROCKS1P3 (0.48g)	-	0.89	0.62
11	ROCKS1P4 (0.32g)	-	0.74	0.64
12	ROCKS1P5 (0.67g)	-	0.79	0.53
13	ROCKS1P6 (0.41g)	-	0.78	0.67
14	ROCKS1P7 (0.4g)	-	0.76	0.56
15	-	ROCKS1N1 (0.7g)	0.52	1.10
16	-	ROCKS1N2 (0.38g)	0.57	1.10
17	-	ROCKS1N3 (0.32g)	0.67	1.23
18	-	ROCKS1N4 (0.34g)	0.65	1.20
19	-	ROCKS1N5 (0.53g)	0.52	1.28
20	-	ROCKS1N6 (0.42g)	0.60	1.30
21	-	ROCKS1N7 (0.36g)	0.56	1.14
22	-	ROCKS1P1 (0.71g)	0.51	1.07
23	-	ROCKS1P2 (0.44g)	0.55	1.07
24	-	ROCKS1P3 (0.48g)	0.51	1.26
25	-	ROCKS1P4 (0.32g)	0.65	1.22
26	-	ROCKS1P5 (0.67g)	0.55	1.31
27	-	ROCKS1P6 (0.41g)	0.61	1.31
28	-	ROCKS1P7 (0.4g)	0.66	1.17

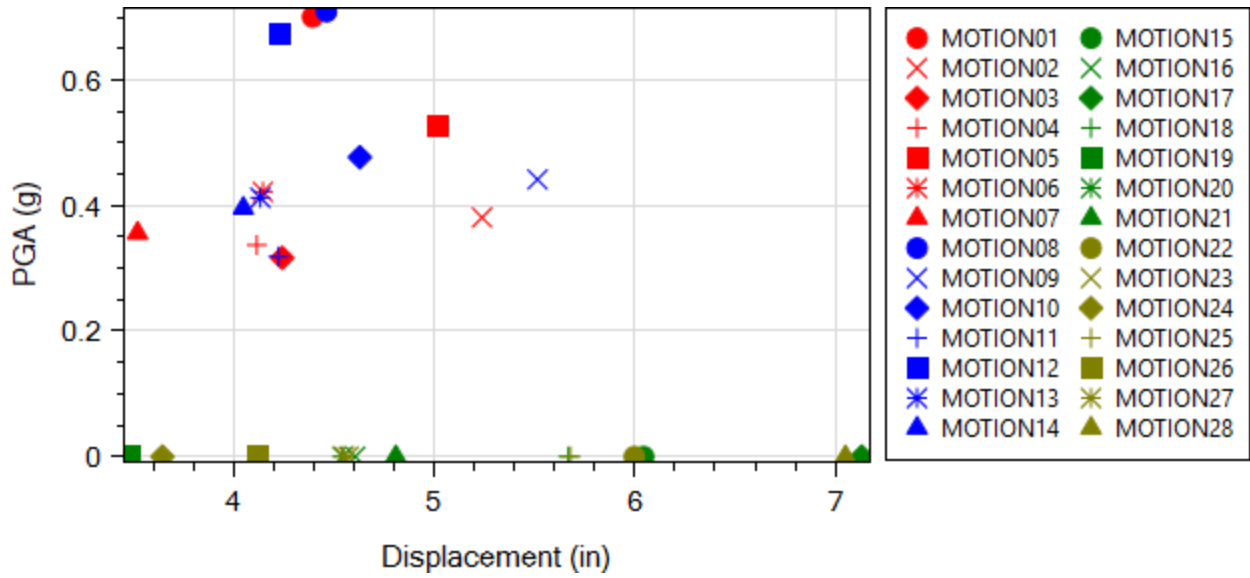


Figure 4.7 Bridge deck maximum longitudinal displacement

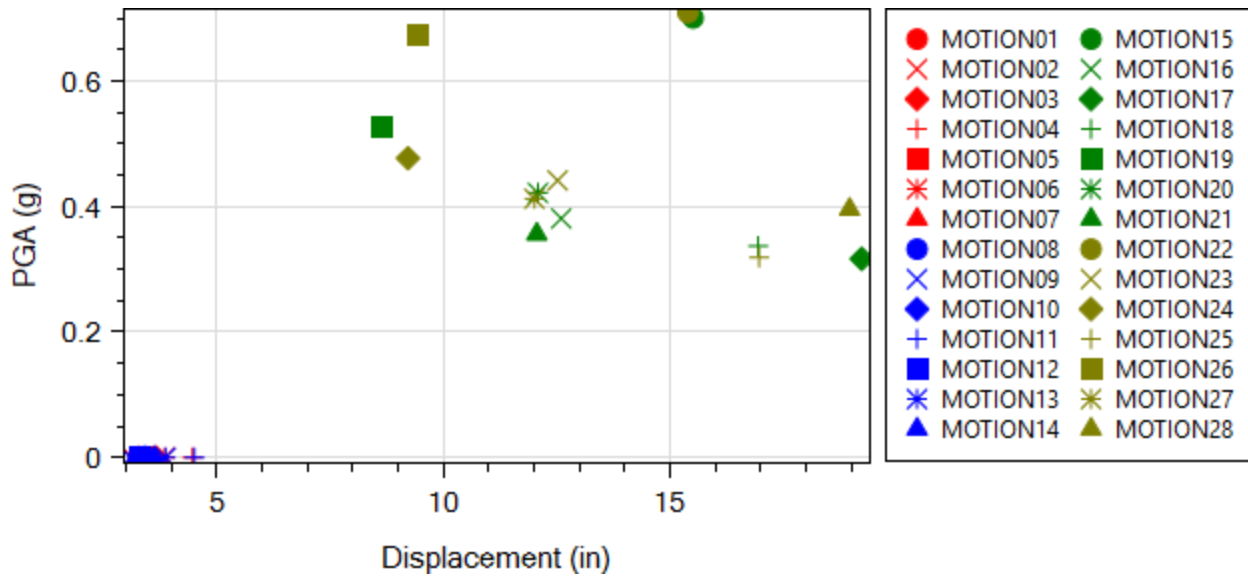


Figure 4.8 Bridge deck maximum transverse displacement

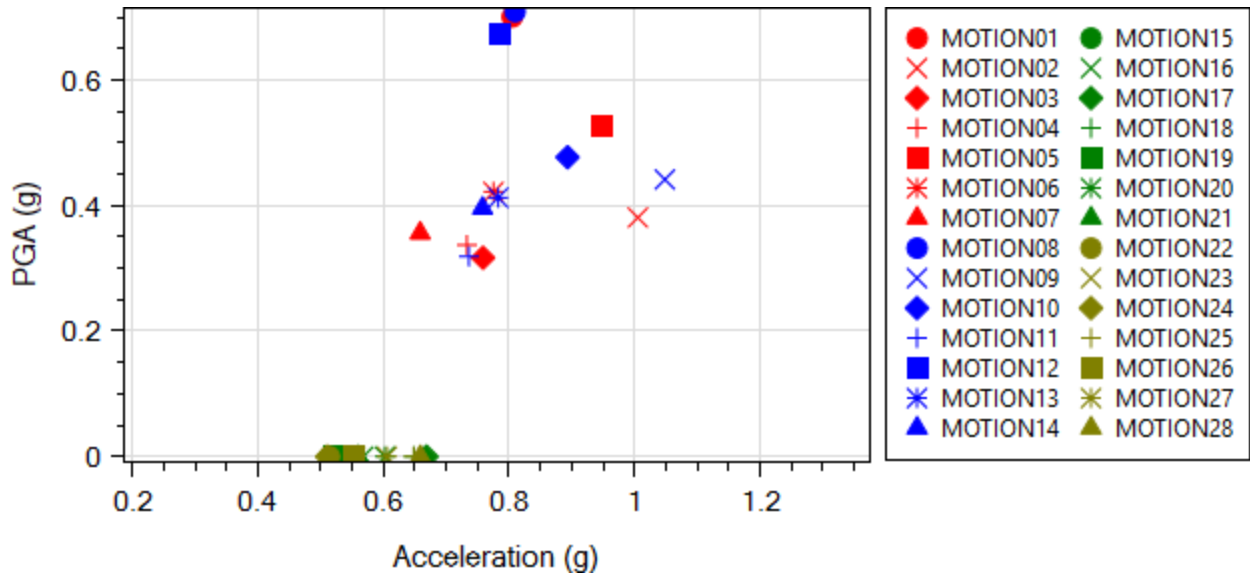


Figure 4.9 Bridge deck maximum longitudinal acceleration

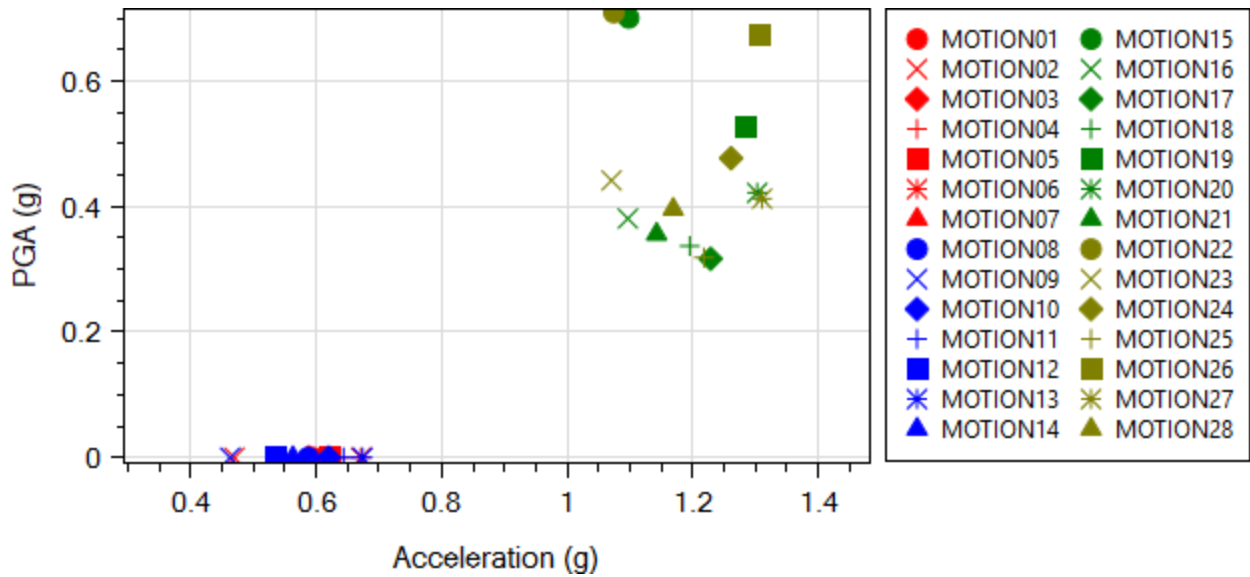


Figure 4.10 Bridge deck maximum transverse acceleration

4.6.2 Response Time History

In this section, response time histories for Pier E-7 (see Figure 4.4) from 2 representative simulations (Simulations 2 and 9) are presented (Longitudinal seismic excitation).

1) Simulation 2 (motion ROCKS1N2)

For Simulation 2, the deck maximum displacement is 5.2 in (Table 4.7). The pier top longitudinal response time histories for Pier E-7 are displayed in Figure 4.11 where the displacement time history refers to the displacement at the pier top. The input motion ROCKS1N2 is also shown in Figure 4.11d for reference.

Figure 4.12 displays the moment-curvature response at the pier top. A maximum bending moment of 22,400 kip-ft was reached (Figure 4.12). The deformed mesh when the deck maximum displacement was reached (i.e., 5.2 in as shown in Table 4.7) is shown in Figure 4.13.

2) Simulation 9 (motion ROCKS1P2)

For Simulation 9, the deck maximum displacement is 5.5 in (Table 4.7). The pier top longitudinal response time histories at Pier E-7 are displayed in Figure 4.14. The input motion ROCKS1P2 is also shown in Figure 4.14d for reference.

Figure 4.15 displays the moment-curvature response at the pier top for selected piers. A maximum bending moment of 20,900 kip-ft was reached for Pier E-7 (Figure 4.15). The deformed mesh when the deck maximum displacement was reached (i.e., 5.5 in as shown in Table 4.7) is shown in Figure 4.16.

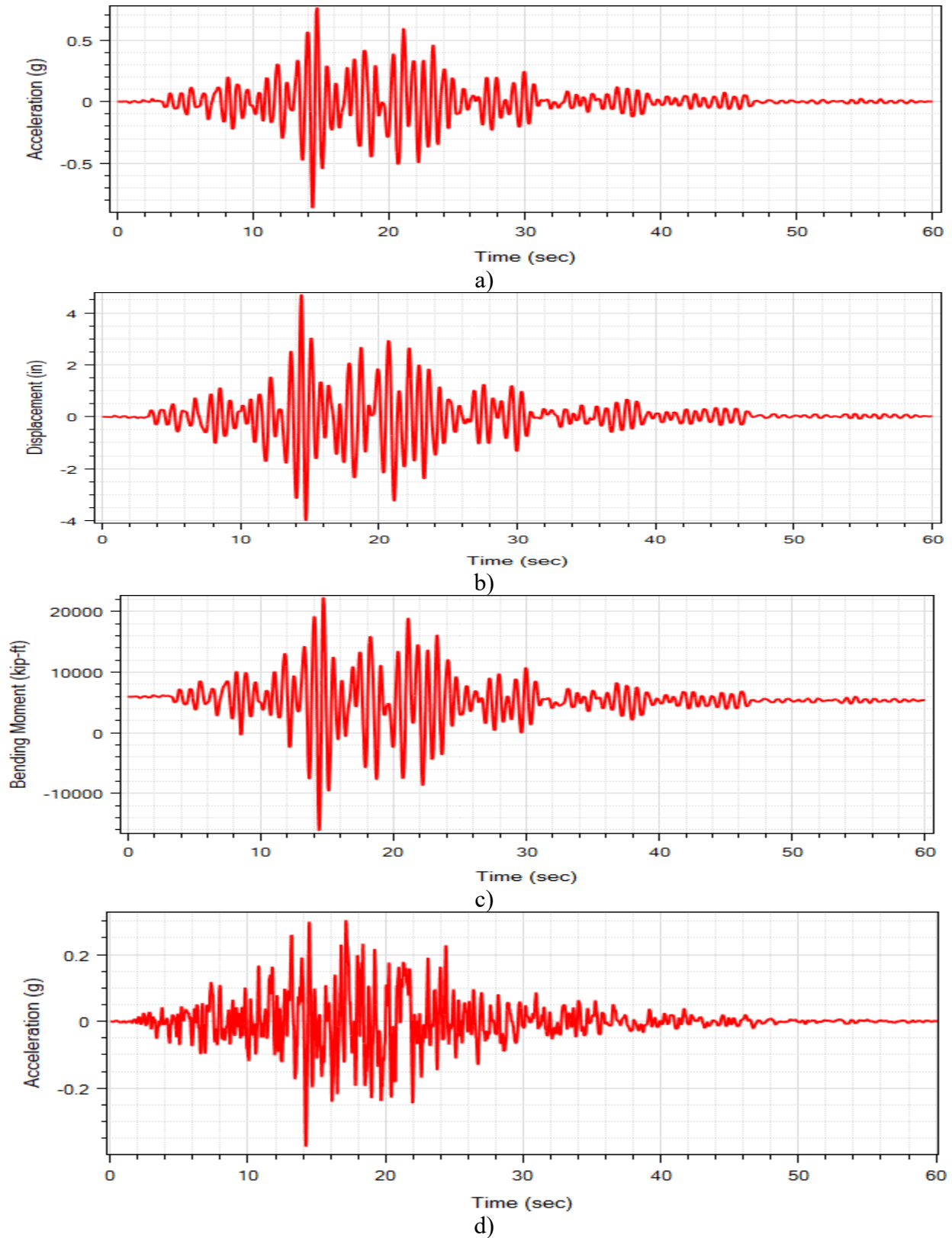
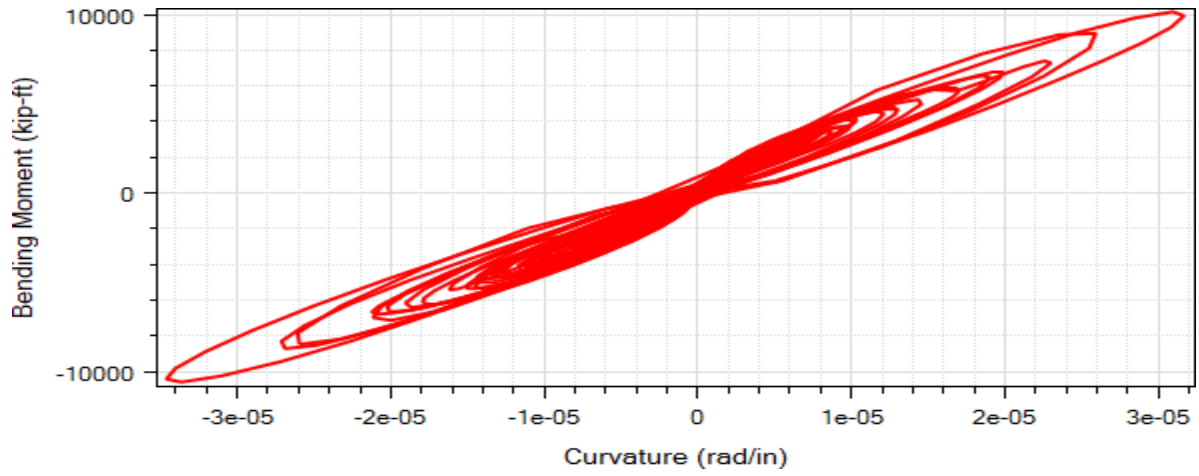
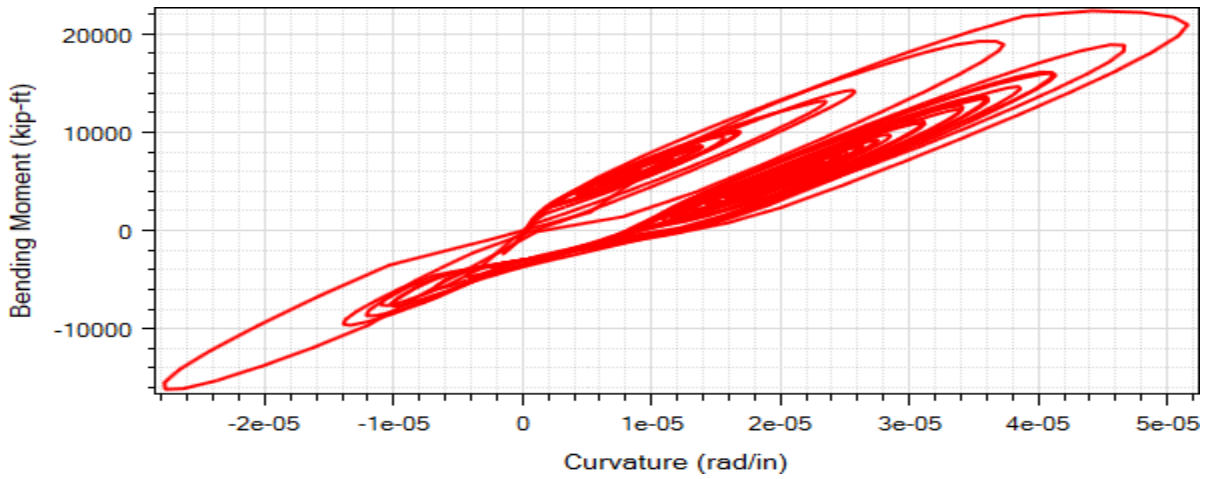


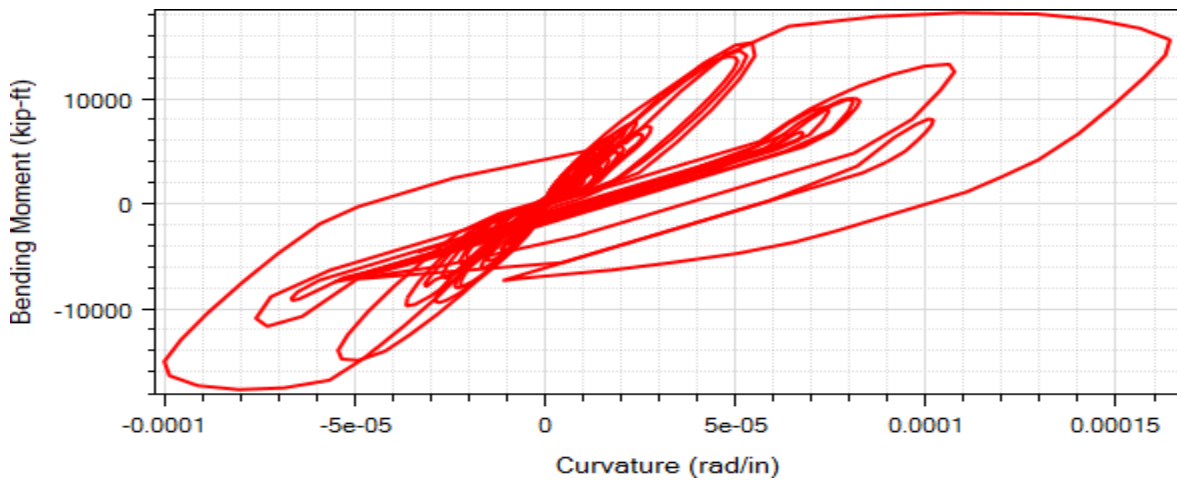
Figure 4.11 Pier E-7 Column top longitudinal response time histories for Simulation 2: a) acceleration; b) displacement; c) bending moment; d) base excitation ROCKS1N2



(a)

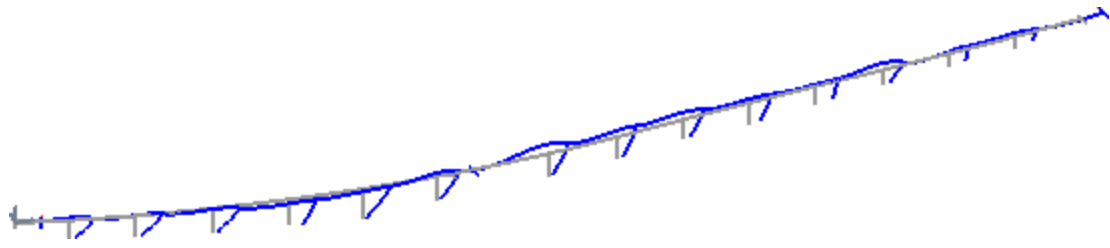


(b)

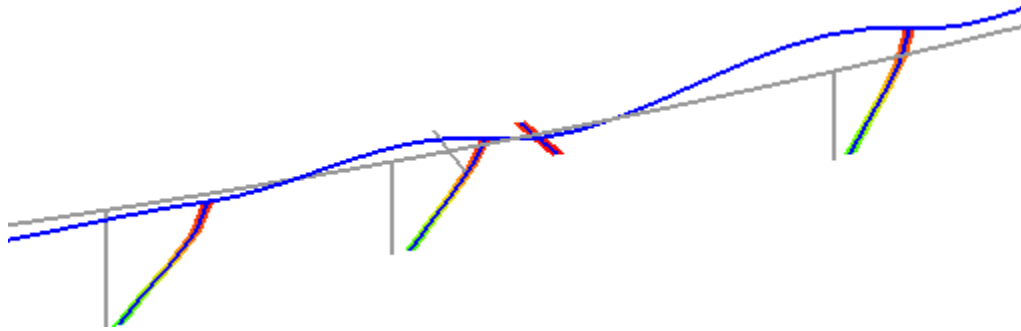


(c)

Figure 4.12 Column top longitudinal moment-curvature response for Simulation 2 (motion ROCKS1N2): (a) Pier E-6; (b) Pier E-7; (c) Pier E-13

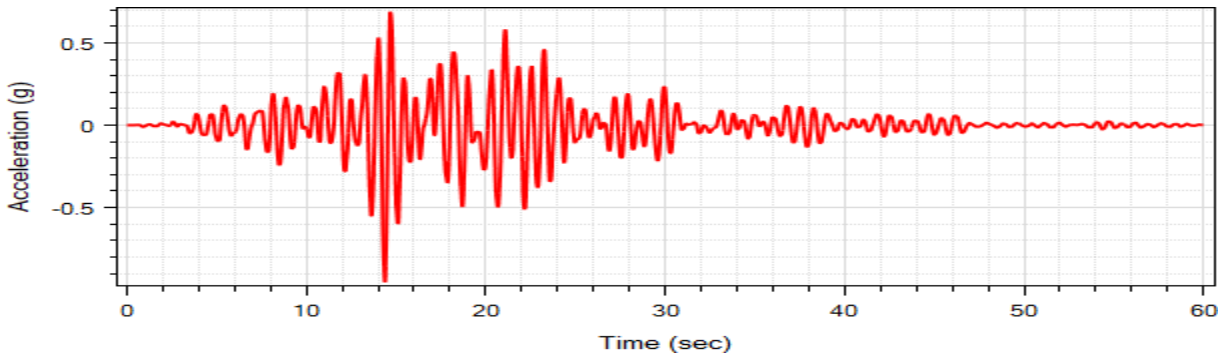


(a)

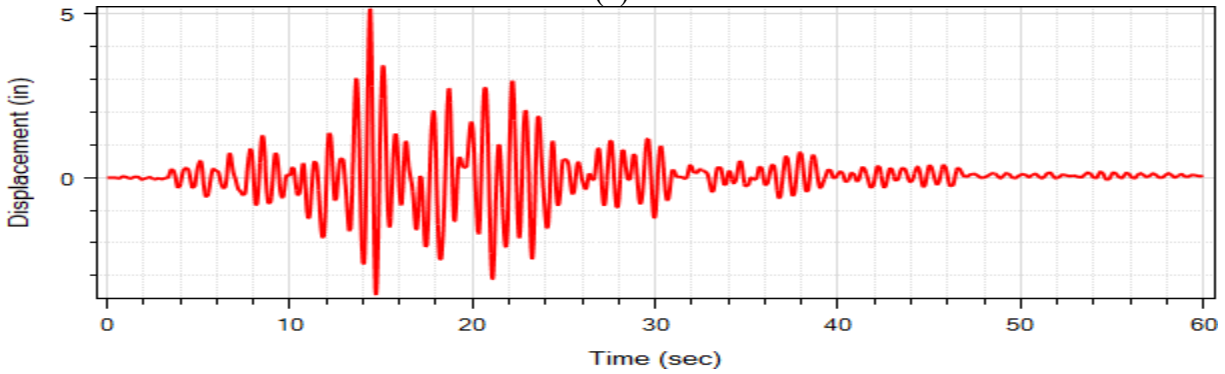


(b)

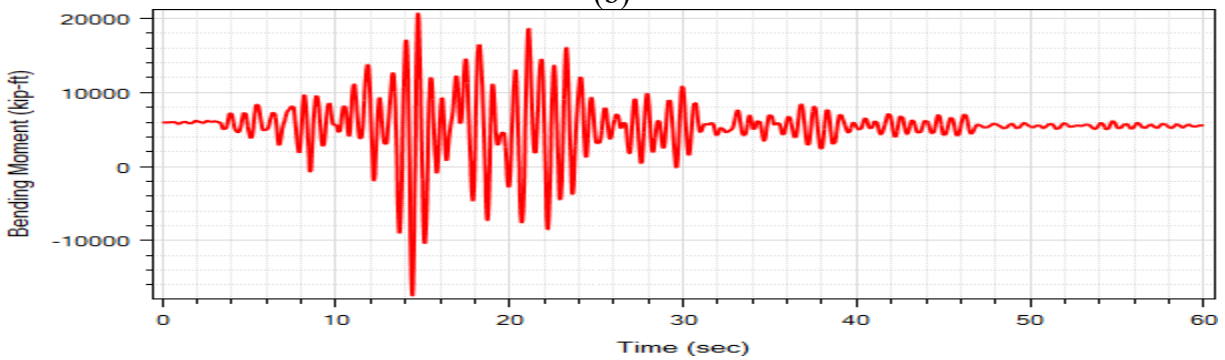
Figure 4.13 Deformed mesh (factor of 100) for Simulation 1 (motion ROCKS1P2) at the maximum displacement step (grey lines represent undeformed mesh): (a) entire bridge; (b) close-up of Piers 6, 7, and 8 (from left to right)



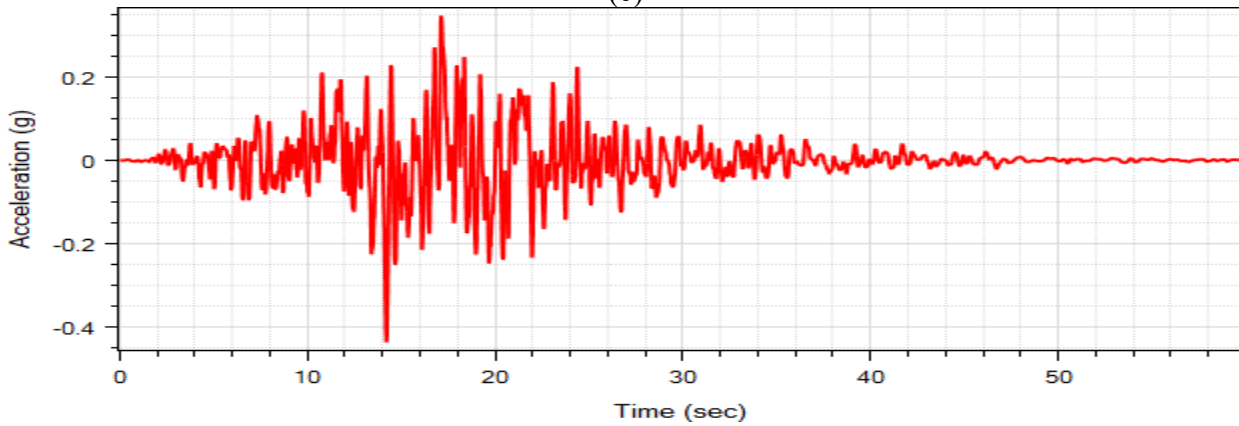
(a)



(b)

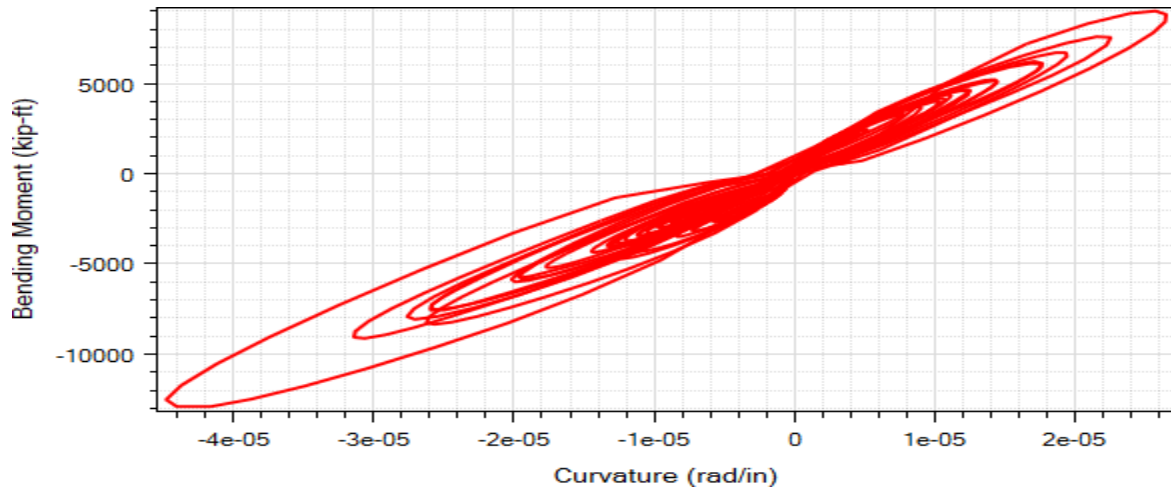


(c)

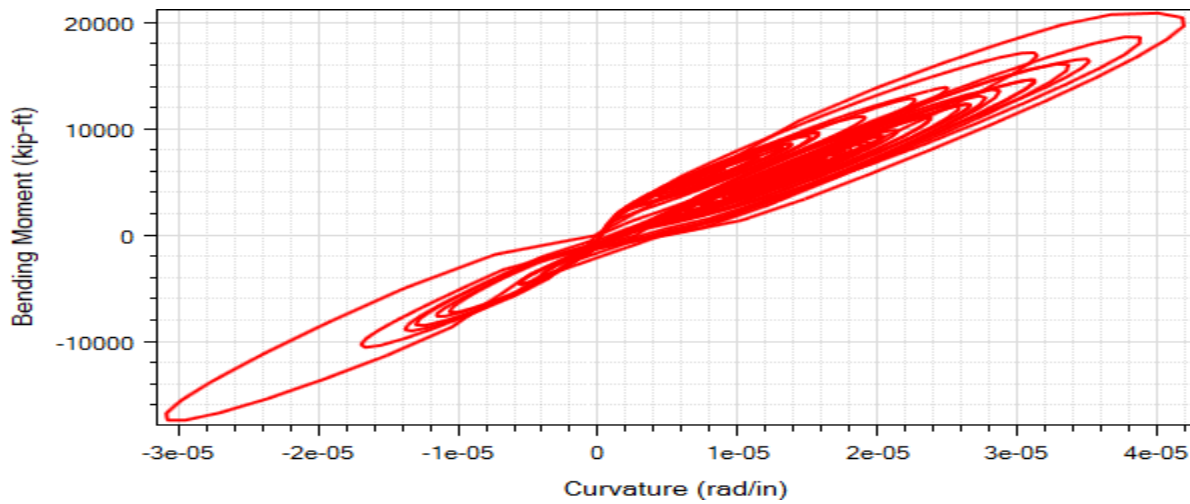


(d)

Figure 4.14 Pier E-7 column top longitudinal response time histories for Simulation 9: (a) acceleration; (b) displacement; (c) bending moment; (d) base excitation ROCKS1P2



(a)



(b)

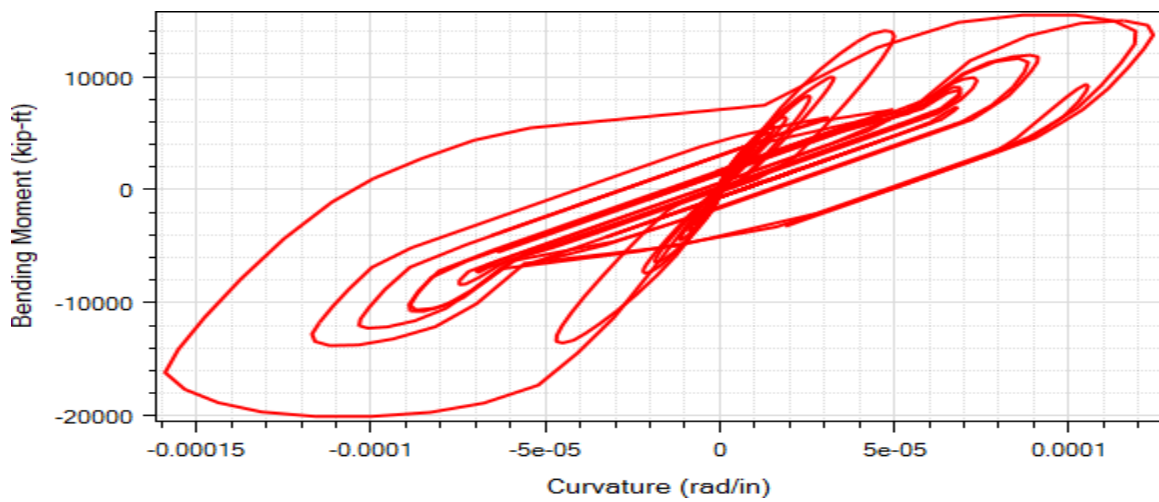


Figure 4.15 Column top longitudinal moment-curvature response for Simulation 9 (motion ROCKS1P2): (a) Pier E-6; (b) Pier E-7; (c) Pier E-13

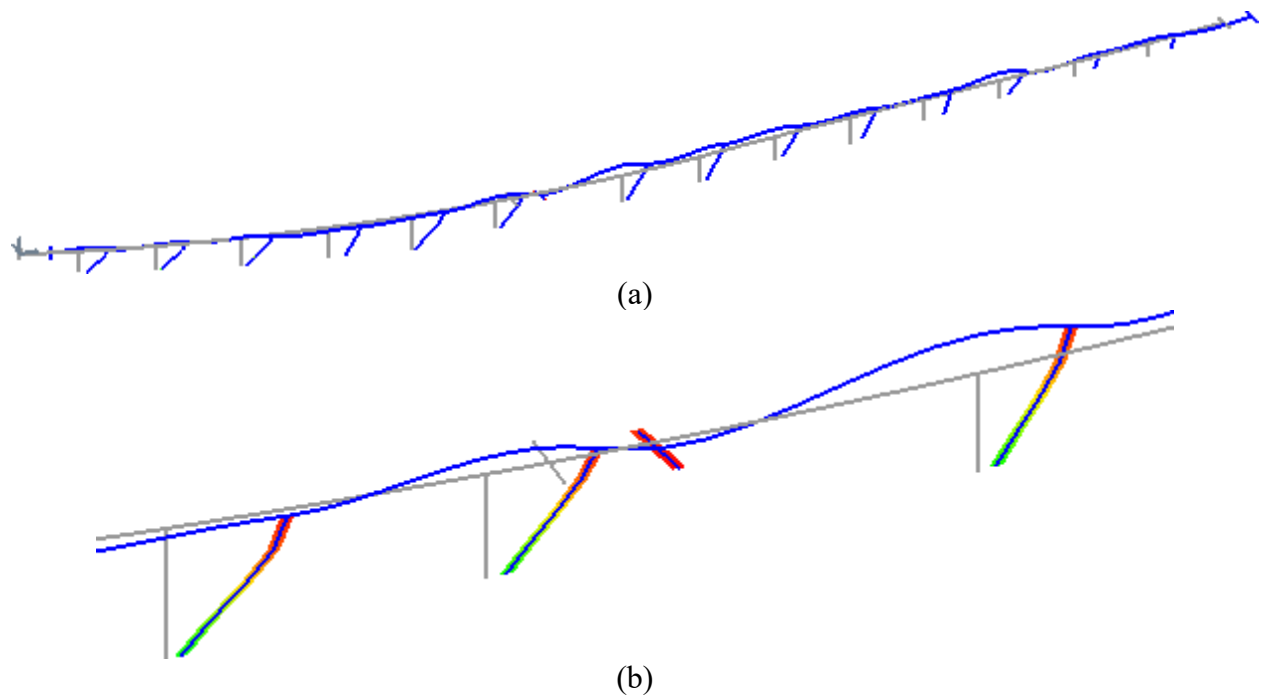


Figure 4.16 Deformed mesh (factor of 100) for Simulation 9 (motion ROCKS1P2) at the maximum displacement step (grey lines represent undeformed mesh): (a) entire bridge; (b) close-up of Piers 6, 7, and 8 (from left to right)

4.7 Summary

Eureka Bridge was modeled in OpenSees. A recently developed user interface MSBridge was employed for pre- and post-processing in the conducted OpenSees analysis. Nonlinear THA was conducted for the 14 input motions provided by Caltrans. The average THA maximum displacement is 4.4 inches in the bridge longitudinal direction and 13.7 inches in the transverse direction. ESA was also conducted for Eureka Bridge using MSBridge.

4.8 Conclusions

1. For the employed ESA spectrum, column displacement demand was 6.1 inches in the longitudinal direction and 13.1 inches in the transverse direction.
2. For the investigated set of ground motions in the OpenSees analysis:
 - 2.1 In the longitudinal direction, none of the shaking events resulted in column displacement demand that exceeded that of the ESA.
 - 2.2 In the transverse direction, about 43% of the shaking events resulted in column displacement demand that exceeded that of the ESA. This demand reached a maximum of 47% in excess of that from the corresponding ESA.

5 SUMMARY AND CONCLUSIONS

5.1 Summary

Three bridges (the Salinas River Bridge, the Samoa Channel Bridge and the Eureka Channel Bridge) were studied using OpenSees. In this context, the seismic response is being investigated from a system level perspective. The deck, columns, abutments, and foundation response mechanisms are integrated within a unified framework. Systematic evaluation of the global system response is conducted under a wide range of expected earthquake input shaking scenarios. The analysis procedures and results for the 3 studied bridges were presented in this report.

For the Salinas River Bridge, an idealized bi-linear moment-curvature relationship was used to model the columns. The force-based beam-column element based on the plastic hinge integration method (`BeamWithHinges`) in OpenSees was employed to model the columns while the deck and bentcap were considered linearly elastic. The column foundation response was modeled by Soil Springs calculated based on p-y and t-z springs. An elastic abutment model was employed. In addition, an effort was also made to compare OpenSees and wFrame pushover analysis results for the Salinas River Bridge model.

For the Samoa Channel Bridge and the Eureka Channel Bridge, the pier foundation response was model by Foundation Matrix. The pier columns were modeled using the nonlinear Fiber section. The force-based beam-column element with the distributed plasticity integration method (`forceBeamColumn`) in OpenSees was employed to model the pier column while the deck was considered linearly elastic. Elastic abutment model was also employed.

To facilitate the conducted analyses in OpenSees, the user interface MSBridge was further developed and employed. Nonlinear THA (Time History Analysis) was conducted for 14 input motions provided by Caltrans. ESA (Equivalent Static Analysis) was performed in OpenSees as well using MSBridge. Furthermore, an effort was made to illustrate and verify the MSBridge salient features and capabilities.

5.2 Conclusions

1. Good agreement was noted in the OpenSees and wFrame results in the longitudinal and transverse ESA Salinas River Bridge study. The relative differences in initial stiffness between OpenSees and wFrame were 1%, and 2.6% in the longitudinal and transverse directions, respectively.
2. Bridge transverse direction study for comparing ESA and THA for a OSB bridge model shows: i) Linear models of the bridge bent resulted in essentially identical responses (ESA and THA); ii) Nonlinearity of the columns and base soil springs (p-y and t-z) caused a difference of about 25 %; and iii) When the abutment effects were included, the difference actually decreased to somewhere in the neighborhood of 10 %.

3. For the Salinas River Bridge, the differences between the ESA displacement demand and the average THA maximum displacement is about 12% (for both longitudinal and transverse directions).
4. For the Samoa Channel Bridge and the Eureka Channel Bridge models, the differences between the ESA displacement demand and the average THA maximum displacement are 5.8% and 27.5%, respectively, in the longitudinal direction. The differences between the ESA and THA results in the transverse direction are 15.8% and 4.5%, respectively, for the above 2 bridges.
5. In the longitudinal direction, for the Salinas River Bridge, about 36% of the shaking events resulted in column displacement demand that exceeded that of the ESA. This demand reached a maximum of 12% in excess of that from the corresponding ESA. For the Samoa Channel Bridge and the Eureka Channel Bridge, 64% and 0%, respectively, of the shaking events resulted in column displacement demand that exceeded that of the ESA. This demand reached a maximum of 32% in excess of that from the corresponding ESA (for the Samoa Channel Bridge).
6. In the transverse direction, for the Salinas River Bridge, about 14% of the shaking events resulted in column displacement demand that exceeded that of the ESA. This demand reached a maximum of 25% in excess of that from the corresponding ESA. For the Samoa Channel Bridge and the Eureka Channel Bridge, 14% and 43%, respectively, of the shaking events resulted in column displacement demand that exceeded that of the ESA. This demand reached a maximum of 20% and 47%, respectively, in excess of that from the corresponding ESA.

APPENDIX A MSBRIDGE: MULTI-SPAN BRIDGE ANALYSIS

A.1 General Overview

MSBridge is a PC-based graphical pre- and post-processor (user-interface) for conducting nonlinear Finite Element (FE) studies for multi-span multi-column bridge systems. This research project was funded by California Department of Transportation (Caltrans). Main features of MSBridge include:

- i) Automatic mesh generation of multi-span (straight or curved) bridge systems
- ii) Options of foundation soil springs and foundation matrix
- iii) Options of deck hinges, isolation bearings, and steel jackets
- iv) A number of advanced abutment models (Elgamal *et al.* 2014; Aviram 2008a, 2008b)
- v) Management of ground motion suites
- vi) Simultaneous execution of nonlinear time history analyses for multiple motions
- vii) Visualization and animation of response time histories

FE computations in MSBridge are conducted using OpenSees (currently ver. 2.5.0 is employed). OpenSees is an open source software framework (McKenna *et al.* 2010, Mazzoni *et al.* 2009) for simulating the seismic response of structural and geotechnical systems. OpenSees has been developed as the computational platform for research in performance-based earthquake engineering at the Pacific Earthquake Engineering Research (PEER) Center. For more information about OpenSees, please visit <http://opensees.berkeley.edu/>.

The analysis options available in MSBridge include:

- i) Pushover analysis
- ii) Mode shape analysis
- iii) Single and multiple 3D base input acceleration analysis
- iv) Equivalent Static Analysis (ESA)
- v) Pushover analysis of soil movements (imposed displacement profile)

MSBridge supports analysis in both the US/English and SI unit systems. The default unit system is US/English units. This unit option can be interchanged during model creation, and MSBridge will convert all input data to the desired unit system.

The global coordinate system employed in MSBridge is shown in Figure A.1. The origin is located at the left deck-end of the bridge. The bridge deck direction in a straight bridge is referred to as “longitudinal direction (X)”, while the horizontal direction perpendicular to the longitudinal direction is referred to as “transverse direction (Y)”. At any time, “Z” denotes the vertical direction.

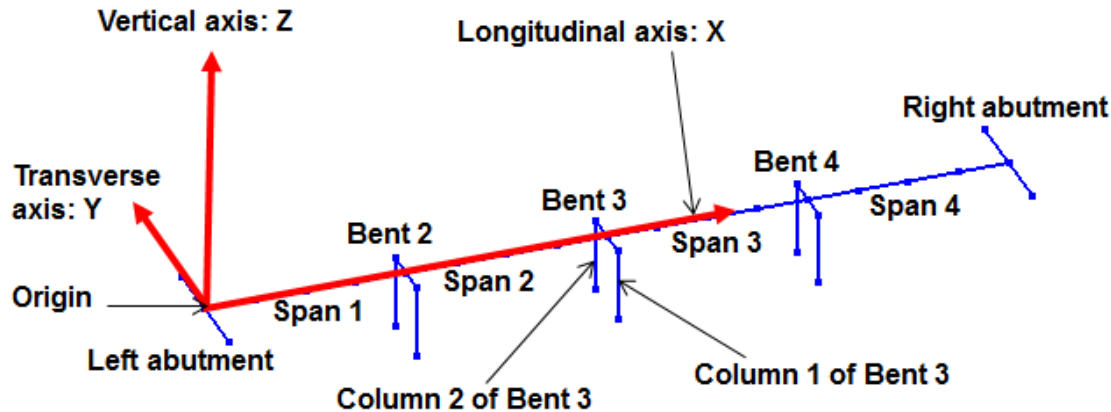


Figure A.1 Global coordinate system employed in MSBridge

In MSBridge, the maximum response quantities (e.g., displacement, acceleration) are reported in the local coordinate system. In a straight bridge, the local coordinate system is parallel to the global one. For a curved bridge, the local coordinate system is defined in such a way that the longitudinal axis (x) is tangent to the bridge curve at a given superstructure location while the transverse axis (y) is another horizontal direction that is perpendicular to the longitudinal axis (x). The vertical axis (z) in a local coordinate system is still parallel to the global one.

MSBridge was written in Microsoft .NET Framework (Windows Presentation Foundation or WPF). OpenTK (OpenGL) library (website: <http://www.opentk.com/>) was used for visualization of FE mesh and the OxyPlot package (<http://oxyplot.codeplex.com/>) was employed for x-y plotting. For more information about MSBridge, please refer to the MSBridge user manual (Elgamal *et al.* 2014).

A.2 Capabilities Added in the Current Updated Version of MSBridge

A number of capabilities and features have been added in the current version of MSBridge. These added features mainly allow MSBridge to address possible variability in the bridge deck, bent cap, column, foundation, and soil configuration/properties (on a bent-by-bent basis). Specifically, the capabilities implemented are:

- (a) A different skew angle can be defined for each individual bent/abutment (in MSBridge, from main window -> **Advanced** -> check **Use Individual Skew Angles** -> **Bent and Abutments**).
- (b) A different skew angle can be defined for each individual deck hinge (from main window -> **Advanced** -> **Define Deck Hinges**).

- (c) Shear key option (using OpenSees **Bilin** material) is included in the deck hinge model. The shear key is not activated by default (From main window -> **Advanced** -> **Define Deck Hinges** -> **Modify**).
- (d) Deck and bent cap are now connected by a rigid link (deck offset is activated in this case). A hinge with 6 Degrees of freedom (DOF's) of linear springs can be activated at the rigid link, at the location that the user specifies (From main window -> **Bentcap**).
- (e) Box girder section graphical representation has been added (for efficient incorporation of the user defined properties). (From main window -> **Deck** -> **Recalculate Section from Box Girder**)
- (f) Option to couple longitudinal and transverse directions of bearing pad nonlinear response has been added (From main window -> **Advanced** -> **Define Isolation Bearings** -> **Couple Longitudinal and Transverse Directions**).
- (g) Definition of the bent cap properties is now allowed on a bent by bent basis (From main window -> **Bentcap**).
- (h) Definition of the column properties is allowed for each individual column. This option gives the user great flexibility and control over assigning different nonlinear fiber sections to columns and pile shafts (Types I & II), (From main window -> **Column**).
- (i) Oblong column cross section with two circular steel cages has been added (From main window -> **Column** -> **Oblong**).
- (j) For the circular cross section, options for Bonded and Un-bonded Column Jackets (i.e., Casing as Fibers in the Bonded case) have been added (From main window -> **Column** -> **Circle** -> check **Activate Steel Jacket**).
- (k) Option to improve computational analysis schemes has been added. Specifically, this option is mainly to allow automatic switching between time integration schemes to achieve convergence in highly nonlinear scenarios (From menu **Execute** -> **Advanced Option: OpenSees Parameters** -> check **Automatic Switching between Time Integration Schemes**).

Furthermore, the following options have been implemented:

- (a) Concrete properties can be manually specified (instead of automatically calculated from the column geometry and reinforcement information) (From main window -> **Column** -> check **Manually Modify Concrete Properties**).
- (b) Option to enter user-defined moment curvature (from main window -> **Column** -> check **User-Defined Moment Curvature** and click **Define Moment Curvature**).

- (c) A separate steel material can be used for the steel jacket (From main window -> **Column** -> **Nonlinear Fiber Section**).
- (d) Option to include the vertical soil springs for the Soil Springs foundation type (From main window -> **Foundation** -> click **Soil Springs** and then **Modify Soil Springs**).
- (e) Option to calculate the vertical soil springs (for the Soil Springs foundation type) based on user-defined T-z and Q-z data (From main window -> **Foundation** -> click **Soil Springs** and then **Modify Soil Springs** -> click **Calculate from User T-z and Q-z**).
- (f) Option to specify a yielding curvature as the yielding criterion for Longitudinal and Transverse ESA (From main window -> click **Longitudinal Direction** (or **Transverse Direction**)).
- (g) A different number of columns can be specified for each individual bent, with locations defined by column offsets (From main window -> **Bridge** -> check **Non-uniform Column Layout** -> **Columns**).
- (h) Column base offset (zero by default) can also be defined, for modeling inclined columns (From main window -> **Bridge** -> check **Non-uniform Column Layout** -> **Columns** -> specify **Base Offset**).
- (i) Different deck properties can be specified on a span-by-span basis (From main window -> **Deck**; from main window -> **Bridge** -> check **Non-uniform Column Layout**).
- (j) For Horizontal Alignment, the global coordinate system can be rotated at the angle specified; or the bridge longitudinal direction can be chosen to coincide with the chord connecting the two abutments (From main window -> **Spans** -> check **Horizontal Alignment** -> **Modify Horizontal Curve**).
- (k) Option to include the bent cap overhang (the portion of the bent cap outside the columns) has been added (From main window -> **Bentcap**).
- (l) Option to include the user defined TCL code snippet for the nonlinear Fiber section has been added. This is an advanced option and the users must proceed with caution (From main window -> **Column** -> check **User-Defined Tcl Script for Nonlinear Fiber Section** -> **Define Fiber Section Tcl Script**).
- (m) Different Foundation Matrix parameters can be assigned to each column base (From main window -> **Foundation** -> check **Foundation Matrix** -> **Modify Foundation Matrix**).
- (n) Option to include pile cap masses and fixity conditions has been added, available only in the foundation types “Soil Springs” and “Foundation Matrix” (From main window -> **Advanced** -> **Pilecap Mass and Rotation Condition**).

- (o) Option to include column P-Delta effect (included by default) has been added (From main window -> **Advanced** -> check/uncheck **Include P-Delta Effect**).
- (p) Option to include Rayleigh (stiffness proportional component) damping for the abutments has been added, with no Rayleigh damping for the abutment stiffness as the default (From main window -> **Advanced** -> check/uncheck **Include Rayleigh Damping**).
- (q) Deck-end fixity conditions can be directly applied (From main window -> **Advanced** -> **Deckend Fixity**)
- (r) For the Soil Springs Foundation option (pile foundation), an analysis option of “Specified Displacement Time History Input” has been added (From main window -> **Time History Input** -> **Change Input**).
- (s) Visualization of pile response (profiles, time histories and relationships) has been added, available for the foundation type “Soil Springs” (From menu **Display** -> **Pile Response Profiles/Pile Response Time Histories/Pile Response Relationships**).
- (t) Option to view OpenSees analysis log (from main menu -> **Execute** -> **OpenSees Analysis Log**).

APPENDIX B BASE INPUT MOTIONS

Table B.1 lists the 14 input motions employed in the study. These motion files were provided by Caltrans. The motion names (Table B.1) have 8 or 9 character with naming convention as follows:

TypeAiBjC , where

Type = ROCK

A = S for Synthetic, N for Natural

i = 1 for base record (1000 year return)

B = P for pulse-like motion, N for non-pulse-like motion

j = Record number for records of same TypeAiB

C = N for normal component, P for Parallel component, nonexistent for one component synthetic

Note that the vertical acceleration input is zero for all motions.

Figure B.1 shows the PGA histograms for the 14 input motions. Most motions are within 0.32g – 0.43g whereas 3 motions (i.e., Motions 1, 8, and 12) are between 0.67g – 0.71g.

Table B.2 displays the Intensity Measures of the 14 motions. The acceleration time histories of the input motion components are shown in Figure B.2-Figure B.3. The Pseudo-Spectral Accelerations of the input motions are displayed in Figure B.4-Figure B.5.

Table B.1. Input Motions Employed in the Nonlinear THA

Motion No.	Name	Peak Acceleration (g)
Motion 1	ROCKS1N1	0.70
Motion 2	ROCKS1N2	0.38
Motion 3	ROCKS1N3	0.32
Motion 4	ROCKS1N4	0.34
Motion 5	ROCKS1N5	0.53
Motion 6	ROCKS1N6	0.42
Motion 7	ROCKS1N7	0.36
Motion 8	ROCKS1P1	0.71
Motion 9	ROCKS1P2	0.44
Motion 10	ROCKS1P3	0.48
Motion 11	ROCKS1P4	0.32
Motion 12	ROCKS1P5	0.67
Motion 13	ROCKS1P6	0.41
Motion 14	ROCKS1P7	0.40

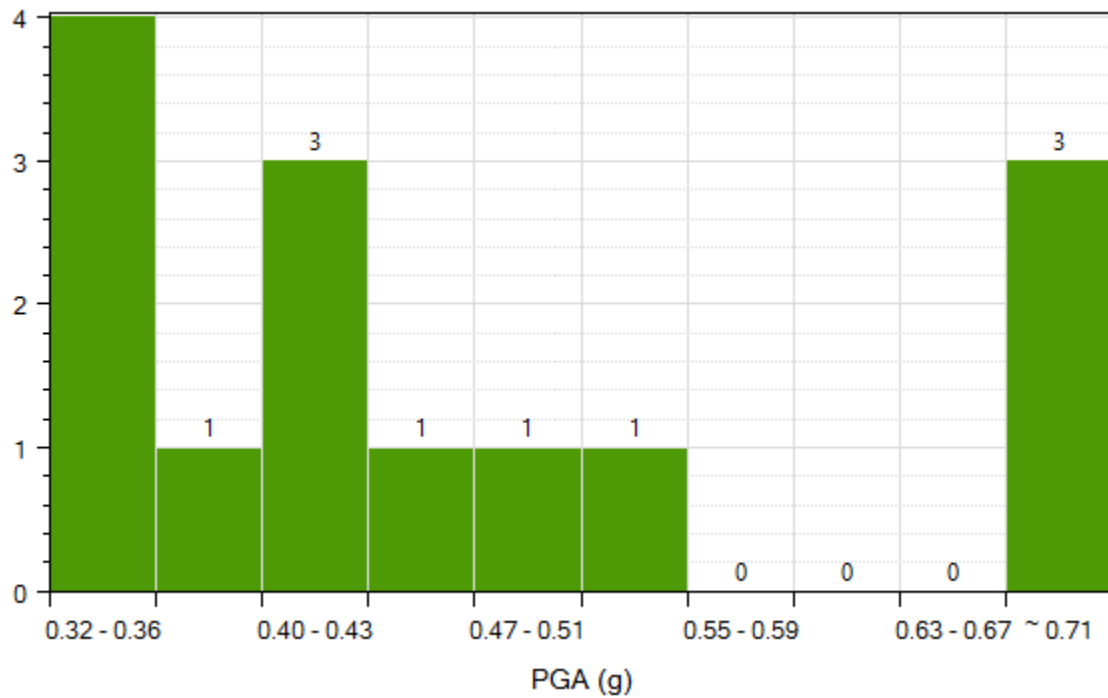


Figure B.1 Longitudinal PGA histograms of the first 14 input motions

Table B.2. Intensity Measures of the 14 Motions

Motion #	PGA (g)	PGV (in/sec)	PGD (in)	D(5-95) (sec)	CAV (in/sec)	Arias Intensity (in/sec)	SD (in)*	PSA (g)*	PSV (in/sec)*
1	0.7	35.231	21.634	86.875	2409.428	844.027	6.369	0.651	40.02
2	0.381	32.859	22.431	86.295	834.813	131.109	7.203	0.736	45.255
3	0.317	29.943	16.469	89.285	794.067	115.058	6.191	0.632	38.897
4	0.337	35.984	43.945	87.145	909.658	146.66	8.242	0.842	51.783
5	0.526	28.869	25.416	83.895	1071.14	195.452	6.887	0.704	43.275
6	0.422	25.616	37.547	83.82	1226.601	219.001	5.642	0.576	35.449
7	0.356	35.106	41.365	88.025	1033.964	170.179	6.74	0.689	42.348
8	0.709	44.435	45.36	86.87	2404.713	835.79	6.606	0.675	41.506
9	0.441	41.297	51.113	85.52	840.053	139.417	7.039	0.719	44.227
10	0.477	45.129	40.75	83.885	1077.207	199.85	7.259	0.742	45.609
11	0.319	40.454	71.431	87.08	922.947	152.089	8.282	0.846	52.04
12	0.672	53.511	60.915	87.95	1442.94	406.681	8.351	0.853	52.473
13	0.412	24.455	37.643	83.83	1228.427	219.589	5.656	0.578	35.538
14	0.396	55.165	53.625	89.09	815.733	125.978	6.228	0.636	39.132

*For period = 1 sec

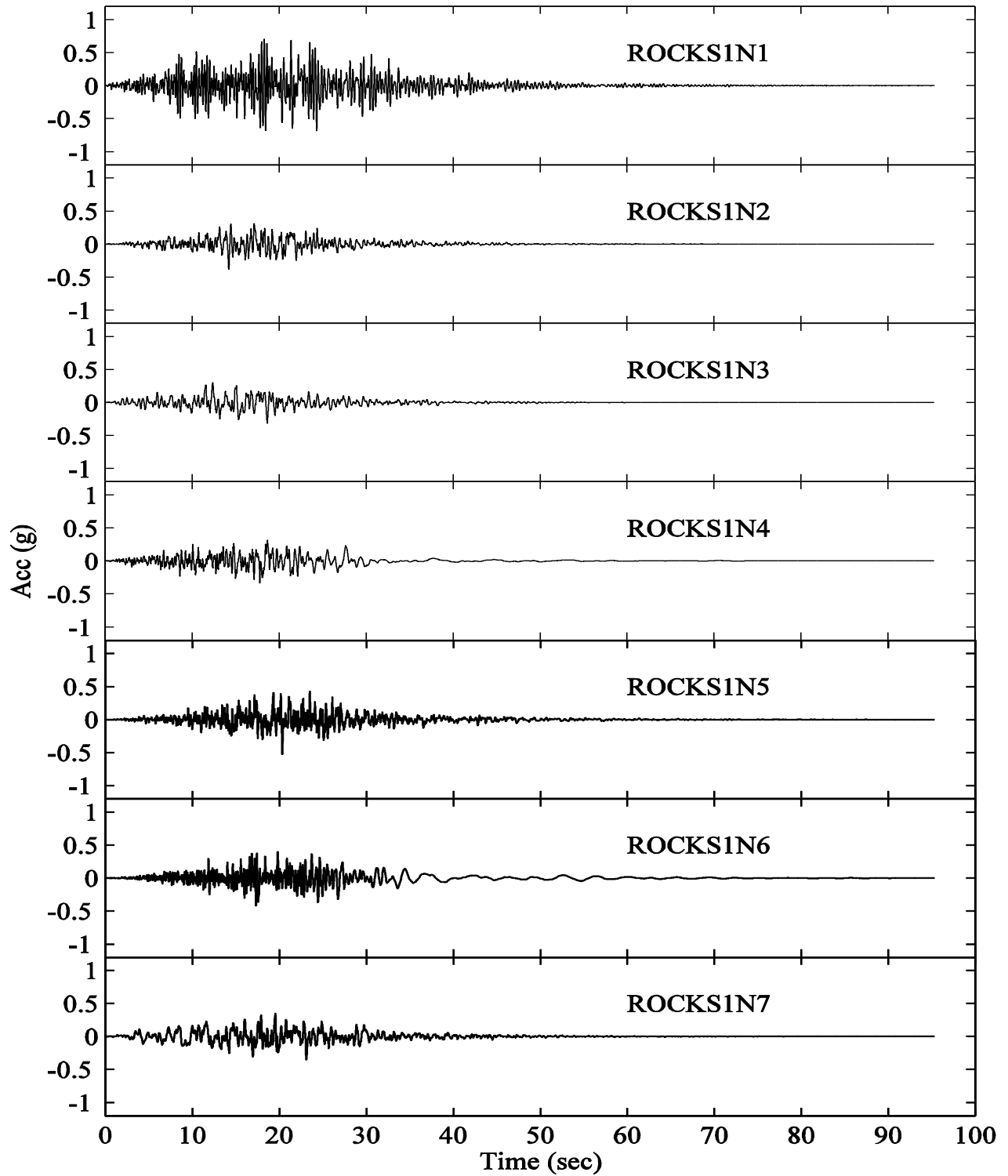


Figure B.2 Acceleration time histories of the input motion components for Rock site (non-pulse-like motions)

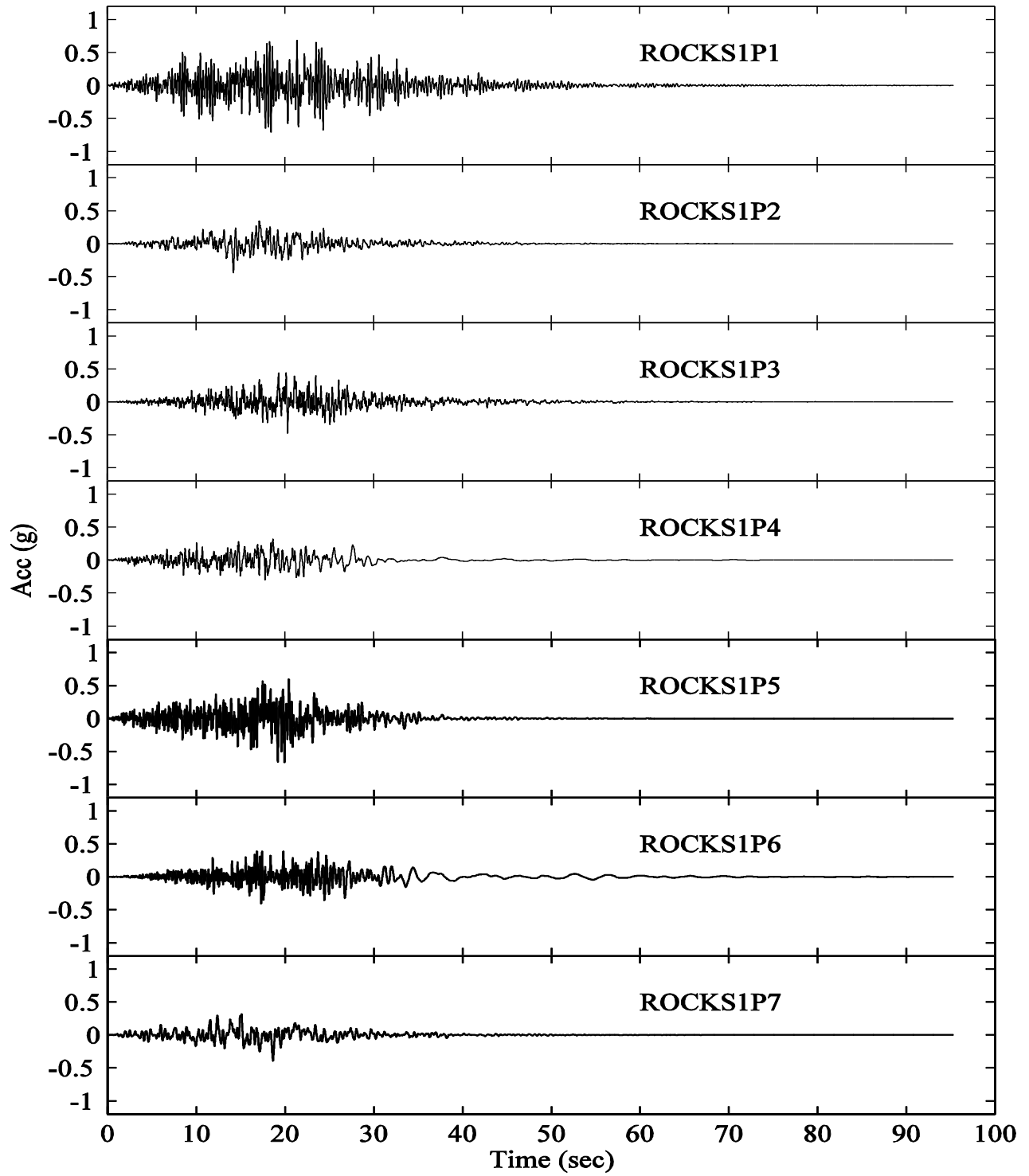


Figure B.3 Acceleration time histories of the input motion components for Rock site (pulse-like motions)

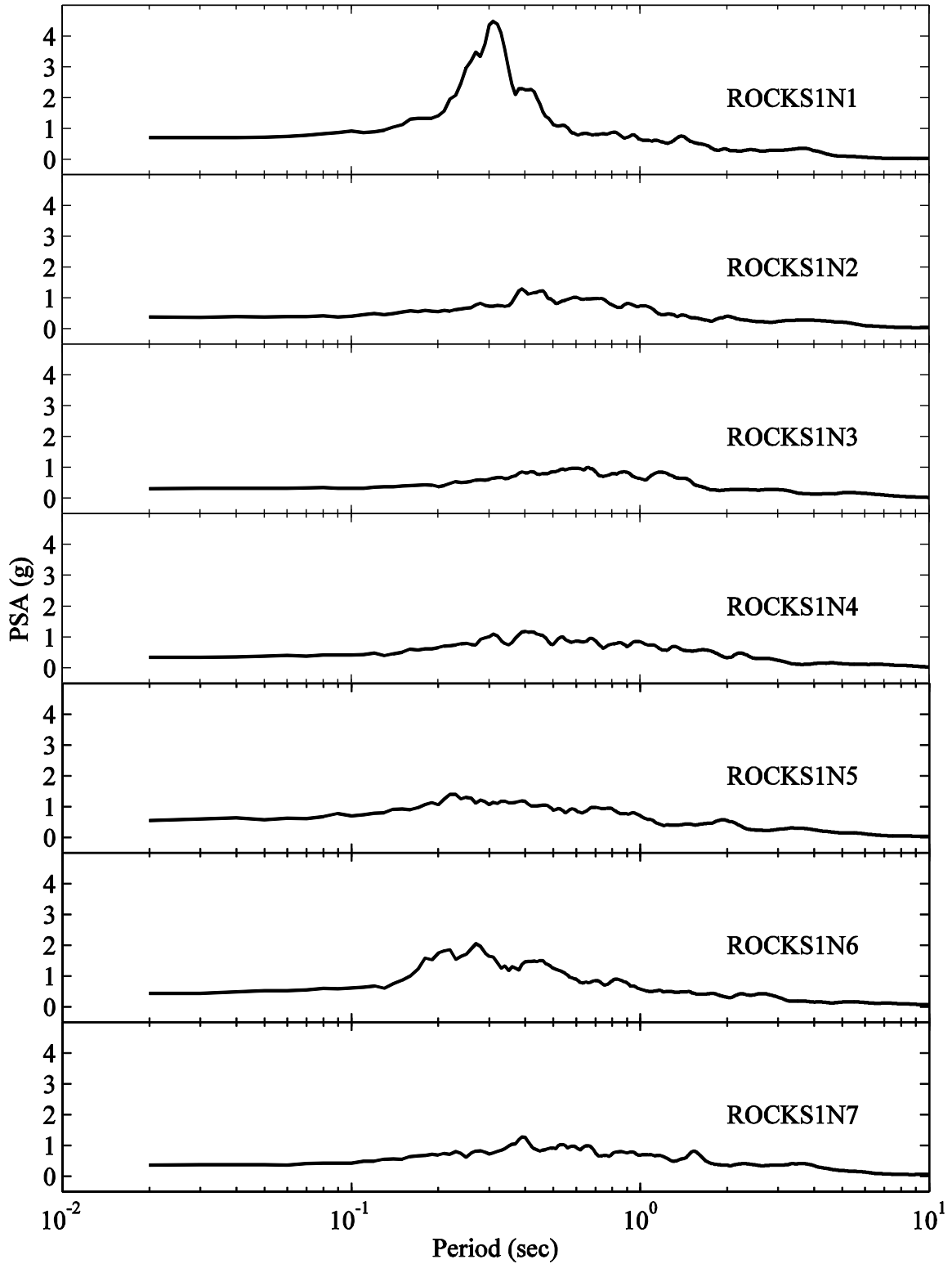


Figure B.4 Pseudo-Spectral Acceleration for rock site (non-pulse-like motions)

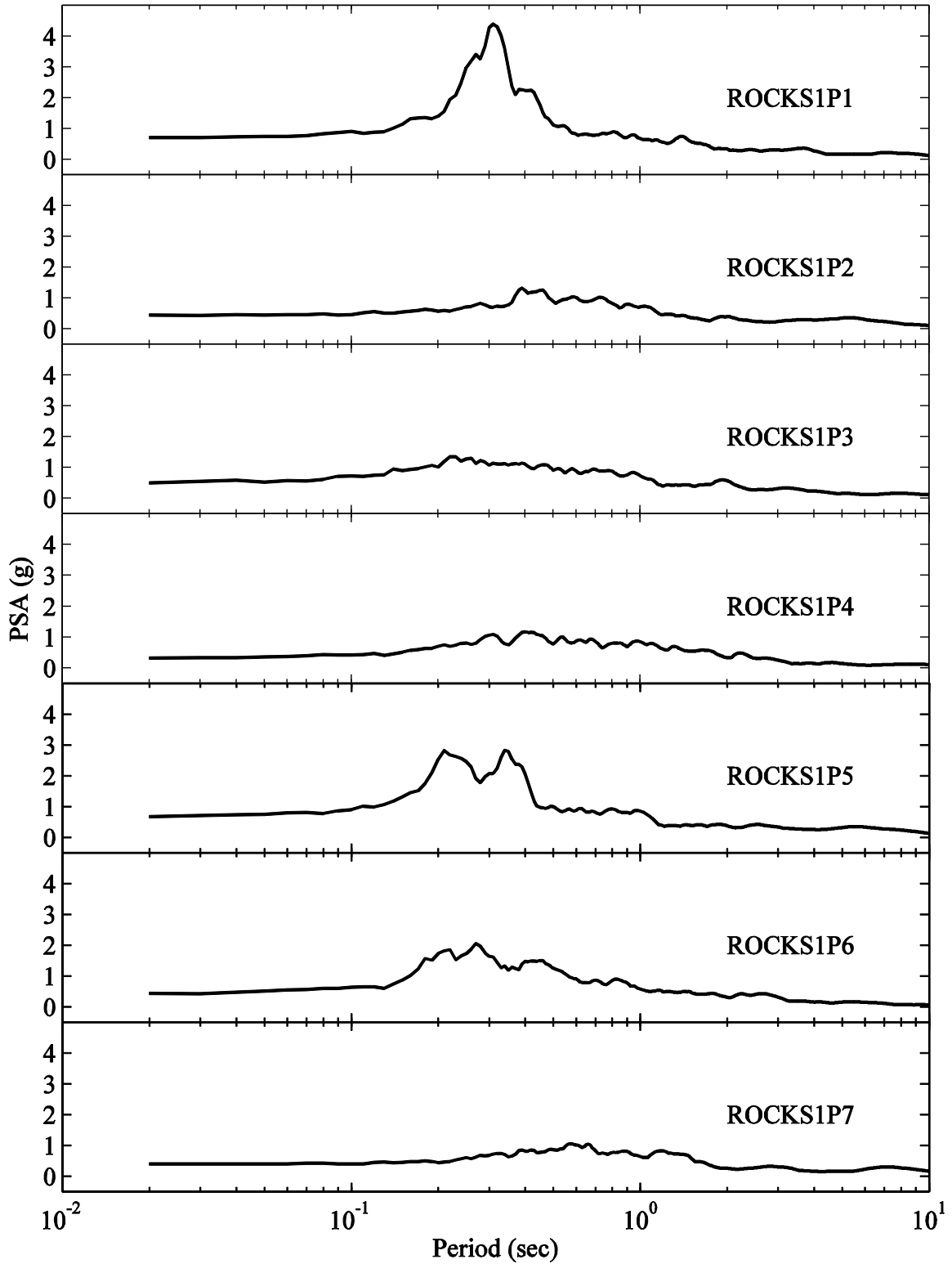


Figure B.5 Pseudo-Spectral Acceleration for rock site (pulse-like motions)

APPENDIX C BRIDGE TRANSVERSE DIRECTION STUDY (COMPARISON OF ESA AND THA RESULTS)

The purpose of this Appendix is to compare ESA (Equivalent Static Analysis) and THA (Time History Analysis) results for a OSB (Ordinary Standard Bridge) model. Focus was placed on the transverse direction response. A series of models of increasing complexity were studied in an attempt to separate influence of column nonlinear response, foundation p-y springs, and the added resistance provided at the bridge end-bents and abutments. A single bent model was studied first, followed by models of the entire bridge (to include the abutment end-effects). On this basis, it was found that:

1. Linear models of the bridge bent resulted in essentially identical responses (ESA and THA).
2. Nonlinearity of the columns and base soil springs (p-y and t-z) caused a difference of about 25 %.
3. When the abutment effects were included, the difference actually decreased to somewhere in the neighborhood of 10 %.

C.1 Introduction

C.1.1 Purpose of Study

The purpose is to compare ESA and THA results for an OSB bridge system. Specifically, comparison of ESA displacement demand and THA maximum displacement was conducted for a set of 14 motions provided by Caltrans. Focus was placed on the transverse direction only. Patterned after the Salinas River Bridge (Caltrans 2005), the bent is supported on two columns (with Type 2 foundation, when activated).

To elucidate the mechanisms behind similarity/difference in ESA and THA estimates, the comparison was conducted for a series of models of increasing complexity according to the following:

To explore linear response under a fixed base scenario

1. **Linear** columns with **fixed base** at mudline

To explore influence of including a p-y and t-z spring foundation

2. **Linear** columns with **linear p-y and t-z spring** foundation.

To explore influence of nonlinear columns

3. **Nonlinear** (bilinear) columns with **fixed base** at mudline
4. **Nonlinear** (bilinear) columns with **linear p-y and t-z spring** foundation.

Towards full bridge model with nonlinear foundation springs, bridge-end bents, and abutment lateral resistance

5. **Nonlinear** (bilinear) columns with **nonlinear p-y and t-z spring** foundation.
6. Same as 5, with 10 bents (to check full model versus single bent behavior)
7. Same as 6, with 2 end bents at the abutments (Salinas River Bridge configuration)
8. Same as 7 with bilinear abutment springs (full Salinas River Bridge model)

As such, it was observed that:

1. As expected, Case 1 (linear with fixed base) shows complete agreement between ESA and THA
2. Also as expected, Case 2 (linear columns with linear p-y and t-z spring foundation) shows good agreement between ESA and THA.
3. Nonlinearity of the columns causes an overall difference of about 23.8%.
4. This difference increased a bit (about 25%) because of nonlinearity of the p-y and t-z springs.
5. The difference decreased to 15% when stiffness from the bridge-end bents was included.
6. Further stiffness introduced by the abutments led to a final overall difference of about 10%.

C.1.2 Salient Modeling Considerations

For simplicity, the bridge weight was assumed uniformly distributed on the superstructure (Caltrans 2005; Mahan 2005). Bentcap and columns were assumed massless (along the logic of a SDOF-type idealization). No resistance from the abutments was assumed for all cases (unless otherwise stated). Finally, connection between the bridge deck and the columns was assumed rigid throughout (including at the abutments).

All analyses (including ESA, THA and Mode shape analysis) were conducted in MSBridge user interface (Elgamal *et al.* 2014) where the Finite Element (FE) framework OpenSees (Mazzoni et al. 2009, McKenna et al. 2010) was employed for the numerical simulations. For the columns and pile shafts, the `forceBeamColumn` (with the distributed plasticity integration method) element was employed (Only one `forceBeamColumn` was used for each column in this study). Rayleigh damping was considered for the soil spring zero-length elements (In OpenSees, Rayleigh damping is not included for `zeroLength` element by default).

C.1.3 Report Layout

This study starts with a single-bent model with rigid base and linear columns (Case 1, see Section C.3). Case 1 is very similar to a SDOF (Single-Degree-Of-Freedom) problem. ESA displacement demand and THA maximum displacement for Case 1 are expected to be identical for this case.

Compared to Case 1, Case 2 (see Section C.4) includes a foundation of linear soil springs (instead of rigid base foundation). Cases 3 (see Section C.5) and 4 (see Section C.6) activate the bilinear moment-curvature behavior for the columns, compared to Cases 1 and 2, respectively.

Compared to Case 4, Case 5 activates nonlinear soil springs (instead of linear springs) for the foundation. Case 5 (Section C.7) essentially represents a typical bent of the Salinas River Bridge model. Case 6 (Section C.8) is multi-bent bridge model with 10 identical bents (each bent is the same as Case 5). No abutment is considered in Case 6. Compared to Case 6, Case 7 (Section C.9) adds 2 end bents. Thus Case 7 represents the idealized Salinas River Bridge model without lateral abutment stiffness. Finally, Case 8 (Section C.10) adds the transverse abutment stiffness, compared to Case 7. Case 8 essentially represents the idealized Salinas River Bridge model.

C.2 Typical Bent

Salinas River Bridge is a reinforced concrete box-girder bridge with 11 spans (Caltrans 2005). Each span is 140 ft long (corresponding to a total weight of 1,912.4 kips lumped at bent). The substructure consists of multiple two-column bents. Figure C.1 shows the side view of a typical bent (column height = 48 ft). For the nonlinear column cases, an idealized bilinear moment-curvature relationship was used to model the columns (Figure C.2) and pile shafts (Figure C.3). As such, one cross section (Figure C.2) defines the column properties and another (Figure C.3) defines pile properties (due to current capabilities of MSBridge). The column foundation response (Figure C.1) was modeled by the approach of p-y and t-z soil springs (Caltrans 2005).

Figure C.4 shows pushover response (for the bent with soil springs). It can be seen that plastic hinges form at column top when the pushover displacement reaches 9.4 inches. At 17.2 inches, plastic hinges form near the base, and ultimate lateral resistance load is reached. As such, the bent ultimate capacity is 508.4 kips (= 2 x 254.2 kips), which corresponds to a lateral bent acceleration of 0.27g.

In the conducted THA numerical simulations, Rayleigh damping of 5% was employed (a value of 5% was specified in the range of first few natural periods of the system).

C.2.1 ESA Comparison for MSBridge and wFrame

Transverse ESA was conducted using MSBridge for the bent (Figure C.1). In the ESA pushover analysis, the bent was pushed at bentcap laterally until initial yielding occurred (at column top in this case).

The ESA outcomes (Table C.1) were compared to the wFrame (Mahan 2005) results reported in Caltrans (2005). In general, good agreement (Table C.1) was noted in the MSBridge and wFrame results. The difference in initial stiffness between MSBridge and wFrame is about 2.6%. Note that in wFrame, 3 cross sections were employed for each column (Caltrans 2005). However, in MSBridge, only 1 cross section was used for the columns and the other 2 sections which are more flexible (but with a higher plastic moment) were not considered due to current capabilities of MSBridge. This simplification resulted in a lower yield displacement (9.4 in) in MSBridge, compared to the yield displacement of 9.76 in obtained in wFrame (Table C.1).

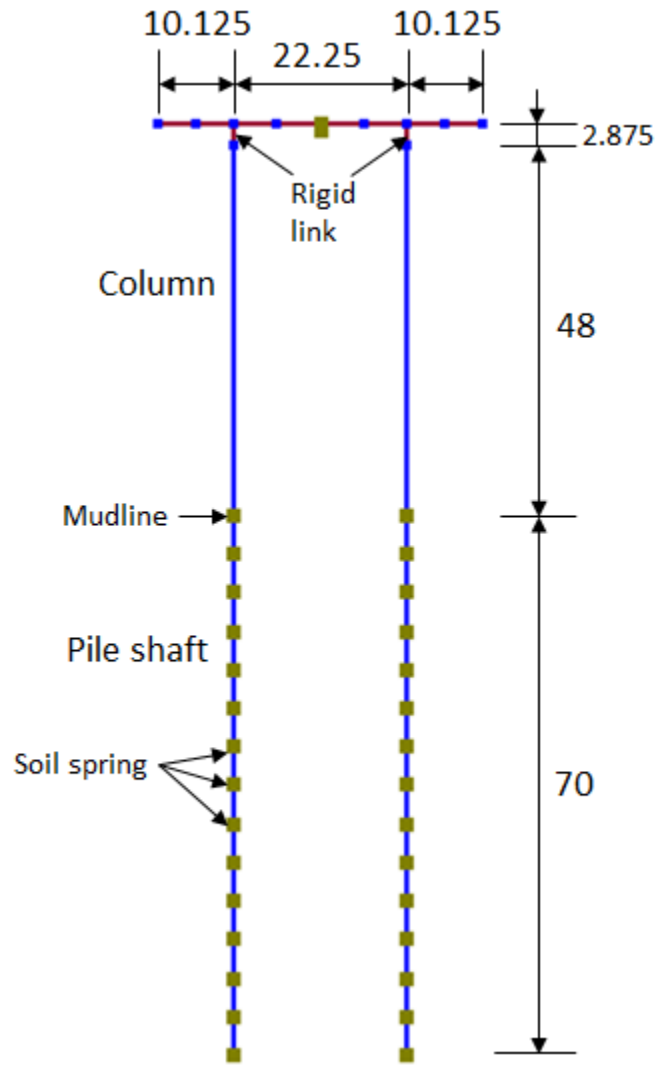


Figure C.1 Typical bent of Salinas Bridge (dimensions in ft)

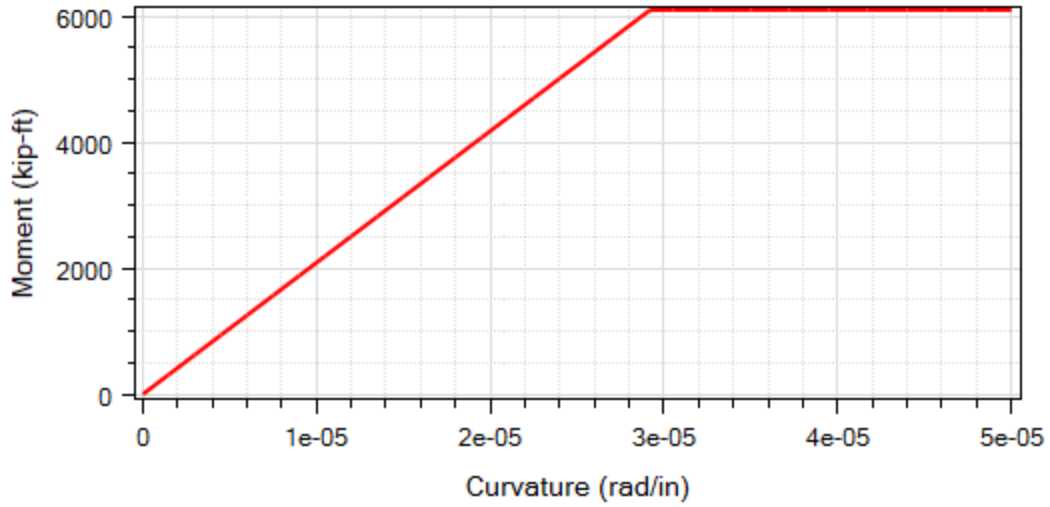


Figure C.2 Idealized bilinear moment-curvature relationship employed for the columns (plastic moment = 6,100 kip-ft; yield curvature = 2.92×10^{-5} rad/in)

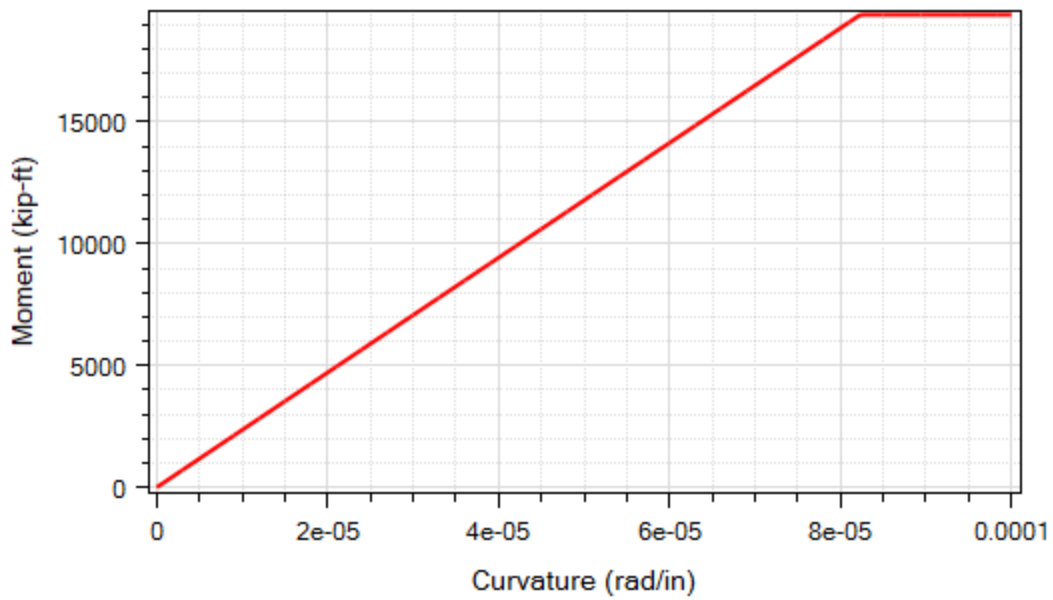


Figure C.3 Idealized bilinear moment-curvature relationship employed for the pile shafts (plastic moment = 19,400 kip-ft; yield curvature = 8.23×10^{-5} rad/in)

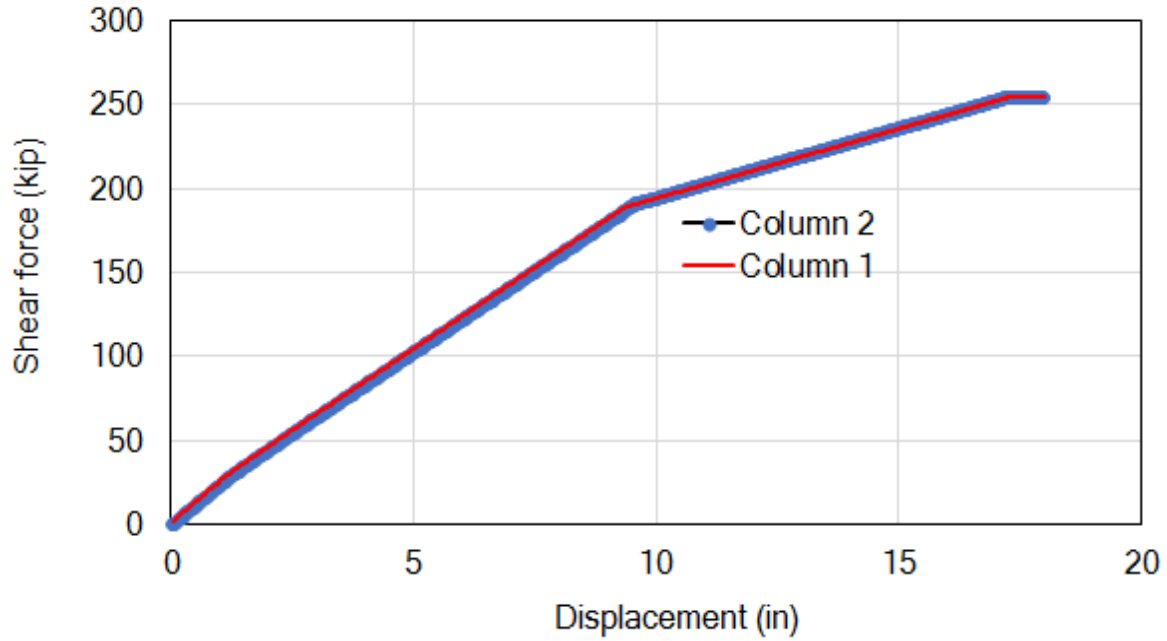


Figure C.4 Shear force versus transverse displacement for pushover analysis

Table C.1. Comparison of MSBridge and wFrame Results for the transverse ESA

Response	Computer Program	wFrame	Difference
	MSBridge	wFrame	Difference
Yield Displacement (in)	9.4	9.76	3.4%
Pushover Load (kips)	376	382.4	1.7%
Initial Stiffness (kip/in)	40	39	2.6%
Period (seconds)	2.21	2.24	1.3%
Displacement Demand (in)	18.8	18.6	1.1%

C.3 Case 1: Single Bent Model with Rigid Base and Linear Columns

Case 1 (Figure C.5) is very similar to a SDOF problem. Mode shape analysis shows the first transverse period is 0.86 seconds, which matches the period calculated by the transverse ESA procedure.

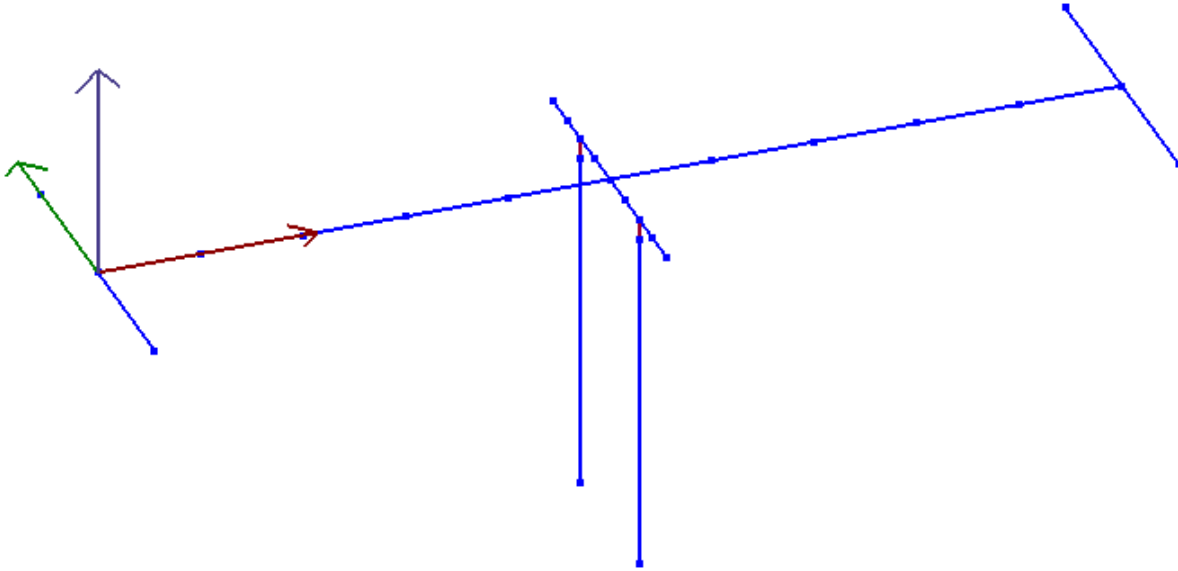


Figure C.5 Single bent model for Case 1 (with rigid base at mudline)

C.3.1 Comparison of ESA and THA Results

For this single-bent bridge model with rigid base and linear columns, Table C.2 shows the ESA displacement demand and the THA maximum displacement are in good agreement (less than 1% difference for most motions while reaching 2.3% for 2 motions). Note that the differences were calculated based on the actual displacement values while the displacement values shown in Table C.2 were rounded to 2 decimal places (for the sake of simplicity).

Table C.3 shows the maximum column bending moments and shear forces for the 14 motions. The maximum column bending moments range from around 18,000 kip-ft – 21,000 kip-ft. Note that, in this linear analysis, all of these maximum bending moments exceed the plastic moment (6,100 kip-ft) to be employed for the nonlinear columns (to be studied in later sections).

Table C.2 Comparison of transverse ESA displacement demand and THA maximum displacement (ESA displacement demand for an individual motion is based on the response spectrum of that motion)

Motion#	Motion (PGA)	THA Maximum Displacement (in)	ESA Displacement Demand (in)	Difference (“-” sign means ESA is less)
1	ROCKS1N1 (0.70g)	5.46	5.49	0.4%
2	ROCKS1N2 (0.38g)	5.30	5.18	-2.3%
3	ROCKS1N3 (0.32g)	6.22	6.16	-0.9%
4	ROCKS1N4 (0.34g)	5.86	5.84	-0.3%
5	ROCKS1N5 (0.53g)	5.65	5.61	-0.7%
6	ROCKS1N6 (0.42g)	6.18	6.17	-0.2%
7	ROCKS1N7 (0.36g)	5.82	5.79	-0.5%
8	ROCKS1P1 (0.71g)	5.52	5.54	0.4%
9	ROCKS1P2 (0.44g)	5.16	5.04	-2.3%
10	ROCKS1P3 (0.48g)	5.29	5.25	-0.7%
11	ROCKS1P4 (0.32g)	5.75	5.73	-0.3%
12	ROCKS1P5 (0.67g)	5.91	5.88	-0.5%
13	ROCKS1P6 (0.41g)	6.17	6.16	-0.2%
14	ROCKS1P7 (0.40g)	5.91	5.85	-0.9%
Average		5.73	5.69	-0.6%

Note: ESA displacement demand based on target ARS is 5.67 inches, corresponding a difference of 1.0%.

Table C.3 Maximum Column Shear Forces and Bending Moments (Transverse)

Motion#	Motion (PGA)	Maximum Bending Moment (kip-ft)	Maximum Shear Force (kips)
1	ROCKS1N1 (0.70g)	18,628.3	753.2
2	ROCKS1N2 (0.38g)	18,080.5	731.4
3	ROCKS1N3 (0.32g)	21,109.6	851.7
4	ROCKS1N4 (0.34g)	19,932.3	805.0
5	ROCKS1N5 (0.53g)	19,242.3	777.6
6	ROCKS1N6 (0.42g)	20,974.3	846.4
7	ROCKS1N7 (0.36g)	19,791.5	799.4
8	ROCKS1P1 (0.71g)	18,822.8	760.9
9	ROCKS1P2 (0.44g)	17,625.2	713.3
10	ROCKS1P3 (0.48g)	18,042.4	729.9
11	ROCKS1P4 (0.32g)	19,562.7	790.3
12	ROCKS1P5 (0.67g)	20,110.1	812.0
13	ROCKS1P6 (0.41g)	20,939.6	845.0
14	ROCKS1P7 (0.40g)	20,080.6	810.9

C.4 Case 2: Single Bent Model with Linear Soil Springs and Linear Columns

Pile shaft was also assumed linear in this case (Figure C.6). Mode shape analysis shows the first transverse period is 2.0 seconds, which also matches the period calculated by the transverse ESA procedure.

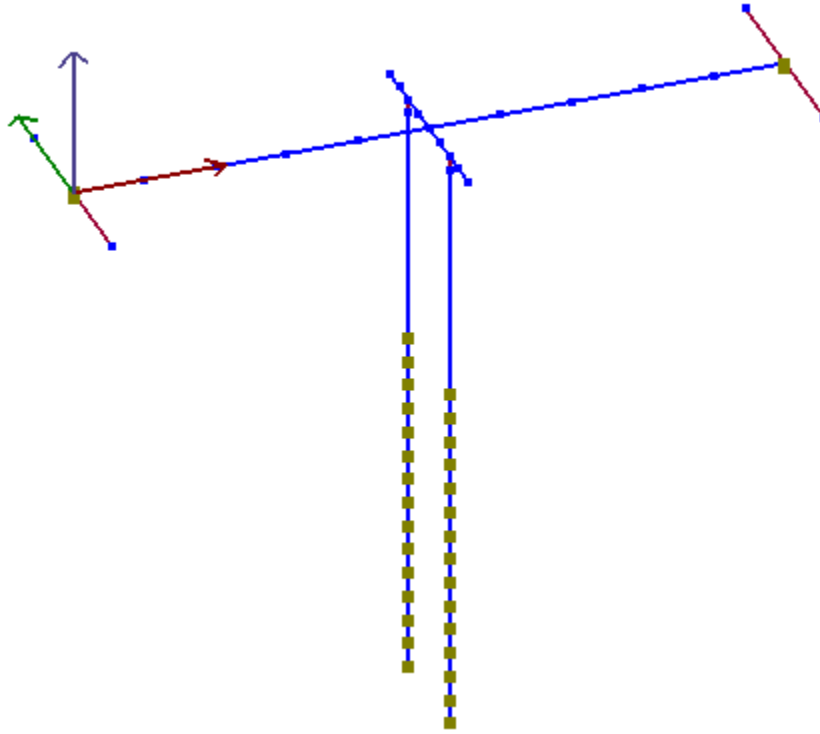


Figure C.6 Single bent model for Case 2

C.4.1 Comparison of ESA and THA Results

Table C.4 displays the comparison of ESA and THA results for Case 2. Essentially, the ESA displacement demand and THA maximum displacement are nearly the same for this linear case (around 1% or less for most motions while reaching about 4% for Motions# 2, 3 and 9). Note that Rayleigh damping was included for the soil spring zero-length elements.

Table C.5 shows the maximum column bending moments and shear forces for the 14 motions. The maximum column bending moments range from around 9,370 kip-ft – 19,900 kip-ft. Note that all of these maximum bending moments also exceed the plastic moment (6,100 kip-ft) to be employed for the nonlinear columns (Figure C.2; to be studied in later sections).

Table C.4 Comparison of transverse ESA displacement demand and THA maximum displacement (ESA displacement demand for an individual motion is based on the response spectrum of that motion)

Motion#	Motion (PGA)	THA Maximum Displacement (in)	ESA Displacement Demand (in)	Difference (“-” sign means ESA is less)
1	ROCKS1N1 (0.70g)	12.9	13.1	1.3%
2	ROCKS1N2 (0.38g)	15.9	15.3	-4.5%
3	ROCKS1N3 (0.32g)	10.9	10.5	-3.8%
4	ROCKS1N4 (0.34g)	13.2	13.1	-0.6%
5	ROCKS1N5 (0.53g)	21.4	21.5	0.2%
6	ROCKS1N6 (0.42g)	12.3	12.4	0.8%
7	ROCKS1N7 (0.36g)	14.0	13.9	-0.9%
8	ROCKS1P1 (0.71g)	13.3	13.4	1.2%
9	ROCKS1P2 (0.44g)	15.7	15.0	-4.5%
10	ROCKS1P3 (0.48g)	22.4	22.5	0.2%
11	ROCKS1P4 (0.32g)	13.2	13.2	-0.1%
12	ROCKS1P5 (0.67g)	14.7	14.9	1.2%
13	ROCKS1P6 (0.41g)	12.3	12.4	0.8%
14	ROCKS1P7 (0.40g)	10.1	10.0	-1.0%
Average		14.5	14.4	-0.6%

Note: ESA displacement demand based on target ARS is 14.8 inches, corresponding a difference of 2.3%.

Table C.5 Maximum Column Shear Forces and Bending Moments (Transverse)

Motion#	Motion (PGA)	Maximum Bending Moment (kip-ft)	Maximum Shear Force (kips)
1	ROCKS1N1 (0.70g)	11,777.4	330.5
2	ROCKS1N2 (0.38g)	14,371.0	405.1
3	ROCKS1N3 (0.32g)	10,084.4	281.9
4	ROCKS1N4 (0.34g)	12,010.7	337.2
5	ROCKS1N5 (0.53g)	19,049.3	539.5
6	ROCKS1N6 (0.42g)	11,273.8	316.1
7	ROCKS1N7 (0.36g)	12,756.3	358.7
8	ROCKS1P1 (0.71g)	12,105.0	340.0
9	ROCKS1P2 (0.44g)	14,156.2	398.9
10	ROCKS1P3 (0.48g)	19,908.7	564.2
11	ROCKS1P4 (0.32g)	12,051.1	338.4
12	ROCKS1P5 (0.67g)	13,352.4	375.8
13	ROCKS1P6 (0.41g)	11,300.8	316.8
14	ROCKS1P7 (0.40g)	9,369.5	261.3

C.5 Case 3: Single Bent Model with Rigid Base and Nonlinear Columns

Compared to Case 1, Case 3 (Figure C.7) activates the bilinear moment-curvature behavior for the columns. Mode shape analysis shows the first transverse period is 0.86 seconds, which also matches the period calculated by the transverse ESA procedure.

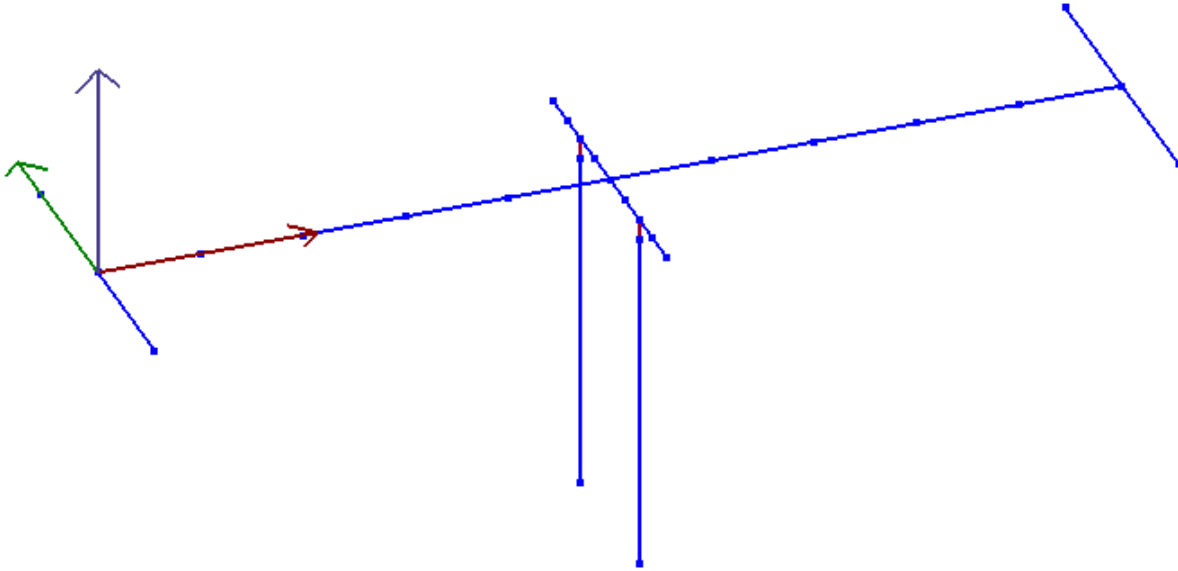


Figure C.7 Single bent model for Case 3 (with rigid base at mudline)

C.5.1 Comparison of ESA and THA Results

Table C.6 displays the comparison of ESA and THA results for Case 3. An overall (average) difference of about 23.8% is observed while some motions significantly exceed this value (Table C.6). It is indicated that these (large) differences are due to the nonlinearity of the columns.

Table C.7 shows the maximum column bending moments and shear forces for the 14 motions. As can be seen, the maximum column bending moment reached the plastic value of 6,100 kip-ft (also see Figure C.8 and Figure C.9), as defined in the moment-curvature relationship for the columns (Figure C.2). The maximum shear force reached the ultimate value of 254.2 kips for all motions (Figure C.4).

Table C.6 Comparison of transverse ESA displacement demand and THA maximum displacement (ESA displacement demand for an individual motion is based on the response spectrum of that motion)

Motion#	Motion (PGA)	THA Maximum Displacement (in)	ESA Displacement Demand (in)	Difference (“-” sign means ESA is less)
1	ROCKS1N1 (0.70g)	5.82	5.82	0.0%
2	ROCKS1N2 (0.38g)	5.70	4.76	-19.7%
3	ROCKS1N3 (0.32g)	6.19	5.41	-14.5%
4	ROCKS1N4 (0.34g)	5.42	5.46	0.7%
5	ROCKS1N5 (0.53g)	9.46	5.53	-71.0%
6	ROCKS1N6 (0.42g)	5.16	6.10	15.3%
7	ROCKS1N7 (0.36g)	6.77	5.35	-26.5%
8	ROCKS1P1 (0.71g)	9.88	5.87	-68.3%
9	ROCKS1P2 (0.44g)	7.36	5.02	-46.7%
10	ROCKS1P3 (0.48g)	10.18	5.19	-96.0%
11	ROCKS1P4 (0.32g)	6.11	5.45	-12.0%
12	ROCKS1P5 (0.67g)	5.01	5.86	14.6%
13	ROCKS1P6 (0.41g)	5.14	6.09	15.7%
14	ROCKS1P7 (0.40g)	7.27	5.22	-39.2%
Average		6.82	5.51	-23.8%

Note: ESA displacement demand based on target ARS is 5.40 inches, corresponding a difference of -26.3%.

Table C.7 Maximum Column Shear Forces and Bending Moments (Transverse)

Motion#	Motion (PGA)	Maximum Bending Moment (kip-ft)	Maximum Shear Force (kips)
1	ROCKS1N1 (0.70g)	6,100	254.2
2	ROCKS1N2 (0.38g)	6,100	254.2
3	ROCKS1N3 (0.32g)	6,100	254.2
4	ROCKS1N4 (0.34g)	6,100	254.2
5	ROCKS1N5 (0.53g)	6,100	254.2
6	ROCKS1N6 (0.42g)	6,100	254.2
7	ROCKS1N7 (0.36g)	6,100	254.2
8	ROCKS1P1 (0.71g)	6,100	254.2
9	ROCKS1P2 (0.44g)	6,100	254.2
10	ROCKS1P3 (0.48g)	6,100	254.2
11	ROCKS1P4 (0.32g)	6,100	254.2
12	ROCKS1P5 (0.67g)	6,100	254.2
13	ROCKS1P6 (0.41g)	6,100	254.2
14	ROCKS1P7 (0.40g)	6,100	254.2

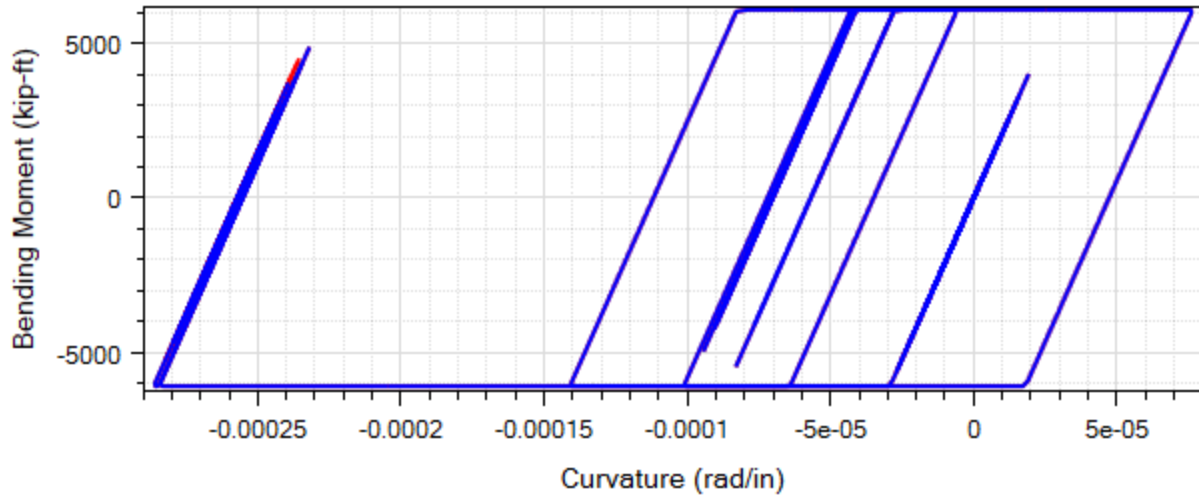


Figure C.8 Moment-curvature response at column top for Motion #1 ROCKS1N1 (Red part shows the end of shaking)

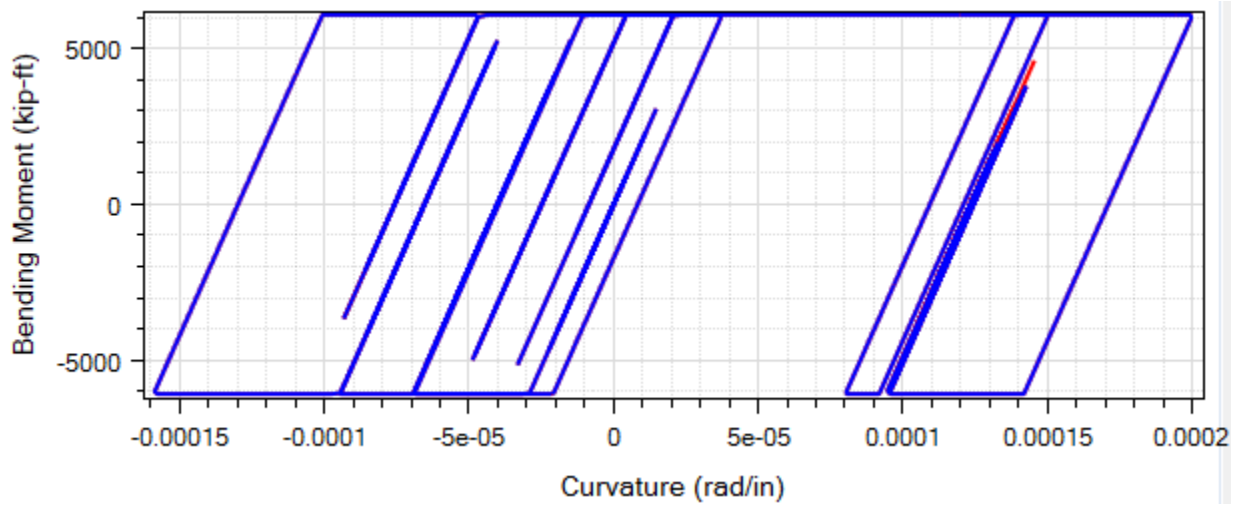


Figure C.9 Moment-curvature response at column top for Motion #2 ROCKS1N2 (Red part shows the end of shaking)

C.6 Case 4: Single Bent Model with Linear Soil Springs and Nonlinear Columns

Compared to Case 2, Case 4 (Figure C.10) activates the bilinear moment-curvature behavior for the columns. Mode shape analysis shows the first transverse period is 2.0 seconds (same as that of Case 2), which also matches the period calculated by the transverse ESA procedure.

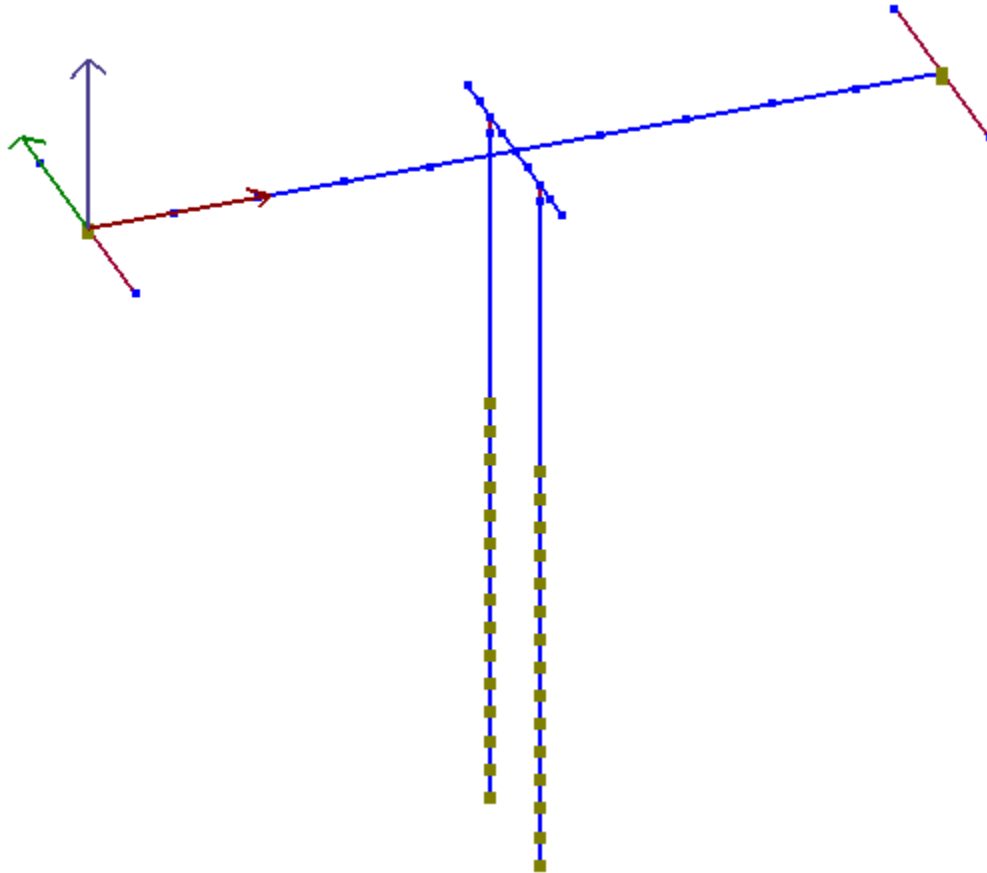


Figure C.10 Single bent model for Case 4

C.6.1 Comparison of ESA and THA Results

Table C.8 displays the comparison of ESA and THA results for Case 4. The differences between the ESA displacement demand and THA maximum displacement are as large as 30% or more. The average difference for the 14 motions is about 11%. These large differences are due to the column nonlinearity.

Table C.9 shows the maximum column bending moments and shear forces for the 14 motions. As can be seen, the maximum column bending moment reached the plastic value of 6,100 kip-ft (also see Figure C.11 and Figure C.12), as defined in the moment-curvature relationship for the columns (Figure C.2).

Table C.8 Comparison of transverse ESA displacement demand and THA maximum displacement (ESA displacement demand for an individual motion is based on the response spectrum of that motion)

Motion#	Motion (PGA)	THA Maximum Displacement (in)	ESA Displacement Demand (in)	Difference (“-” sign means ESA is less)
1	ROCKS1N1 (0.70g)	11.0	13.1	15.7%
2	ROCKS1N2 (0.38g)	16.2	15.3	-5.4%
3	ROCKS1N3 (0.32g)	10.7	10.5	-1.7%
4	ROCKS1N4 (0.34g)	13.1	13.1	-0.3%
5	ROCKS1N5 (0.53g)	13.5	21.5	37.3%
6	ROCKS1N6 (0.42g)	10.8	12.4	12.8%
7	ROCKS1N7 (0.36g)	11.5	13.9	17.9%
8	ROCKS1P1 (0.71g)	12.4	13.4	7.5%
9	ROCKS1P2 (0.44g)	15.0	15.1	0.4%
10	ROCKS1P3 (0.48g)	15.4	22.5	31.8%
11	ROCKS1P4 (0.32g)	12.1	13.2	8.4%
12	ROCKS1P5 (0.67g)	17.0	14.9	-14.0%
13	ROCKS1P6 (0.41g)	10.8	12.4	12.9%
14	ROCKS1P7 (0.40g)	9.8	10.0	1.8%
Average		12.8	14.4	11.0%

Note: ESA displacement demand based on target ARS is 14.8 inches, corresponding a difference of 13.6%.

Table C.9 Maximum Column Shear Forces and Bending Moments (Transverse)

Motion#	Motion (PGA)	Maximum Bending Moment (kip-ft)	Maximum Shear Force (kips)
1	ROCKS1N1 (0.70g)	6,100	208.5
2	ROCKS1N2 (0.38g)	6,100	254.1
3	ROCKS1N3 (0.32g)	6,100	205.8
4	ROCKS1N4 (0.34g)	6,100	226.9
5	ROCKS1N5 (0.53g)	6,100	230.5
6	ROCKS1N6 (0.42g)	6,100	207.0
7	ROCKS1N7 (0.36g)	6,100	212.9
8	ROCKS1P1 (0.71g)	6,100	220.3
9	ROCKS1P2 (0.44g)	6,100	243.9
10	ROCKS1P3 (0.48g)	6,100	247.0
11	ROCKS1P4 (0.32g)	6,100	218.2
12	ROCKS1P5 (0.67g)	6,100	254.2
13	ROCKS1P6 (0.41g)	6,100	207.1
14	ROCKS1P7 (0.40g)	6,100	198.1

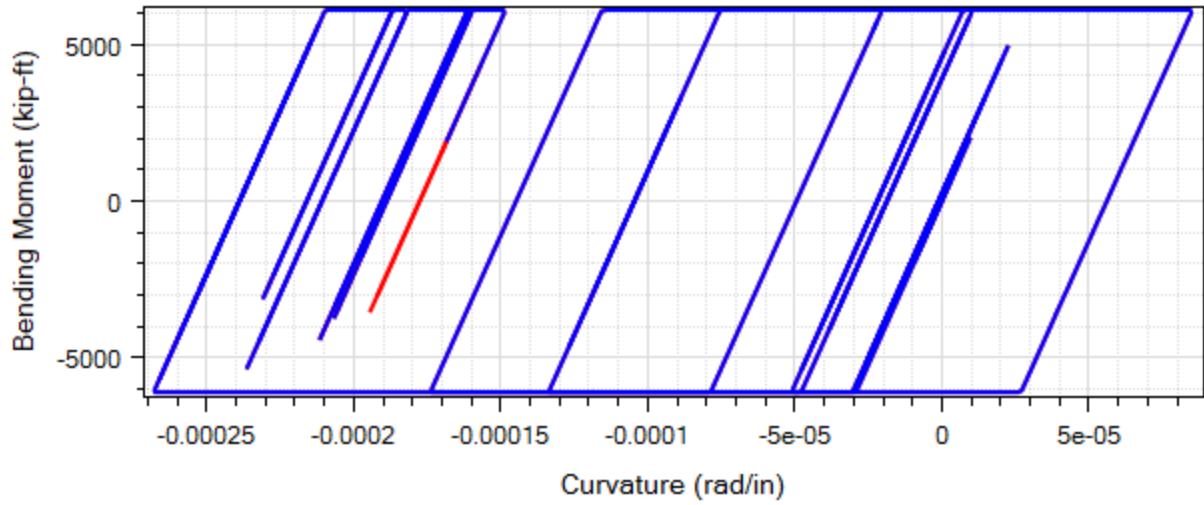


Figure C.11 Moment-curvature response at column top for Motion #1 ROCKS1N1 (Red part shows the end of shaking)

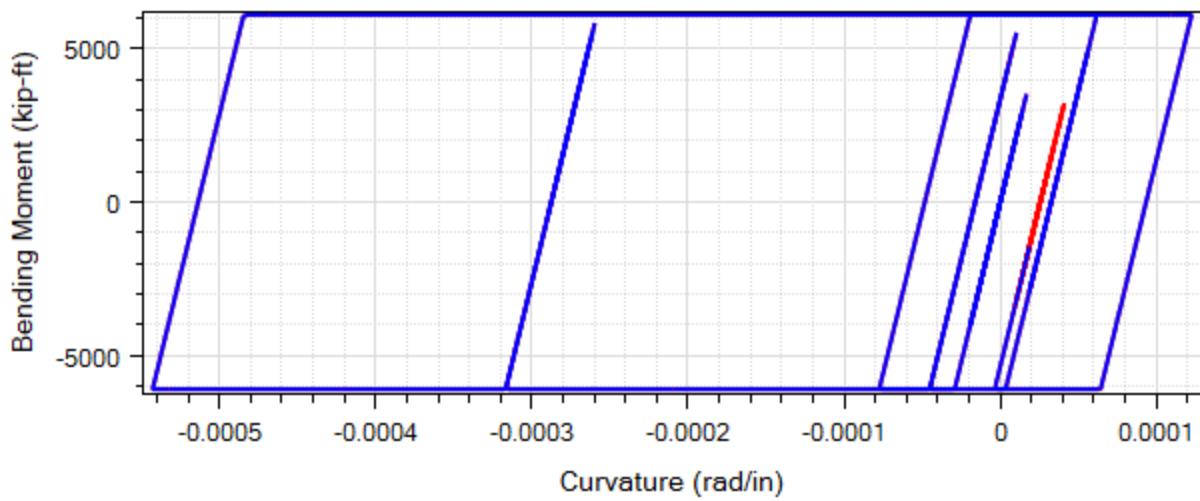


Figure C.12 Moment-curvature response at column top for Motion #2 ROCKS1N2 (Red part shows the end of shaking)

C.7 Case 5: Single Bent Model with Nonlinear Soil Springs and Nonlinear Columns

Compared to Case 4, Case 5 (Figure C.13) employs nonlinear soil springs (instead of linear soil springs). The bilinear model (Figure C.3) was also employed for the pile shaft. As such, Case 5 essentially represents a typical bent of the Salinas River Bridge model. Mode shape analysis shows the first transverse period is 2.0 seconds (the period calculated by the transverse ESA procedure is 2.21 seconds).

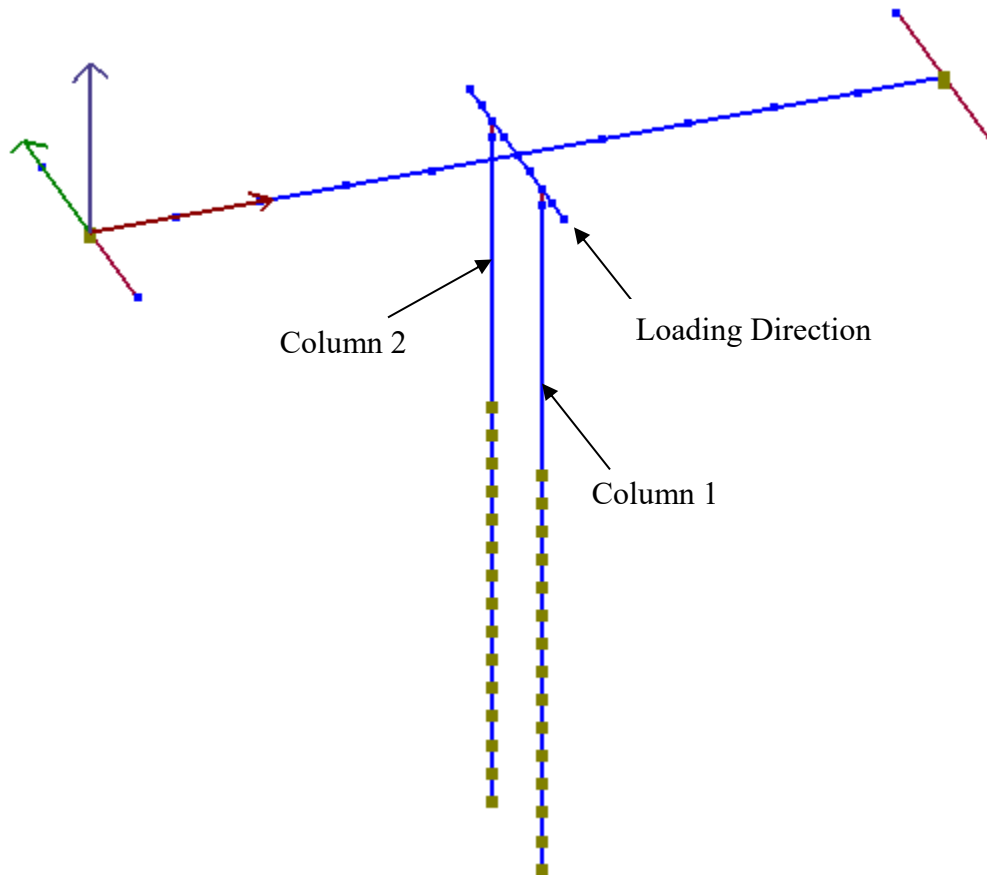


Figure C.13 Single bent model for Case 5

C.7.1 Transverse Pushover Loading

Pushover analysis was conducted by applying a load at the bentcap in 500 steps (in the transverse direction). Figure C.14 shows the pushover load-displacement response of the pushover analysis. The first batch of 2 plastic hinges formed at column top (for the 2 columns) when the pushover displacement reaches 9.4 in (at a load of about 376 kips). The second batch of 2 plastic hinges formed at column base (for the 2 columns) when the pushover displacement reached about 17.2 in (at a load of about 508 kips). After that, the bent cannot resist any additional lateral load (Figure C.14).

Based on Figure C.4, the ESA initial stiffness is 40 kip/in (= 376 kips / 9.4 in). The bending moment-curvature and shear force-displacement response at column top are shown in Figure C.2 and Figure C.4, respectively. During the pushover analysis, the axial force of one column increased when the other one decreased while both were in compression (Figure C.15).

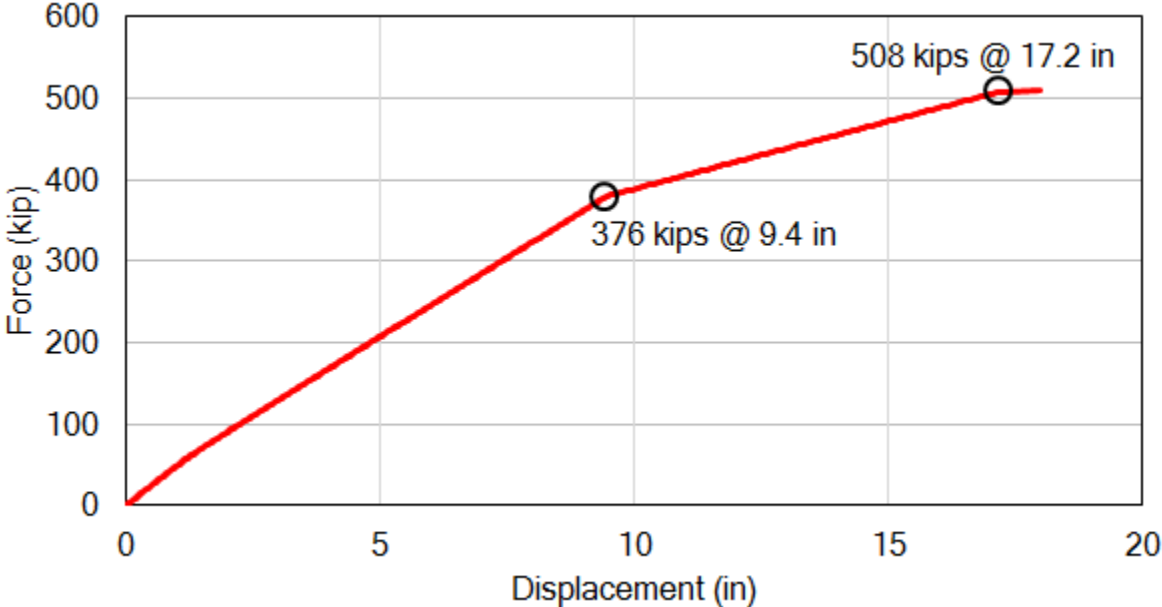


Figure C.14 Pushover load versus transverse displacement for the transverse ESA

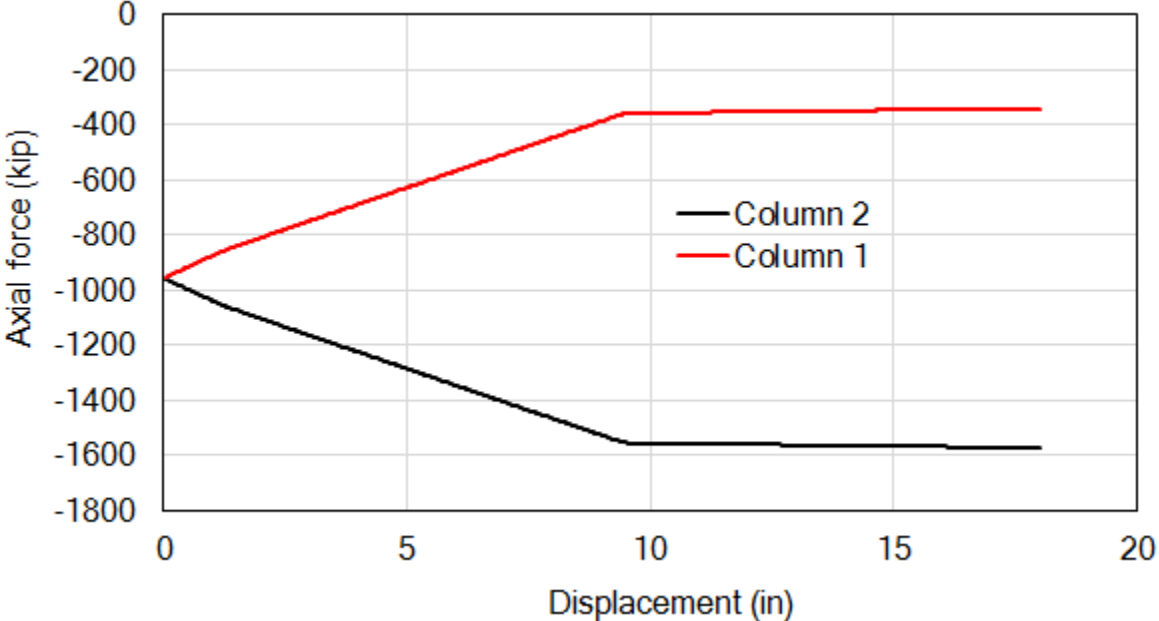


Figure C.15 Axial force versus transverse displacement for the transverse ESA

C.7.2 Comparison of ESA and THA Results

Table C.10 displays the comparison of ESA and THA results for Case 5. An overall (average) difference between the ESA displacement demand and THA maximum displacement is about 25% (while some motions resulted in more than 40%). These (large) differences are mainly due to the nonlinearity of the columns and the soil-spring foundation.

Table C.11 shows the maximum column bending moments and shear forces for the 14 motions. As can be seen, the maximum column bending moment reached the plastic value of 6,100 kip-ft (also see Figure C.16 and Figure C.17), as defined in the moment-curvature relationship for the columns (Figure C.2).

Table C.10 Comparison of transverse ESA displacement demand and THA maximum displacement (ESA displacement demand for an individual motion is based on the response spectrum of that motion)

Motion#	Motion (PGA)	THA Maximum Displacement (in)	ESA Displacement Demand (in)	Difference (“-” sign means ESA is less)
1	ROCKS1N1 (0.70g)	9.9	13.4	26.1%
2	ROCKS1N2 (0.38g)	15.7	14.7	-6.4%
3	ROCKS1N3 (0.32g)	10.5	13.8	23.8%
4	ROCKS1N4 (0.34g)	13.6	23.1	40.9%
5	ROCKS1N5 (0.53g)	13.7	18.5	26.3%
6	ROCKS1N6 (0.42g)	11.0	19.9	45.1%
7	ROCKS1N7 (0.36g)	11.8	19.2	38.3%
8	ROCKS1P1 (0.71g)	11.2	13.7	18.4%
9	ROCKS1P2 (0.44g)	15.0	14.6	-2.7%
10	ROCKS1P3 (0.48g)	15.7	18.3	14.1%
11	ROCKS1P4 (0.32g)	13.0	23.3	44.2%
12	ROCKS1P5 (0.67g)	16.8	15.4	-8.9%
13	ROCKS1P6 (0.41g)	11.0	20.0	45.2%
14	ROCKS1P7 (0.40g)	10.1	10.9	7.5%
Average		12.8	17.1	25.1%

Note: ESA displacement demand based on target ARS is 17.0 inches, corresponding a difference of 24.6%.

Table C.11 Maximum Column Shear Forces and Bending Moments (Transverse)

Motion#	Motion (PGA)	Maximum Bending Moment (kip-ft)	Maximum Shear Force (kips)
1	ROCKS1N1 (0.70g)	6,100	193.7
2	ROCKS1N2 (0.38g)	6,100	241.1
3	ROCKS1N3 (0.32g)	6,100	198.4
4	ROCKS1N4 (0.34g)	6,100	224.4
5	ROCKS1N5 (0.53g)	6,100	225.0
6	ROCKS1N6 (0.42g)	6,100	202.5
7	ROCKS1N7 (0.36g)	6,100	209.7
8	ROCKS1P1 (0.71g)	6,100	203.1
9	ROCKS1P2 (0.44g)	6,100	235.1
10	ROCKS1P3 (0.48g)	6,100	241.7
11	ROCKS1P4 (0.32g)	6,100	219.2
12	ROCKS1P5 (0.67g)	6,100	250.8
13	ROCKS1P6 (0.41g)	6,100	202.5
14	ROCKS1P7 (0.40g)	6,100	195.3

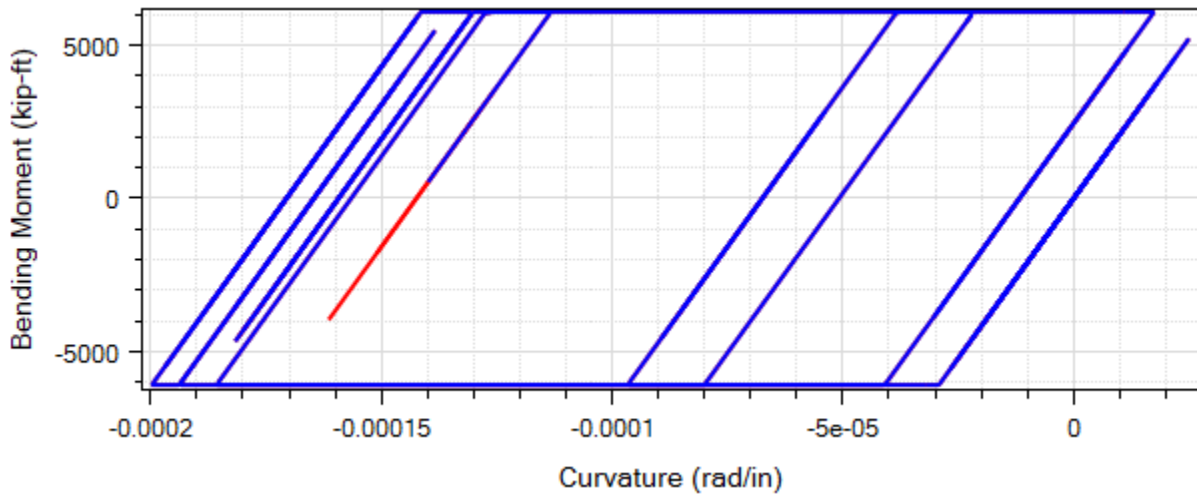


Figure C.16 Moment-curvature response at column top for Motion #1 ROCKS1N1 (Red part shows the end of shaking)

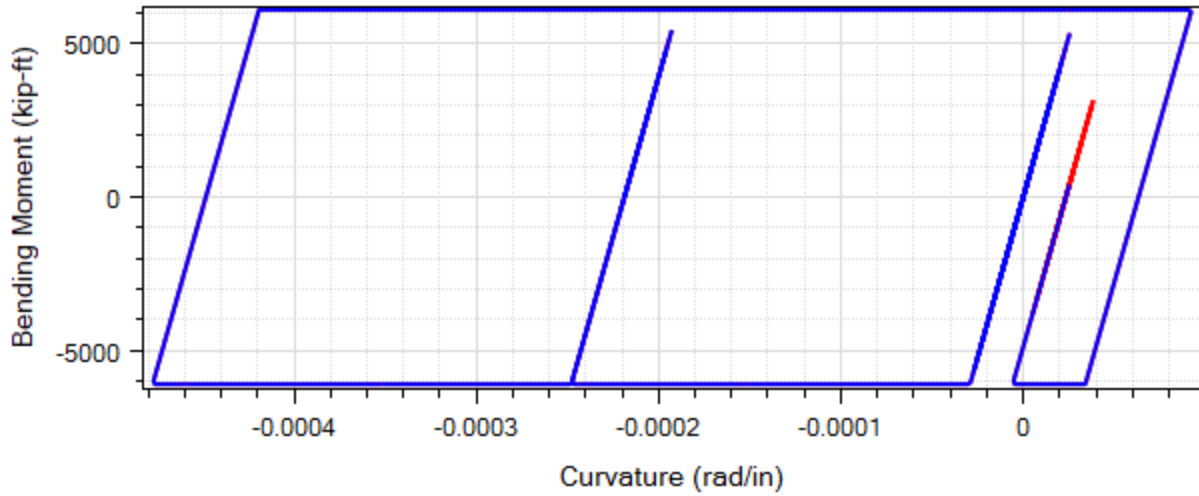


Figure C.17 Moment-curvature response at column top for Motion #2 ROCKS1N2 (Red part shows the end of shaking)

C.8 Case 6: Multi-bent Model with Nonlinear Soil Springs and Nonlinear Columns

Case 6 (Figure C.18) is a multi-bent bridge model with 10 identical bents (each bent is the same as Case 5). No abutment was considered in Case 6. Mode shape analysis (Figure C.19) showed the first transverse period is 2.0 seconds (the period calculated by the transverse ESA procedure is 2.21 seconds).

THA numerical simulations were conducted for Case 6. The THA results show the response of Case 6 is the same as that of Case 5.

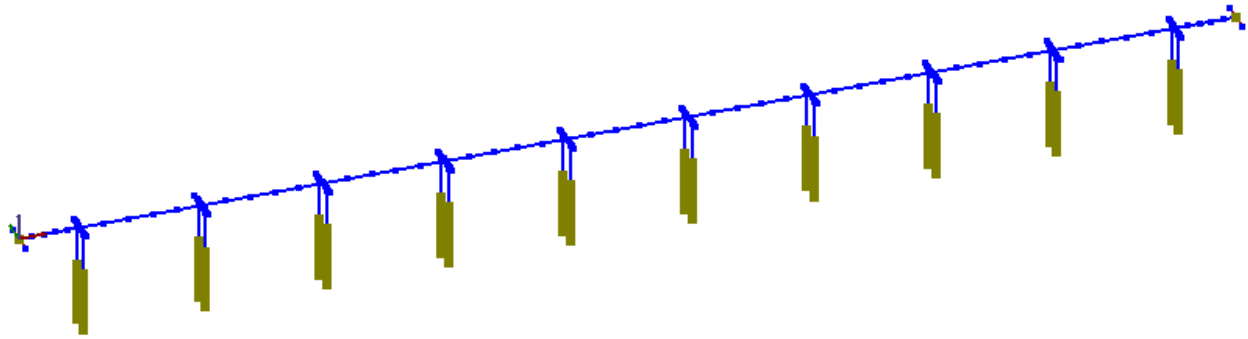


Figure C.18 Multi-bent model for Case 6

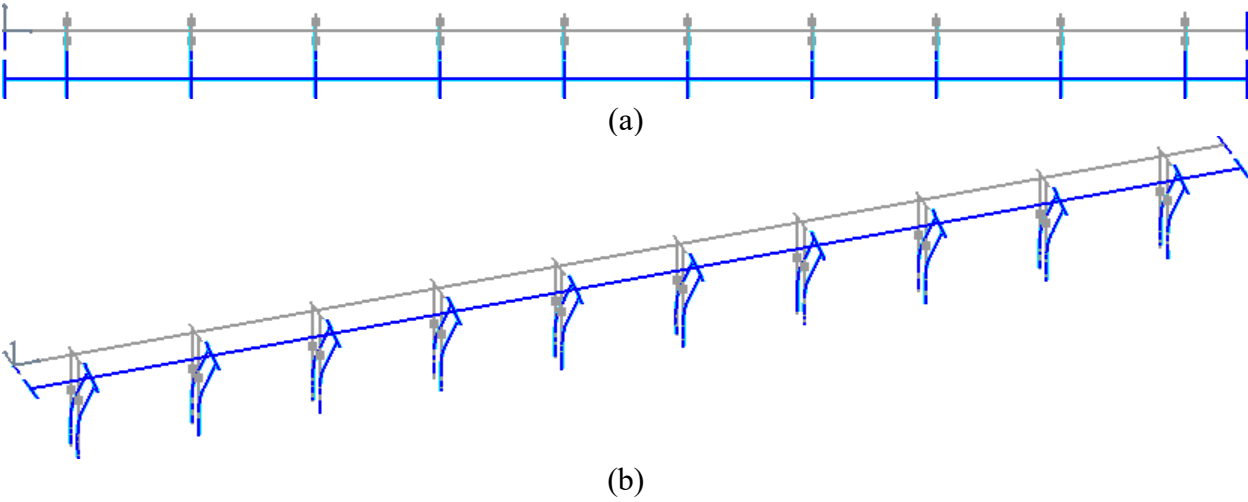


Figure C.19 First transverse mode of the multi-bent model (period = 2.0 seconds): (a) plan view; (b) 3D view

C.9 Case 7: Multi-bent Model with End-bents

Compared to Case 6, Case 7 (Figure C.20) included 2 end-bents (same as the other bents) at the abutment locations. However, lateral abutment stiffness was not considered in Case 7. Mode shape analysis (Figure C.21) showed the first transverse period is 1.94 seconds (the period calculated by the transverse ESA procedure is 2.21 seconds).

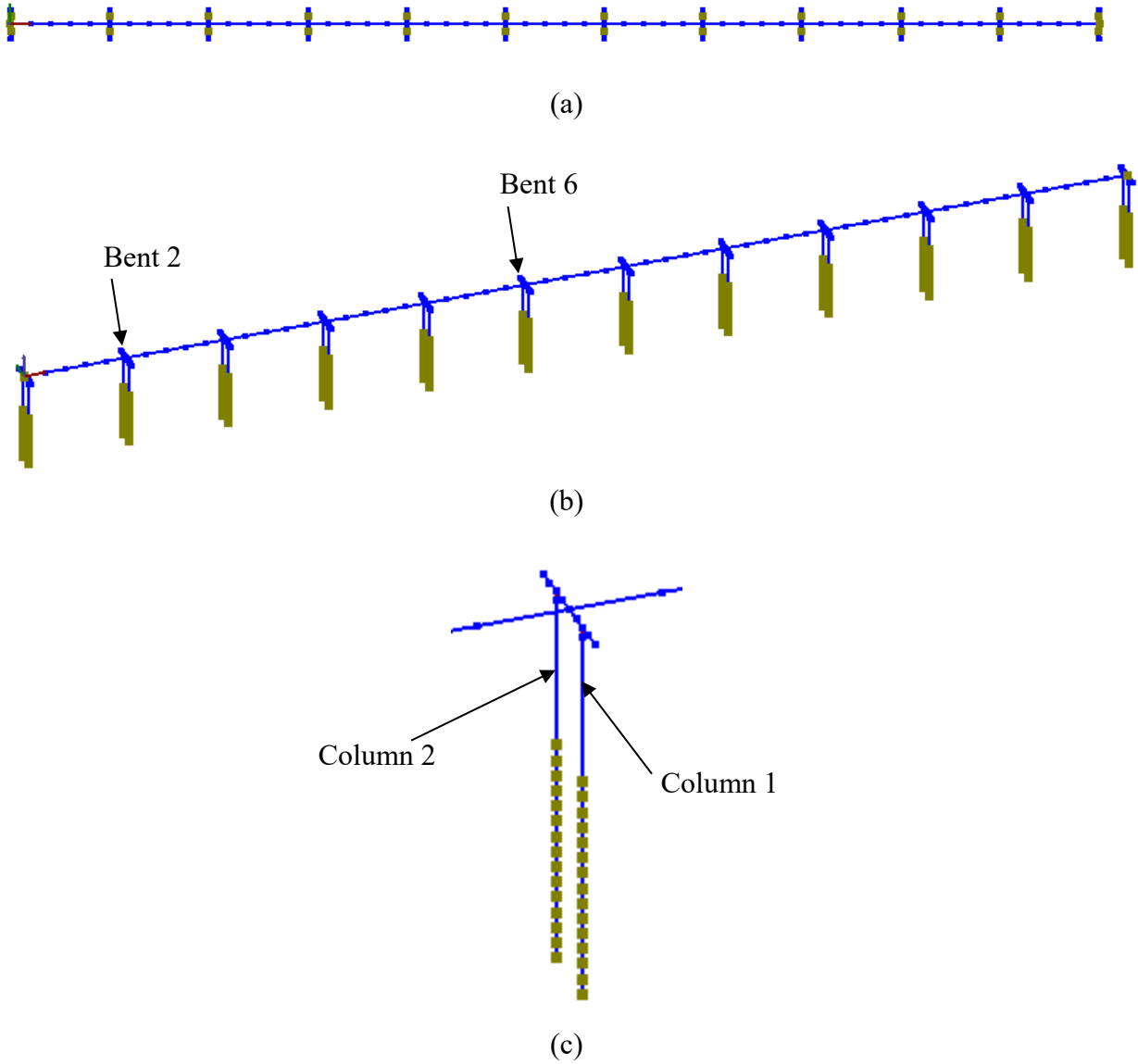


Figure C.20 Multi-bent model with end-bents: (a) plan view; (b) 3D view; (c) bent close-up

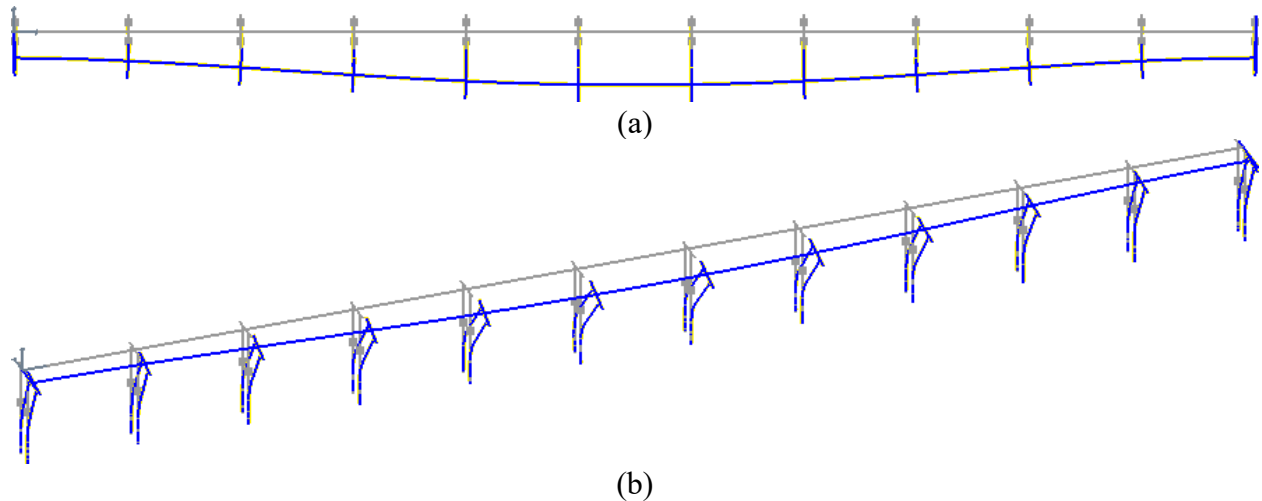


Figure C.21 First transverse mode of the multi-bent model (period = 1.94 seconds)

C.9.1 Comparison of ESA and THA Results

Table C.12 displays the comparison of ESA and THA results for Case 7. The differences between the ESA displacement demand and THA maximum displacement are as large as about 44%. An overall difference of 15% between ESA and THA was observed (Table C.12). These (large) differences are mainly due to the nonlinearity of the columns and the soil-spring foundation. Table C.13 shows the comparison of THA maximum displacement for Cases 5 and 7 where Case 7 shows higher maximum displacement.

Table C.14 shows the maximum column bending moments and shear forces for the 14 motions. As can be seen, the maximum column bending moment reached the plastic value of 6,100 kip-ft (also see Figure C.22 and Figure C.23), as defined in the moment-curvature relationship for the columns (Figure C.2).

Table C.12 Comparison of transverse ESA displacement demand and THA maximum displacement (ESA displacement demand for an individual motion is based on the response spectrum of that motion)

Motion#	Motion (PGA)	THA Maximum Displacement (in)	ESA Displacement Demand (in)	Difference (“-” sign means ESA is less)
1	ROCKS1N1 (0.70g)	12.2	13.4	8.7%
2	ROCKS1N2 (0.38g)	16.1	14.7	9.0%
3	ROCKS1N3 (0.32g)	10.7	13.8	22.3%
4	ROCKS1N4 (0.34g)	14.3	23.1	38.0%
5	ROCKS1N5 (0.53g)	17.4	18.5	6.4%
6	ROCKS1N6 (0.42g)	13.1	19.9	34.4%
7	ROCKS1N7 (0.36g)	12.5	19.2	34.6%
8	ROCKS1P1 (0.71g)	14.0	13.7	2.5%
9	ROCKS1P2 (0.44g)	15.7	14.6	8.0%
10	ROCKS1P3 (0.48g)	19.7	18.3	7.2%
11	ROCKS1P4 (0.32g)	13.1	23.3	43.6%
12	ROCKS1P5 (0.67g)	20.6	15.4	33.7%
13	ROCKS1P6 (0.41g)	13.1	20.0	34.6%
14	ROCKS1P7 (0.40g)	10.5	10.9	3.7%
Average		14.5	17.1	15.0%

Note: ESA displacement demand based on target ARS is 17.0 inches, corresponding to a difference of 14.5%.

Table C.13 Comparison of Cases 5 and 7 for THA maximum displacement

Motion#	Motion (PGA)	THA Maximum Displacement (in)		
		Case 5	Case 7	Difference (“-” sign means Case 7 is less)
1	ROCKS1N1 (0.70g)	9.9	12.2	19.0%
2	ROCKS1N2 (0.38g)	15.7	16.1	2.3%
3	ROCKS1N3 (0.32g)	10.5	10.7	1.9%
4	ROCKS1N4 (0.34g)	13.6	14.3	4.8%
5	ROCKS1N5 (0.53g)	13.7	17.4	21.2%
6	ROCKS1N6 (0.42g)	11.0	13.1	16.2%
7	ROCKS1N7 (0.36g)	11.8	12.5	5.6%
8	ROCKS1P1 (0.71g)	11.2	14.0	20.4%
9	ROCKS1P2 (0.44g)	15.0	15.7	4.8%
10	ROCKS1P3 (0.48g)	15.7	19.7	19.9%
11	ROCKS1P4 (0.32g)	13.0	13.1	1.0%
12	ROCKS1P5 (0.67g)	16.8	20.6	18.5%
13	ROCKS1P6 (0.41g)	11.0	13.1	16.2%
14	ROCKS1P7 (0.40g)	10.1	10.5	4.0%
Average		12.8	14.5	11.9%

Table C.14 Maximum Column Shear Forces and Bending Moments (Transverse)

Motion#	Motion (PGA)	Maximum Bending Moment (kip-ft)	Maximum Shear Force (kips)		
			Case 5	Case 7	Difference (“-” sign means Case 7 is less)
1	ROCKS1N1 (0.70g)	6,100	193.7	213.2	9.1%
2	ROCKS1N2 (0.38g)	6,100	241.1	244.8	1.5%
3	ROCKS1N3 (0.32g)	6,100	198.4	200.2	0.9%
4	ROCKS1N4 (0.34g)	6,100	224.4	229.6	2.3%
5	ROCKS1N5 (0.53g)	6,100	225.0	254.2	11.5%
6	ROCKS1N6 (0.42g)	6,100	202.5	220.1	8.0%
7	ROCKS1N7 (0.36g)	6,100	209.7	215.7	2.8%
8	ROCKS1P1 (0.71g)	6,100	203.1	227.0	10.5%
9	ROCKS1P2 (0.44g)	6,100	235.1	241.8	2.8%
10	ROCKS1P3 (0.48g)	6,100	241.7	254.2	4.9%
11	ROCKS1P4 (0.32g)	6,100	219.2	220.6	0.7%
12	ROCKS1P5 (0.67g)	6,100	250.8	254.2	1.3%
13	ROCKS1P6 (0.41g)	6,100	202.5	220.2	8.0%
14	ROCKS1P7 (0.40g)	6,100	195.3	198.9	1.8%

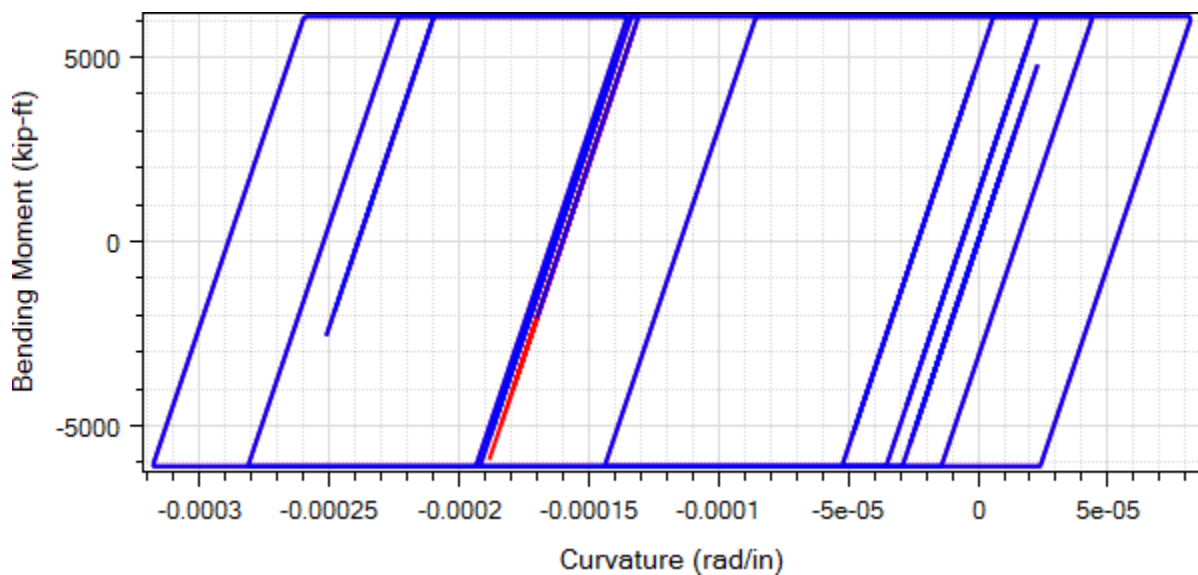


Figure C.22 Moment-curvature response at column top for Column 1 of Bent 6 for Motion #1 ROCKS1N1 (Red part shows the end of shaking)

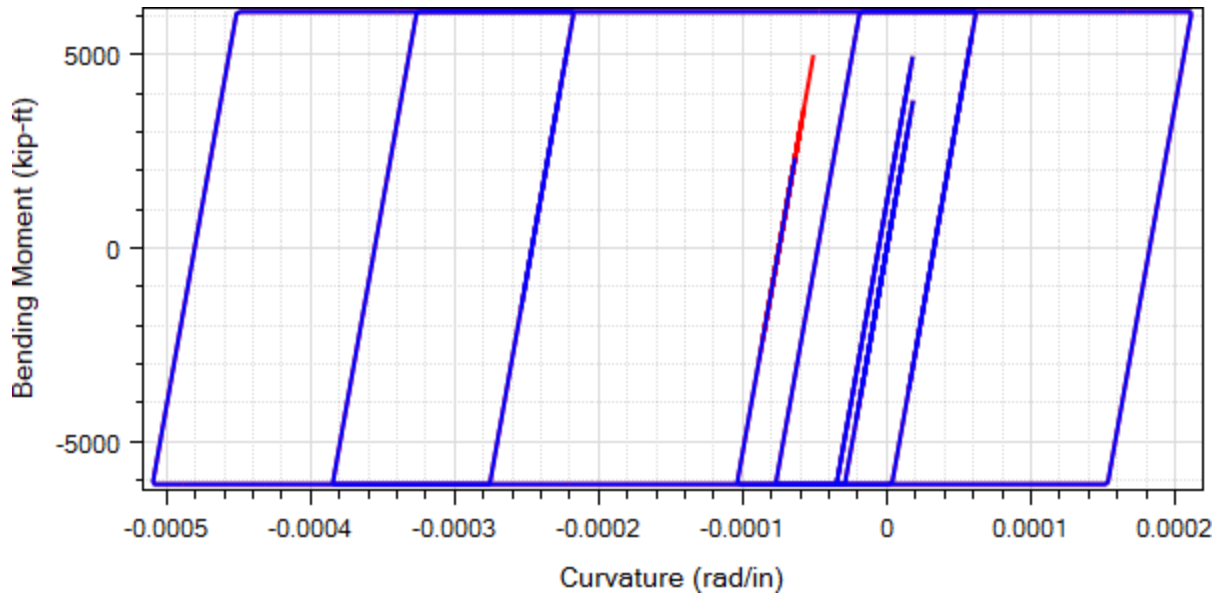


Figure C.23 Moment-curvature response at column top for Column 1 of Bent 6 for Motion #2 ROCKS1N2 (Red part shows the end of shaking)

C.10 Case 8: Salinas River Bridge Model

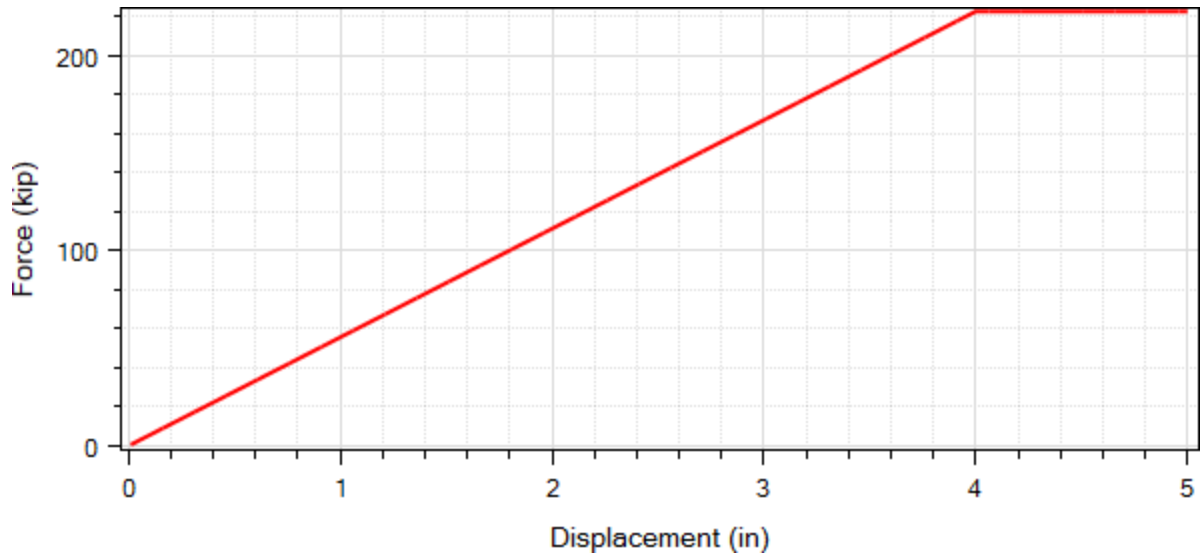
Compared to Case 7, Case 8 (see Figure C.20) included abutment resistance in the transverse direction. The transverse abutment resistance was taken as a fraction of the longitudinal resistance (Aviram *et al.* 2008a, 2008b). According to Caltrans SDC Example (2005), a bilinear model of initial stiffness of 128.25 kip/in and yield displacement of 4 in was employed for the longitudinal direction of each abutment for the Salinas River Bridge model. As a result, a bilinear model with a yield force of 222.5 kips at a yield displacement of 4 in was employed (Figure C.24a) for the transverse direction of each abutment (Aviram *et al.* 2008a, 2008b; Caltrans 2013; Mahan 2005). Note that Rayleigh damping was not included in the zeroLength elements of the abutments. Compared to the response of a typical bent (Figure C.24b), it may be seen that:

1. Total stiffness from bridge bents is 480 kip/in (= 40 kip/in x 12 bents), compared to 111.25 kip/in (=55.625 kip/in x 2) from the abutments.
2. Abutments yield first at a displacement of 4 inches.
3. First yield of intermediate bents occurs at 9.4 inches, and full resistance is reached at 17.2 inches.

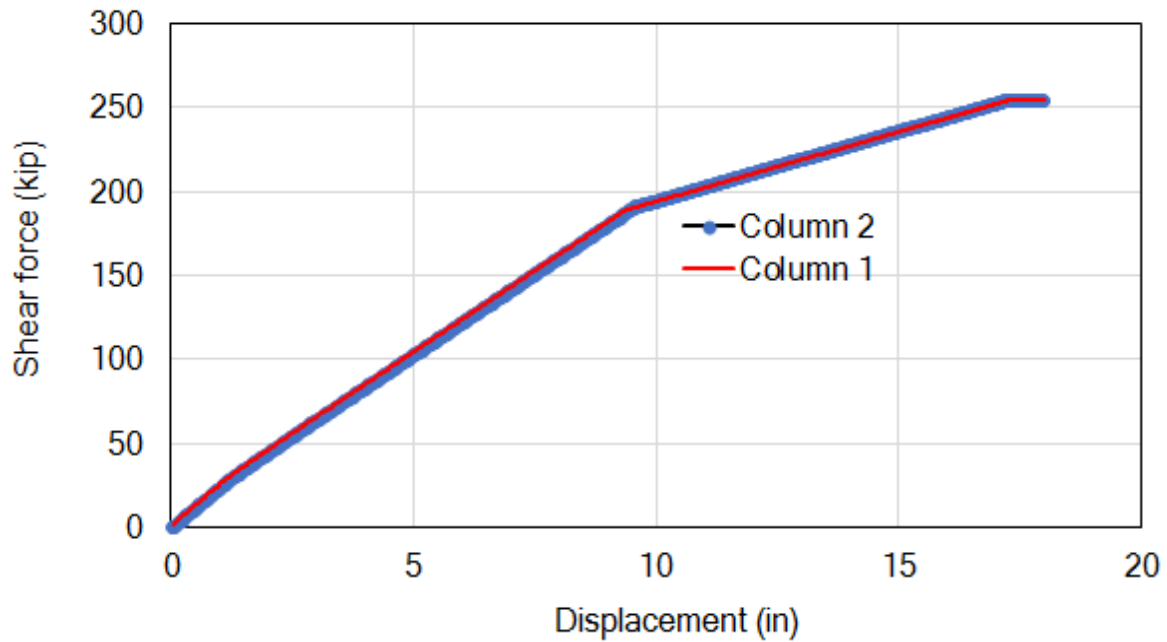
Abutment total ultimate resistance is $222.5 \times 2 = 445$ kips, compared to total ultimate resistance from the bridge bents of $254.2 \times 24 = 6,100.8$ kips.

The quantities above can be used to assess the level of deformation reached in each earthquake shaking event below (Table 2.17).

Mode shape analysis (Figure C.25) shows the first transverse period is 1.91 seconds, which is a bit lower than Case 7 due to the increased transverse abutment resistance (the period reported by the transverse ESA for a typical bent is 2.21 seconds).



(a) Idealized bilinear force-displacement relationship employed for the abutment in the transverse direction (ultimate passive pressure force = 222.5 kips; yield displacement = 4 in; thus the abutment stiffness = 55.625 kip/in)



(b) Column shear force vs. displacement response in pushover analysis

Figure C.24 Abutment and column response in pushover analysis

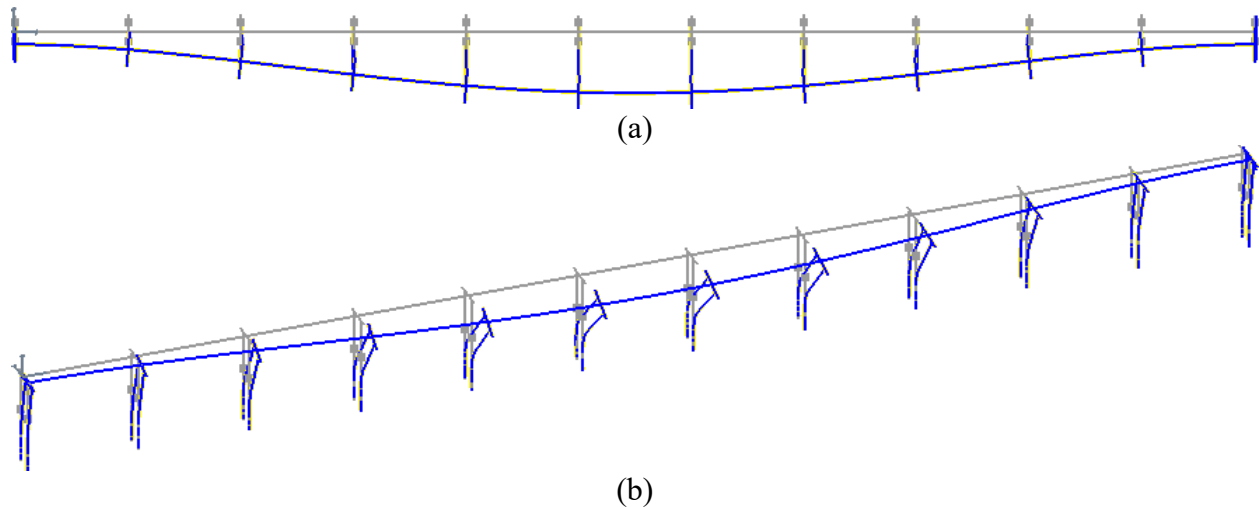


Figure C.25 First transverse mode of Salinas River Bridge (period = 1.91 seconds): (a) plan view; (b) 3D view

C.10.1 Comparison of ESA and THA Results

Table C.15 displays the comparison of ESA and THA results for Case 8. An overall (average) difference of about 10% was observed (while some motions resulted in 30% or more). These (large) differences are mainly due to the nonlinearity of the columns and the soil-spring foundation. Table C.16 shows the comparison of THA maximum displacement for Cases 5 and 8 where Case 8 shows higher maximum displacement (in general).

Table C.17 shows the maximum column bending moments and shear forces for the 14 motions. As can be seen, the maximum column bending moment and the ultimate abutment resistance force reached 6,100 kip-ft (also see Figure C.26), and 222.5 kips (also see Figure C.27), respectively, as defined in Figure C.2 and Figure C.24. Figure C.26 and Figure C.27 show the column and abutment response for Column 1 of Bent 6 (center bent) for Motion #1 ROCKS1N1. Figure C.28 and Figure C.29 display the response for Motion #2 ROCKS1N2.

Table C.15 Comparison of transverse ESA displacement demand and THA maximum displacement (ESA displacement demand for an individual motion is based on the response spectrum of that motion)

Motion#	Motion (PGA)	THA Maximum Displacement (in)	ESA Displacement Demand (in)	Difference (“-” sign means ESA is less)
1	ROCKS1N1 (0.70g)	14.7	13.4	-9.7%
2	ROCKS1N2 (0.38g)	14.9	14.7	-1.4%
3	ROCKS1N3 (0.32g)	10.4	13.8	24.3%
4	ROCKS1N4 (0.34g)	16.2	23.1	29.6%
5	ROCKS1N5 (0.53g)	17.1	18.5	7.8%
6	ROCKS1N6 (0.42g)	13.9	19.9	30.1%
7	ROCKS1N7 (0.36g)	14.7	19.2	23.4%
8	ROCKS1P1 (0.71g)	15.7	13.7	-14.9%
9	ROCKS1P2 (0.44g)	15.6	14.6	-6.9%
10	ROCKS1P3 (0.48g)	18.9	18.3	-3.2%
11	ROCKS1P4 (0.32g)	14.9	23.3	35.9%
12	ROCKS1P5 (0.67g)	21.1	15.4	-36.7%
13	ROCKS1P6 (0.41g)	14.0	20.0	30.2%
14	ROCKS1P7 (0.40g)	12.5	10.9	-14.5%
Average		15.3	17.1	10.1%

Note: ESA displacement demand based on target ARS is 17.0 inches, corresponding a difference of 9.5%.

Table C.16 Comparison of Cases 5 and 8 for THA maximum displacement

Motion#	Motion (PGA)	THA Maximum Displacement (in)		Difference (“-” sign means Case 8 is less)
		Case 5	Case 8	
1	ROCKS1N1 (0.70g)	9.9	14.7	32.6%
2	ROCKS1N2 (0.38g)	15.7	14.9	-5.0%
3	ROCKS1N3 (0.32g)	10.5	10.4	-0.7%
4	ROCKS1N4 (0.34g)	13.6	16.2	16.1%
5	ROCKS1N5 (0.53g)	13.7	17.1	20.1%
6	ROCKS1N6 (0.42g)	11.0	13.9	21.4%
7	ROCKS1N7 (0.36g)	11.8	14.7	19.4%
8	ROCKS1P1 (0.71g)	11.2	15.7	29.0%
9	ROCKS1P2 (0.44g)	15.0	15.6	3.9%
10	ROCKS1P3 (0.48g)	15.7	18.9	16.8%
11	ROCKS1P4 (0.32g)	13.0	14.9	13.0%
12	ROCKS1P5 (0.67g)	16.8	21.1	20.3%
13	ROCKS1P6 (0.41g)	11.0	14.0	21.5%
14	ROCKS1P7 (0.40g)	10.1	12.5	19.2%
Average		12.8	15.3	16.7%

Table C.17 Maximum Column Shear Forces and Bending Moments (Transverse)

Motion#	Motion (PGA)	Maximum Bending Moment (kip-ft)	Maximum Shear Force (kips)		
			Case 5	Case 8	Difference (“-” sign means Case 8 is less)
1	ROCKS1N1 (0.70g)	6,100	193.7	233.3	17.0%
2	ROCKS1N2 (0.38g)	6,100	241.1	235.4	-2.4%
3	ROCKS1N3 (0.32g)	6,100	198.4	197.8	-0.3%
4	ROCKS1N4 (0.34g)	6,100	224.4	245.6	8.6%
5	ROCKS1N5 (0.53g)	6,100	225.0	253.7	11.3%
6	ROCKS1N6 (0.42g)	6,100	202.5	227.3	10.9%
7	ROCKS1N7 (0.36g)	6,100	209.7	233.3	10.1%
8	ROCKS1P1 (0.71g)	6,100	203.1	241.0	15.7%
9	ROCKS1P2 (0.44g)	6,100	235.1	240.5	2.2%
10	ROCKS1P3 (0.48g)	6,100	241.7	254.2	4.9%
11	ROCKS1P4 (0.32g)	6,100	219.2	234.6	6.6%
12	ROCKS1P5 (0.67g)	6,100	250.8	254.2	1.3%
13	ROCKS1P6 (0.41g)	6,100	202.5	227.4	11.0%
14	ROCKS1P7 (0.40g)	6,100	195.3	215.3	9.3%

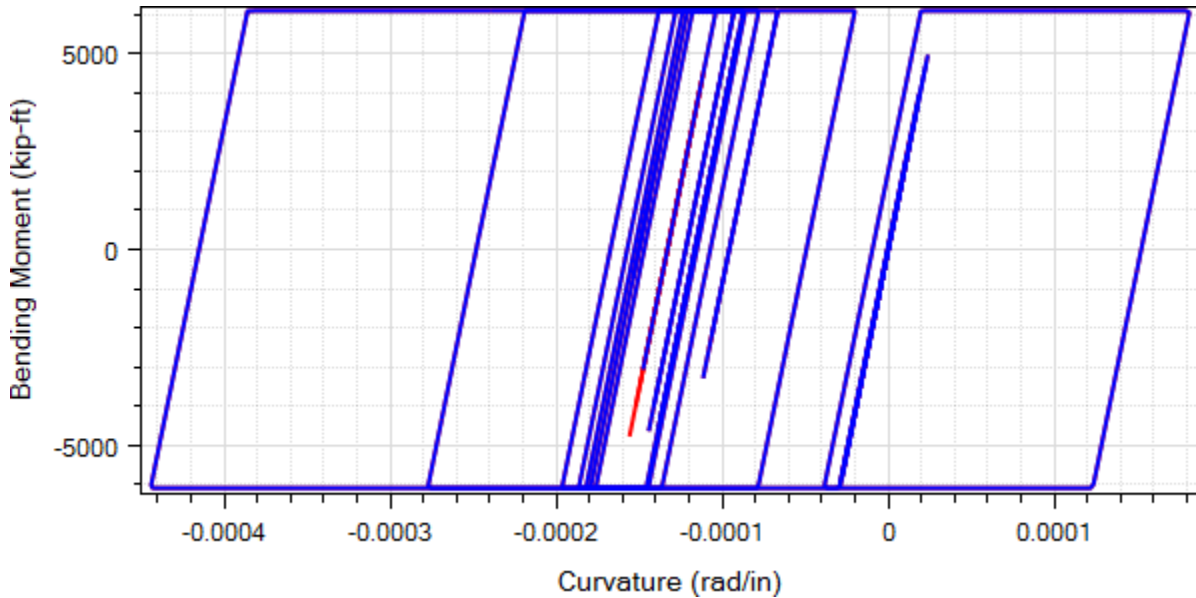


Figure C.26 Moment-curvature response at column top for Column 1 of Bent 6 for Motion #1 ROCKS1N1 (Red part shows the end of shaking)

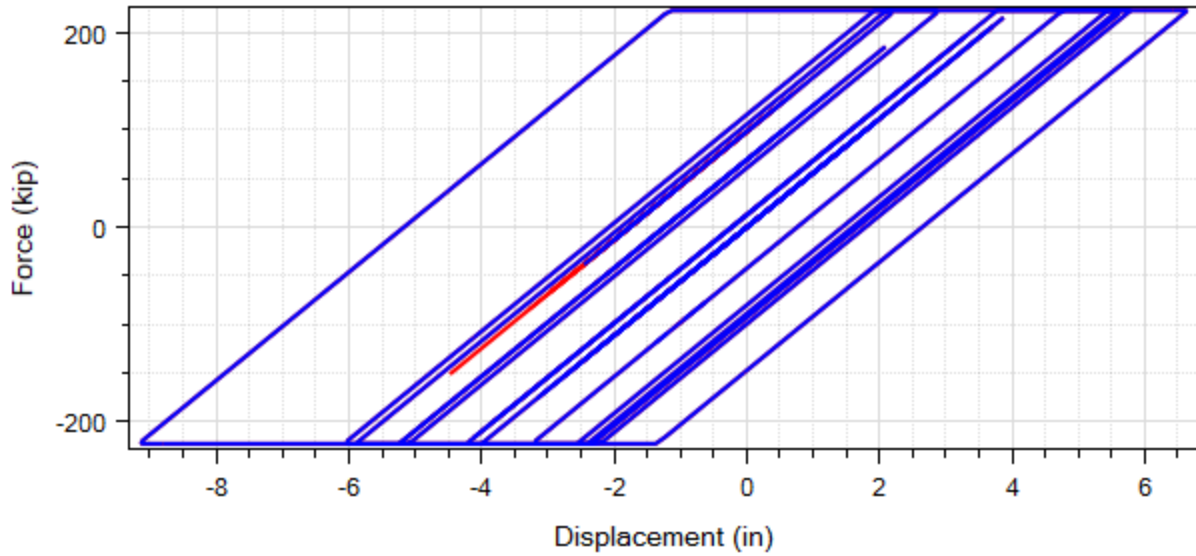


Figure C.27 Abutment (left or right) transverse resisting force-displacement response for Motion #1 ROCKS1N1 (Red part shows the end of shaking)

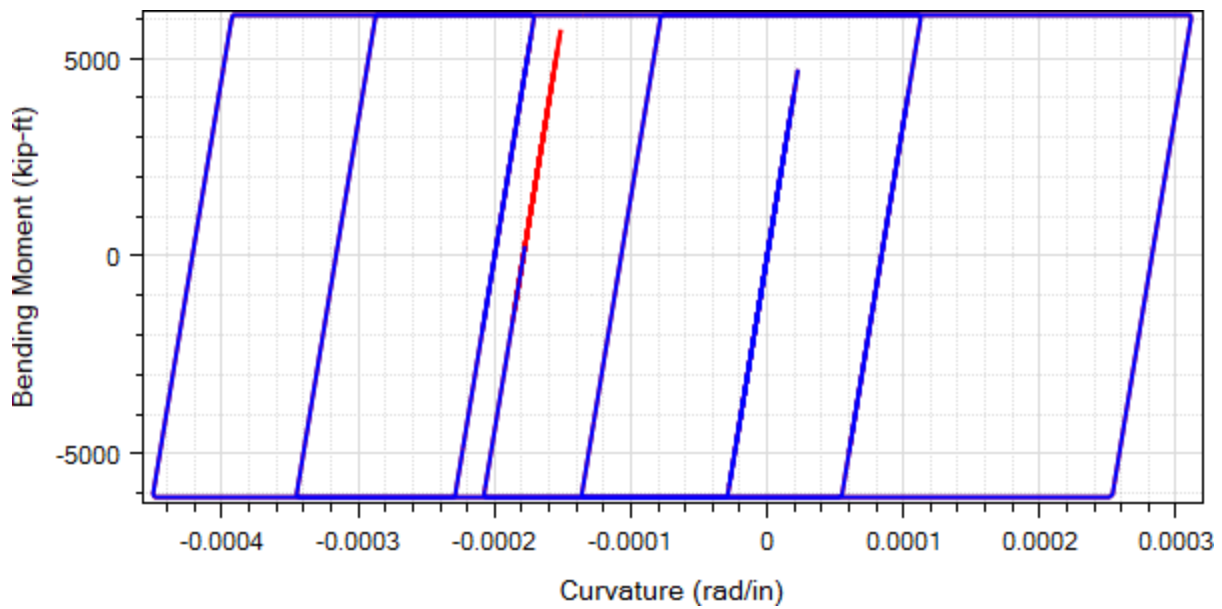


Figure C.28 Moment-curvature response at column top for Column 1 of Bent 6 for Motion #2 ROCKS1N2 (Red part shows the end of shaking)

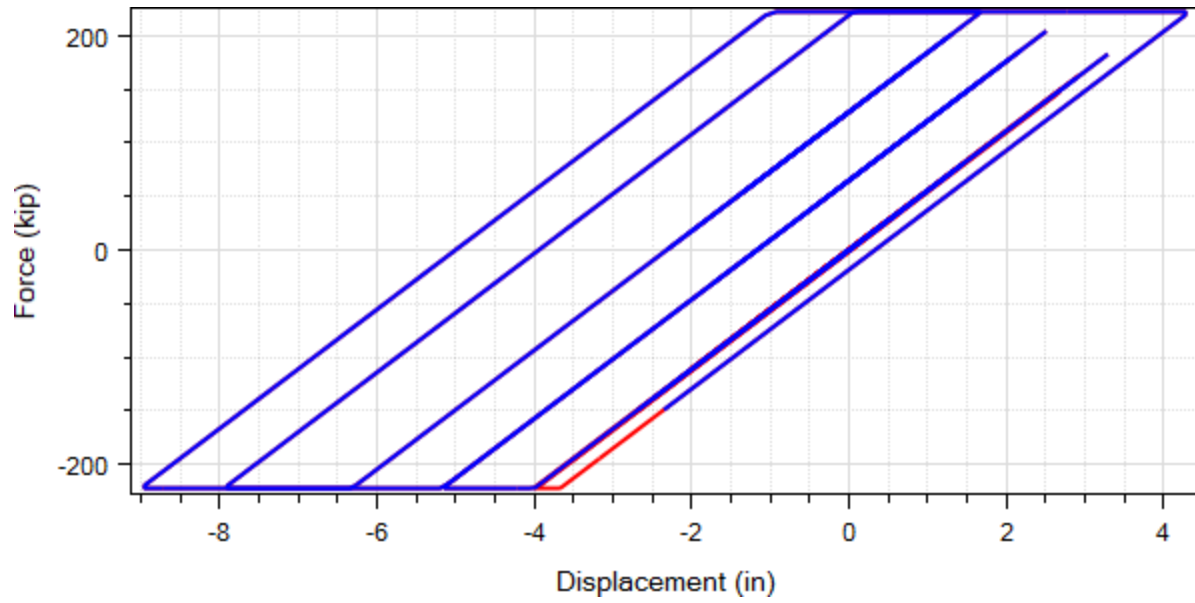


Figure C.29 Abutment (left or right) transverse resisting force-displacement response for Motion #2 ROCKS1N2 (Red part shows the end of shaking)

C.11 Summary and Conclusions

C.11.1 Summary

Comparison of ESA displacement demand and THA maximum displacement was conducted for a OSB bridge model (in the transverse direction only). A series of models of increasing complexity were studied in an attempt to separate influence of column nonlinear response, foundation p-y springs, and the added resistance provided at the bridge abutments. A set of 14 motions (and target ARS) provided by Caltrans was employed. Comparison of the average ESA and THA results (for the 14 motions) for all the studied models is summarized in Table C.18.

Table C.18 Comparison of the average ESA displacement demand and THA maximum displacement for all the studied models

Case#	Case Description	Average of THA Maximum Displacement (in)	Average of ESA Displacement Demand (in)	Difference*
Case 1	Linear columns with fixed base	5.73	5.69	-0.6%
Case 2	Linear columns with linear p-y and t-z spring foundation	14.5	14.4	-0.6%
Case 3	Nonlinear columns with fixed base	6.82	5.51	-23.8%
Case 4	Nonlinear columns with linear p-y and t-z spring foundation	12.8	14.4	11.0%
Case 5	Nonlinear columns with nonlinear p-y and t-z spring foundation	12.8	17.1	25.1%
Case 6	Same as 5, with 10 bents		Same as Case 5	
Case 7	Case as 6, with 2 end-bents at the abutment	14.5	17.1	15.0%
Case 8	Same as 7, with bilinear abutment springs	15.3	17.1	10.1%

Note: * “-” sign means ESA is less

C.11.2 Conclusions

The main findings are:

- 1) For the single bent model studied, the difference between ESA displacement demand and THA maximum displacement is about 25% (overall).
- 2) Ultimately, for the full Salinas River Bridge model, an overall difference of about 10% was observed between ESA and THA due to: i) nonlinearity of the bridge columns and p-y / t-z foundation springs; and ii) the added lateral resistance provided by the bridge-end bents and the abutments.
- 3) For linear cases (case of linear columns with rigid base, and case of linear columns with linear soil springs), the ESA displacement demand and the THA maximum displacement are in good agreement (around 1% or less for most shaking events).

APPENDIX D SALINAS BRIDGE MODELING DETAILS

D.1 Column

The Salinas Bridge model created in MSBridge was based on the wFrame model reported in Caltrans (2005). As such, a bi-linear moment-curvature relationship was used to model the columns and pile shafts (Caltrans 2005). Figure D.1 shows the user-defined bi-linear moment-curvature relationships for the columns above the mudline (Figure D.1a) as well as for the pile shafts (Figure D.1b), respectively. An axial compressive load of 1,000 kip was applied in the moment-curvature analysis. For the columns, plastic moment is 6100 kip-ft (at the curvature of 2.92×10^{-5} rad/in). For the pile shafts, plastic moment is 19,400 kip-ft (at the curvature of 8.23×10^{-5} rad/in).

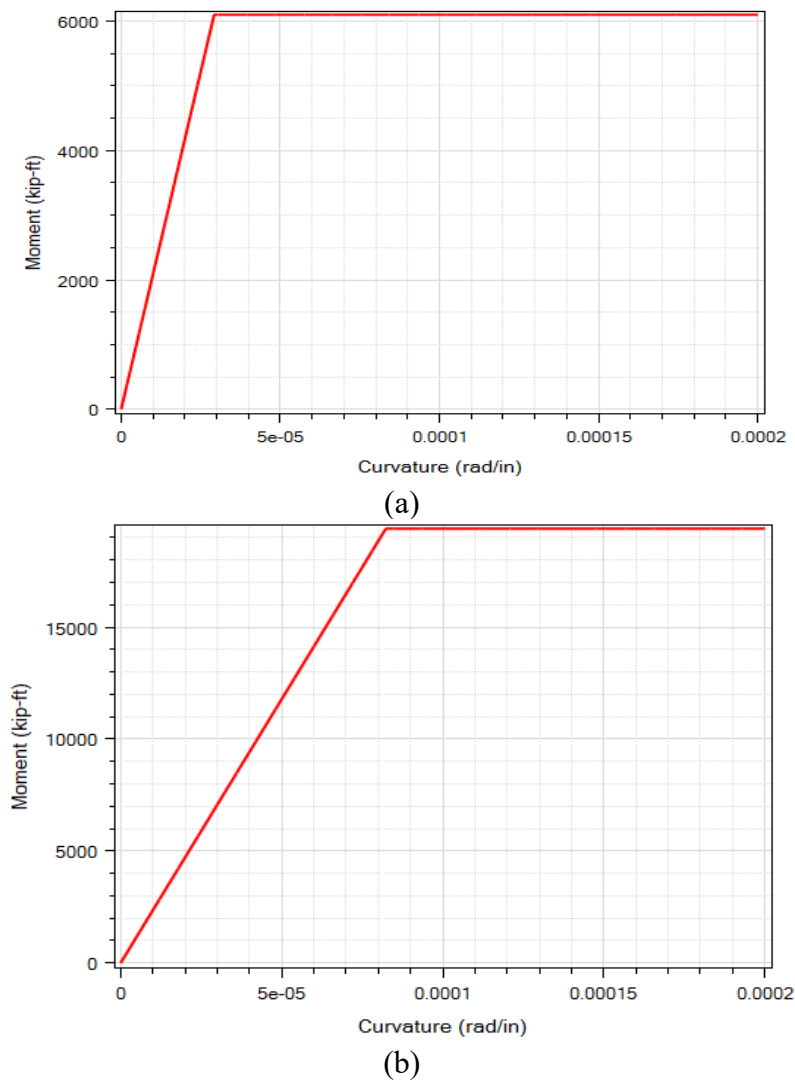


Figure D.1 Bi-linear moment-curvature relationship: (a) column; (b) pile shaft

D.2 Soil Springs

Figure D.2 to Figure D.5 show the p-y curves used to account for stiffness of the underlying pile foundations and the resulting soil-foundation-structure interaction. The values of these curves are converted to proper soil springs within the push analysis. In addition, Figure D.6 and Figure D.7 show the T-Z and Q-Z curves, respectively.

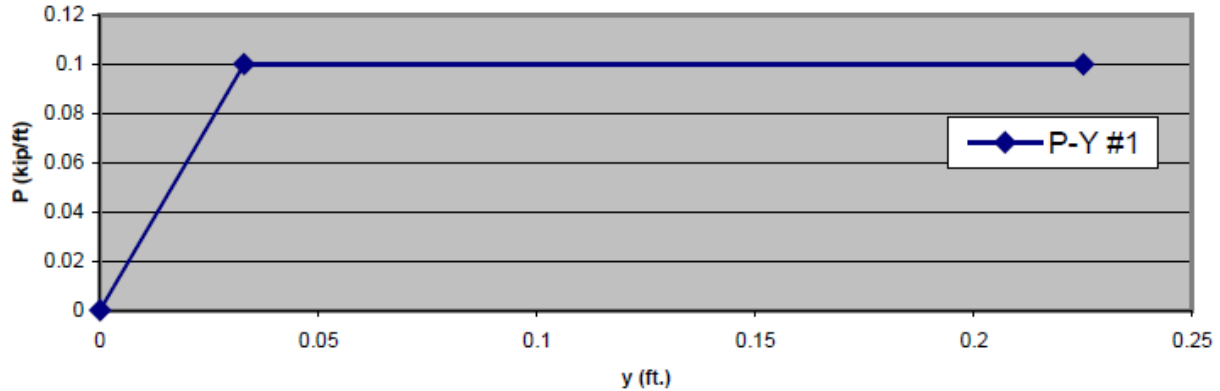


Figure D.2 Idealized soil P-Y curve at depth of 0.5 ft (Caltrans, 2005)

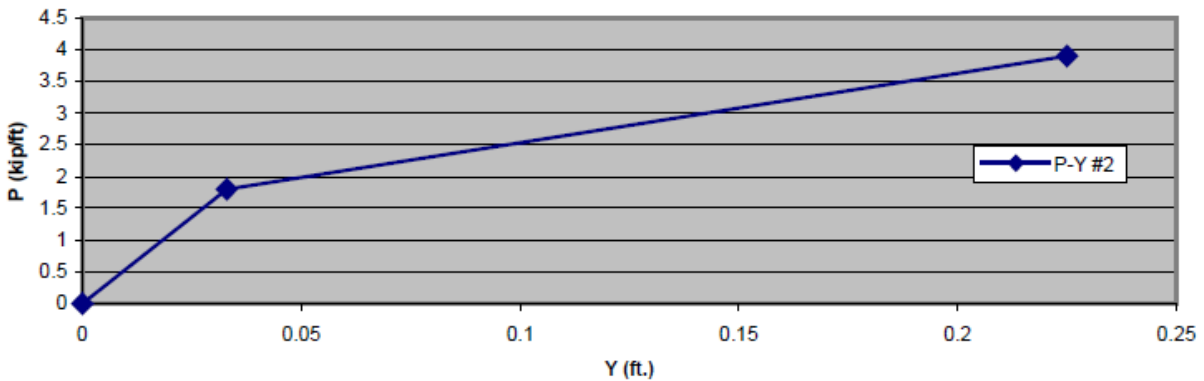


Figure D.3 Idealized soil P-Y curve at depth of 16.5 ft (Caltrans, 2005)

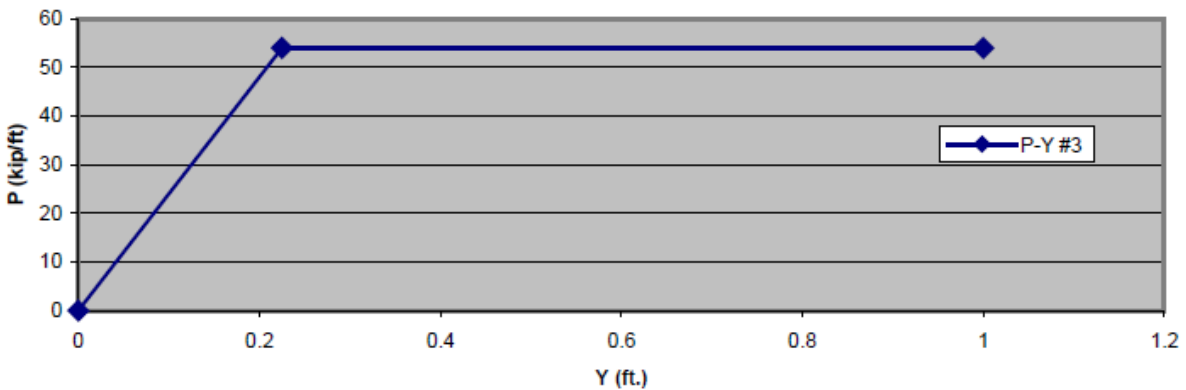


Figure D.4 Idealized soil P-Y curve at depth of 17.5 ft (Caltrans, 2005)

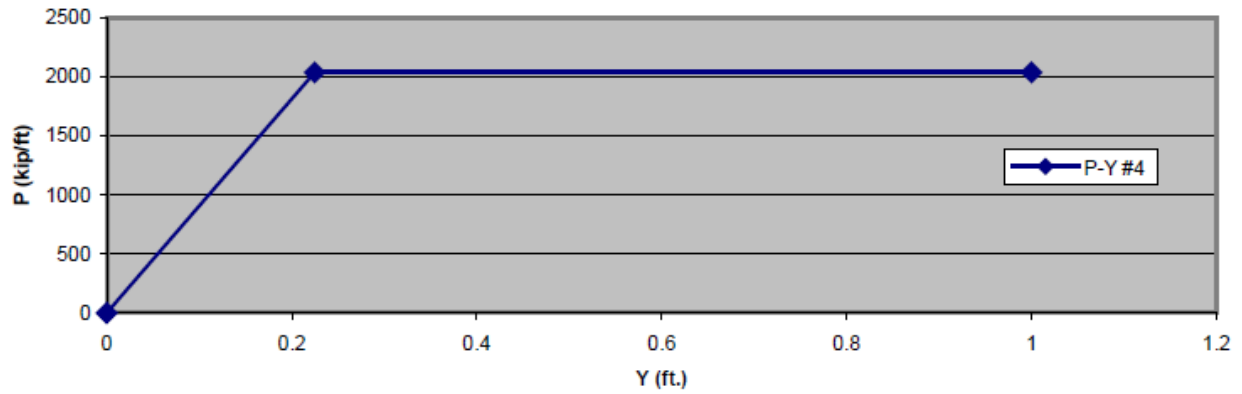


Figure D.5 Idealized soil P-Y curve at depth of 106.5 ft (Caltrans, 2005)

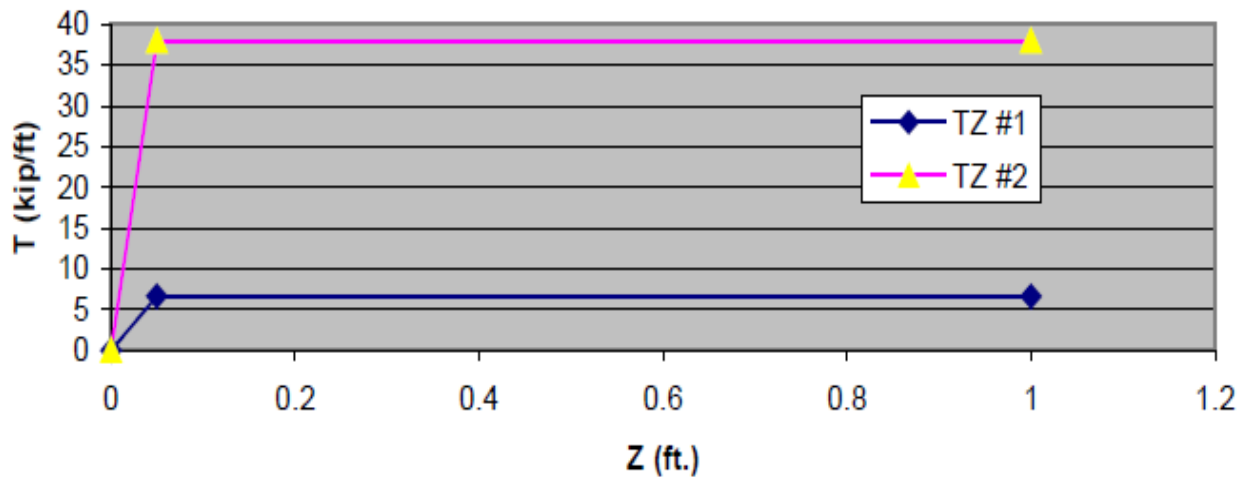


Figure D.6 Idealized soil T-Z curves (Caltrans, 2005)

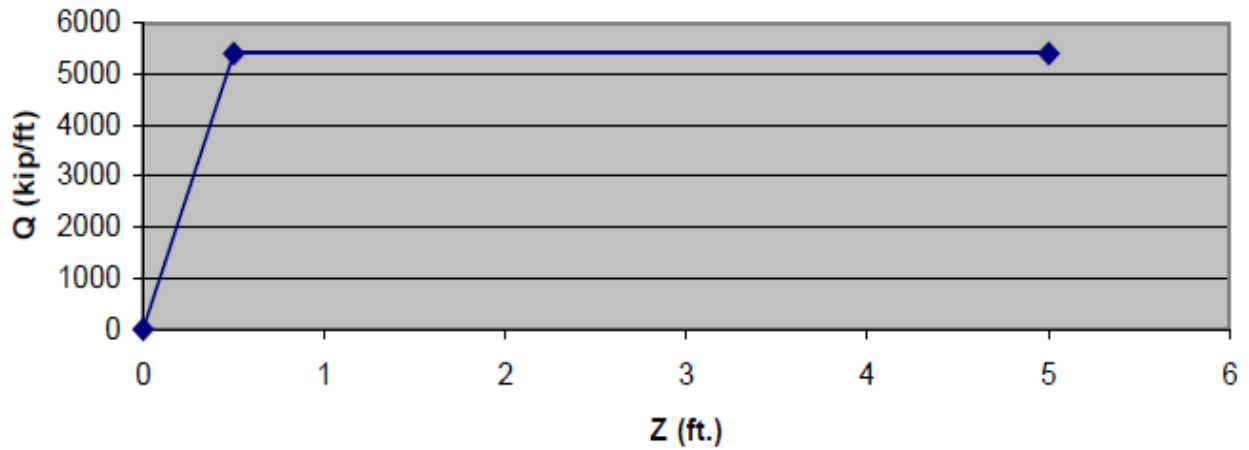


Figure D.7 Idealized soil Q-Z curves (Caltrans, 2005)

D.3 Deck and Bentcap

The material and section properties of the box-girder are listed in Table D.1. The weight of the bridge deck per unit length is 10.445 kip/ft (= 69.64 ft² x 0.15 kcf).

The material and section properties of the bentcap are listed in Table D.2. The weight of the bridge bentcap per unit length is 5.175 kip/ft (= 34.5 ft² x 0.15 kcf).

Table D.1. Salinas River Bridge Deck Material and Section Properties

Parameter	Value
Young's modulus (ksi)	4,031
Shear modulus (ksi)	1,668
Unit weight (kcf)	0.15
Area of cross section (ft ²)	69.64
Moment of inertia @ horizontal axis (ft ⁴)	327.44
Moment of inertia @ vertical axis (ft ⁴)	10105.6
Torsion constant (ft ⁴)	934

Table D.2. Salinas River Bridge Bentcap Properties

Parameter	Value
Young's modulus (ksi)	4,031
Shear modulus (ksi)	1,668
Unit weight (kcf)	0.15
Area of cross section (ft ²)	34.5
Moment of inertia @ horizontal axis (ft ⁴)	95.1
Moment of inertia @ vertical axis (ft ⁴)	103.5
Torsion constant (ft ⁴)	166.79

D.4 Abutment

Elastic abutment model with a stiff vertical spring and 3 stiff rotational springs was employed. In the longitudinal direction, a spring of stiffness $k = 128.25$ kip/in was applied at each of the 2 abutments (Caltrans 2005). In the transverse direction, a spring of stiffness $k = 55.625$ kip/in was employed (for each of the 2 abutments). In addition, the abutment was considered to have a pinned connection with the pile foundation.

APPENDIX E THE SAMOA CHANNEL BRIDGE MODELING DETAILS

E.1 Column

Nonlinear Fiber section in OpenSees was used to model the columns. APPENDIX G lists the OpenSees Tcl code snippet for the Fiber section for Piers S-8 and S-9 of Samoa Bridge (Section I) while the Tcl code snippet for other piers (except Piers S-8 and S-9) (Section II).

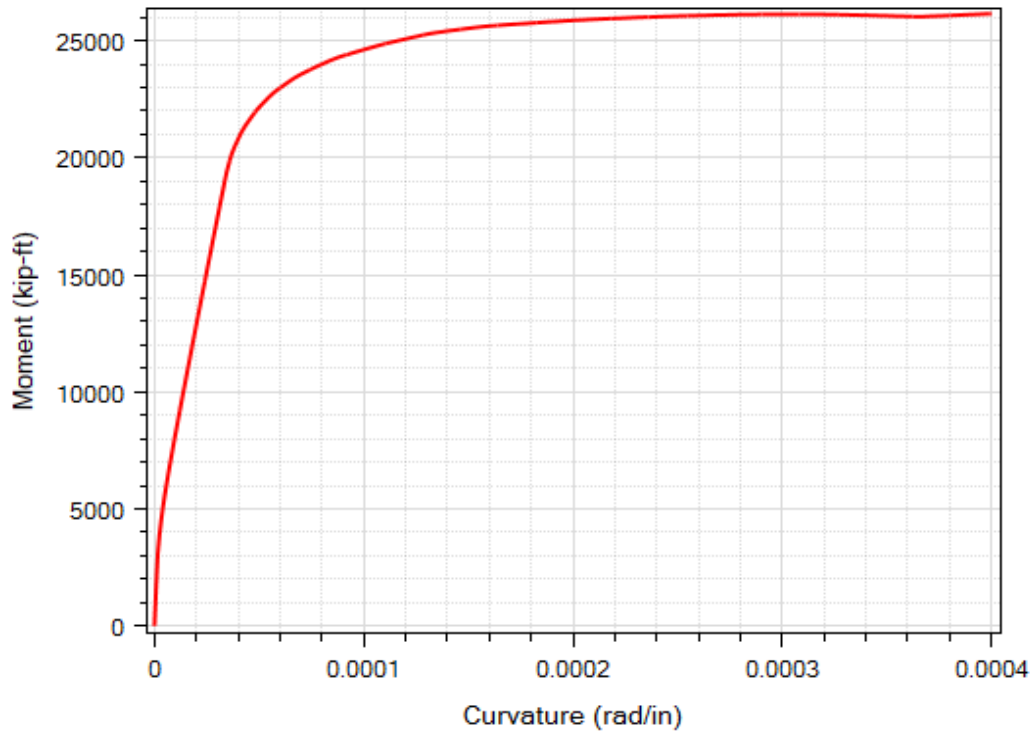
The moment-curvature response of the column Fiber section for Pier S-8 and S-9 is shown in Figure E.1a. An axial compressive load of 2,000 kip was applied in the moment-curvature analysis in the transverse direction.

For other piers (except Piers S-8 and S-9), the moment-curvature response of the column Fiber section is shown in Figure E.1b. An axial compressive load of 1,300 kip was applied in the moment-curvature analysis in this case for the transverse direction.

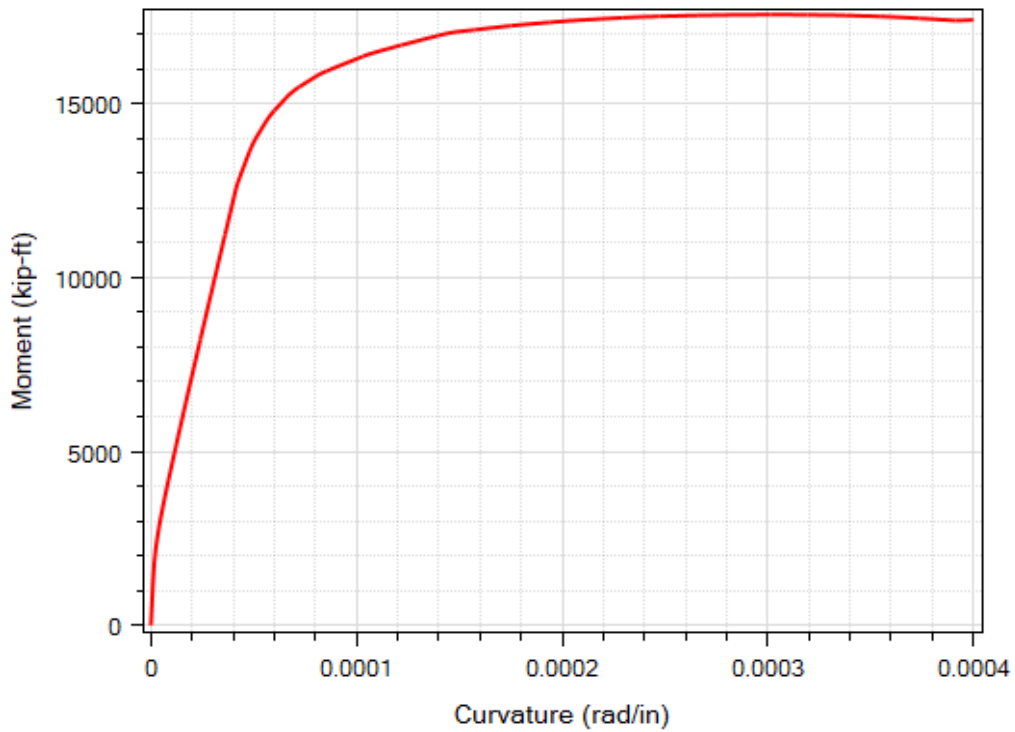
Similarly, Figure E.2a shows the moment-curvature response of the column Fiber section in the longitudinal direction with the same applied axial load for Pier S-8 and S-9. Furthermore, Figure E.2b shows the moment-curvature response of the other piers (except Piers S-8 and S-9) in the longitudinal direction.

E.2 Foundation Matrix

The **Foundation Matrix model** is represented by the coupled foundation stiffness matrix (Lam and Martin). Specifically, the stiffness of a single pile is represented by a 6 x 6 matrix associated with all six degrees of freedom at the pile head (Figure E.3). However, the overall pile-soil stiffness should reflect the soil characteristics and the structural properties of the pile as well. Moreover, Table E.1 and Table E.2 show the foundation matrix coefficients of all bents (Wang 2015).

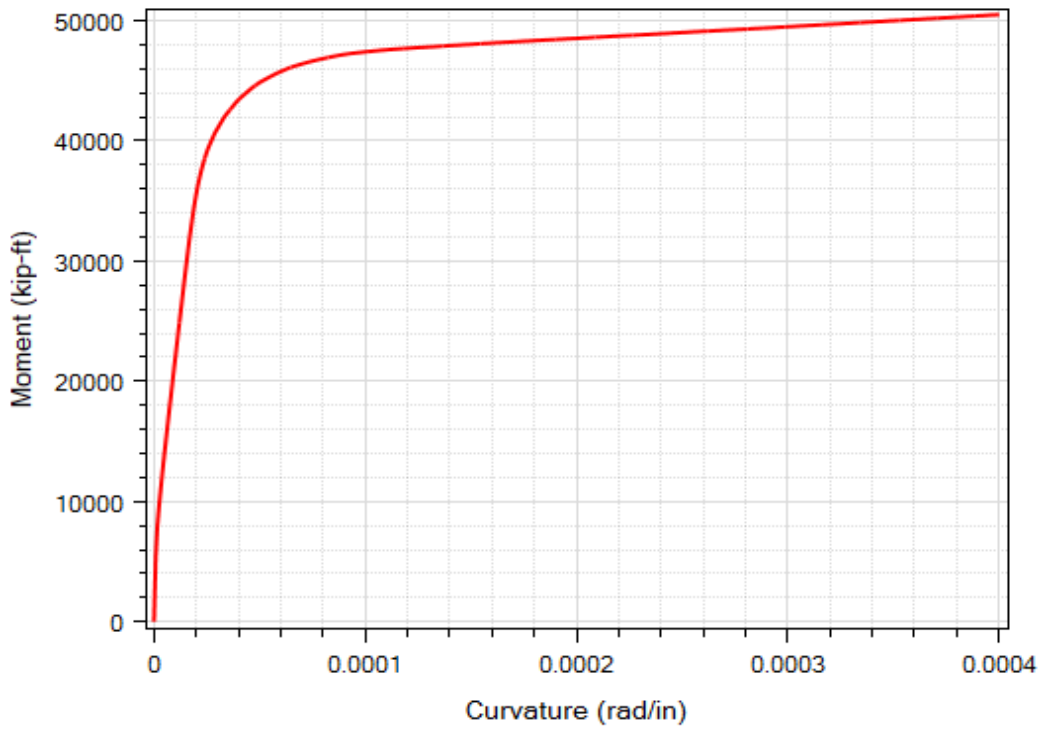


(a)

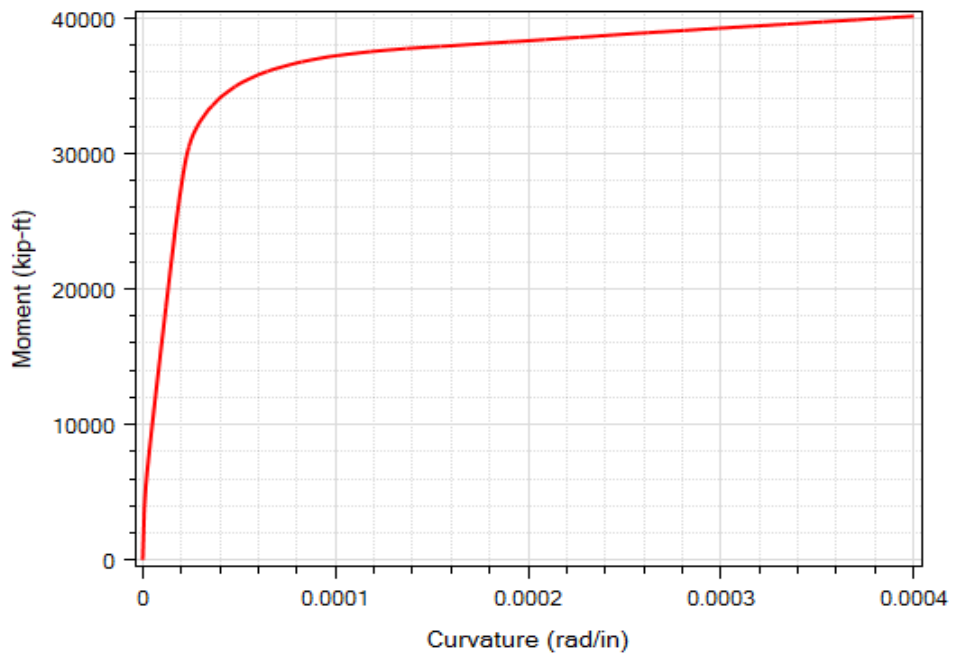


(b)

Figure E.1 Column moment-curvature relationship in the longitudinal direction for: (a) Pier S-8 and Pier S-9; (b) other piers



(a)



(b)

Figure E.2 Column moment-curvature relationship in the transverse direction for: (a) Pier S-8 and Pier S-9; (b) other piers

$$[k] = \begin{bmatrix} k_x & 0 & 0 & 0 & k_{x-ry} & 0 \\ 0 & k_y & 0 & k_{y-rx} & 0 & 0 \\ 0 & 0 & k_z & 0 & 0 & 0 \\ 0 & k_{rx-y} & 0 & k_{rx} & 0 & 0 \\ k_{ry-x} & 0 & 0 & 0 & k_{ry} & 0 \\ 0 & 0 & 0 & 0 & 0 & k_t \end{bmatrix}$$

Figure E.3 Foundation matrix definition

Table E.1. Samoa Bridge Foundation Matrix Coefficients (Wang 2015)

Bent #	K_x or K_y translational stiffness (kip/in)
Bent 2	624.786
Bent 3	78.412
Bent 4	669.903
Bent 5	290.177
Bent 6	151.970
Bent 7	100.286
Bent 8	223.015
Bent 9	289.949
Bent 10	209.081
Bent 11	145.802
Bent 12	230.268
Bent 13	221.359
Bent 14	1,333.52
Bent 15	1,333.52
Bent 16	1,333.52
Bent 17	704.74
Bent 18	704.74
Bent 19	704.74
Bent 20	704.74

Table E.2. Samoa Bridge Constant Foundation Matrix Coefficients for All Bents (Wang 2015)

Parameter	Value
k_z (kip/in)	30,000
k_{rx} (kip/in)	20,000,000
k_{ry} (kip/in)	20,000,000
k_t (kip-in/rad)	77,477.88
k_{y-rx} (kip)	10,000
k_{x-ry} (kip)	-10,000

E.3 Deck

The employed linear elastic material and section properties of the I-girder are listed in Table E.3. The weight of the bridge deck per unit length is 8.687 kip/ft (126.82 kN/m).

Table E.3. Bridge Deck Material and Section Properties for Samoa Bridge (Wang 2015)

Parameter	Value
Young's modulus	3.67×10^3 ksi (2.53×10^7 kPa)
Shear modulus	1.53×10^3 ksi (1.05×10^7 kPa)
Unit weight	160 pcf (25.11 kPa)
Area of cross section	54.3 ft ² (5.05 m ²)
Moment of inertia @ horizontal axis	783.82 ft ⁴ (6.78 m ⁴)
Moment of inertia @ vertical axis	4.84×10^3 ft ⁴ (41.89 m ⁴)
Torsion constant	113.29 ft ⁴ (0.98 m ⁴)

E.4 Abutment

Elastic abutment model with a stiff vertical spring and 3 stiff rotational springs was employed. In the longitudinal direction, a spring of stiffness $k = 102.6$ kip/in (value obtained by scaling the Salinas River Bridge spring stiffness by the ratio of the 2 bridge deck widths) was applied at each of the 2 abutments. In the transverse direction, a spring of stiffness $k = 44.5$ kip/in (value obtained also by the scaling scheme similar to the above) was employed (for each of the 2 abutments).

E.5 ESA

The ESA was conducted in the longitudinal and transverse directions. Figure E.4 shows the acceleration response spectrum (ARS) used in the ESA of Samoa and Eureka Bridges.

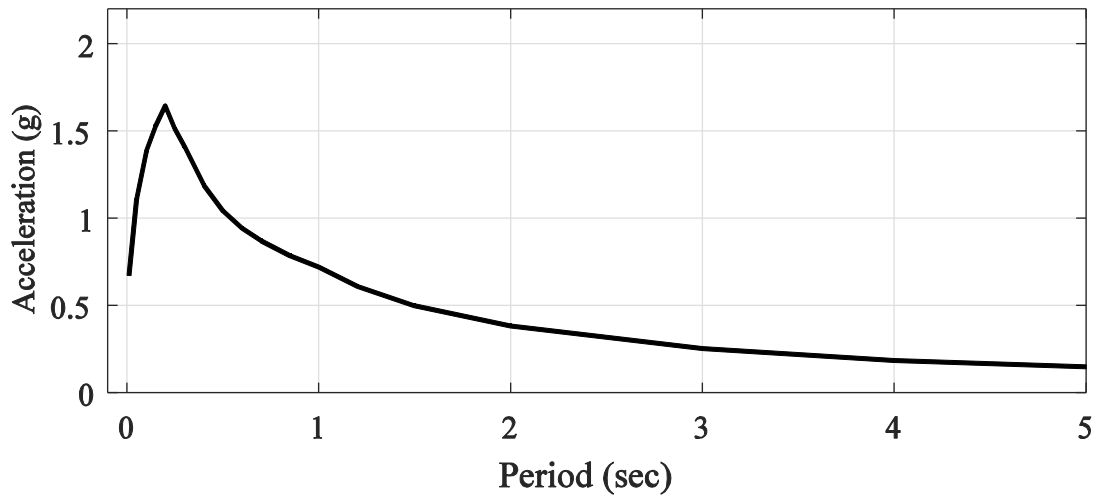


Figure E.4 Acceleration response spectrum employed in the ESA

APPENDIX F THE EUREKA CHANNEL BRIDGE MODELING DETAILS

F.1 Column

Nonlinear Fiber section in OpenSees was used to model the columns. APPENDIX G lists the OpenSees Tcl code snippet for the Fiber section for Piers E-6 and E-7 of Eureka Bridge (Section I) while the Tcl code snippet for other piers (except Piers E-6 and E-7) (Section II).

The moment-curvature response of the column Fiber section for Pier E-6 and E-7 is shown in Figure E.1a. An axial compressive load of 2,000 kip was applied in the moment-curvature analysis.

For other piers (except Piers E-6 and E-7), the moment-curvature response of the column Fiber section is shown in Figure E.1b. An axial compressive load of 1,300 kip was applied in the moment-curvature analysis in this case.

In addition, the moment-curvature responses of the column Fiber section in the longitudinal direction are shown in Figure E.2a and Figure E.2b.

F.2 Foundation Matrix

The **Foundation Matrix model** is represented by the coupled foundation stiffness matrix (Lam and Martin). Moreover, Table F.1 shows the foundation matrix translational coefficients of all bents and Table E.2 shows the other stiffness coefficients (Wang 2015).

Table F.1. Bent Foundation Matrix Coefficients for Eureka Bridge (Wang 2015)

Bent #	K_x or K_y translational stiffness (kip/in)
Bent 2	805.254
Bent 3	885.209
Bent 4	651.057
Bent 5	190.748
Bent 6	725.300
Bent 7	942.319
Bent 8	942.319
Bent 9	560.251
Bent 10	560.251
Bent 11	280.982
Bent 12	190.748
Bent 13	902.342
Bent 14	280.98
Bent 15	205.03

F.3 Deck

The employed linear elastic material and section properties of the I-girder are listed in Table F.2. The weight of the bridge deck per unit length is 6.48 kip/ft (94.6783 kN/m).

Table F.2. Material and Section Properties of the Bridge Deck for Eureka Bridge (Wang 2015)

Parameter	Value
Young's modulus	3.67×10^3 ksi (2.53×10^7 kPa)
Shear modulus	1.53×10^3 ksi (1.05×10^7 kPa)
Unit weight	160 pcf (25.11 kPa)
Area of cross section	40.53 ft ² (3.77 m ²)
Moment of inertia @ horizontal axis	194.22 ft ⁴ (1.68 m ⁴)
Moment of inertia @ vertical axis	3.80×10^3 ft ⁴ (32.9 m ⁴)
Torsion constant	40.46 ft ⁴ (0.35 m ⁴)

F.4 Abutment

Elastic abutment model with the same spring stiffness coefficients as those of Samoa Bridge was employed for Eureka Bridge.

APPENDIX G COLUMN NONLINEAR FIBER SECTIONS FOR THE SAMOA CHANNEL BRIDGE AND THE EUREKA CHANNEL BRIDGE

This section lists the Tcl code snippet for the column nonlinear fiber section of Piers S-8 and S-9 for Samoa Bridge (Wang 2015). In addition, the same code snippet was also employed for Piers E-6 and E-7 of Eureka Bridge (Section I). Furthermore, it lists the Tcl code snippet for the column nonlinear fiber section of typical piers (except Piers S-8 and S-9 of Samoa Bridge and Piers E-6 and E-7 of Eureka Bridge) (Section II).

Section I (Units in SI: kN, m)

```
set in2m 2.54e-2
set kips2Ton 0.4535929
set g 9.81
set kips2KN [expr $kips2Ton*$g]
set pierWidth 2.1336
set pierDepth 1.2192
set triDepth 0.5334
set cover 0.0762
set As [expr 10.06e-004]; # area of longitudinal-reinforcement bars
# Area of no. 11 bar in the columns, in2
set fy 303000.0; # Yield strength of reinforcing steel
set E 20.0e+7; # Young's modulus of reinforcing steel
set np 5; # Number of Gauss-Lobato points per beam-column element
set fcCore -34700.0;
set fcuCore -30700.0
set fcCover -34000.0; # f'c of cover concrete, ksi
set fcuCover 0.0; # f'cu of cover concrete, ksi
set epscCore -0.0025;
set epscuCore -0.006;
set epscCover -0.002;
set epscuCover -0.005;
set columnSectionArea [expr $pierWidth*$pierDepth+$triDepth*$pierDepth]

#Define materials for nonlinear columns
#Columns material #1/3::Core concrete (confined)
#CONCRETE tag f'c ec0 f'cu ecu
uniaxialMaterial Concrete01 1421 $fcCore $epscCore $fcuCore $epscuCore
#Column Material #2/3::Cover concrete (unconfined)
#CONCRETE tag f'c ec0 f'cu ecu
uniaxialMaterial Concrete01 1422 $fcCover $epscCover $fcuCover $epscuCover
#Column Material #3/3::Reinforcing steel
#STEEL tag fy E0 b
uniaxialMaterial Steel01 1423 $fy $E 0.008

set columnSectionY1 [expr $pierDepth/2.0-$cover]
set columnSectionZ1 [expr $pierWidth/2.0]

# Define Retrofit
uniaxialMaterial Concrete01 1431 -35700.0 $epscCore -33200.0 -0.0155; #Columns
material #1/3::Core concrete (confined)
```

```

uniaxialMaterial Concrete01 1432 -28000.0 $sepscCover $fcuCover $sepscCover;
#Column Material #2/3::Cover concrete (unconfined)
uniaxialMaterial Steel01 1433 414000.0 $E 0.008;
#Column Material #3/3::Reinforcing steel
set cover2 0.075
set columnSectionY2 [expr 1.83/2.0-$cover2]; #cover
set columnSectionZ2 [expr 1.195]
set triDepth2 [expr 0.915-0.075]; #0.84
set As2 [expr 2.84e-004]; #19
set cover3 0.305;
set columnSectionY3 [expr 1.83/2.0-$cover3]; #Middle
set columnSectionZ3 [expr 1.195]
set triDepth3 [expr 3.355/2-1.195]
set Tricover3 0.4325;
set delta_S [expr (305-75-50)/pow(2,0.5)*0.001]

set pSection 2005
section Fiber $pSection {
    # Create the concrete core fibers (checked)
    patch quad 1421 10 20 -0.5334 -1.0668 0.0 -1.6002 0.0 1.6002 -0.5334 1.0668
    patch quad 1421 20 10 0.5334 -1.0668 0.5334 1.0668 0.0 1.6002 0.0 -1.6002

    #Create the concrete cover fibers (checked)
    patch quad 1422 20 1 -0.6096 1.067 -0.6096 -1.067 -0.533 -1.067 -0.533 1.0668
    patch quad 1422 20 1 0.533 1.0668 0.5334 -1.0668 0.6096 -1.0668 0.6096 1.0668
    patch quad 1422 1 10 0.0 -1.6764 0.0 -1.6002 -0.5334 -1.0668 -0.6096 -1.0668
    patch quad 1422 1 10 0.0 -1.6002 0.0 -1.6764 0.6096 -1.0668 0.5334 -1.0668
    patch quad 1422 1 10 -0.6096 1.0668 -0.5334 1.0668 0.0 1.6002 0.0 1.6764
    patch quad 1422 1 10 0.5334 1.0668 0.6096 1.0668 0.0 1.6764 0.0 1.6002

    #Create the reinforcing fibers (checked)
    layer straight 1423 1 0.001006 0.0 -1.6002 0.0 -1.6002
    layer straight 1423 2 0.001006 -0.13335 -1.46685 0.13335 -1.46685
    layer straight 1423 2 0.001006 -0.2667 -1.3335 0.2667 -1.3335
    layer straight 1423 2 0.001006 -0.40005 -1.20015 0.40005 -1.20015
    layer straight 1423 2 0.001006 -0.5334 -1.0668 0.5334 -1.0668
    layer straight 1423 2 0.001006 -0.5334 -0.85344 0.5334 -0.85344
    layer straight 1423 2 0.001006 -0.5334 -0.64008 0.5334 -0.64008
    layer straight 1423 2 0.001006 -0.5334 -0.42672 0.5334 -0.42672
    layer straight 1423 2 0.001006 -0.5334 -0.21336 0.5334 -0.21336
    layer straight 1423 2 0.001006 -0.5334 -0.0 0.5334 0.0
    layer straight 1423 2 0.001006 -0.5334 0.21336 0.5334 0.21336
    layer straight 1423 2 0.001006 -0.5334 0.42672 0.5334 0.42672
    layer straight 1423 2 0.001006 -0.5334 0.64008 0.5334 0.64008
    layer straight 1423 2 0.001006 -0.5334 0.85344 0.5334 0.85344
    layer straight 1423 2 0.001006 -0.5334 1.0668 0.5334 1.0668
    layer straight 1423 2 0.001006 -0.40005 1.20015 0.40005 1.20015
    layer straight 1423 2 0.001006 -0.2667 1.3335 0.2667 1.3335
    layer straight 1423 2 0.001006 -0.13335 1.46685 0.13335 1.46685
    layer straight 1423 1 0.001006 0.0 1.6002 0.0 1.6002

    # Create concrete core fibers of retrofit (confined) (checked)
    patch quad 1431 20 1 -0.84 1.195 -0.84 -1.195 -0.61 -1.0668 -0.61 1.0668
    patch quad 1431 20 1 0.61 1.0668 0.61 -1.0668 0.84 -1.195 0.84 1.195
    patch quad 1431 1 10 0.0 -2.035 0.0 -1.6775 -0.61 -1.0668 -0.84 -1.195
    patch quad 1431 1 10 0.0 -1.6775 0.0 -2.035 0.84 -1.195 0.61 -1.0668
    patch quad 1431 1 10 -0.84 1.195 -0.61 1.0668 0.0 1.6775 0.0 2.035

```

```

patch quad 1431 1 10 0.61 1.0668 0.84 1.195 0.0 2.035 0.0 1.6775

# Create concrete cover3 fibers of retrofit (unconfined) (checked)
patch quad 1432 20 1 -0.915 1.195 -0.915 -1.195 -0.84 -1.195 -0.84 1.195
patch quad 1432 20 1 0.84 1.195 0.84 -1.195 0.915 -1.195 0.915 1.195
patch quad 1432 1 10 0.0 -2.11 0.0 -2.035 -0.84 -1.195 -0.915 -1.195
patch quad 1432 1 10 0.0 -2.035 0.0 -2.11 0.915 -1.195 0.84 -1.195
patch quad 1432 1 10 -0.915 1.195 -0.84 1.195 0.0 2.035 0.0 2.11
patch quad 1432 1 10 0.84 1.195 0.915 1.195 0.0 2.11 0.0 2.035

#Create the reinforcing fibers of retrofit
layer straight 1433 1 0.000284 0.0 -2.003934 0.0 -2.003934
layer straight 1433 1 0.000284 0.0 -1.7275 0.0 -1.7275
# inner
layer straight 1433 2 0.001006 -0.6596 -1.1168 0.6596 -1.1168
layer straight 1433 2 0.001006 -0.4947 -1.2692 0.4947 -1.2692
layer straight 1433 2 0.001006 -0.3298 -1.4216 0.3298 -1.4216
layer straight 1433 2 0.001006 -0.1649 -1.574 0.1649 -1.574
# outer
layer straight 1433 2 0.001006 -0.621979 -1.396479 0.621979 -1.396479
layer straight 1433 2 0.001006 -0.457079 -1.548879 0.457079 -1.548879
layer straight 1433 2 0.001006 -0.292179 -1.701279 0.292179 -1.701279
# outer
layer straight 1433 2 0.000284 -0.84 -1.195 0.84 -1.195
layer straight 1433 2 0.000284 -0.84 -0.915 0.84 -0.915
layer straight 1433 2 0.000284 -0.84 -0.61 0.84 -0.61
layer straight 1433 2 0.000284 -0.84 -0.305 0.84 -0.305
layer straight 1433 2 0.000284 -0.84 -0.0 0.84 0.0
layer straight 1433 2 0.000284 -0.84 0.915 0.84 0.915
layer straight 1433 2 0.000284 -0.84 0.61 0.84 0.61
layer straight 1433 2 0.000284 -0.84 0.305 0.84 0.305
layer straight 1433 2 0.000284 -0.84 1.195 0.84 1.195
# inner
layer straight 1433 2 0.000284 -0.66 -0.915 0.66 -0.915
layer straight 1433 2 0.000284 -0.66 -0.61 0.66 -0.61
layer straight 1433 2 0.000284 -0.66 -0.305 0.66 -0.305
layer straight 1433 2 0.000284 -0.66 -0.0 0.66 0.0
layer straight 1433 2 0.000284 -0.66 0.915 0.66 0.915
layer straight 1433 2 0.000284 -0.66 0.61 0.66 0.61
layer straight 1433 2 0.000284 -0.66 0.305 0.66 0.305

# outer
layer straight 1433 2 0.001006 -0.621979 1.396479 0.621979 1.396479
layer straight 1433 2 0.001006 -0.457079 1.548879 0.457079 1.548879
layer straight 1433 2 0.001006 -0.292179 1.701279 0.292179 1.701279

# inner
layer straight 1433 2 0.001006 -0.6596 1.1168 0.6596 1.1168
layer straight 1433 2 0.001006 -0.4947 1.2692 0.4947 1.2692
layer straight 1433 2 0.001006 -0.3298 1.4216 0.3298 1.4216
layer straight 1433 2 0.001006 -0.1649 1.574 0.1649 1.574
layer straight 1433 1 0.000284 0.0 2.003934 0.0 2.003934
layer straight 1433 1 0.000284 0.0 1.7275 0.0 1.7275
}

```

Section II (Units in SI: kN, m)

```
set in2m 2.54e-2
set kips2Ton 0.4535929
set g 9.81
set kips2KN [expr $kips2Ton*$g]
set pierWidth 2.1336
set pierDepth 1.524
set triDepth 0.6858
set cover 0.0762
set As [expr 10.06e-004]; # area of longitudinal-reinforcement bars
# Area of no. 11 bar in the columns, in2

set fy 303000.0; # Yield strength of reinforcing steel
set E 20.0e+7; # Young's modulus of reinforcing steel
set np 5; # Number of Gauss-Lobato points per beam-column element

set fcCore -34700.0;
set fcuCore -30700.0
set fcCover -34000.0; # f'c of cover concrete, ksi
set fcuCover 0.0; # f'cu of cover concrete, ksi
set epscCore -0.0025;
set epscuCore -0.006;
set epscCover -0.002;
set epscuCover -0.005;
set columnSectionArea [expr $pierWidth*$pierDepth+$triDepth*$pierDepth]

#Define materials for nonlinear columns
#Columns material #1/3::Core concrete (confined)
#CONCRETE tag f'c ec0 f'cu ecu
uniaxialMaterial Concrete01 21 $fcCore $epscCore $fcuCore $epscuCore

#Column Material #2/3::Cover concrete (unconfined)
#CONCRETE tag f'c ec0 f'cu ecu
uniaxialMaterial Concrete01 22 $fcCover $epscCover $fcuCover $epscuCover

#Column Material #3/3::Reinforcing steel
#STEEL tag fy E0 b
uniaxialMaterial Steel01 23 $fy $E 0.008

set columnSectionY1 [expr $pierDepth/2.0-$cover]
set columnSectionZ1 [expr $pierWidth/2.0]

# Define Retrofit
uniaxialMaterial Concrete01 31 -35700.0 $epscCore -33200.0 -0.0155; #Columns
material #1/3::Core concrete (confined)
uniaxialMaterial Concrete01 32 -28000.0 $epscCover $fcuCover $epscuCover;
#Column Material #2/3::Cover concrete (unconfined)
uniaxialMaterial Steel01 33 414000.0 $E 0.008;
#Column Material #3/3::Reinforcing steel

set cover2 0.075
set columnSectionY2 [expr 2.13/2.0-$cover2]; #cover
set columnSectionZ2 [expr 1.195]
set triDepth2 [expr 1.065-0.075]; #0.84
set As2 [expr 2.84e-004]; #19
```

```

set As25 [expr 5.1e-004]; #25
set cover3 0.305;
set columnSectionY3 [expr 2.13/2.0-$cover3]; #Middle
set columnSectionZ3 [expr 1.195]
set triDepth3 [expr 3.66/2-1.195]
set Tricover3 [expr (4.52-3.66)/2];
set deltaS [expr 0.305/pow(2, 0.5)]

# User-Defined Fiber Section (Fiber)
set pSection 2015
section Fiber $pSection {

    # Create the concrete core fibers
    patch quad 21 10 20 -0.6858 -1.0668 0.0 -1.7526 0.0 1.7526 -0.6858 1.0668
    patch quad 21 20 10 0.6858 -1.0668 0.6858 1.0668 0.0 1.7526 0.0 -1.7526

    #Create the concrete cover fibers
    patch quad 22 20 1 -0.762 1.067 -0.762 -1.067 -0.6858 -1.0668 -0.6858 1.067
    patch quad 22 20 1 0.6858 1.067 0.6858 -1.0668 0.762 -1.0668 0.762 1.0668
    patch quad 22 1 10 0.0 -1.8288 0.0 -1.7526 -0.6858 -1.0668 -0.762 -1.0668
    patch quad 22 1 10 0.0 -1.7526 0.0 -1.8288 0.762 -1.0668 0.6858 -1.0668
    patch quad 22 1 10 -0.762 1.0668 -0.6858 1.0668 0.0 1.7526 0.0 1.8288
    patch quad 22 1 10 0.6858 1.0668 0.762 1.0668 0.0 1.8288 0.0 1.7526

    #Create the reinforcing fibers
    layer straight 23 1 0.001006 0.0 -1.7526 0.0 -1.7526
    layer straight 23 2 0.001006 -0.13716 -1.61544 0.13716 -1.61544
    layer straight 23 2 0.001006 -0.27432 -1.47828 0.27432 -1.47828
    layer straight 23 2 0.001006 -0.41148 -1.34112 0.41148 -1.34112
    layer straight 23 2 0.001006 -0.54864 -1.20396 0.54864 -1.20396

    layer straight 23 2 0.001006 -0.6858 -1.0668 0.6858 -1.0668
    layer straight 23 2 0.001006 -0.6858 -1.0668 0.6858 -1.0668
    layer straight 23 2 0.001006 -0.6858 -0.85344 0.6858 -0.85344
    layer straight 23 2 0.001006 -0.6858 -0.64008 0.6858 -0.64008
    layer straight 23 2 0.001006 -0.6858 -0.42672 0.6858 -0.42672
    layer straight 23 2 0.001006 -0.6858 -0.21336 0.6858 -0.21336
    layer straight 23 2 0.001006 -0.6858 -0.0 0.6858 0.0
    layer straight 23 2 0.001006 -0.6858 0.21336 0.6858 0.21336
    layer straight 23 2 0.001006 -0.6858 0.42672 0.6858 0.42672
    layer straight 23 2 0.001006 -0.6858 0.64008 0.6858 0.64008
    layer straight 23 2 0.001006 -0.6858 0.85344 0.6858 0.85344
    layer straight 23 2 0.001006 -0.6858 1.0668 0.6858 1.0668
    layer straight 23 2 0.001006 -0.6858 1.0668 0.6858 1.0668

    layer straight 23 2 0.001006 -0.54864 1.20396 0.54864 1.20396
    layer straight 23 2 0.001006 -0.41148 1.34112 0.41148 1.34112
    layer straight 23 2 0.001006 -0.27432 1.47828 0.27432 1.47828
    layer straight 23 2 0.001006 -0.13716 1.61544 0.13716 1.61544

    layer straight 23 1 0.001006 0.0 1.7526 0.0 1.7526

    # Create concrete core fibers of retrofit (confined) (checked)
    patch quad 31 20 1 -0.99 1.195 -0.99 -1.195 -0.76 -1.0668 -0.76 1.0668
    patch quad 31 20 1 0.76 1.0668 0.76 -1.0668 0.99 -1.195 0.99 1.195
    patch quad 31 1 10 0.0 -2.185 0.0 -1.83 -0.76 -1.0668 -0.99 -1.195
    patch quad 31 1 10 0.0 -1.83 0.0 -2.185 0.99 -1.195 0.76 -1.0668

```

```

patch quad 31 1 10 -0.99 1.195 -0.76 1.0668 0.0 1.83 0.0 2.185
patch quad 31 1 10 0.76 1.0668 0.99 1.195 0.0 2.185 0.0 1.83

# Create concrete cover3 fibers of retrofit (unconfined) (checked)
patch quad 32 20 1 -1.065 1.195 -1.065 -1.195 -0.99 -1.195 -0.99 1.195
patch quad 32 20 1 0.99 1.195 0.99 -1.195 1.065 -1.195 1.065 1.195
patch quad 32 1 10 0.0 -2.26 0.0 -2.185 -0.99 -1.195 -1.065 -1.195
patch quad 32 1 10 0.0 -2.185 0.0 -2.26 1.065 -1.195 0.99 -1.195
patch quad 32 1 10 -1.065 1.195 -0.99 1.195 0.0 2.185 0.0 2.26
patch quad 32 1 10 0.99 1.195 1.065 1.195 0.0 2.26 0.0 2.185

#Create the reinforcing fibers of retrofit
layer straight 33 1 0.000284 0.0 -2.153934 0.0 -2.153934
layer straight 33 1 0.00051 0.0 -2.153934 0.0 -2.153934
layer straight 33 1 0.000284 0.0 2.153934 0.0 2.153934
layer straight 33 1 0.00051 0.0 2.153934 0.0 2.153934

# outer
layer straight 33 2 0.000284 -0.9246 -1.265 0.9246 -1.265
layer straight 33 2 0.000284 -0.7532 -1.429 0.7532 -1.429
layer straight 33 2 0.000284 -0.5817 -1.593 0.5817 -1.593
layer straight 33 2 0.000284 -0.4103 -1.757 0.4103 -1.757
layer straight 33 2 0.000284 -0.2388 -1.921 0.2388 -1.921

layer straight 33 2 0.00051 -0.9246 -1.265 0.9246 -1.265
layer straight 33 2 0.00051 -0.7532 -1.429 0.7532 -1.429
layer straight 33 2 0.00051 -0.5817 -1.593 0.5817 -1.593
layer straight 33 2 0.00051 -0.4103 -1.757 0.4103 -1.757
layer straight 33 2 0.00051 -0.2388 -1.921 0.2388 -1.921

# inner
layer straight 33 2 0.000284 -0.7974 -1.138 0.7974 -1.138
layer straight 33 2 0.000284 -0.6259 -1.301 0.6259 -1.301
layer straight 33 2 0.000284 -0.4545 -1.465 0.4545 -1.465
layer straight 33 2 0.000284 -0.283 -1.629 0.283 -1.629
layer straight 33 2 0.000284 -0.1116 -1.793 0.1116 -1.793

# width outer
layer straight 33 2 0.000284 -0.99 -1.195 0.99 -1.195
layer straight 33 2 0.000284 -0.99 -0.915 0.99 -0.915
layer straight 33 2 0.000284 -0.99 -0.61 0.99 -0.61
layer straight 33 2 0.000284 -0.99 -0.305 0.99 -0.305
layer straight 33 2 0.000284 -0.99 -0.0 0.99 0.0
layer straight 33 2 0.000284 -0.99 0.915 0.99 0.915
layer straight 33 2 0.000284 -0.99 0.61 0.99 0.61
layer straight 33 2 0.000284 -0.99 0.305 0.99 0.305
layer straight 33 2 0.000284 -0.99 1.195 0.99 1.195

layer straight 33 2 0.00051 -0.99 -1.195 0.99 -1.195
layer straight 33 2 0.00051 -0.99 -0.915 0.99 -0.915
layer straight 33 2 0.00051 -0.99 -0.61 0.99 -0.61
layer straight 33 2 0.00051 -0.99 -0.305 0.99 -0.305
layer straight 33 2 0.00051 -0.99 -0.0 0.99 0.0
layer straight 33 2 0.00051 -0.99 0.915 0.99 0.915
layer straight 33 2 0.00051 -0.99 0.61 0.99 0.61
layer straight 33 2 0.00051 -0.99 0.305 0.99 0.305
layer straight 33 2 0.00051 -0.99 1.195 0.99 1.195

# width inner

```

```

layer straight 33 2 0.000284 -0.81 -0.915 0.81 -0.915
layer straight 33 2 0.000284 -0.81 -0.61 0.81 -0.61
layer straight 33 2 0.000284 -0.81 -0.305 0.81 -0.305
layer straight 33 2 0.000284 -0.81 -0.0 0.81 0.0
layer straight 33 2 0.000284 -0.81 0.915 0.81 0.915
layer straight 33 2 0.000284 -0.81 0.61 0.81 0.61
layer straight 33 2 0.000284 -0.81 0.305 0.81 0.305

# outer
layer straight 33 2 0.000284 -0.9246 1.265 0.9246 1.265
layer straight 33 2 0.000284 -0.7532 1.429 0.7532 1.429
layer straight 33 2 0.000284 -0.5817 1.593 0.5817 1.593
layer straight 33 2 0.000284 -0.4103 1.757 0.4103 1.757
layer straight 33 2 0.000284 -0.2388 1.921 0.2388 1.921

layer straight 33 2 0.00051 -0.9246 1.265 0.9246 1.265
layer straight 33 2 0.00051 -0.7532 1.429 0.7532 1.429
layer straight 33 2 0.00051 -0.5817 1.593 0.5817 1.593
layer straight 33 2 0.00051 -0.4103 1.757 0.4103 1.757
layer straight 33 2 0.00051 -0.2388 1.921 0.2388 1.921

# inner
layer straight 33 2 0.000284 -0.7974 1.138 0.7974 1.138
layer straight 33 2 0.000284 -0.6259 1.301 0.6259 1.301
layer straight 33 2 0.000284 -0.4545 1.465 0.4545 1.465
layer straight 33 2 0.000284 -0.283 1.629 0.283 1.629
layer straight 33 2 0.000284 -0.1116 1.793 0.1116 1.793
}

```

APPENDIX H VERIFICATIONS OF MSBRIDGE RESPONSE MECHANISMS

The main purpose of this verification effort is to illustrate and verify the salient new features and capabilities of MSBridge using appropriate idealized bridge configurations. Each of these configurations allowed for simple and systematic assessment of the particular response feature being verified.

Table H.1 presents the cases studied.

G.1 Bridge Model

Aim: Pushover analysis was done with an equivalent bridge model of rigid deck, no abutment effects and the same columns height of 50 ft to check the linear response. Linear column results are shown below for both longitudinal and transverse directions.

G.1.1 Longitudinal Column Response Profile

G.1.1.1 Deformed Shape

Figure H.1 shows the deformed shape of the bridge, the response is as expected for the behavior of the linear columns, where $E = 4,000$ ksi, $I = 30.68$ ft⁴ and $L = 50$ ft.

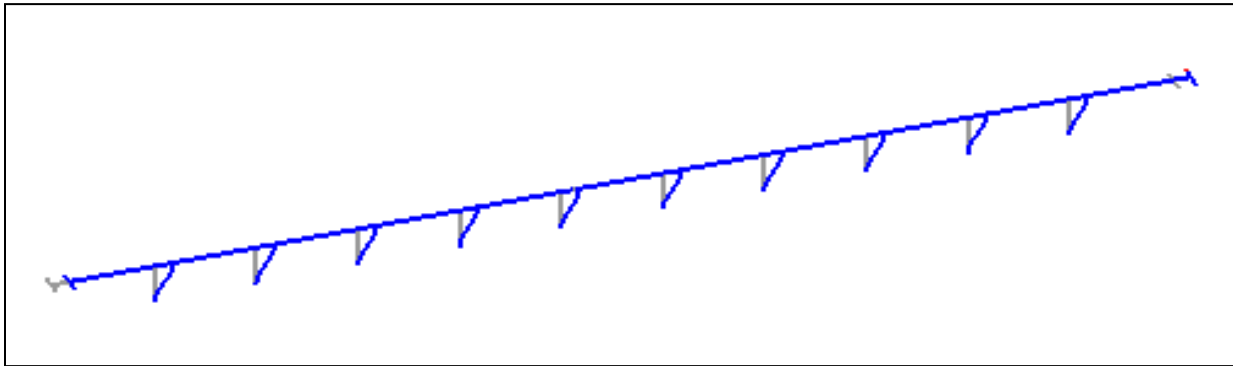


Figure H.1 Bridge deformed shape in the longitudinal direction

Discussion: The deformed shape shows that as the load applied in the longitudinal direction; the bridge will move accordingly. Since the deck is rigid there will be no flexural deformation. In addition, the roller abutment will not resist the movement.

Table H.1 MSBridge Feature-Verification Cases

Section	Aim	Configuration	Conclusion
G.1 Bridge Model	To verify the lateral stiffness of linear columns in a multi-span bridge configuration via Pushover and Mode shape analyses	Bridge model with equal height columns (50 ft), single column per bent, rigid deck and roller abutment	Deformed shapes and displacement for all columns are identical. Column bending stiffness in fixed-fixed configuration is verified to match the value of $12EI/L^3$ (long. direction), with corresponding mode shapes and resonant frequencies.
G.2 Pushover Analysis			
G.3 Mode Shape Analysis			
G.4 Abutment Model	To verify stiffness contribution of different abutment models in multi-span bridge configuration	Same as above	Roller, SDC, and Elastic abutment models function as expected, according to the underlying modeling assumptions.
G.5.2 Soil Springs	To verify the p-y soil spring results with the beam-on-elastic-foundation solution	A simplified single linear pile model	Pushover analysis results match the analytical response of the rigid beam on elastic foundation.
G.5.3 Foundation Matrix	To verify the performance of the Foundation Matrix model	Same as above	Column base displacement and rotation are in accordance with the specified values of the corresponding foundation matrix coefficients.
G.6 Advanced Options, Deck Hinge	To document the deck hinge performance under Pushover loading	Bridge model with equal height columns (30 ft), two columns per bent, rigid deck and roller abutment	<ol style="list-style-type: none"> 1. Increasing the bearing stiffness causes the two sides of the bridge deck to move as one unit. 2. Gap closure works as expected. When the gap reaches the value specified, the tension cables are engaged and behave as expected. 3. Increasing the number of bearings increases the stiffness as expected.

G.1.1.2 Column Response (Deflected Shape)

Figure H.2 shows the column deformation, since the connection is fixed-fixed with the same load applied by the Pushover analysis, the columns should have the same shape. Therefore, only one plot is displayed, and it would be the column of the middle bent, since the Pushover force is applied at the bridge deck center.

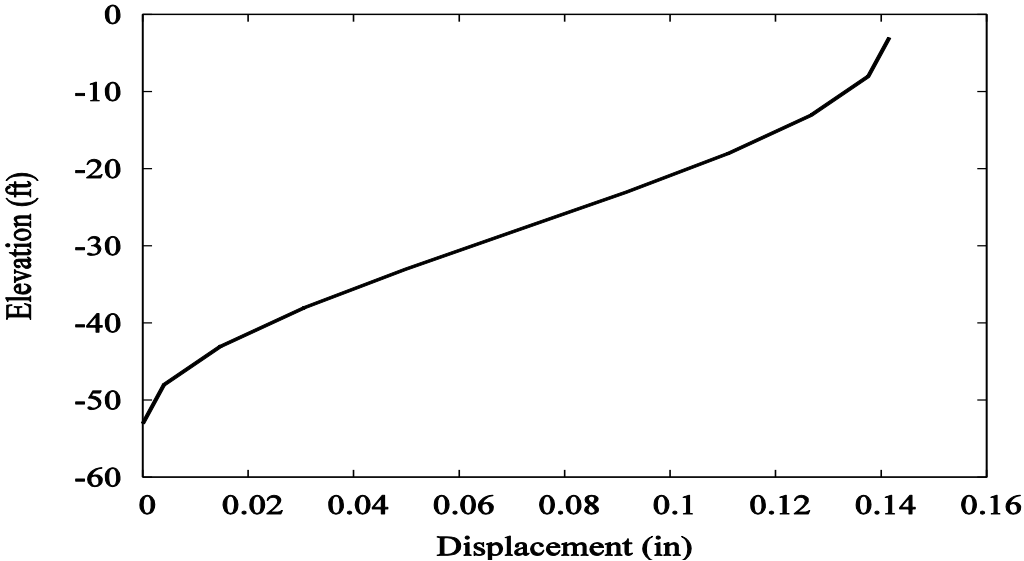


Figure H.2 Longitudinal displacement response profile for column 1 of bent 6

Discussion: the deformed shapes for all columns are the same; the shapes are as expected for linear columns. However, it is good to note that the shape would be smoother if finer mesh was chosen and would be clear that the rotation is zero at the top and bottom connections.

G.1.2 Transverse Column Response Profile

G.1.2.1 Deformed Shape

Similarly, Figure H.3 shows the deformed shape in the transverse direction. However, since the columns are circular, then they have the same stiffness in both directions.

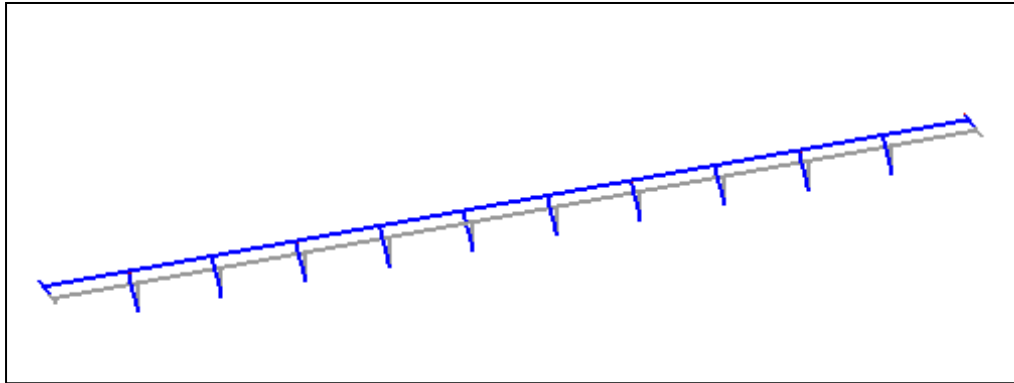


Figure H.3 Bridge deformed shape in the transverse direction

G.1.2.2 Column Response (Deflected Shape)

In this section the columns' deformed shapes are shown in the transverse direction, since the connection is fixed-fixed with the same load applied by the Pushover analysis, the columns should have the same shape (Figure H.4).

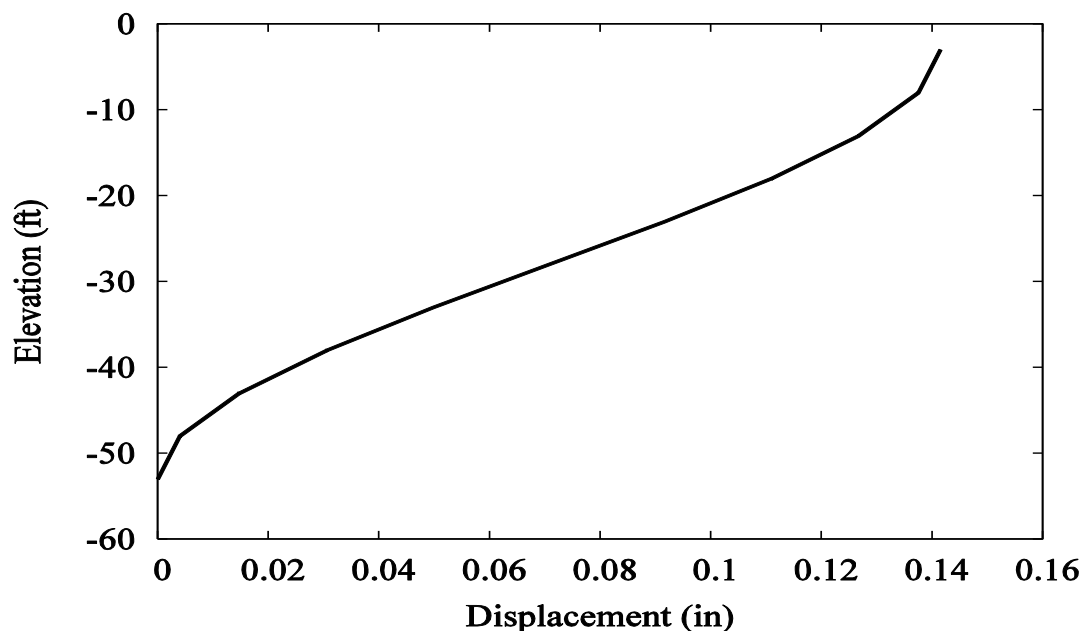


Figure H.4 Transverse displacement response profile for column 1 of bent 6

Discussion: similar results for both directions since the columns are linear, the deck is rigid, and no abutment resistance of movement.

G.2 Pushover Analysis

The pushover options consist of Monotonic Pushover, Cyclic Pushover, and U-Push (pushover by a user-defined loading pattern). However, in this report only the monotonic Pushover is presented and discussed. Moreover, two methods of pushover are available: force-based and displacement-based.

G.2.1 Forced-based Pushover Analysis

In the Force-Based Method, a force increment is applied per step, where the pushover load linearly increases per step in a monotonic pushover mode. The pushover load is applied at the bridge deck center or at the bent as chosen by the user.

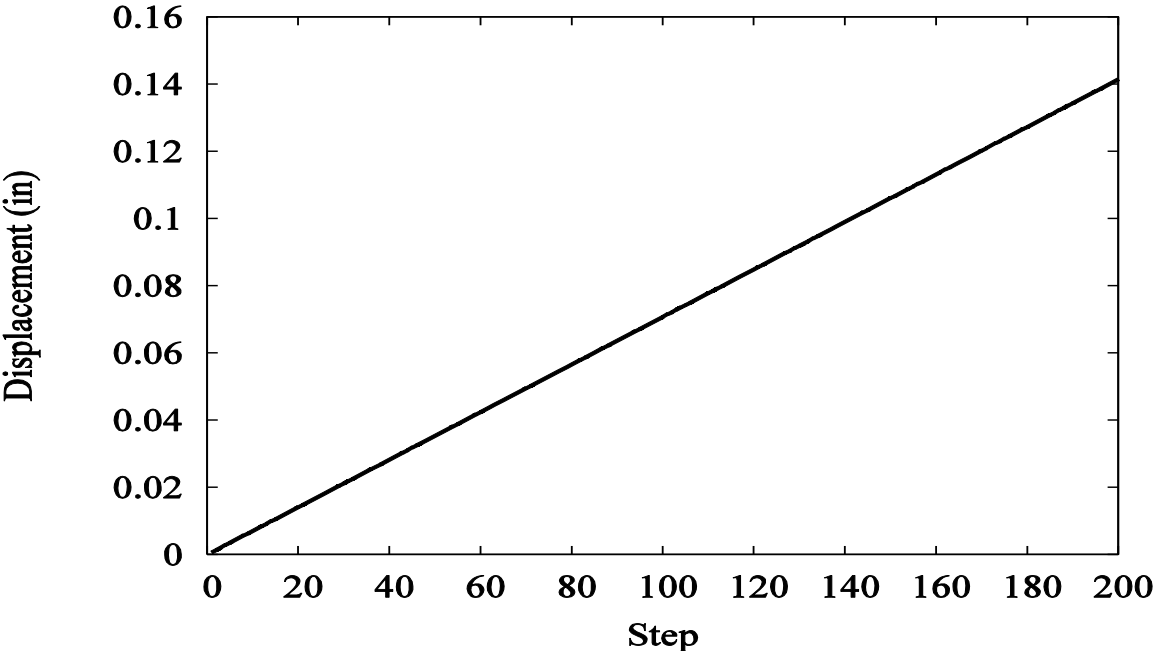


Figure H.5 Longitudinal displacement response time history at elevation of -3 ft for column 1 of bent 6

Since the deck is rigid and the two abutments are roller types, then all the column time histories are the same, so only one figure of column 1 of bent 6 at the bridge deck center is shown since the load is applied at the bridge center (Figure H.5).

The column stiffness for fixed-fixed connection (K) = $12EI/L^3$ for each column
 Where: $E = 4,000$ ksi, and $I = 30.68$ ft⁴, where $I = \frac{\pi}{64}D^4$ and D is the diameter.

$$K = \frac{12 EI}{L^3} = \frac{12 \times 4000 \text{ ksi} \times 30.68 \text{ ft}^4 \times 12^4 \text{ in}^4/\text{ft}^4}{(50 \text{ ft} \times 12 \text{ in}/\text{ft})^3} = 141 \text{ K/in}$$

The total bridge stiffness = $141 \frac{K}{in} \times 10 \text{ bents} = 1410 \text{ K/in}$

And the average stiffness from the Pushover analysis is $200 \text{ kips}/0.141 \text{ in} = 1410 \text{ K/in}$

Conclusion: The results from MSBridge satisfy the structural laws of force and stiffness. Moreover, the same conclusion will result if the Displacement-Based Analysis was performed.

G.2.2 Displacement-based Pushover Analysis

In this section, the same Pushover analysis was performed, but using the displacement-based method. By this method a displacement increment is applied per step. The pushover displacement linearly increases with step in a monotonic pushover mode. The pushover displacement is applied at the bridge deck center or at the bent as chosen by the user.

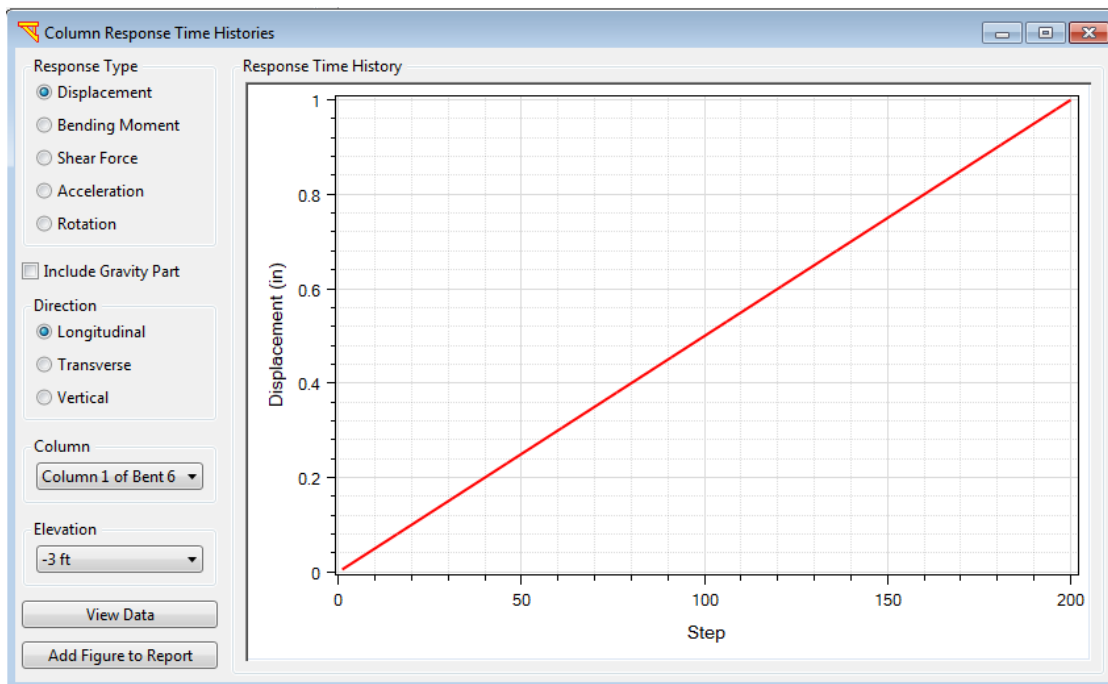


Figure H.6 Longitudinal displacement response time history at elevation of -3 ft for column 1 of bent 6

The column stiffness for fixed-fixed connection (K) = $12EI/L^3$ for each column

$$K = \frac{12 EI}{L^3} = \frac{12 \times 4000 \text{ ksi} \times 30.68 \text{ ft}^4 \times 12^4 \text{ in}^4/\text{ft}^4}{(50 \text{ ft} \times 12 \text{ in/ft})^3} = 141 \text{ K/in}$$

The total bridge stiffness = $141 \frac{K}{in} \times 10 \text{ bents} = 1410 \text{ K/in}$

And the force from the Pushover analysis is $1410 \frac{K}{in} \times 1 \text{ in} = 1410 \text{ K}$

By using Force-Based method with total force of 1410 kips, 1 in. displacement is expected to verify that the Displacement-based method gives similar results to the Force based method.

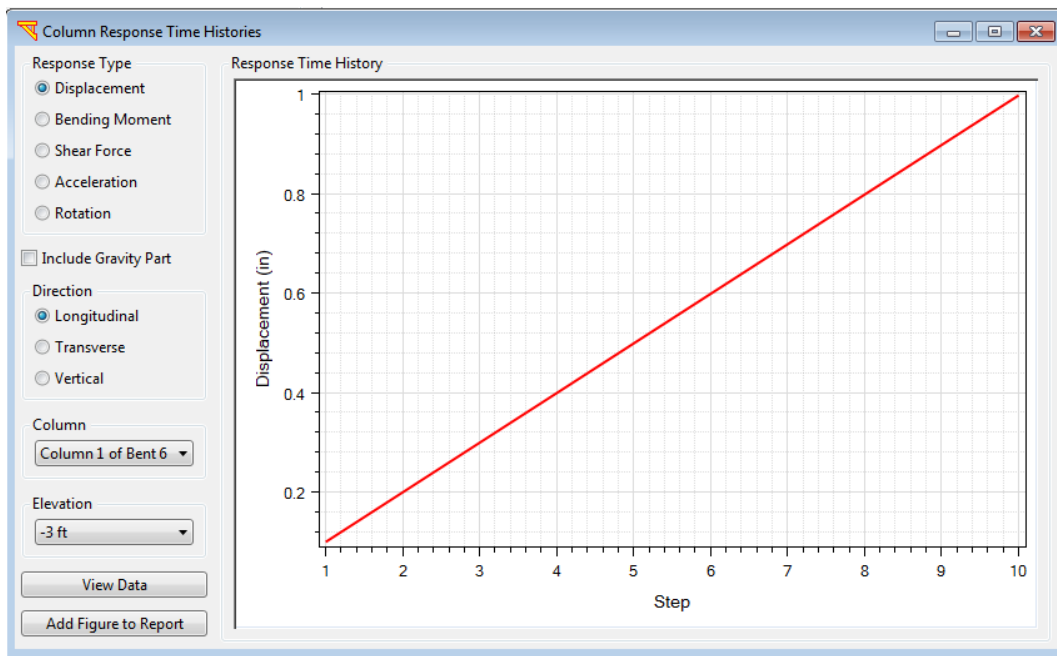


Figure H.7 Longitudinal displacement response time history at elevation of -3 ft for column 1 of bent 6

Conclusion: The Displacement-based method shows same results as the Force-based method (Figure H.6).

G.2.3 Nonlinear Fiber Section

Aim: to run the Pushover Analysis with the nonlinear columns, then compare the results with the linear columns model. However, the pushover load was increased to 12 kips per step for 200 steps, so that it will extend to nonlinear range.

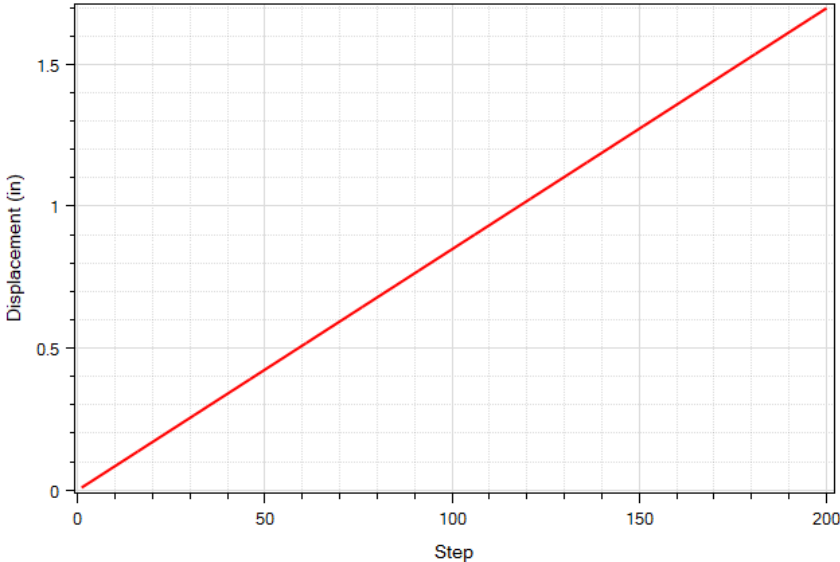


Figure H.8 Longitudinal Displacement Response Time History at Elevation of -3 ft for Column 1 of Bent 6 [Linear Columns]

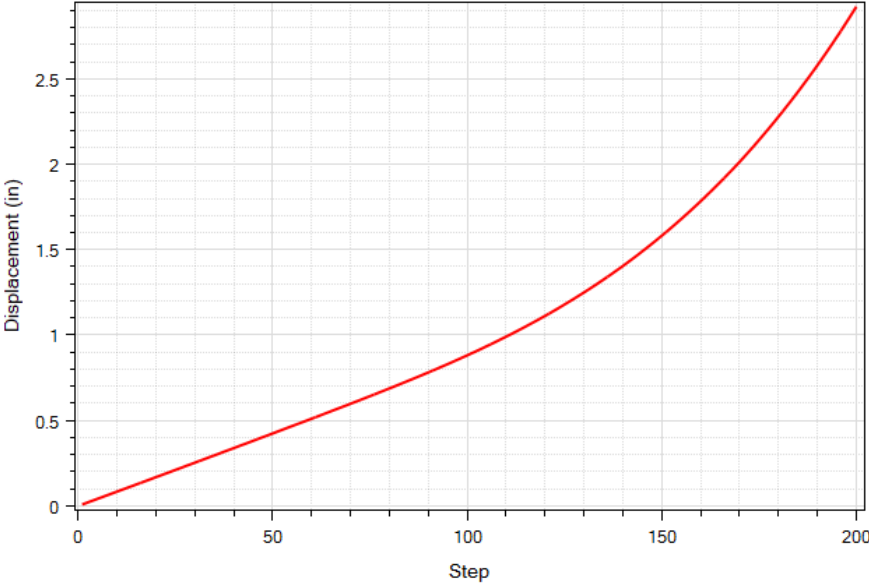
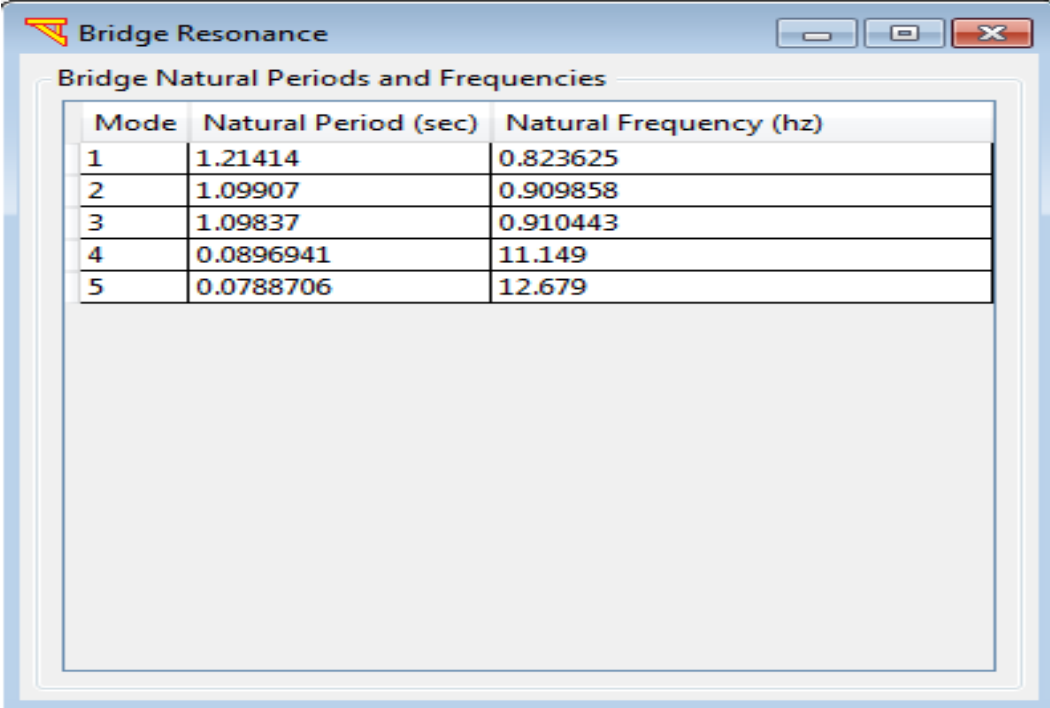


Figure H.9 Longitudinal Displacement Response Time History at Elevation of -3 ft for Column 1 of Bent 6 [Non-linear Columns]

Conclusion: The nonlinear columns displacements are higher than the linear ones, since the nonlinear are softer, as shown in Figure H.9. However, nonlinear columns are showing same results for small displacements when they are still in the linear range. Therefore, the Pushover analysis should be applied for large displacements to make the results more obvious.

G.3 Mode Shapes Analysis

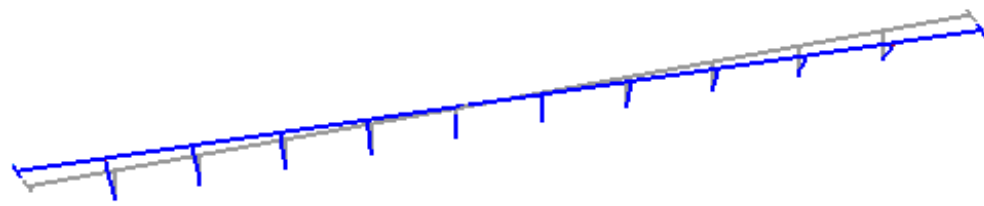
Figure H.10 shows the natural periods and frequencies of the first five modes after performing the Mode Shapes Analysis, and the corresponding mode shapes are shown in Figure H.11.



The screenshot shows a software window titled "Bridge Resonance" with a standard Windows-style title bar (minimize, maximize, close buttons). The main content area is titled "Bridge Natural Periods and Frequencies" and contains a table with three columns: "Mode", "Natural Period (sec)", and "Natural Frequency (hz)". The table lists five modes with their respective values.

Mode	Natural Period (sec)	Natural Frequency (hz)
1	1.21414	0.823625
2	1.09907	0.909858
3	1.09837	0.910443
4	0.0896941	11.149
5	0.0788706	12.679

Figure H.10 Bridge natural periods and natural frequencies



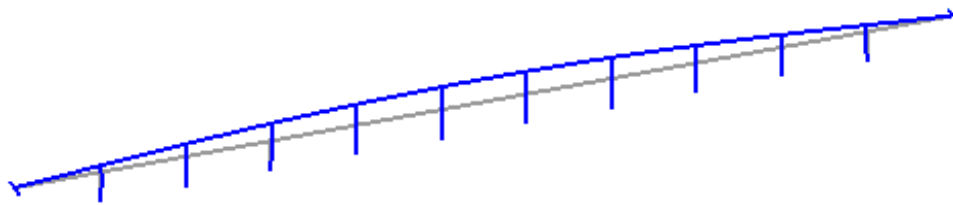
(a)



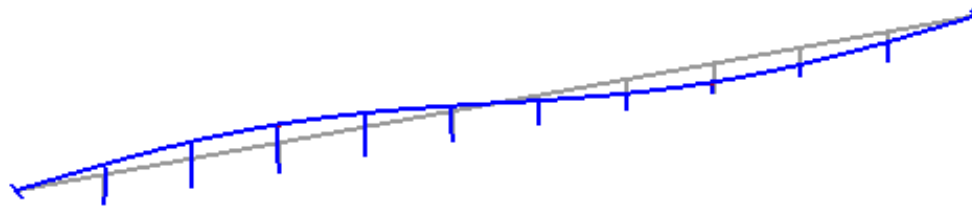
(b)



(c)



(d)



(e)

Figure H.11 Mode Shapes for the bridge model: (a) first mode; (b) second mode; (c) third mode; (d) fourth mode; and (e) fifth mode

Longitudinal Mode Shape Verification

The bridge natural frequency of vibration is determined by equations and compared with the value obtained by the MSBridge. Figure H.11c shows the longitudinal mode shape. Therefore, a value of 0.91 Hz is expected.

Given: deck cross-sectional area = 69.64 ft²

$$\text{Deck weight} = 69.64 \text{ ft}^2 \times 145 \text{ pcf} = 10.1 \text{ Kips/ft}$$

Also, column cross-sectional area = 69.64 ft²

$$\text{Deck weight} = 19.63 \text{ ft}^2 \times 145 \text{ pcf} = 2.85 \text{ Kips/ft}$$

$$\text{Total bridge length} = 2 \times 142.25 \text{ ft} + 9 \times 140 \text{ ft} = 1544.5 \text{ ft}$$

$$\text{Half Column height} = 25 \text{ ft, the total heights} = 25 \text{ ft} * 10 \text{ columns} = 250 \text{ ft}$$

The gravity acceleration (g) = 386 in/s²

$$\text{Mass} = \frac{10.1 \frac{k}{ft} \times 1544.5 \text{ ft} + 2.85 \frac{k}{ft} \times 250 \text{ ft}}{386 \text{ in/s}^2} = 42.26 \frac{K \cdot s^2}{in}$$

$$K = 10 \times \frac{12EI}{L^3} = 1410 \frac{k}{in} \text{ (refer to section G.2)}$$

$$\omega = \sqrt{\frac{K}{m}} = \sqrt{\frac{1410}{42.26}} = 5.77 \text{ s}^{-1}$$

$f = \frac{\omega}{2\pi} = \frac{5.77}{2\pi} = 0.91 \text{ Hz}$	OK
---	----

Discussion: The mode shapes obtained from MSBridge satisfy the structural laws. Also, it is worth noting that the previous mode shapes are for the equivalent bridge with equal height columns and a single column per bent.

G.4 Abutment Model

Aim: To assign each abutment model to the bridge, then to apply the Pushover analysis and check the effects of the abutment model on the bridge response. In addition, to find correlations between the models.

The abutment models implemented in MSBridge consist of seven types; and are defined as Elastic, Roller, SDC 2004, SDC 2010 Sand, SDC 2010 Clay, EPP-Gap and HFD abutment models. The abutment type has a significantly influence the response of the entire bridge system under moderate to strong intensity ground motions. However, the differences between only three types (Elastic, Roller, SDC 2010 Sand) will be studied and presented in this section.

Implementation:

Similar to the previous section, an equivalent bridge model was used to run the analysis. It has the same number of spans with equal height columns, linear columns and rigid deck to study the effect of the abutment models.

G.4.1 Elastic Abutment Model

The Elastic Abutment Model consists of a total of six elastic springs, three of which are translational in the longitudinal, transverse and vertical directions, and three rotational around the longitudinal, transverse and vertical directions. All the series of springs are assigned at each node at the end of the bridge. By default, there will be two series of springs at the ends of the rigid element along the deck width, where the rigid element width is the same as the deck width. However, the user can define multiple distributed springs (equal spacing within deck width). For the longitudinal direction (translational and rotational), each of the distributed (Elastic) springs carries its tributary amount. In addition, it is worth noting that the results from the elastic abutment model depend on the stiffness values associated with the abutment. For instance, making the stiffness values very minimal as if there no motion resistance and the vertical translational stiffness is infinity; would make the abutment model as a roller. As a matter of fact, this will be one of the checks for this section and similar results should be maintained for zero stiffness values elastic abutment model with the vertical translational stiffness is infinity and roller abutment model (Figure H.12).

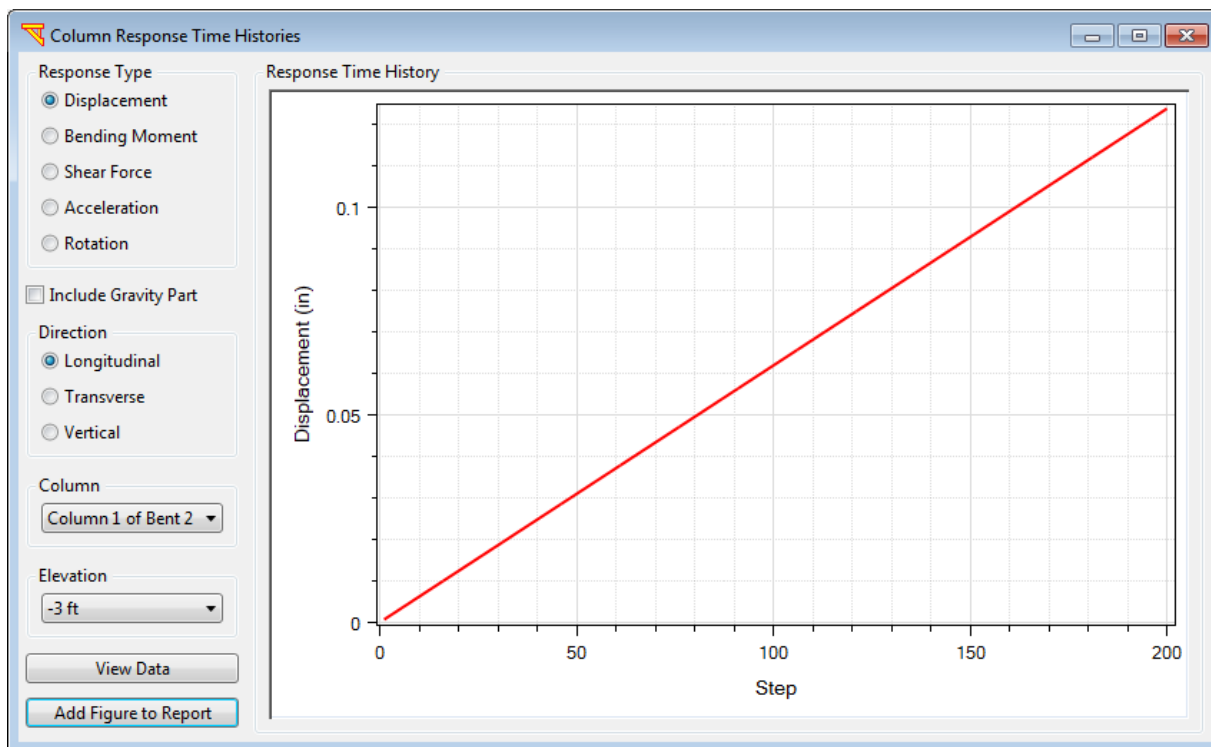


Figure H.12 Longitudinal displacement response time history at elevation of -3 ft for column 2 of bent 6 [Elastic Abutment]

G.4.2 Roller Abutment Model

The Roller Abutment Model acts as single-point constraints against displacement in the vertical direction. Therefore, it consists of rollers in the transverse and longitudinal directions only; the vertical restraint also provides a boundary that prevents rotation of the deck about its axis (torsion). Similar to the elastic abutment model; there will be two rollers at the ends of the rigid element along the deck width, where the rigid element width is the same as the deck width. However, the user can define multiple rollers (equal spacing within deck width). Each of the assigned roller acts as resist the motion in the vertical direction only.

In addition, this model can be used to provide a lower-bound estimate of the longitudinal and transverse resistance of the bridge that may be displayed through a pushover analysis. The roller abutment model result is shown in Figure H.13.

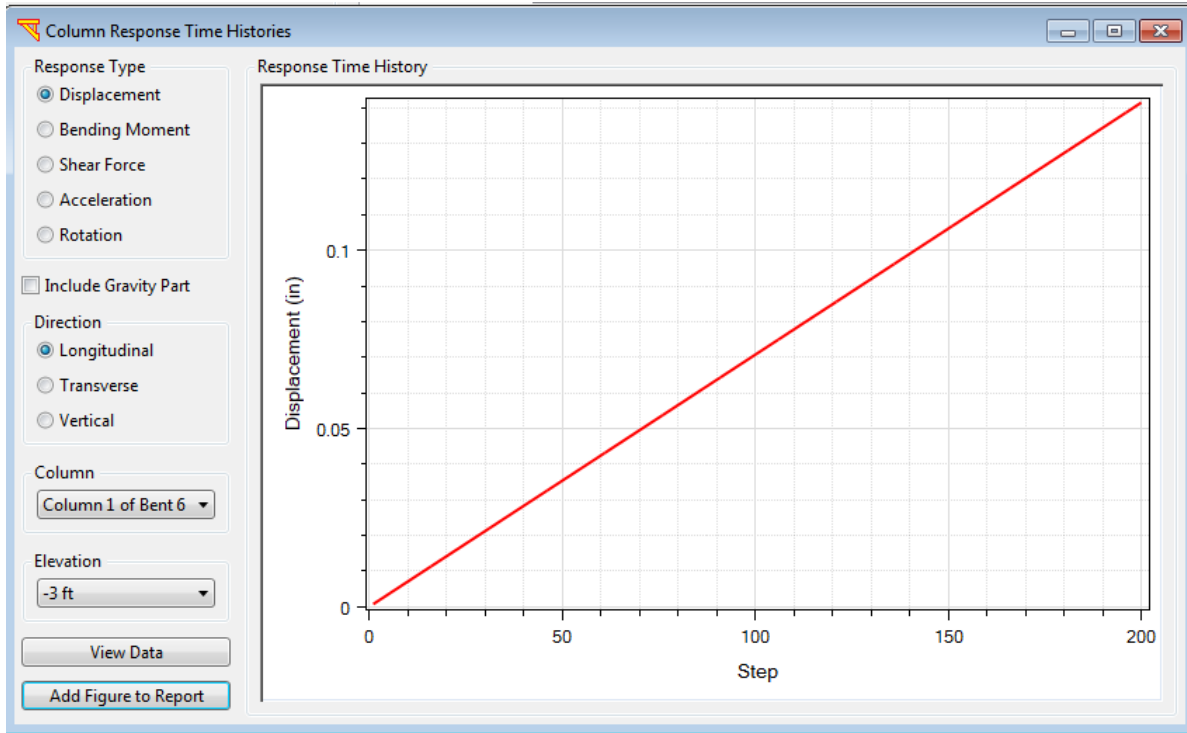


Figure H.13 Longitudinal displacement response time history at elevation of -3 ft for column 2 of bent 6 [Roller Abutment]

G.4.3 SDC Abutment Model

Unlike the other abutment models, the SDC model requires defining more than one parameter. The user should define the elastomeric bearing pads, gap, abutment back wall, abutment piles, and soil backfill material. Prior to impact or gap closure, the superstructure forces are transmitted through the elastomeric bearing pads to the stem wall, and subsequently to the piles and backfill, in a series system. After gap closure, the superstructure bears directly on the abutment back wall and mobilizes the full passive backfill pressure.

The SDC consist of three types, SDC 2004, SDC 2010 Sand and SDC 2010 Clay. By default, there will be two distributed springs at the ends of the rigid element along the deck width, where the rigid element width is the same as the deck width. However, the user can define multiple rollers (equal spacing within deck width). Figure H.14 shows the pushover result for the SDC 2010 Sand abutment model.

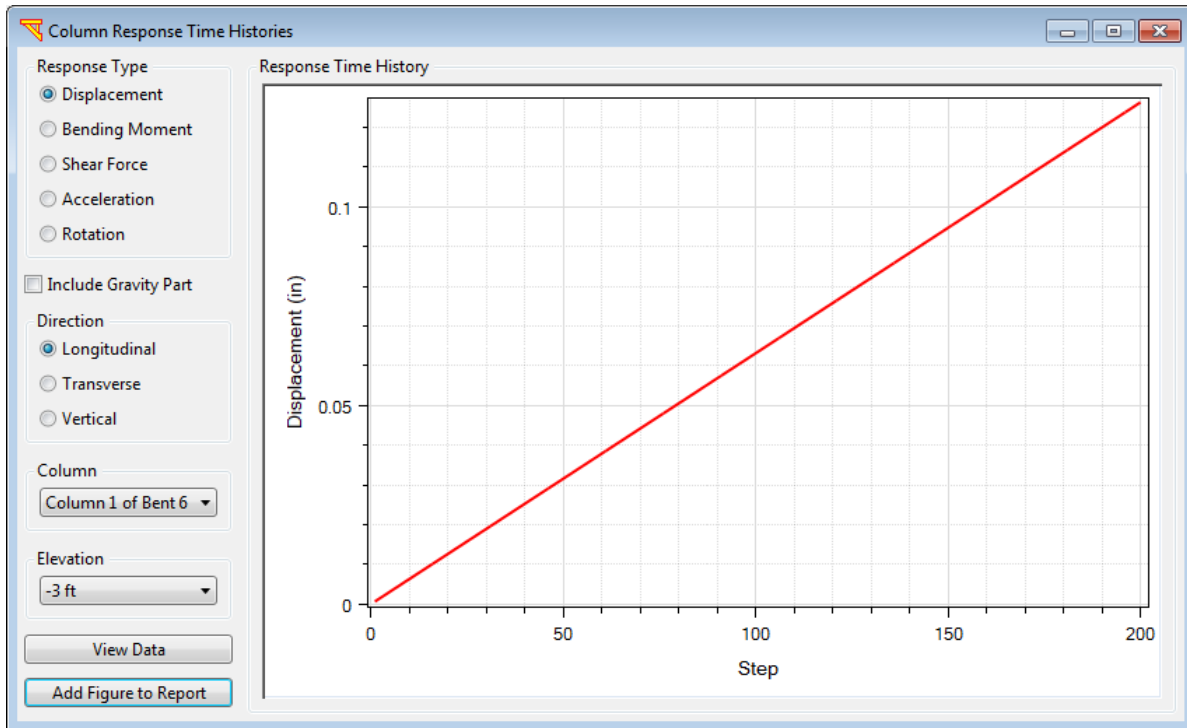


Figure H.14 Longitudinal displacement response time history at elevation of -3 ft for column 2 of bent 6 [SDC 2010 Sand]

Discussion: Since all columns are equal in height and the bridge deck is rigid, then all columns time histories are the same, so only the column at bent 6 results are shown and the rest of the columns are following the same pattern.

Conclusion:

The highest Pushover displacement is found with the roller abutment type. On the other hand, the lowest displacement is associated with the SDC 2010 abutment type. Therefore, the MSBridge satisfy the structural laws as the stiffness is increased, the displacement will decrease while all other components effect is restricted.

Correlations:

The elastic abutment model with zero stiffness and the vertical translational stiffness is infinity is used and its results are shown to compare them with the roller one. They should show identical results. The result shown in Figure H.15 is the column time history.

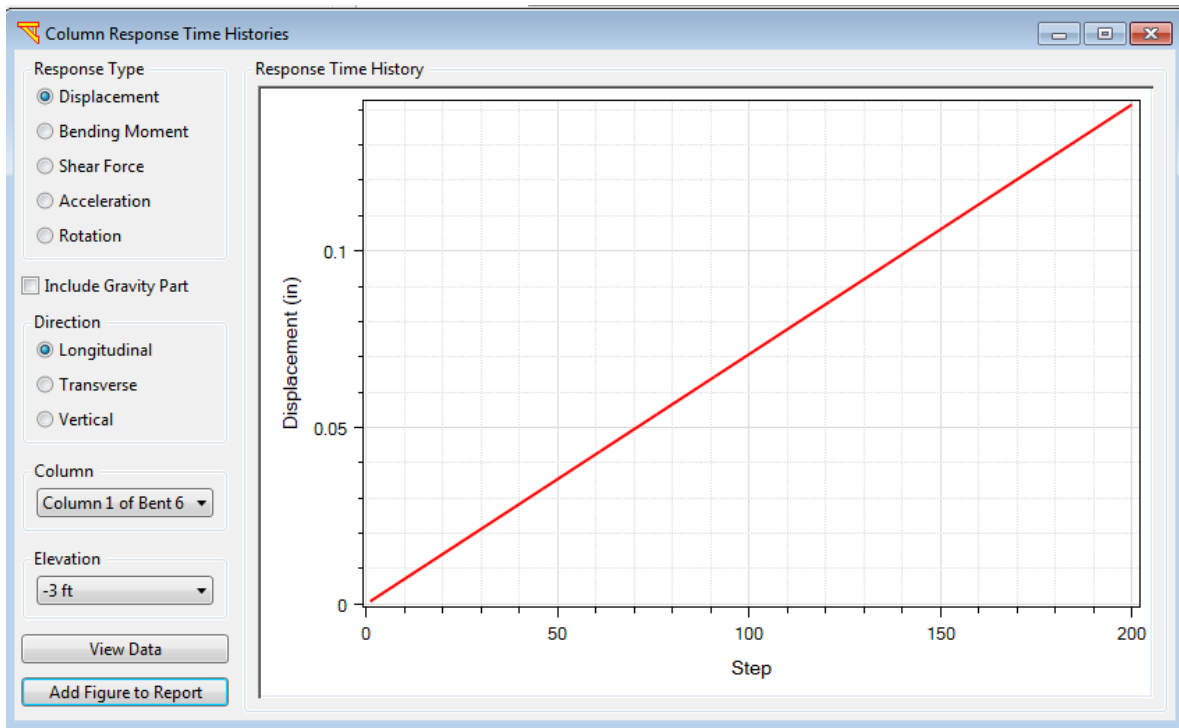


Figure H.15 Longitudinal displacement response time history at elevation of -3 ft for column 2 of bent 6 [Elastic zero stiffness Abutment]

Discussion: the roller abutment model shows similar results to the zero stiffness elastic abutment model with the vertical translational stiffness is infinity.

G.5 Foundation Model

There are three types of foundations available as shown in Figure H.16: **Rigid Base**, **Soil Springs** and **Foundation Matrix**. It is worth noting that for the previous analysis the rigid foundation model was used, and it is the model assigned by default.

G.5.1 Rigid Base

The Rigid Base is where all column bases will be fixed (in 3 translational and 3 rotational directions). In that case, the “fixity” nodes of the abutment models are also fixed. It is consider being as the upper-bound of the foundation stiffness values, and it could be maintained by the other type if very high values were used.

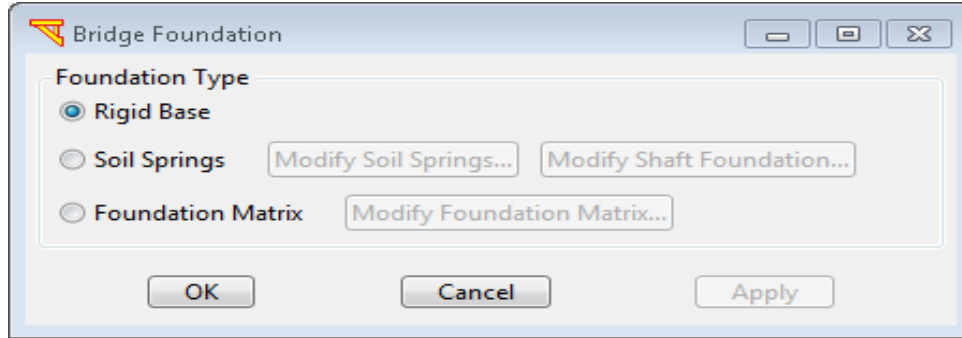


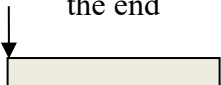
Figure H.16 Foundation types available in MSBridge

G.5.2 Soil Springs

Aim: to compare the maximum deflection from the rigid beam on elastic foundation (the Winkler Foundation) with that from MSbridge using soil springs (Figure H.17).

The Winkler Foundation is the simplest elastic foundation that relates the vertical pressure acting on the solid surface, and the vertical deflection, w , is given by $p = k_0w$. Table H.2 shows the special case of the concentrated load at the end. In addition, Figure H.17 shows the general layout of the soil springs window.

Table H.2 Special Cases for Rigid Beam on Elastic Foundation (Hetenyi 1946)

Case	Deflection, w	Moment, M	Shear, Q
Concentrated load at the end 	$2V_1\lambda D_{\lambda x}/k$	$-V_1B_{\lambda x}/\lambda$	$-V_1C_{\lambda x}$

Where,

$$D_{\lambda x} = e^{-\lambda x}(\cos \lambda x);$$

$$C_{\lambda x} = e^{-\lambda x}(\cos \lambda x - \sin \lambda x);$$

$$\lambda = \sqrt[4]{\frac{k}{4EI}};$$

k = stiffness pressure (ksi) = subgrade coefficient \times beam width

Special Case: Concentrated load at the end

$$\text{Maximum Deflection } (w) = \frac{2P\lambda}{k}, \quad \text{where } D_{\lambda x} = 1.$$

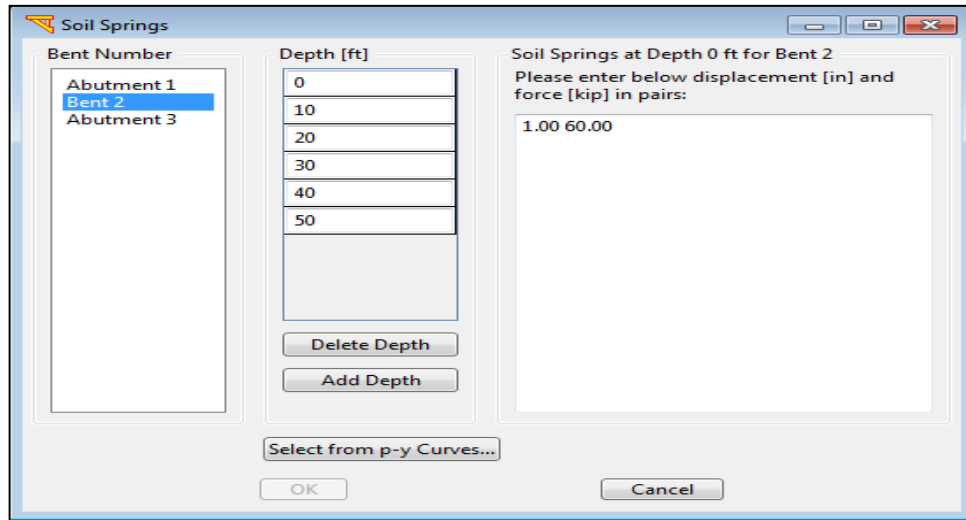


Figure H.17 Soil springs foundation type

Implementation:

A semi-infinite steel bar ($E = 200\text{GPa}$) has a square cross section ($b = h = 80\text{mm}$) and rests on a Winkler foundation of modulus $k_o = 0.25 \text{ N/mm}^2/\text{mm}$. A downward force of 50 kN is applied to the end as shown in Figure H.18

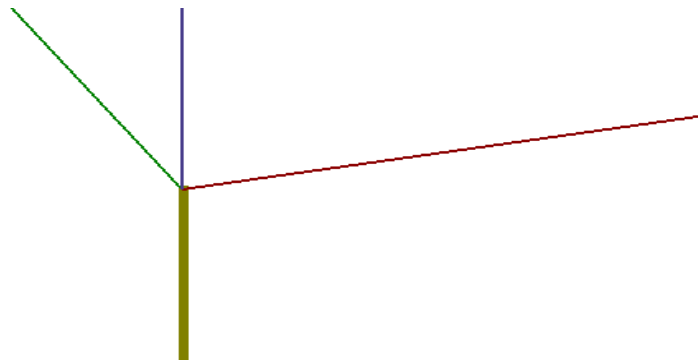


Figure H.18 A simplified single pile model

Analytical Solution

$$P = 50 \text{ kN}, k = \text{width} \times k_o = 20 \text{ N/mm/mm}, \lambda = \sqrt[4]{\frac{20 \frac{\text{N}}{\text{mm}}/\text{mm}}{4 \times 6.827 \times 10^{11} \text{ N.mm}^2}} = 0.001645/\text{mm}$$

$$\text{Deflection at end } (w) = \frac{2 \times 50,000 \text{ N} \times 0.001645/\text{mm}}{20 \frac{\text{N}}{\text{mm}}/\text{mm}} = 8 \text{ mm}$$

Deformed Shape:

Figure H.19 shows the deformed shape of the single pile after applying the pushover load. However, the shape is similar to the expected behavior of the linear pile.

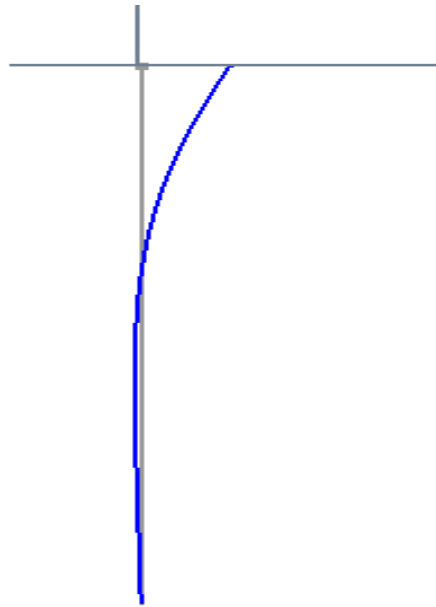


Figure H.19 Deformed shape with soil springs foundation model

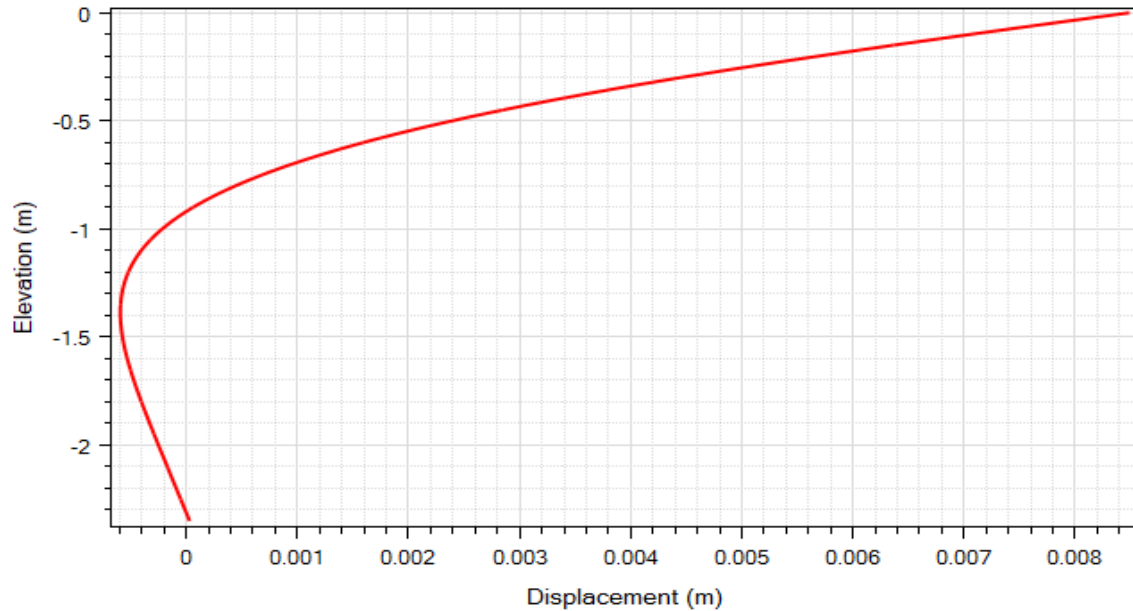


Figure H.20 Longitudinal pile response

Conclusion: The Pushover analysis results are very similar for both the analytical solution (The Winkler Springs) and MSBridge output as shown in Figure H.20 for the pile response.

G.5.3 Foundation Matrix

Aim: to assign the foundation matrix type to the bridge foundation, then to compare the pushover analysis with different foundation types, and show how the foundation stiffness would affect the results.

The third foundation type available is **Foundation Matrix**. In this method, the foundation (only for bent columns) is represented by the coupled foundation stiffness matrix (Lam and Martin 1986). Specifically, the stiffness of a single pile is represented by a 6 x 6 matrix representing stiffness associated with all six degrees of freedom at the pile head as shown in Figure H.21. The local coordination system employed for the foundation matrix is parallel to the global coordination system.

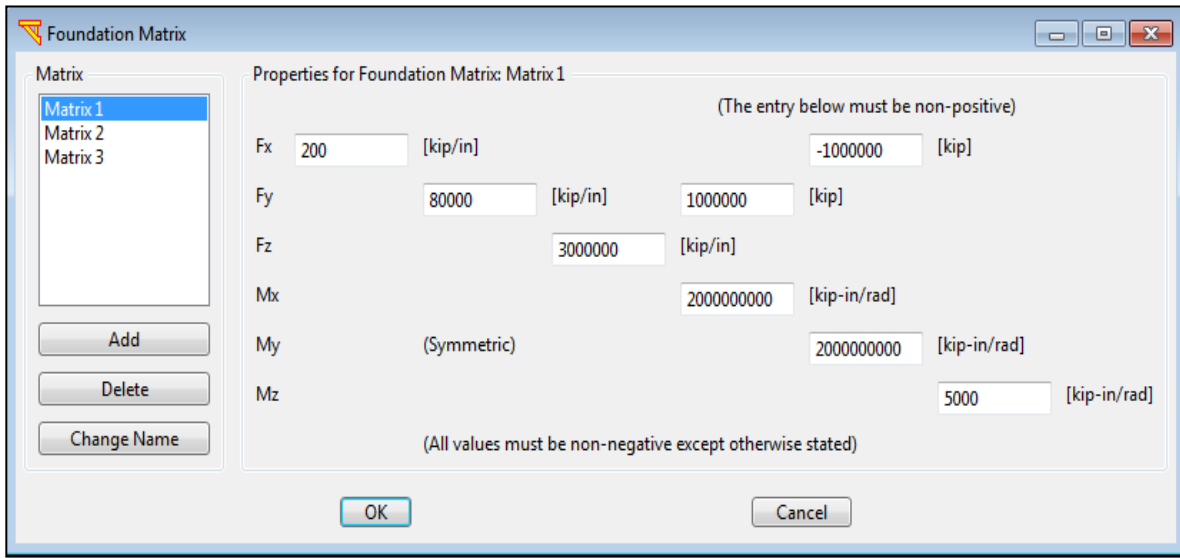


Figure H.21 Foundation matrix for each bent

Implementation

A simplified two-span bridge model is used to run the analysis for the foundation type as shown in Figure H.22. Also, the Pushover analysis time steps were reduced to only 2 steps, since the linear columns results follow the same pattern.

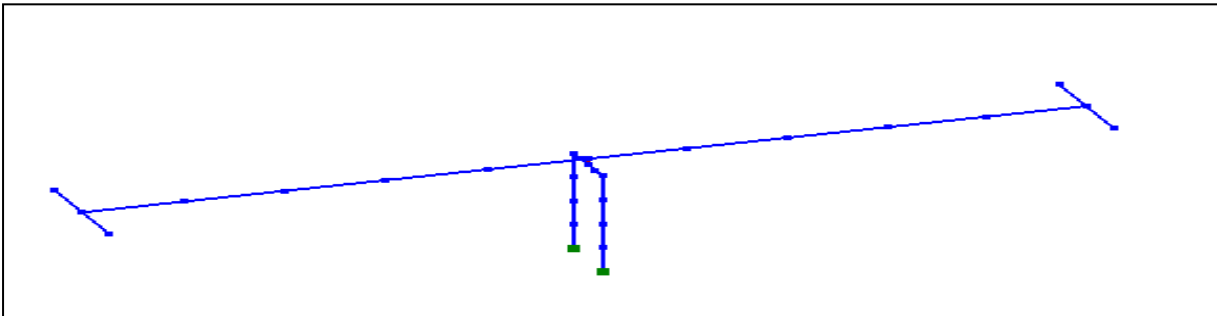


Figure H.22 A simplified two-span bridge model

Deformed Shape

Figure H.23 shows the deformed shape of the bridge, and it functions as expected based on linear columns, rigid deck, and no abutment effect.

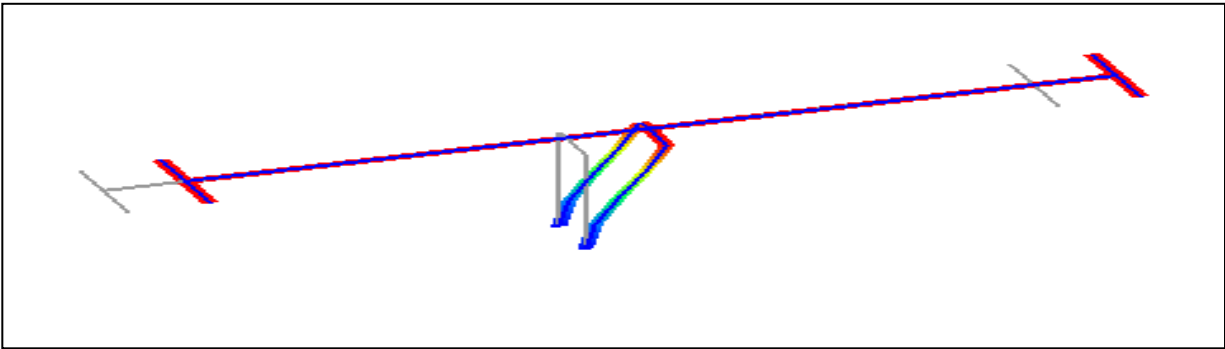


Figure H.23 Deformed shape with foundation matrix model

Case 1: rigid foundation vs. infinite stiffness foundation matrix

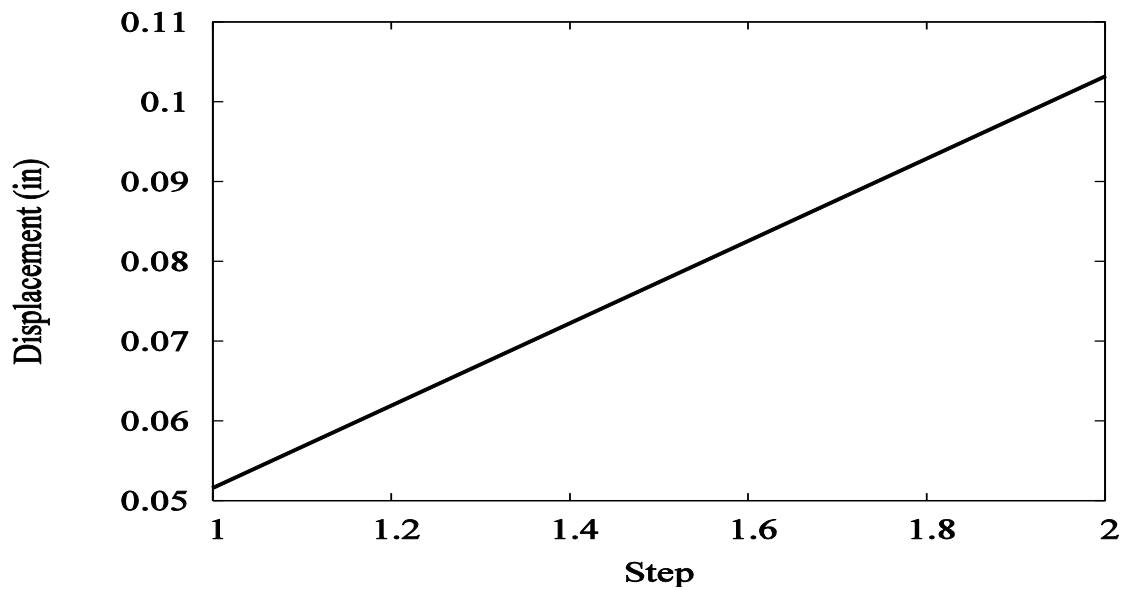


Figure H.24 Longitudinal displacement response time history at elevation of -3 ft for column 1 of bent 2 [rigid]

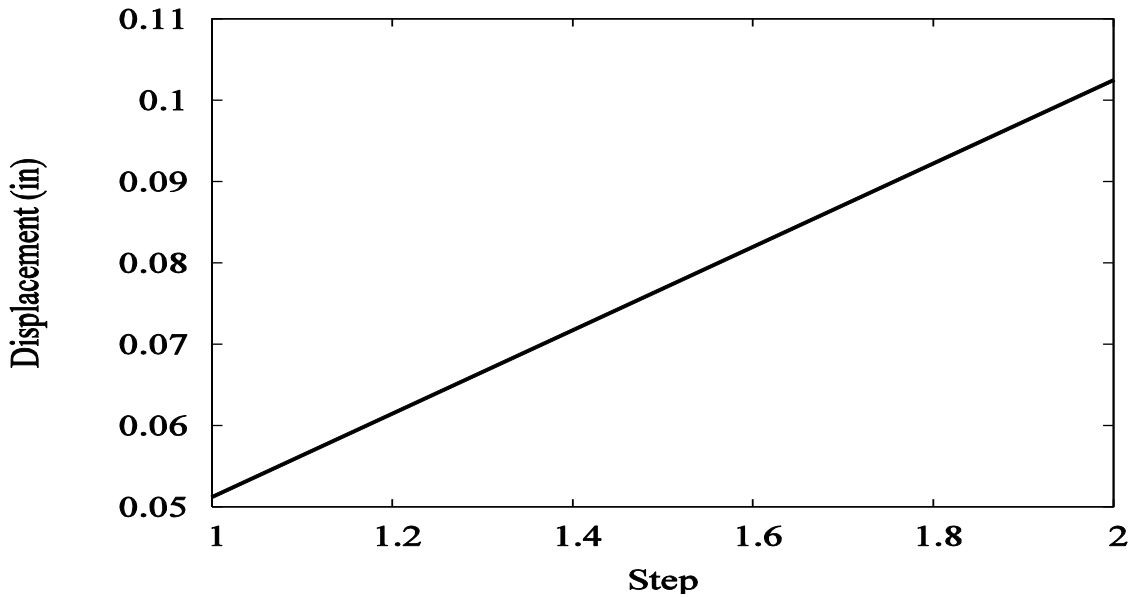


Figure H.25 Longitudinal displacement response time history at elevation of -3 ft for column 1 of bent 2 [infinite foundation stiffnesses]

Conclusion: The Pushover analysis results are identical for both rigid and infinite stiffness in the foundation matrix as shown in Figure H.24 and Figure H.25.

Case 2: rigid foundation vs. reduced lateral stiffness

In this case, only the horizontal displacement of the foundation is allowed (Figure H.26), this can be implemented by provide a finite stiffness value for F_x in Figure H.27 and restrained all other degrees of freedom.

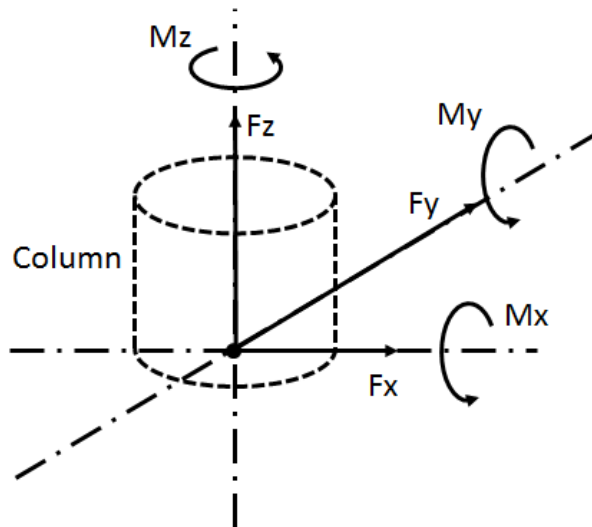


Figure H.26 Local coordination system for the foundation matrix (Elgamal et al. 2014)

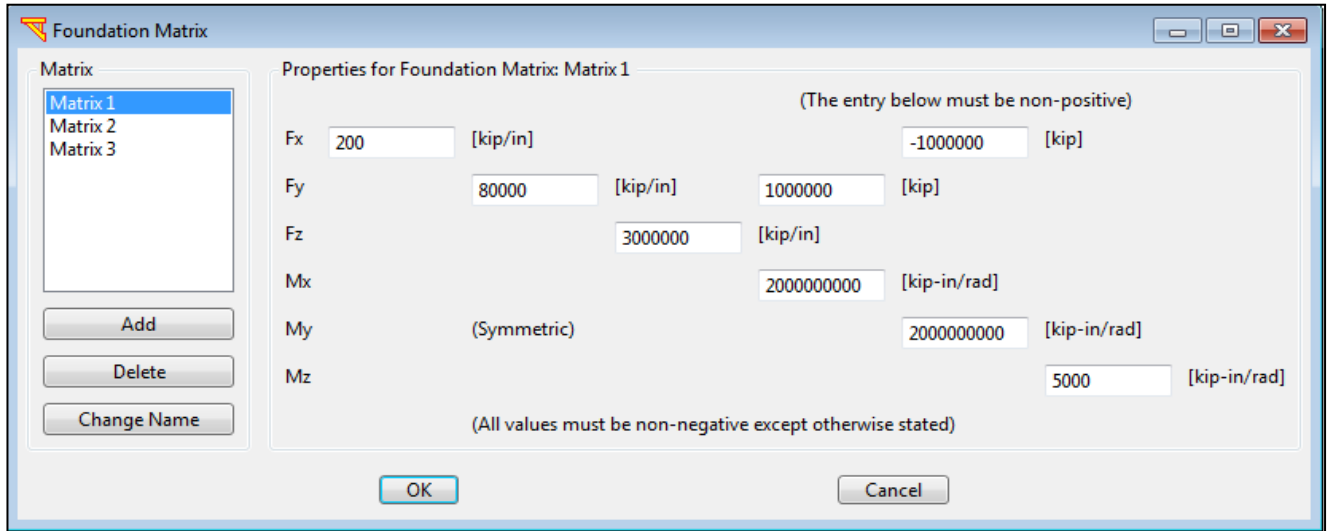


Figure H.27 Foundation matrix for each bent

Deformed Shape:

Figure H.28 shows the deformed shape of the equivalent model with a reduced horizontal stiffness value as explained in case 2.

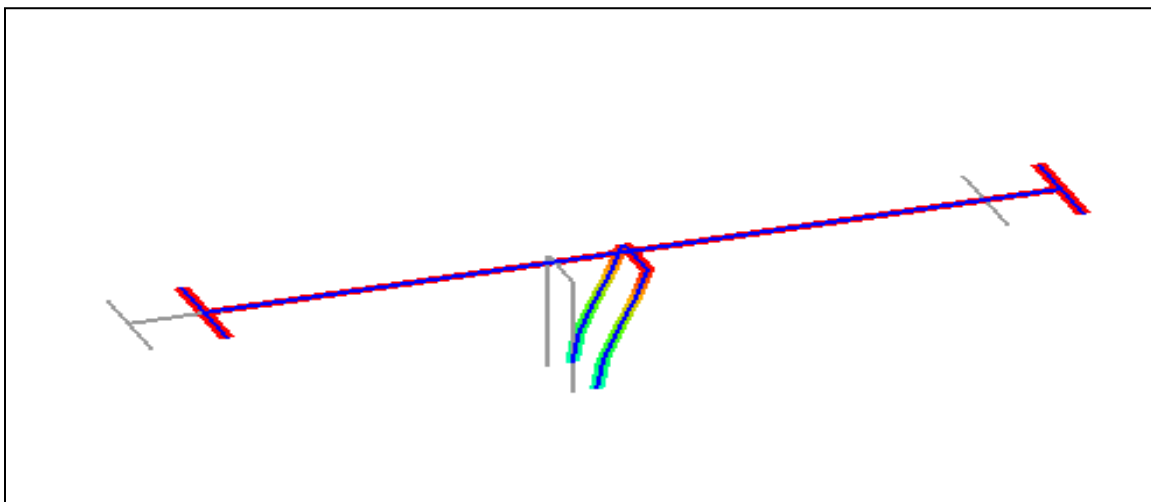


Figure H.28 Deformed Shape with foundation matrix model [case 2]

Calculation:

The displacement for the rigid foundation = 0.1 in

The horizontal foundation stiffness $k_x = 200 \text{ K/in/spring}$.

The applied force from the Pushover = 20 kips

$$\text{The increase in the displacement} = \frac{20 \text{ kips} / 200 \frac{\text{kips}}{\text{in}} / \text{spring}}{2 \text{ springs}} = 0.05 \text{ in}$$

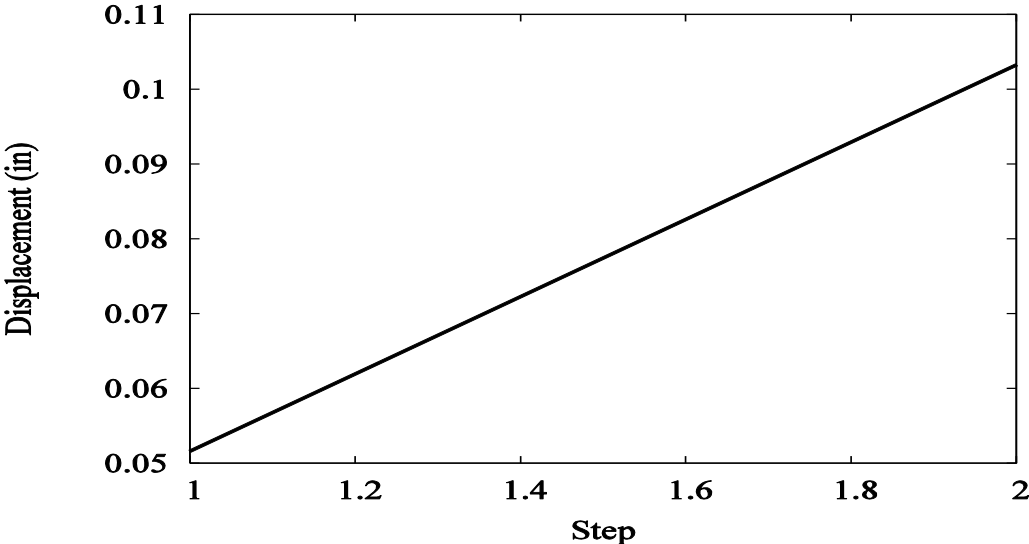


Figure H.29 Longitudinal displacement response time history at elevation of -3 ft for column 1 of bent 2 [rigid]

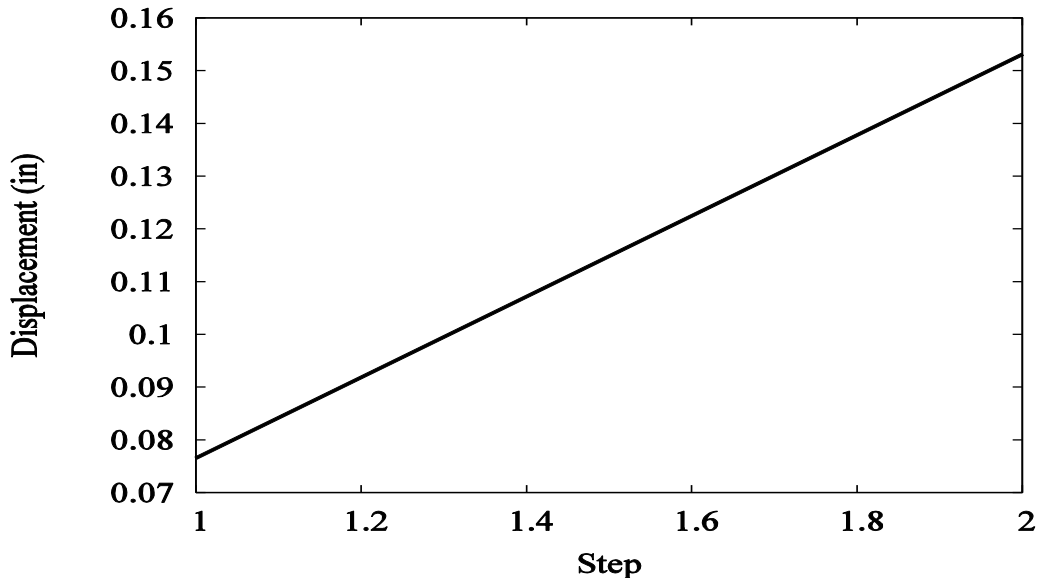


Figure H.30 Longitudinal displacement response time history at elevation of -3 ft for column 1 of bent 2 [horizontal displacement is permitted]

Conclusion: The displacement from reducing the foundation horizontal stiffness equals the sum of that due to the Pushover and the spring compression as shown in Figure H.29 and Figure H.30.

Case 3: rigid foundation vs. reduced rotational stiffness

In this case, only the rotation around the y-axis of the foundation is allowed, this can be implemented by provide a finite stiffness value for M_y in Figure H.31 and restrained all other degrees of freedom.

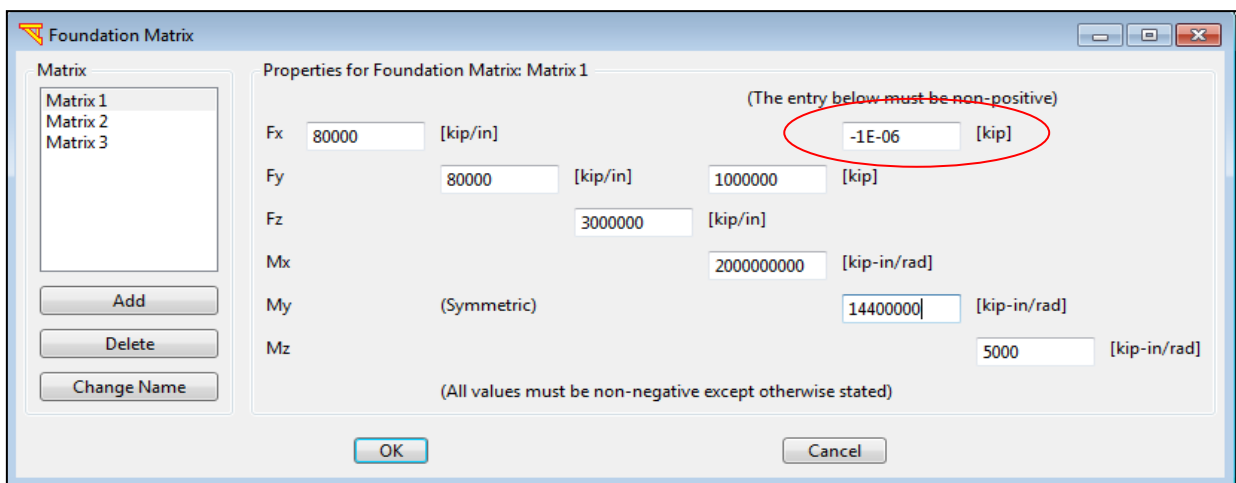


Figure H.31 Foundation matrix for each bent

Deformed Shape:

Figure H.32 shows the deformed shape of the equivalent model with a reduced horizontal stiffness value as explained in case 3.

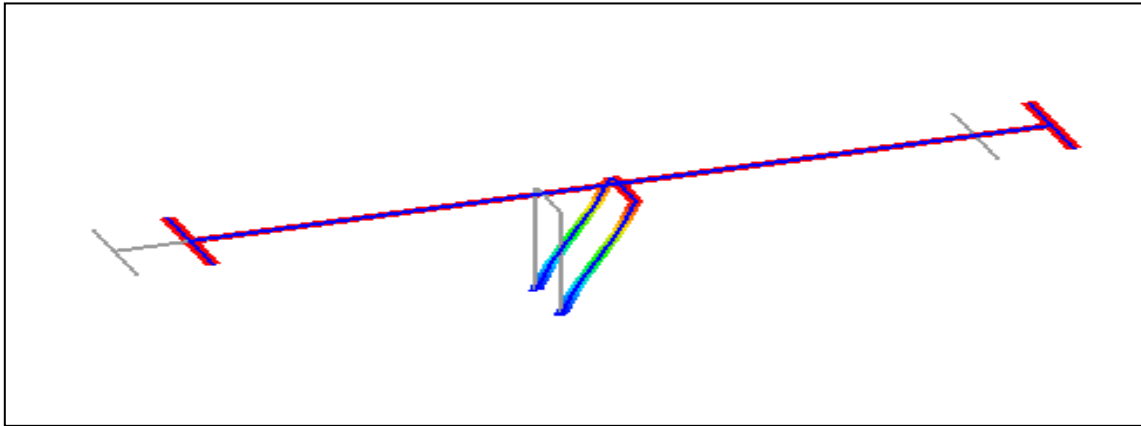


Figure H.32 Deformed shape with foundation matrix mode [case 3]

Calculation:

The displacement for the rigid foundation = 0.1 in

The applied force from the Pushover = 20 kips

The rotational foundation stiffness $k_{\text{rotational}_y} = 14400000$ K-in/rad/spring.

The rotation = 1/600 rad

The displacement = $1/600 * 50' * 12''/' = 1$ in

The increase in the displacement = $\frac{1 \text{ in}}{2 \text{ springs}} = 0.05 \text{ in}$

Remark: the rotational stiffness was calculated to give 1 in horizontal displacement per spring, so that the same load will be applied for case 4, the combined case.

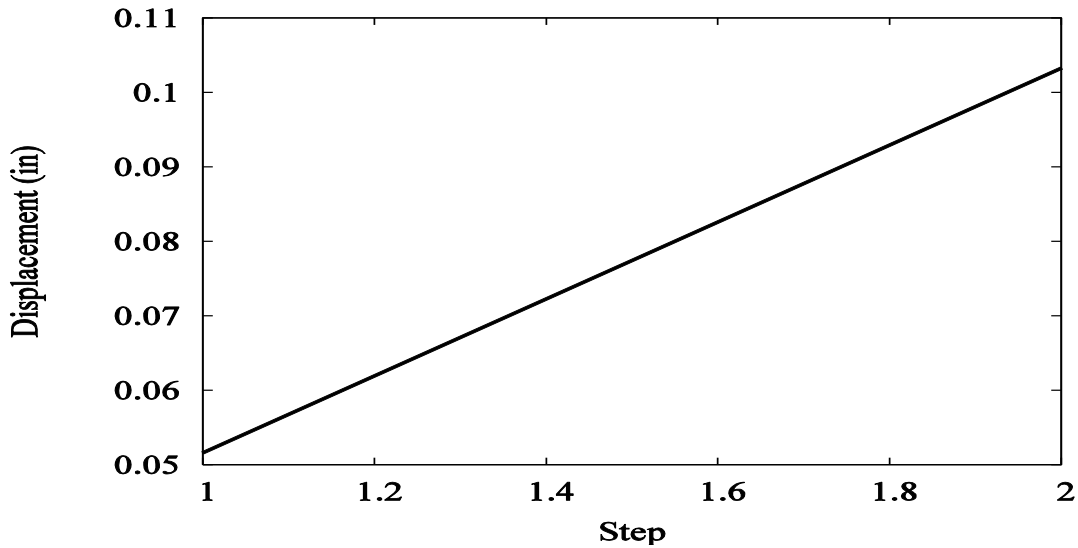


Figure H.33 Longitudinal displacement response time history at elevation of -3 ft for column 1 of bent 2 [rigid]

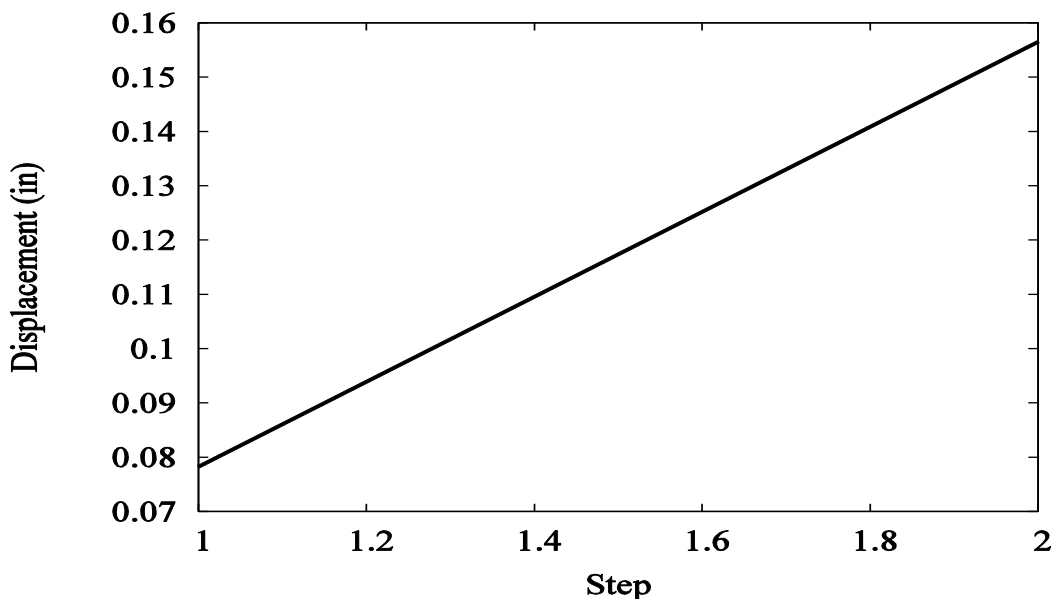


Figure H.34 Longitudinal displacement response time history at elevation of -3 ft for column 1 of bent 2 [rotation is permitted]

Conclusion: The displacement from reducing the foundation rotational stiffness equals the sum of that due to the Pushover and the spring compression as shown in Figure H.33 and Figure H.34.

Case 4: rigid foundation vs. reduced lateral and rotational stiffness

In this case, only the horizontal displacement and rotation around y-axis of the foundation are allowed, this can be implemented by provide a finite stiffness value for F_x and M_y in Figure H.35 and restrained all other degrees of freedom.

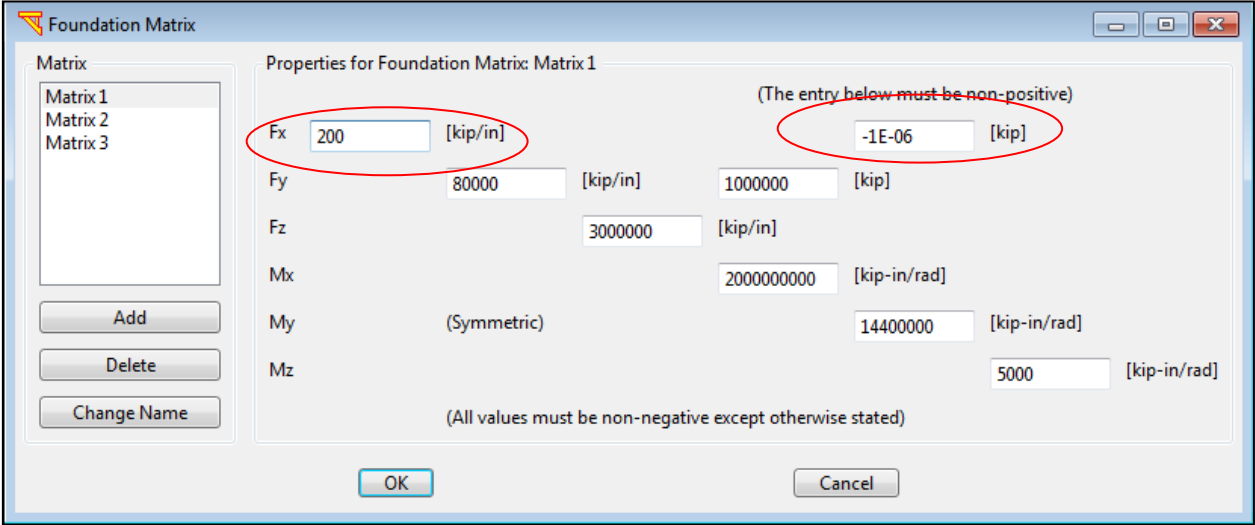


Figure H.35 Foundation matrix for each bent

Deformed Shape:

Figure H.36 shows the deformed shape of the equivalent model with a reduced horizontal stiffness value as explained in case 4.

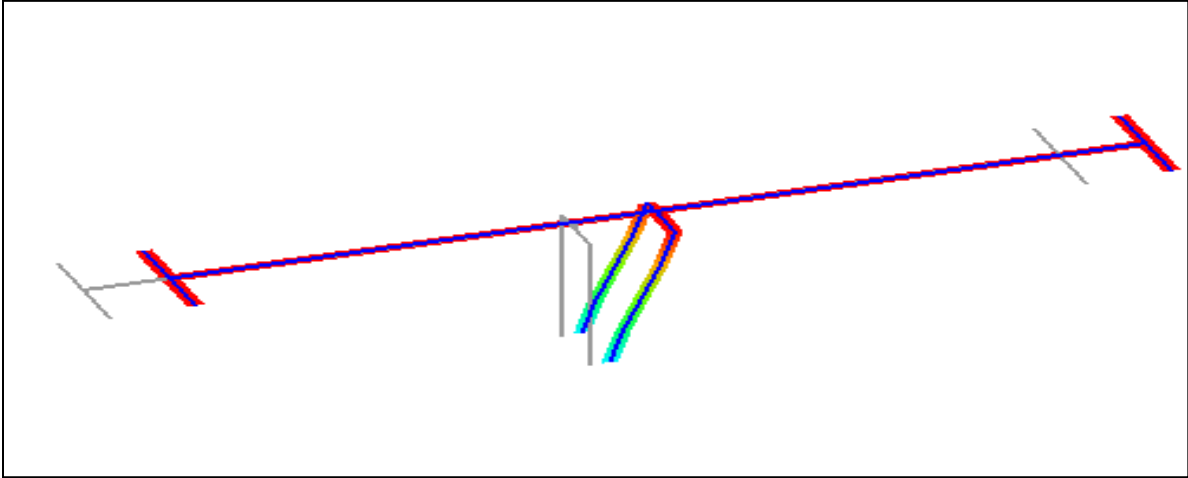


Figure H.36 Deformed shape with foundation matrix [case 4]

Calculation:

The displacement for the rigid foundation = 0.1 in

The horizontal foundation stiffness $k_x = 200$ K/in/spring.

The applied force from the Pushover = 20 kips

The rotational foundation stiffness $k_{\text{rotational}_y} = 14400000$ K-in/rad/spring.

The increase in the displacement = case 2 + case 3 = 1 in

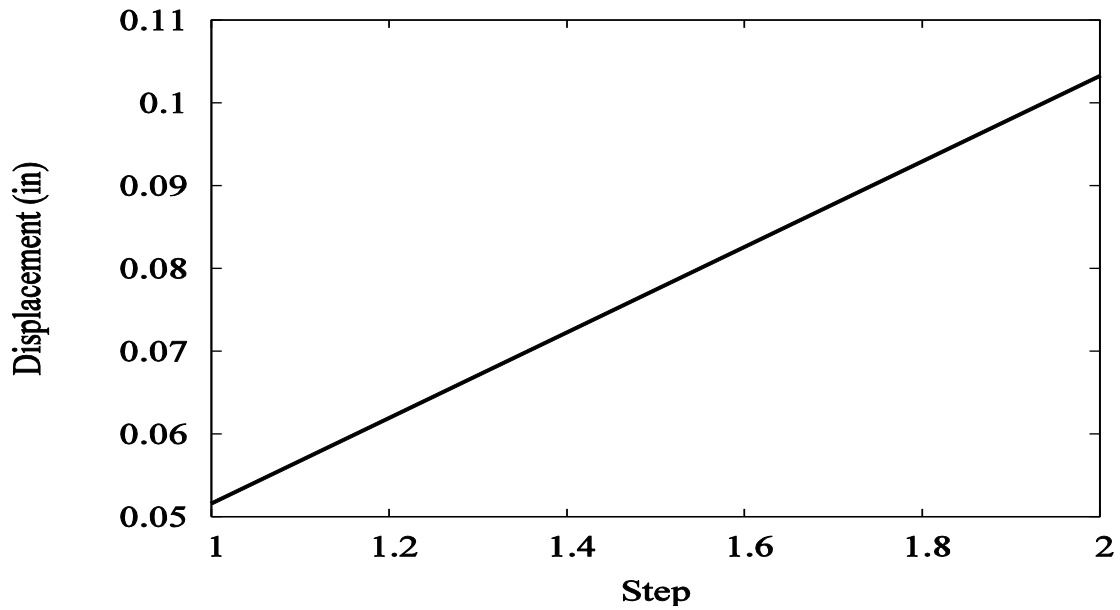


Figure H.37 Longitudinal displacement response time history at elevation of -3 ft for column 1 of bent 2 [rigid]

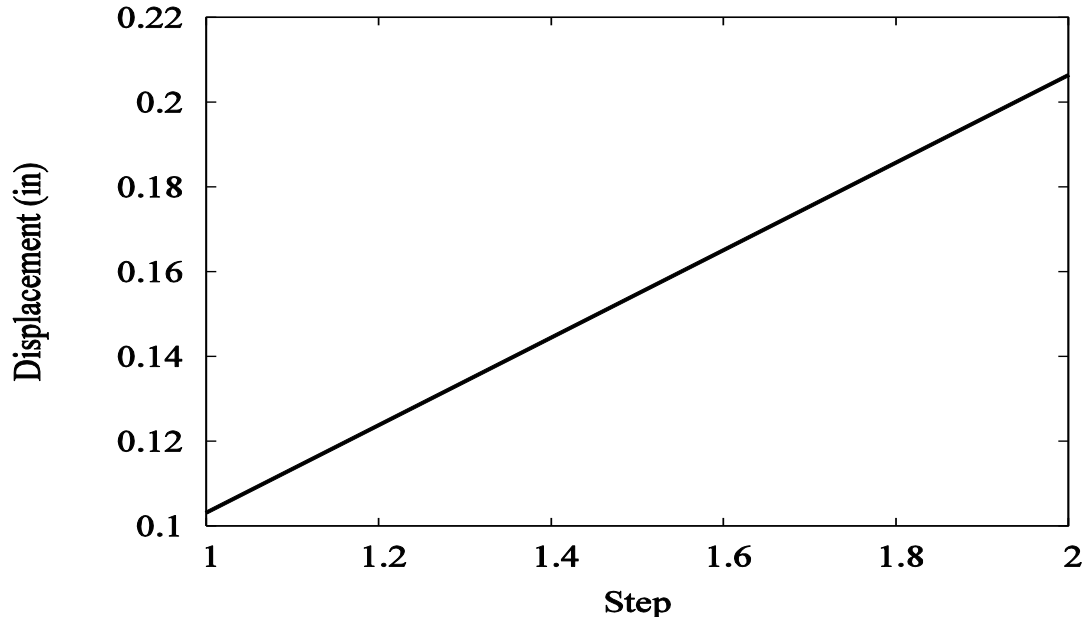


Figure H.38 Longitudinal displacement response time history at elevation of -3 ft for column 1 of bent 2 [horizontal displacement and rotation are permitted]

Conclusion: The displacement from reducing the foundation horizontal and rotational stiffness values equals the sum of that due to the Pushover and the spring compressions as shown in Figure H.37 and Figure H.38.

G.6 Advanced Options

The advanced options in MSBridge include Deck Hinges, Isolation Bearings and Skew Angles as shown in Figure H.39. The focus in this section is on the deck hinge.

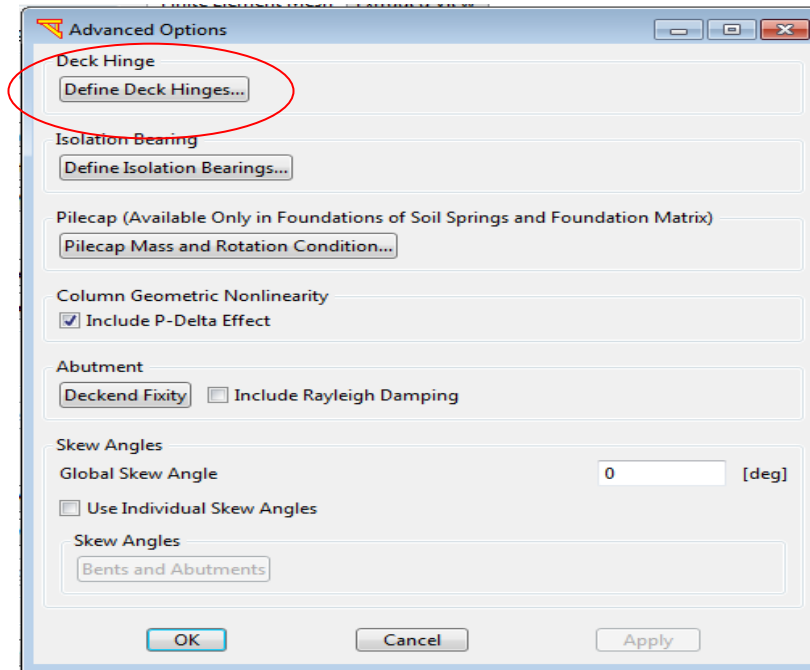


Figure H.39 Advanced options

Deck Hinges

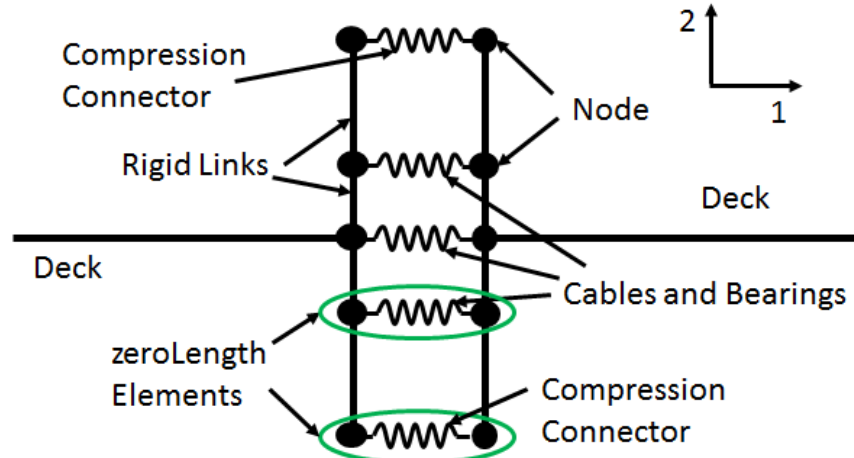


Figure H.40 the general scheme of a deck hinge, which consists of 2 compression connectors (located at both deck edges) and cables. (Elgamal et al. 2014)

“Zero-Length elements are used for cables and compression connectors. The bearing pads are included in the cables. For each zero-Length element, both nodes are interacted in the longitudinal direction (denoted as direction “1” in Figure H.40) but tied in the vertical direction “3” (not shown in Figure H.40) as well as the transverse direction (denoted as direction “2” in Figure H.40). The above conditions would force both sides of deck segments to move in the same plane.

Distance to Bent: The distance to the nearest (left) bent. Foot and meter are used for English and SI units, respectively

Spacing: The space between transverse left and right deck connectors. This space should usually approximately equal to the Deck Width.

Skew Angle: The skew angle of the deck hinge. A zero skew angle means the deck hinge is perpendicular to the bridge deck direction

Of Cables: The total number of cables of the deck hinge

Cable Spacing: The spacing between cables. Symmetric layout of cables is assumed. Foot and meter are used for English and SI units, respectively” (Elgamal et al. 2014)

The default values of properties for the compression connectors, cables, bearing pads are also shown in Figure H.41.

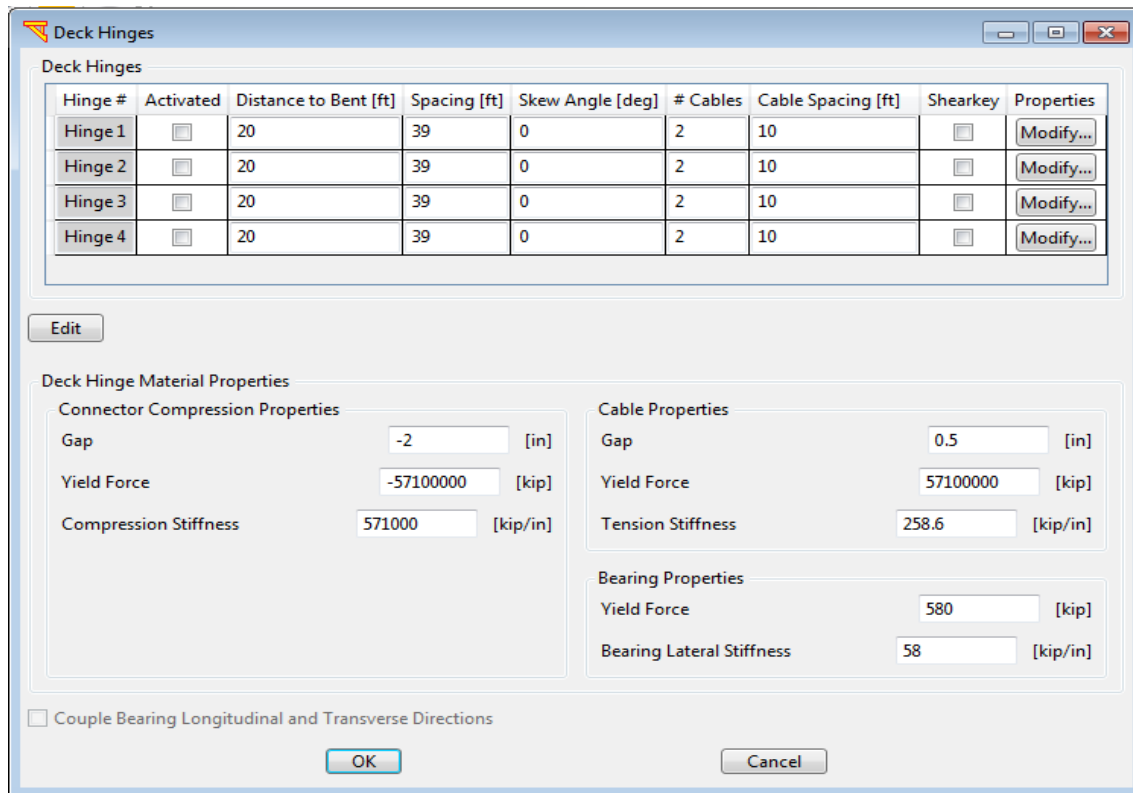


Figure H.41 Definition of deck hinges

Aim: to implement the deck hinge in the bridge model shown in Figure H.42, then check the effect of the deck hinge in the Pushover analysis. The hinge consists of three main elements, the bearing, the cables (for tension) and compression connectors (for compression). Each of these elements will be checked individually by applying the load on the side that will make the corresponding element active.

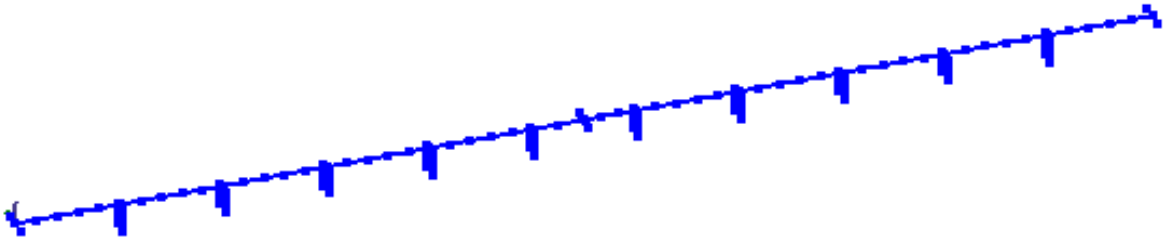


Figure H.42 FE mesh of 11-span model with one deck hinge included

Infinitely High Bearing Stiffness

In this case, the bearing stiffness will be increased to infinity, then compare it with the case of no deck hinge, since increasing the stiffness will result in one bridge without a gap. By this neither the cables nor the connectors will be in action, since the much-stiffed bearings will not allow the gap to propagate.

Deformed Shape

Figure H.43 shows the deformed shape of the bridge with infinitely high bearing stiffness. the bridge is moving as one object as expected.

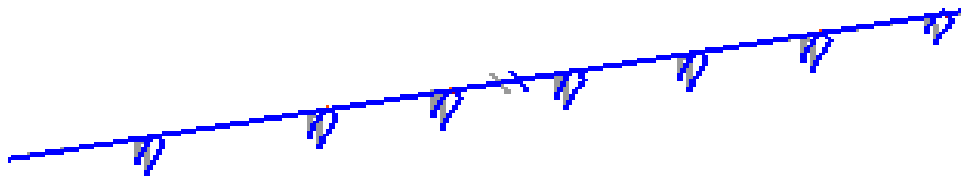


Figure H.43 Deformed shape with deck hinge

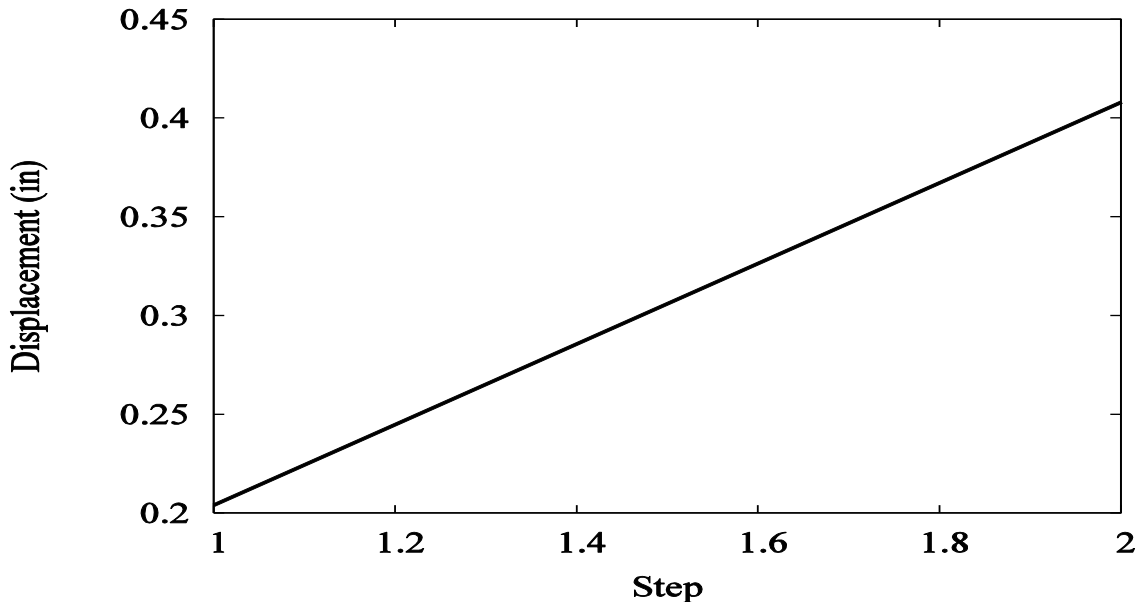


Figure H.44 Longitudinal displacement response time history at elevation of -3 ft for column 1 of bent 6 [without deck hinge]

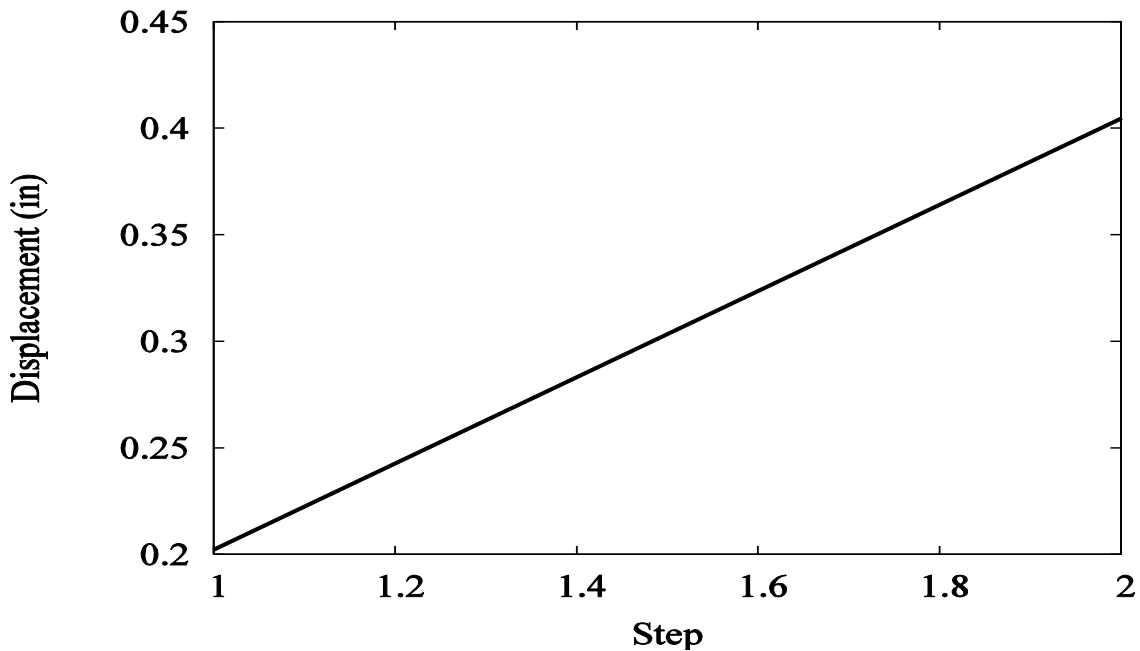


Figure H.45 Longitudinal displacement response time history at elevation of -3 ft for column 1 of bent 6 [with high stiffness bearing]

Conclusion:

The Pushover analysis results for the high bearing stiffness match the case without the hinge as shown in Figure H.44 and Figure H.45; this makes sense as the deformed shape shows that the two segments of the deck act as one object.

Force-Displacement for the Deck Hinge Response

In this case the displacement based Pushover analysis was used to show that after the cables had started to be in action, the stiffness increased. The gap is 0.5 in, so as the displacement reaches this value; there will be a jump in the force-displacement graph (Figure H.46).

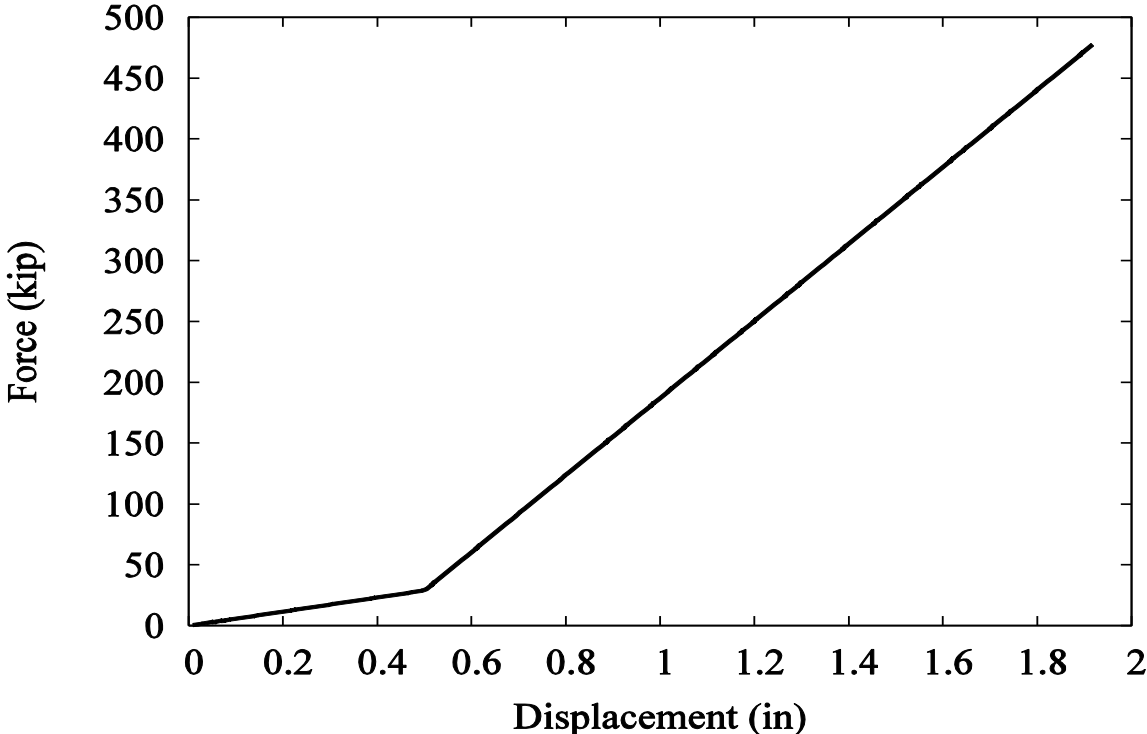


Figure H.46 Deck hinge Force-Displacement response

Deformed Shape

Figure H.47 and Figure H.48 show the deformed shape for different time step in the pushover analysis.

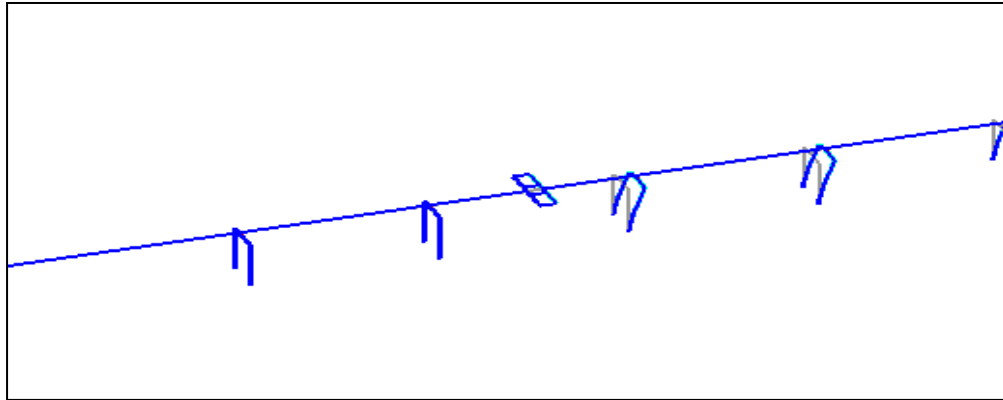


Figure H.47 Deformed shape for time step 1

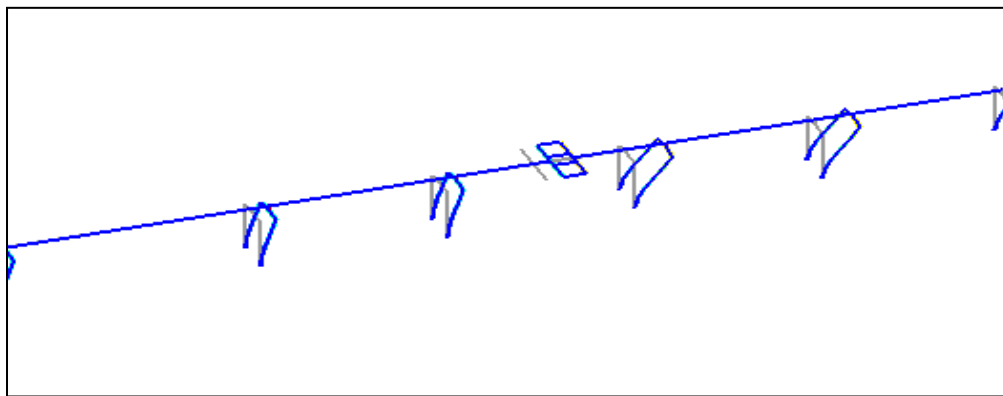


Figure H.48 Deformed shape for time step 3

Conclusion:

The Pushover analysis results show that as the displacement reaches the value where cables are in action; there will be a jump in the force-displacement graph. In addition, the deck section will act as one object since the cables stiffness values are infinitely high.

Compression Connectors

For the deck hinge under compression, only the bearing will play a role in resisting the movement. However, as the displacement reaches the gap value of 2 in, the compression connector will work along with the other side of the deck.

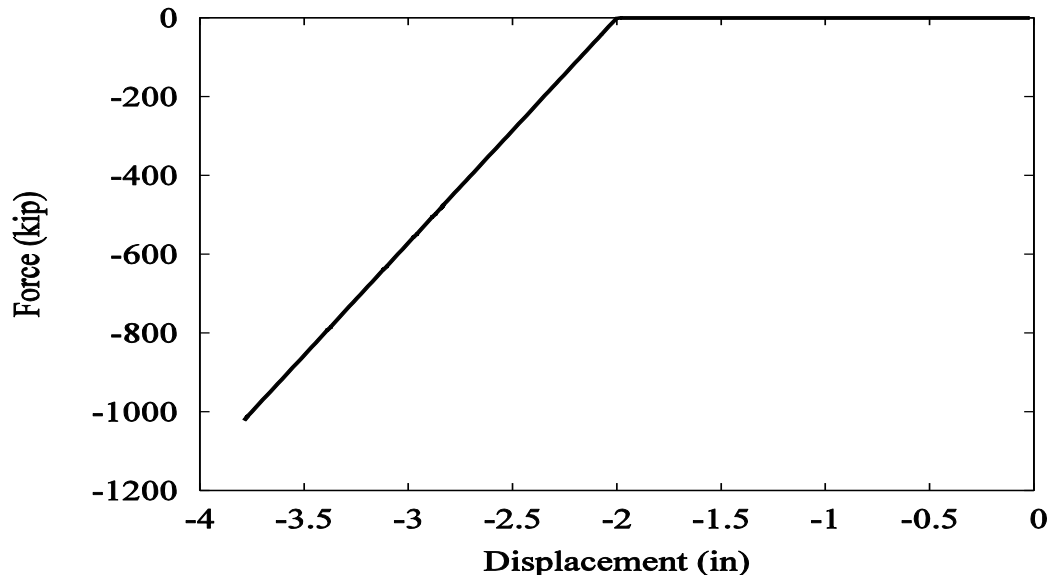


Figure H.49 Deck hinge Force-Displacement response

Conclusion:

The Pushover analysis result (Figure H.49) shows that as the displacement reaches the value where compression connectors are in action; there will be a jump in the force-displacement graph.

Multi Bearings Effect

Aim: In this section, bearings were used to check the effect of having more bearings on the bridge deck response. Less displacement is predicted from the Pushover results, since increasing the number of bearing will result in higher deck stiffness.

Implementation

The same bridge model will be used, but with reduced cable stiffness values so that only the bearings resisted the motion, since even the gap has reached to the value by which the cables start to work, it will not resist the motion because of low stiffness values.

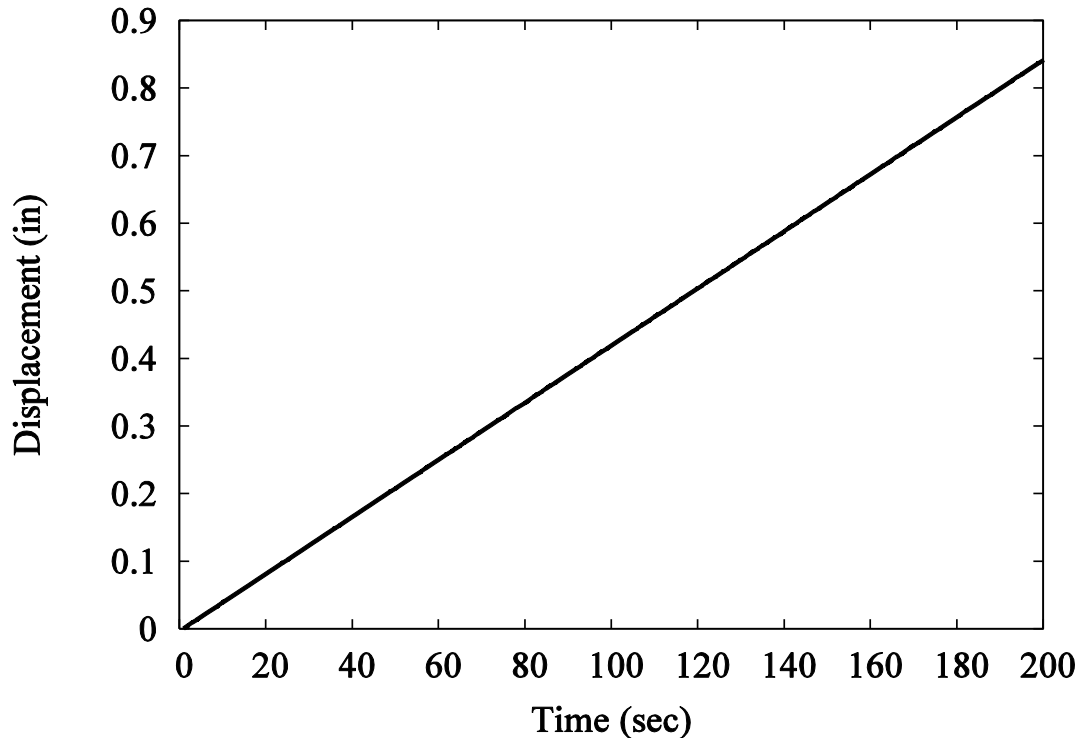


Figure H.50 Deck hinge displacement response time history [1 bearing]

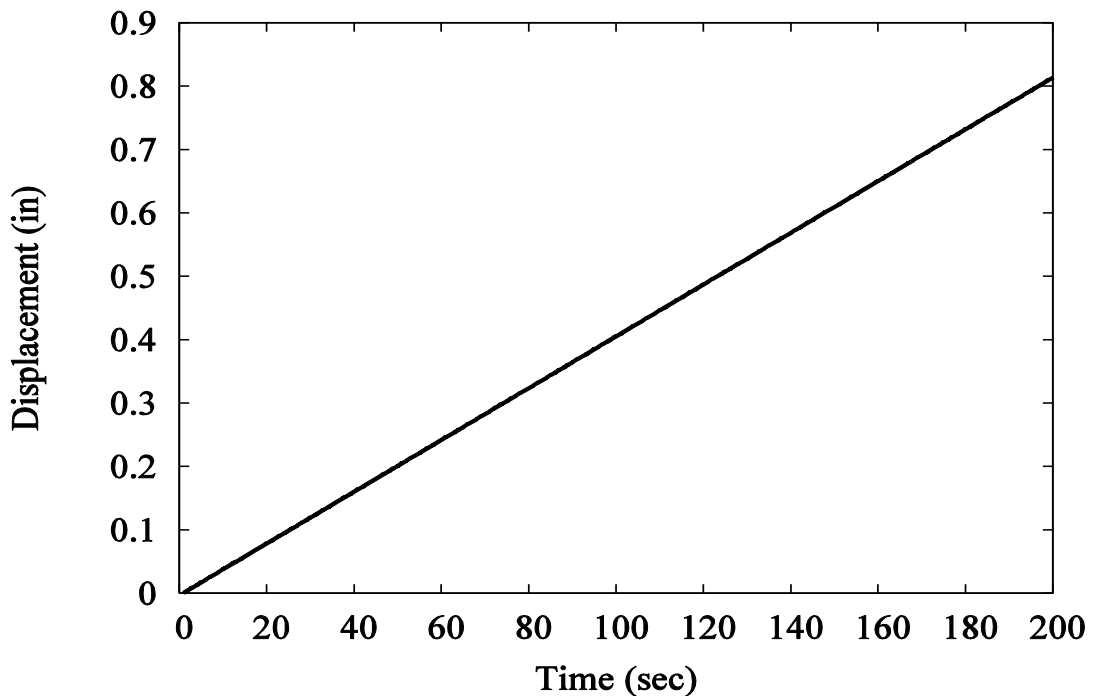


Figure H.51 Deck hinge displacement response time history [3 bearings]

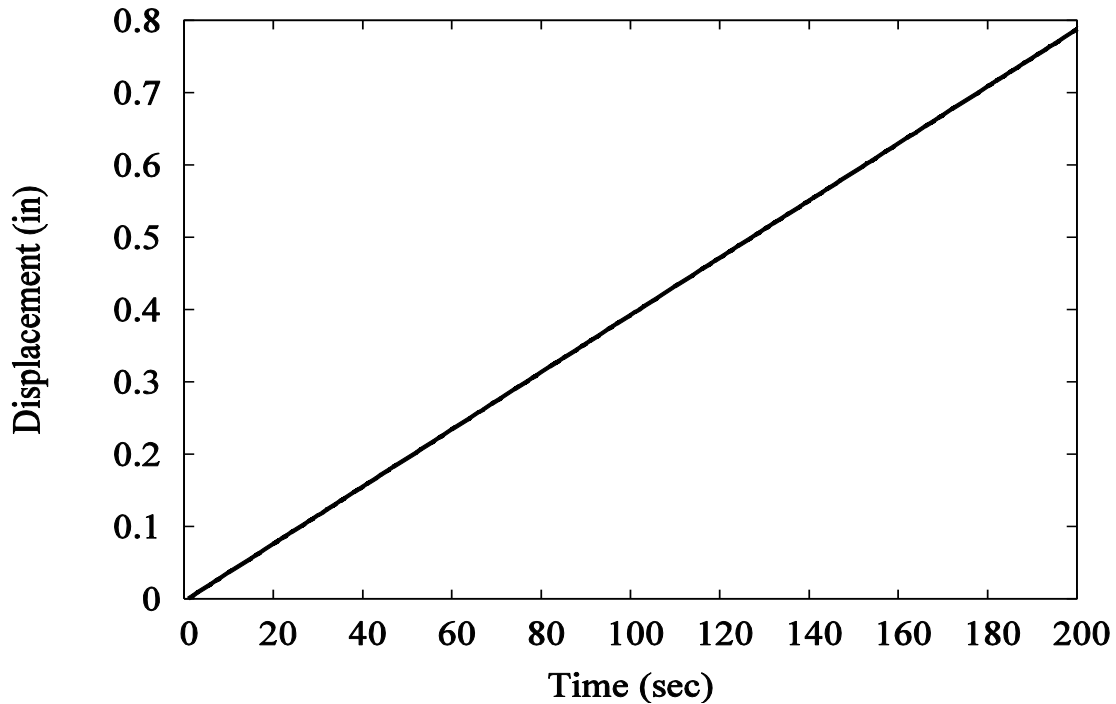


Figure H.52 Deck hinge displacement response time history [5 bearings]

Conclusion:

The Pushover analysis results show that as the numbers of bearings are increased, the stiffness will increase accordingly. Therefore, the displacement of the deck hinge is higher for one bearing than multi-bearings.

Transverse Direction

As the load was applied transversally, the two sides of the deck hinge started to rotate; so, one end will be in compression (end 1) and the other end will be in tension (end 2). Therefore, cables and compression connectors started to work together whenever the gap value had reached the critical one.

Aim: To check the effect of the transverse loading on the deck hinge response. The stiffness in the compression end will increase as the displacement reaches the compression gap value, 2 in. On the other hand, the stiffness in the tension end will increase whenever the cables are in action and the 0.5 in has been reached.

Implementation

In this section two cables, two bearings, and two compression connectors were used to check the transverse loading, since more than one element is required to show the rotation of the deck hinge.

Deformed Shape

The deformed shape shows how the two sides of the deck hinge rotate when the Pushover load is applied transversely. Thus, one side will be in compression and the connectors will resist if the gap closes (Figure H.54). On the other end, the cables will resist the motion if the gap has reached the defined value for the cables to start working, since this end of the hinge is in tension.

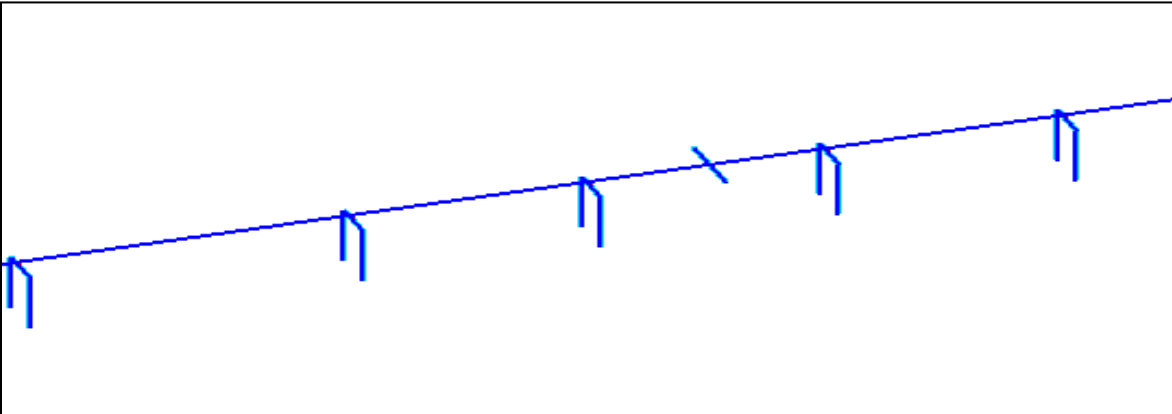


Figure H.53 Deformed shape for time step 1

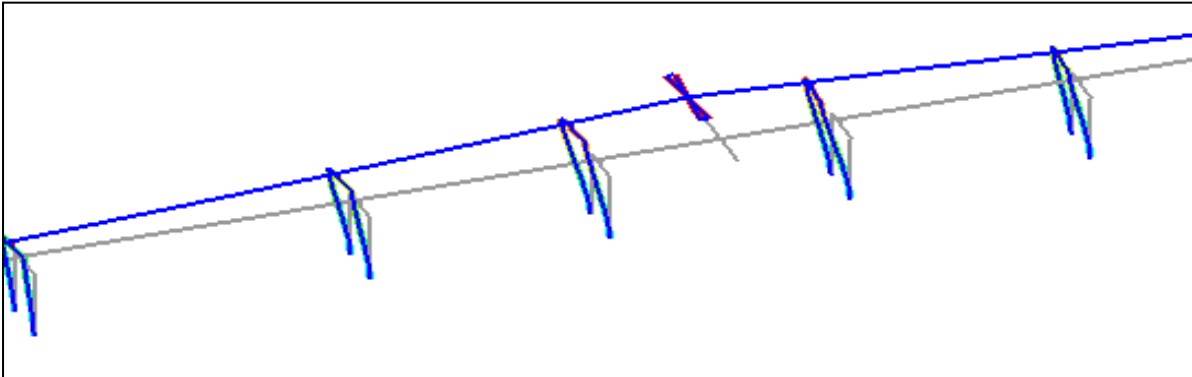


Figure H.54 Deformed shape for time step 200

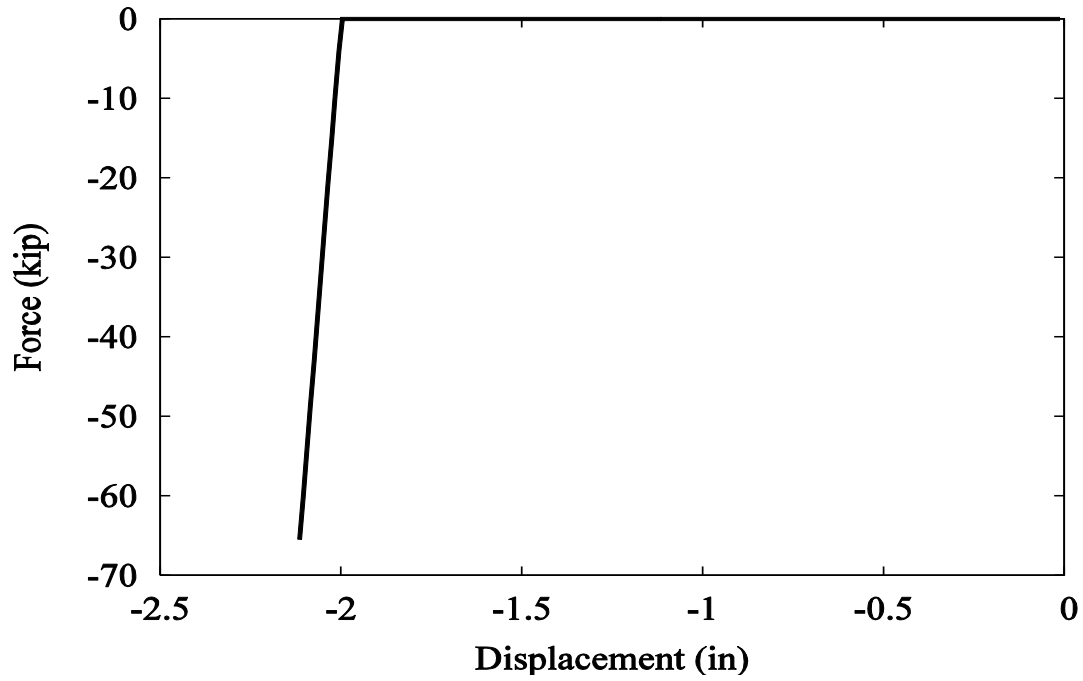


Figure H.55 Deck hinge Force-Displacement response [Edge Element 1]

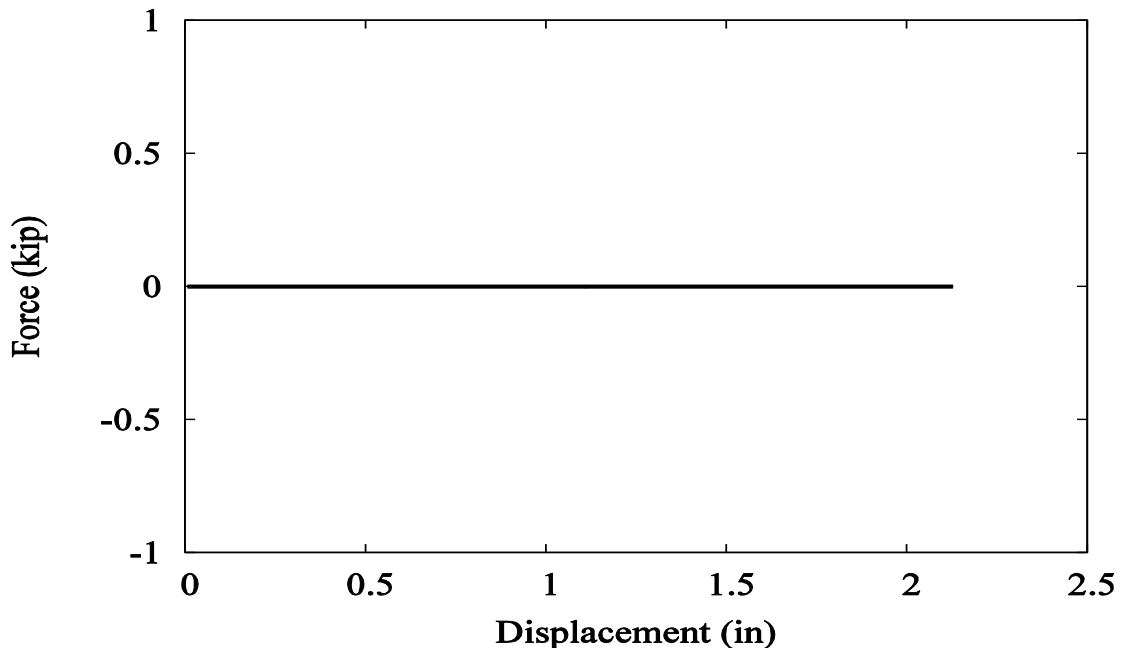


Figure H.56 Deck hinge Force-Displacement response [Edge Element 2]

Figure H.55 shows that the edge element 1 stiffness increases when the displacement reached 2 in which is the gap value, since the end 1 was in compression. On the other hand, Figure H.56 shows that the edge element 2 remains unchanged since the end 2 was in tension.

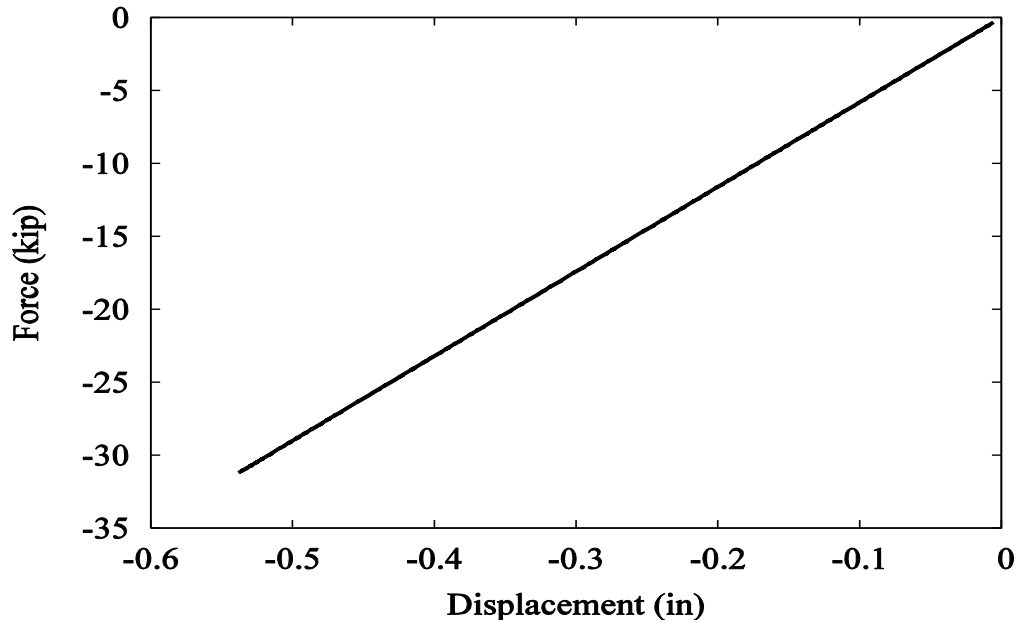


Figure H.57 Deck hinge Force-Displacement response [Cable Element 1]

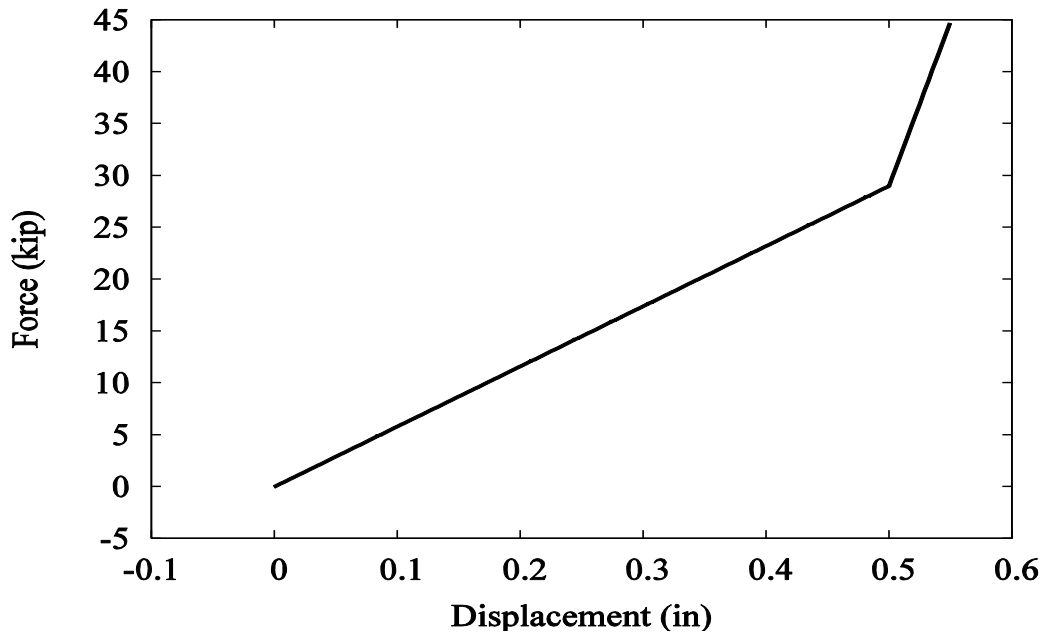


Figure H.58 Deck hinge Force-Displacement response [Cable Element 2]

Figure H.57 shows that the cable element 1 remained unchanged since the end 1 was in compression. On the other hand, Figure H.58 shows that the cable element 2 stiffness increased when the displacement reached 0.5 in. (i.e. the gap value) since the end 1 was in tension.

REFERENCES

- Aviram, A., Mackie, K.R., and Stojadinovic, B. (2008a). "Effect of abutment modeling on the seismic response of bridge structures." *Earthquake Engineering and Engineering Vibration*, 7(4), 395-402.
- Aviram, A., Mackie, K.R., and Stojadinovic, B. (2008b). "Guidelines for nonlinear analysis of bridge structures in California." *PEER Report No. 2008/03*, Pacific Earthquake Engineering Research Center, University of California, Berkeley.
- Caltrans (2005). "SDC Example A: Pushover Design Example (Version 1.2), Salinas River Bridge (Right Replace), Br. No. 44-002R", California Department of Transportation, Sacramento, California.
- Caltrans (2013). *Caltrans Seismic Design Criteria, Version 1.7*, California Department of Transportation, Sacramento, California.
- Caltrans (2016). Personal communication. California Department of Transportation, Sacramento, California.
- Elgamal, A., Lu, J., and Mackie, K. (2014). "MSBridge: OpenSees pushover and earthquake Analysis of multi-span bridges - user manual." *Structural Systems Research Project SSRP-14/04*, University of California at San Diego, La Jolla.
- Hetenyi, M. (1946). *Beams on Elastic Foundation*, The University of Michigan Press, Ann Arbor, MI
- Lu, J., Elgamal, A., and Mackie, K. (2015). "Parametric Study of Ordinary Standard Bridges using OpenSees and CSiBridge." *Structural Systems Research Project SSRP-14/03*, University of California at San Diego, La Jolla.
- Mahan, M. (2005). *wFrame - Pushover Analysis of Bridge Bents and Frames*, California Department of Transportation, Sacramento, California.
- Mazzoni, S., McKenna, F., Scott, M. H., Fenves, G. L., et al. (2009). *Open System for Earthquake Engineering Simulation, User Command-Language Manual*, Pacific Earthquake Engineering Research Center, University of California, Berkeley, OpenSees version 2.0, May.
- McKenna, F., Scott, M., and Fenves, G. (2010). "Nonlinear Finite-Element Analysis Software Architecture Using Object Composition". *J. Comput. Civ. Eng.*, 24(1), 95–107.
- Scott, M. and G. Fenves. (2006). "Plastic Hinge Integration Methods for Force-Based Beam-Column Elements", *Journal of Structural Engineering*, 132(2), 244-252.
- Scott, M. and K. Ryan. (2013). "Moment-Rotation Behavior of Force-Based Plastic Hinge Elements", *Earthquake Spectra*, 29(2), 597-607.

Shamsabadi, A. and Taciroglu, E. (2013). "A Frequency-Time Domain Handshake Method For Seismic SoilFoundation-Structure Interaction Analysis of Long-Span Bridges", *Seventh National Seismic Conference on Bridge and Highways*, Oakland, California.

Terzaghi, K. (1955). "Evaluation of Coefficients of Subgrade Reaction." *Geotechnique*, Vol. 5, pp. 297

Wang, N. (2015). "Three-Dimensional Modeling of Ground-Pile Systems and Bridge Foundations", PhD Thesis, Department of Structural Engineering, University of California, San Diego, La Jolla, CA.